

Functional characterization of npcRNAs
Intercellular trafficking of generegulatory components via exosomes

Dissertation for the award of the degree

„Doctor of Philosophy“ (Ph.D.)

Molecular Biology of Cells Program
Georg August University Göttingen
Faculty of Biology

Submitted by

Kai Oliver Böker

Born 18.09.1985 in Herford

Göttingen 2016

PhD Thesis Committee:

Dr. Jens Gruber

Medical RNA Biology

German Primate Center, Göttingen

Prof. Dr. Reinhard Jahn

Director at the Max Planck Institute for Biophysical Chemistry

Department Neurobiology

Max-Planck-Institute for Biophysical Chemistry, Göttingen

Prof. Dr. Michael Simons

Department of Neurology

Cellular Neuroscience

Max-Planck Institute of Experimental Medizin, Göttingen

Prof. Dr. Lutz Walter

Department of Primate Genetics

German Primate Center, Göttingen

Dr. Julia Gross

Department of Developmental Biochemistry

Extracellular Signaltransduction

University Medical Center (UMG)

Prof. Dr. Uwe Groß

Head of the Institute for Medical Microbiology

Department Medical Microbiology

University Medical Center (UMG)

Date of the oral examination: 15.12.2016

Affidavit

Herewith I declare, that I prepared this thesis “Functional characterization of npcRNAs - Intercellular trafficking of generegulatory components via exosomes“ independently and with no other sources and aids than quoted.

Göttingen, 31.10.2016

Kai Böker

Table of contents

Table of contents

Table of contents	I
List of Figures.....	V
List of tables.....	VII
Original publications.....	VIII
1. Introduction.....	1
1.1 Extracellular vesicles.....	1
1.2 Exosomes: Classification, biogenesis and marker proteins	2
1.3 Methods of extracellular vesicle isolation.....	6
1.4 Biogenesis of miRNAs and RNA interference (RNAi)	7
1.5 Cell-cell communication via extracellular vesicles.....	10
1.6 Gene delivery via lentiviruses or virus-like particles (VLPs).....	11
1.7 Aim of thesis	14
2. Materials & Methods.....	15
2.1 Molecular biology	15
2.1.1 <i>Escherichia coli</i> transformation, cultivation and plasmid isolation.....	15
2.1.2 DNA separation by Agarose Gel Electrophoresis.....	15
2.1.3 Polymerase chain reaction	15
2.1.4 Gel purification.....	16
2.1.5 Ligation of two DNA fragments.....	17
2.1.6 Transformation of bacteria.....	17
2.1.7 Restriction digestion of DNA.....	17
2.1.8 Isolation of extracellular vesicles.....	18
2.1.9 Extracellular vesicle characterization by Nanoparticle Tracking	18
Analysis	18
2.1.10 RNA Isolation, size and integrity detection and cDNA synthesis.....	18
2.1.11 Quantitative PCR analysis	19
2.1.12 NGS library preparation	19
2.1.13 Next generation sequencing and data analysis.....	19
2.1.14 Preparing samples for electron microscopy.....	20
2.2 Cell biology	22
2.2.1 Cell culture	22
2.2.2 Fluorescence microscopy.....	22
2.2.3 Generation of lentiviral constructs.....	22

Table of contents

2.2.4	Lentivirus production, concentration and titration.....	23
2.2.5	Generation of stable CD9 _{GFP} , Alix ⁻ mCherry and TSG101 _{mCherry} cell lines.....	23
2.2.6	Primary cortical culture.....	24
2.2.7	Immunohistochemistry and confocal microscopy	24
2.2.8	Flow cytometry analysis (FACS).....	25
2.2.9	Transfection of pUTA2.0 plasmids and data analysis	25
2.2.10	Virus like particle loading with DNA or RNA for <i>in vitro</i> use	25
2.2.11	Virus like particle loading with NanoGold particles	26
2.2.12	Virus like particle loading for <i>in vivo</i> use	26
2.3	Protein biochemistry.....	27
2.3.1	Preparation of exosome or cellular samples for protein analysis.....	27
2.3.2	Determination of protein concentration.....	27
2.3.3	Polyacrylamid gel electrophoresis	27
2.3.4	Western Blot.....	28
2.3.5	VLP production and purification.....	29
2.4	Materials.....	30
2.4.1	Machines.....	30
2.4.2	Buffers and Solutions.....	31
2.4.3	Chemicals and Materials.....	32
2.4.4	Bacterial strains information.....	36
2.4.5	Cell lines.....	36
2.4.6	Cell culture media and additives	36
3.	Results.....	38
3.1.	Comparison of three isolation techniques for exosomes.....	38
3.1.1	Different isolation techniques yield various size profiles of EVs.....	38
3.1.2	All tested isolation techniques show exosomal marker protein expression like CD9, CD63 or Alix.....	41
3.1.3	Confirmation of EV isolation by electron microscopy	43
3.2.	Small RNA profiles of cellular and exosomal RNA.....	44
3.2.1	Cellular and exosomal RNA differ in size distribution.....	44
3.2.2	Next generation sequencing workflow.....	45
3.2.3	Reproducibility of NGS data on the IonTorrent system	46
3.2.4	Exosomal and intracellular small RNA profiles of human B-lymphocytes (Raji).....	47
3.2.5	Exosomal and intracellular small RNA profiles of human T-lymphocytes (Jurkat)	49
3.2.6	Exosomal and intracellular small RNA profiles of human B-lymphocytes (DG75)	51

Table of contents

3.2.7	Exosomal and intracellular small RNA profiles of human cervical cancer cells (HeLa)	54
3.2.8	Cluster analysis of cellular and exosomal small RNAs.....	56
3.2.9	Comparison of miRNA distribution in exosomes and sequence motifs	58
3.3	Comparison of exosome isolation techniques.....	61
3.4	Overexpression of exosomal marker proteins and influence on EVs and LVs	64
3.4.1	Overexpression of TSG101, Alix or CD9 alters both amount and mean sizes of EVs.....	64
3.4.2	CD9 overexpression affects size and amount of extracellular vesicles in different cell types	66
3.4.3	Cellular localization of CD9 _{GFP} , Alix _{mCherry} and TSG101 _{mCherry}	69
3.4.4	LV production workflow and produced LVs.....	70
3.4.5	The CD9 mediated increase of extracellular vesicles boosts the transduction efficiency of lentiviral vectors	71
3.4.6	Overexpression of CD9 yields transduction competent LVs in absence of viral envelope proteins	75
3.4.7	Influence of CD9 on LV production and amount tested by ELISA	76
3.4.8	Performance of CD9 LVs on primary cell material.....	77
3.4.9	Cytoplasmic relocalization of CD9 during lentivirus production	78
3.4.10	CD9 influence on exosomal small RNA content.....	80
3.5.	Role of EVs in cell-cell communication	82
3.5.1	Sequence motifs of secreted miRNAs of Jurkat and Raji.....	82
3.5.2	Cell-cell communication between Raji and Jurkat cells.....	83
3.5.3	Cell-cell communication analysis by a novel dual reporter gene toolbox..	87
3.6	Manipulation of human B-lymphocytes and <i>in vivo</i> studies	96
3.6.1	Transduction of human B-lymphocytes via virus-like particles (VLPs)	96
3.6.2	Tracking of miR-451a inside human B-lymphocytes via NanoGold particles.....	97
3.6.3	Studying cell-cell communication between Raji and SW837	98
3.6.4	<i>In vivo</i> siRNA delivery by virus-like particles (VLPs).....	100
4.	Discussion.....	102
4.1	Comparison of exosome isolation techniques.....	102
4.2	Cellular and extracellular small RNA profiles of four human cell lines.....	105
4.3	Comparison of PEG precipitation and Ultracentrifugation	108
4.4	Overexpression of exosomal marker proteins and influence on EVs and LVs	110
4.5	Role of EVs in cell-cell communication	114
4.6	Manipulation of human B-lymphocytes and <i>in vivo</i> studies	117

5. Summary	121
6. Reference	122
7. Acknowledgements.....	135
8. Abbreviations	136
9. Appendix.....	138
9.1 Raji sequencing reports.....	138
9.1.1 Intracellular Raji library (Raji cell1).....	138
9.1.2 Intracellular Raji library (Raji cell3).....	138
9.1.3 Intracellular Raji (Raji cell2) and exosomal Raji library (Raji exo3).....	139
9.1.4 Exosomal Raji library (Raji exo1)	139
9.1.4 Exosomal Raji library (Raji exo2)	140
9.2 Jurkat sequencing run reports.....	140
9.2.1 Intracellular Jurkat library.....	140
9.2.2 Exosomal Jurkat library	141
9.3 DG75 sequencing reports	141
9.3.1 Intracellular DG75 library.....	141
9.3.2 Exosomal DG75 library	142
9.4 HeLa sequencing reports.....	142
9.4.1 Intracellular HeLa library.....	142
9.4.2 Exosomal HeLa library	143
9.5 Raji small RNA sequencing results.....	143
9.6 Jurkat small RNA sequencing results (log2foldchange >±2)	151
9.7 DG75 small RNA sequencing results (log2foldchange >±2)	160
9.8 HeLa small RNA sequencing results (log2foldchange >±1)	167
9.9 Plasmid maps	177
9.9.1 Destiny vector for lentiviral construct generation.....	177
9.9.2 Lentivirus vector for stable CD9 _{GFP} expression	177
9.9.3 Lentivirus vector for stable Alix _{mCherry} expression.....	178
9.9.4 Lentivirus vector for stable TSG101 _{mCherry} expression	178
9.10 Curriculum vitae	179

List of Figures

Figure 1: Release of extracellular vesicles and their properties.	1
Figure 2: Diagram of endosome pathways and exosome biogenesis in mammalian cells.....	3
Figure 3: Schematic representation of exosome composition..	5
Figure 4: MiRNA biogenesis and function.	8
Figure 5: RNAi pathway and exosome biogenesis.	9
Figure 6: Cell-cell communication by exosomes	10
Figure 7: Comparison of lentiviruses, exosomes and virus-like particles.	13
Figure 8: Generation of pUTA2.0 construct.	21
Figure 9: Comparison of three exosome isolation techniques.	38
Figure 10: Comparing size and yield of extracellular vesicles (EVs) isolated by three different techniques.	40
Figure 11: Detection of three different exosome marker proteins via Western Blot.	42
Figure 12: Detection of extracellular vesicles by electron microscopy.	43
Figure 13: RNA size-profile of cellular (purified / total RNA) and exosomal RNA.....	45
Figure 14: Illustration of the next generation sequencing workflow.	46
Figure 15: Reproducibility of NGS data generated by IonTorrent System.....	47
Figure 16: Cellular and exosomal small RNA distribution of Raji small RNA libraries..	48
Figure 17: Small RNA distribution in cells and exosomes of Jurkat.	50
Figure 18: Cellular and exosomal small RNA expression of human B-lymphocytes (DG75).	52
Figure 19: Cellular and exosomal small RNA expression of human cervical cancer cells (HeLa).	54
Figure 20: Cellular and exosomal small RNA expression of Raji and Jurkat.	57
Figure 21: Cellular and exosomal small RNAs of Raji, Jurkat, DG75 and HeLa.	58
Figure 22: Expression pattern and sequence motifs of exosomal miRNAs in HeLa, Jurkat, DG75 and Raji exosomes.	59
Figure 23: Distinct small RNA sequence motifs of three different human B- and T- lymphocytes.....	60
Figure 24: RNA- and vesicle size-profiles of EVs isolated from Raji cells.	61
Figure 25: Small RNA profiles of cellular and exosomal RNA isolated by ultracentrifugation or PEG precipitation.....	62
Figure 26: Overexpression of exosomal marker proteins CD9, Alix and TSG101 in HEK293 cells affects vesicle amounts and sizes.....	64
Figure 27: Overexpression of exosomal marker proteins CD9, Alix and TSG101 in HEK293 cells affects vesicle amounts and sizes.....	66
Figure 28: CD9 overexpression in HEK293 FT, HeLa, Jurkat and Raji cells.....	67
Figure 29: CD9 locate to the plasma membrane and cell-cell-contact surfaces in stably CD9-GFP expressing cell lines.	69
Figure 30: Alix and TSG101 overexpression in HEK293 cells visualized by fluorescence microscopy.....	70
Figure 31: Procedure of Lentivirus production and comparison between exosomes and LVs.....	71
Figure 32: Lentiviral transduction of Raji and Jurkat	72
Figure 33: Transduction efficiency of LV-VSVG and LV-VSVG-CD9.	72
Figure 34: Transduction efficiency of LV-VSVG and LV-VSVG-CD9..	73

List of tables

Figure 35: Transduction efficiency of LV-VSVG and LV-VSVG-CD9 determined by FACS analysis.....	74
Figure 36: CD9 mediates fusion with target cell membrane.	75
Figure 37: Negative control setup for transduction efficiency comparison of CD9, VSVG and CD9-VSVG virus.....	76
Figure 38: Physical titer of tested lentiviruses measured by Elisa.	77
Figure 39: Lentivirus function on primary rat brain culture.	78
Figure 40: Localization of CD9GFP in HEK293FT-CD9GFP cells.	79
Figure 41: CD9 influence on exosomal miRNA content.	80
Figure 42: Exosomal miRNAs of Raji und Jurkat and their sequence motifs..	82
Figure 43: Co-cultivation of Raji cells with Jurkat cell culture supernatant and the resulting change of intracellular miRNA composition	83
Figure 44: QPCR analysis of BCL2 and DNMT1 in Raji cells.....	86
Figure 45: Principle of the dual fluorescence reporter gene toolbox and miRNA characterization.	87
Figure 46: Non cognate controls for dual reporter gene assay.	88
Figure 47: Functional characterization of miR-451a, miR-148a-3p and GL-2.....	89
Figure 48: Functional characterization of miR-15a-5p and influence of exosome treatment.	90
Figure 49: Functional characterization of miR-21-5p and influence of exosome treatment. .	91
Figure 50: Functional characterization of miR-19b-3p and influence of exosome treatment.	92
Figure 51: Exosomal secretion motif and comparison to GL-2 siRNA sequence.	92
Figure 52: Functional characterization of non-endogenous GL-2 transferred by lipofection or extracellular vesicles.	93
Figure 53: Functional characterization of non-endogenous GL-2 transferred by CD9 or WT exosomes	95
Figure 54: CAG-GFP expression cassette supply into B-lymphocytes via VLP transduction....	96
Figure 55: Delivery of NanoGold particles via virus-like particles into human B-lymphocytes (Raji)..	97
Figure 56: Raji secretion motif and comparison to Cy3 siRNA sequence.	98
Figure 57: Analysis of cell-cell communication between Rajhi and SW837 cells.	99
Figure 58: <i>In vivo</i> siRNA delivery against RANKL in rat tibiae via virus-like particles	101
Figure 59: Key findings evaluated in this thesis.....	120

List of tables

List of tables

Table 1: Antibiotic concentrations for bacteria selection	15
Table 2: Pipetting scheme for polymerase chain reaction	16
Table 3: Standard protocol for PCR amplification	16
Table 4: Pipetting scheme for DNA ligation	17
Table 5: Sequence information of qPCR primers	19
Table 6: Generated plasmids for miRNA efficiency detection by UTA system.. ..	21
Table 7: Plasmids for LV generation with depositor and Addgene information	23
Table 8: Blasticidin concentration for selection of lentivirus transduced cell lines	24
Table 9: Recipe for separation gel	28
Table 10: Stacking gel recipe	28
Table 11: Antibody information for Western Blot analysis	29
Table 12: Used machines and manufacturer information	30
Table 13: Informations about buffers and solutions	31
Table 14: Chemicals and Materials	32
Table 15: Used bacterial strains for transformation and plasmid generation	36
Table 16: Cell lines for in vitro tests	36
Table 17: Different media for cell culture use	36
Table 18: Mean particle size and yield of different EV isolated from four different human cell lines by three isolation methods	41
Table 19: Sequencing information for Raji libraries	46
Table 20: MiRNA candidates of Raji and distribution in cells compared to exosomes	48
Table 21: MiRNA candidates exclusively present in exosomes (log ₂ foldchange = Inf) or intracellular (log ₂ foldchange = -Inf)	49
Table 22: MiRNA candidates of Jurkat and distribution in cells compared to exosomes	50
Table 23: MiRNA candidates exclusively present in Jurkat exosomes (log ₂ foldchange = Inf) or intracellular (log ₂ foldchange = -Inf)	51
Table 24: MiRNA candidates of DG75 and distribution in cells compared to exosomes	52
Table 25: MiRNA candidates exclusively present in DG75 exosomes (log ₂ foldchange = Inf) or intracellular (log ₂ foldchange = -Inf)	53
Table 26: Top 5 cellular and exosomal miRNAs in HeLa	55
Table 27: Exclusively extracellular (log ₂ foldchange = Inf) or intracellular (log ₂ foldchange = -Inf) HeLa miRNA candidates	55
Table 28: Exosomal miRNA distribution among four human cell lines	60
Table 29: Small RNA content of PEG precipitated or ultracentrifuged extracellular vesicles	63
Table 30: miRNAs only detectable after PEG precipitation	64
Table 31: Summary of CD9, Alix and TSG overexpression and influence on EVs	68
Table 32: Comparison of LV-VSVG and LV-VSVG-CD9GFP transduction efficiency	74
Table 33: Top5 overrepresented extracellular small RNA candidates of wildtype and CD9 overexpressing B-lymphocytes	81
Table 34: MiRNAs exclusively present in exosomes of wildtype Raji	81
Table 35: Increased and decreased miRNA candidates after Jurkat exosome treatment	84
Table 37: High represented miRNAs in Jurkat exosomes and change in Raji cells upon treatment with Jurkat exosomes	85
Table 38: In silico analysis of miRNA targets	85
Table 39: Sequence and modification of miR-451a	98
Table 40: Three different doses of siRNA loaded virus-like particles	100

Original publications

The following publications base on this thesis and are further described in the literature bibliography.

Hoffmann, DB, **Böker, K. O.**, Schneider, S., Eckermann-Felkl, E., Schuder, A., Komrakova, M., Sehmisch, S. Gruber, J. (2016). In Vivo siRNA Delivery Using JC Virus-like Particles Decreases the Expression of RANKL in Rats. *Molecular therapy Nucleic acids* **5**: e298.

Hoffmann and Böker contributed equally to this work

Lemus-Diaz, N, **Böker, K. O.**, Rodriguez-Polo, I., Mitter, M., Preis, J., Gruber, J. (2016). Dissecting the gene regulatory activity of miRNAs at the single cell level. *Scientific Reports* **(Accepted)**

Böker, K. O., Lemus, N., Rinaldi Ferreira, R., Schiller, L. T., Schneider, S., Gruber, J. (2016). The impact of the CD9 tetraspanin on exosome secretion and lentivirus infectivity. *Molecular Therapy* **(in revision)**.

Schneider, S, Schiller, L. T., **Böker, K. O.**, Lemus-Diaz, N., Gruber, J. (2016). Retargeted JC polyoma derived virus-like particles as efficient and specific cell transduction tool. *Journal of controlled release* **(in review)**.

1. Introduction

1.1 Extracellular vesicles

Extracellular vesicles (EVs) are defined as extracellular particles containing cytosolic components from the secreting cell, which are encapsulated by lipid bilayers. The secretion of these EVs is conserved throughout evolution including simple and multicellular eukaryotes (e.g. *Caenorhabditis elegans* [1], *Leishmania donovani* [2], *Toxoplasma gondii* [3] and fungi [4]) but also prokaryotic cells [5] and mammalian cells [6, 7]. Extracellular vesicles have a diverse repertoire of features and in recent years various nomenclatures have been used in literature. Vesicles were designated by their size (microvesicles, nanovesicles, nanoparticles), their tissue of origin (prostasomes, oncosomes) or by their presence outside of cells (exosomes, ectosomes or exovesicles). The nomenclature of extracellular vesicles is still in discussion [8]. Nevertheless, according to the latest research, EVs can be divided into three subclasses: apoptotic bodies, microvesicles and exosomes (Figure 1).

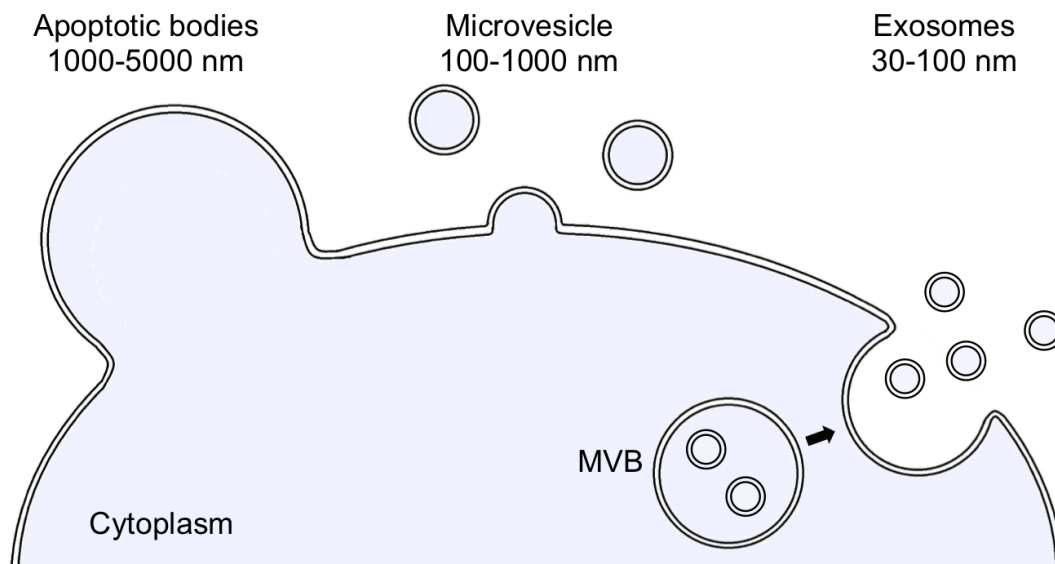


Figure 1: Release of extracellular vesicles and their properties. Extracellular vesicles can be classified into three main classes: Apoptotic bodies (AB), microvesicles (MV) and exosomes. Apoptotic bodies are shed from the cell membrane during stress or apoptosis and are 1000-5000 nm in size. Microvesicles were shed from the cell membrane too, while they are smaller in size with 100-1000 nm. Exosomes are the smallest known extracellular vesicles with a diameter of 30-100 nm. Internal vesicles are formed inside multivesicular bodies (MVB), which fuse with the cell membrane and release these internal vesicles now called exosomes.

1. Introduction

The typical diameter of apoptotic bodies or apoptotic vesicles ranges from 1000 nm – 5000 nm and they are released upon apoptotic cell death [9-11]. These vesicles directly bud from the plasma membrane and carry cytoplasmic, nuclear and endoplasmic proteins [12, 13] as well as DNA and histones [14]. Oncosomes share the biogenesis route and size distribution of apoptotic bodies but are cancer specific and may have unique properties *in vivo* through transferring the oncoprotein EGFRvIII to the membrane of tumour cells lacking this protein [15]. Compared to apoptotic bodies, microvesicles (MV) are smaller in size (100-1000 nm) but share a similar biogenesis route. Both vesicle types are shed from the plasma membrane of the sending cell, while microvesicles are released under non-apoptotic conditions, for example after stimulation of cells by cytokines [16, 17]. Recent studies reported the transfer of mRNA and miRNA from one cell to another by MVs [18], therefore MVs are discussed to play a role in cell-cell communication [19]. A similar role in horizontal transfer of information is also postulated for exosomes. These 30-100 nm extracellular vesicles are formed by invagination of internal vesicles in multivesicular bodies. These intraluminal vesicles can further fuse with the lysosome leading to degradation or fuse with the plasma membrane, releasing the internal vesicles to the extracellular space [20]. More detail of the biogenesis of exosomes is provided in the next chapter (1.2 Exosomes: Classification, biogenesis and marker proteins). Since the cargo (e.g. small RNAs, proteins, DNA) differs among diverse types of EVs [21], a pure population of e.g. exosomes is needed for specific small RNA detection, which is the base of this thesis. However, there are still limitations of current EV isolation methods providing high yield and purity due to the similarity of MVs and exosomes, which will also be described in the next chapters

1.2 Exosomes: Classification, biogenesis and marker proteins

Exosomes are 30 – 100 nm sized extracellular vesicles of endocytic origin, which are secreted by a multitude of cell types *in vitro* as well as *in vivo* [22]. The endocytic pathway consists of dynamic membranous compartments involving early endosomes, which originate by endocytosis at the plasma membrane [23] (Figure 2). Molecules, such as receptors of the plasma membrane, are transferred by endocytic vesicles to early endosomes (1). Due to the acidic pH of 6.2 inside these cell compartments the receptors are uncoupled from their

1. Introduction

ligands and partially recycled back to the plasma membrane (2). Late endosomes even comprise a pH of 5.0-5.5 and accumulate intraluminal vesicles within their lumen (3), while they mature to multivesicular bodies (MVBs) [24, 25]. MVBs can either fuse with the lysosome leading to a degradation of their content by lysosomal hydrolases (5) or fuse with the plasma membrane to release their content as extracellular vesicles, also called exosomes (6). The process, which determines exocytosis or degradation, is not fully understood. However, in 1993 Vidal and Stahl found that MVBs fusing with the plasma membrane bear markers of rather early endosomes than late endosomes, suggesting different subpopulations of MVBs inside the cell [26].

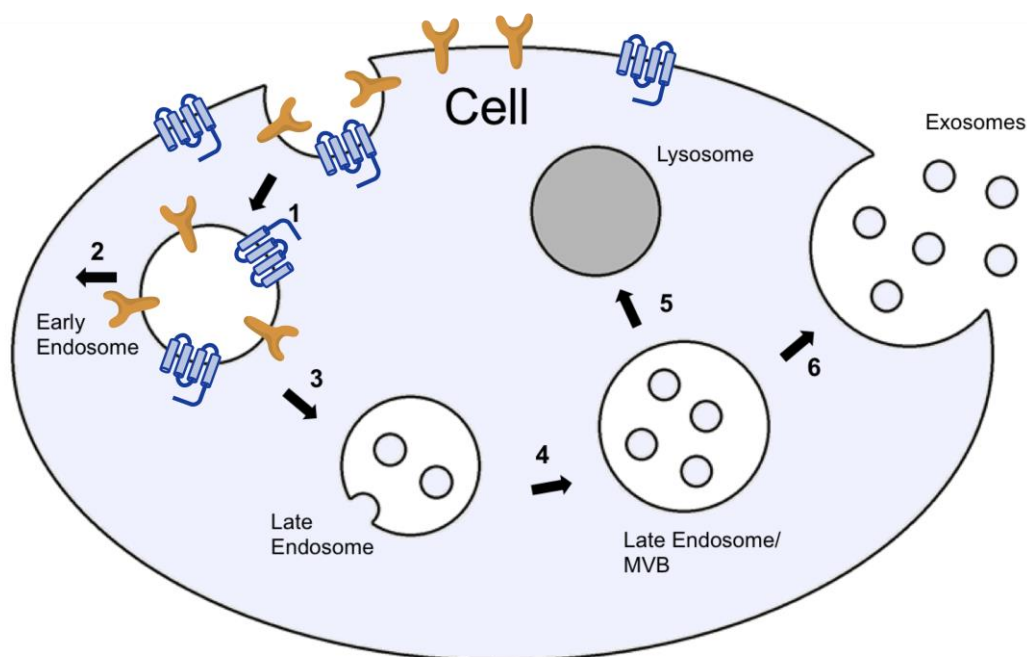


Figure 2: Diagram of endosome pathways and exosome biogenesis in mammalian cells. Membrane proteins (for example transferrin- or EGF-receptors) are internalized upon receptor binding and transported to early endosomes (1). Here the receptor proteins are released from their ligand and are recycled to the plasma membrane (2). During maturation of the endosome vesicles are internalized (3) and multivesicular bodies are formed (4). These cell compartments can fuse with the lysosome leading to a degradation of cargo (5) or they fuse with the plasma membrane (6). Upon fusion the internal vesicles of the MVBs are released into extracellular space, now called exosomes.

Exosomes are unleashed by a variety of cells, including but not limiting to reticulocytes [27], platelets [7], dendritic cells [20] and cancer cells [6, 28]. Due to this fact, exosomes are naturally found in a variety of body fluids like blood [29], saliva [30, 31], urine [32] and amniotic fluid [33]. They are secreted by donor cells and often reach specific sets of recipient cells via fusion with the plasma membrane or via endocytosis [34]. An important role in cell-cell communication is postulated for these secreted vesicles [35], which will be further

1. Introduction

introduced and evaluated in chapter 1.5.

Recent studies focussed on the lipid analysis of exosomes. When comparing the plasma membrane with secreted vesicles an enrichment of sphingomyelin, phosphatidylserine and cholesterol was detected in exosomes [36]. A first description of exosomes carrying RNA was made in 2007, while in recent years numerous groups have analysed the presence of nucleic acids in more detail [28, 32, 37]. Most of these studies describe the small RNA and mRNA content of EVs, while a few workgroups focus on rRNA [38]. However, the rRNA content of exosomes is controversially discussed, since in 2013 a comparison of RNA sizes in apoptotic bodies, MV and exosomes indicated, that the presence of rRNA was limited to apoptotic bodies and large MVs populations. The small RNA content of exosomes seems to be different compared to intracellular small RNAs, which suggests a controlled import mechanism of RNAs into exosomes [6, 39]. In 2013 Villarroya-Beltri described sequence motifs, that were specific for exosomal miRNAs, as was evaluated by micro array analysis [40]. However, up to now the underlying mechanism is not completely understood and needs further investigations.

In accordance with intracellular formation, all proteins and small RNAs can be found inside the cell as well. However, as a result of specific transport- and synthesis steps, which are not fully clarified yet, specific proteins, but also lipids and RNAs as described above, are enriched in exosomes. In the last few years exosomal marker proteins like tetraspanins (CD9, CD63 and CD81) or proteins which are involved in the biosynthesis of MVBs, for example Tumor susceptibility Gene 101 (TSG101) or ALG2 interacting protein (Alix), were discovered [41-43]. CD9, CD63 and CD81 belong to the tetraspanin superfamily [44-46], which is characterized by four transmembrane regions and two exposed extracellular loops [47]. CD9 is involved in cell motility, adhesion, fusion [48] and the loss of CD9 expression leads to tumor progression and metastasis in several types of cancer [49-51]. Furthermore, CD9, CD63 and CD81 are expressed on the mammalian oocyte surface and an essential role of CD9 for sperm-egg fusion was identified [52]. Miyados *et al.* showed that CD9 containing vesicles induce fusion between sperm and eggs *in vitro*, a finding that delivered first insight into gamete fusion (and other membrane fusion) events [53]. TSG101 and Alix are soluble cytoplasmic components of the “endosomal sorting complex required for transport” (ESCRT) machinery, which is required for Multivesicular Body (MVB) formation and cargo sorting into intraluminal vesicles (ILV) [54].

1. Introduction

Both ESCRT complexes and tetraspanins play major roles during exosome assembly from intraluminal membranes [41]. Tetraspanins consist of four transmembrane helices and have the capacity to interact with surface receptors or signalling molecules, forming tetraspanin-enriched microdomains (TEMs) that play an important role in EV biogenesis and EV release [22]. Furthermore, exosomes contain cell specific proteins, for example exosomes deriving from antigen presenting cells contain MHC I and MHC II molecules [55], whereas exosomes from reticulocytes harbour transferrin receptors [27] and exosomes from T-lymphocytes include CD3 in their membrane [56]. Since there is no exclusively exosomal marker protein known so far, these differential expression of proteins can be used to identify exosomes from different sources, for example in blood plasma. A schematic drawing of an exosome and its major components is depicted in Figure 3.

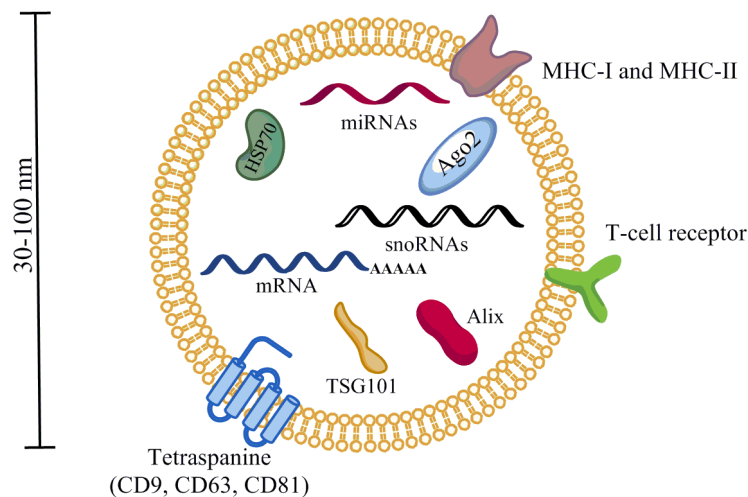


Figure 3: Schematic representation of exosome composition. Exosomes are defined as 30-100 nm sized extracellular vesicles of endocytic origin. They contain enriched proteins like tetraspanins (CD9, CD63 or CD81) or proteins of the ESCRT machinery (for example TSG101 and Alix). Besides proteins small RNAs (miRNAs, snoRNAs) and mRNAs are present inside these extracellular vesicles. However, the transport route of small RNAs and mRNAs remains elusive at the current stage.

In summary, exosomes show distinct lipid, RNA and protein profiles that allow differentiation from secreting cells and other EVs like AB or MVs. According to these observations an important role in cell-cell communication is postulated for exosomes, which will be further evaluated in the chapter 1.5 [57].

1. Introduction

1.3 Methods of extracellular vesicle isolation

The research on extracellular vesicles has recently emerged because of the potential for exosomes to be used as biomarkers in diagnosis of diseases. However, the isolation of EVs is still challenging, time consuming and hard to adapt to clinical practice [58]. A lot of investigation effort was invested to isolate exosomes with high purity and quantity. Especially for clinical applications it is important to have an efficient, quick, reliable and economic workflow for exosome isolation, since highly complex biological fluids with limited amounts like plasma are mainly used. Exosomes can be isolated by their size, density, protein content or biochemical properties. Ultracentrifugation is the most commonly used technique for exosome isolation [59]. This method involves different centrifugation steps to remove cells, cell debris and bigger microvesicles. A final centrifugation step at high g-forces (≥ 100.000 xg) is performed to collect exosomes, which can be washed and centrifuged one more time to increase purity [32, 60]. An alternative method, which is often used for exosome isolation, is based on precipitation by polyethylene glycol (PEG) [61]. PEG is a nontoxic synthetic polymer which is capable of sterically excluding proteins from the solvent until the concentration of protein is very high and the solubility exceeded, which in turn leads to precipitation of e.g. exosomes [62]. Some commercially available kits use this technique to isolate exosomes, for example ExoQuick TC (System Bioscience) [63]. Moreover, exosomes can be isolated by their density (for exosomes between 1.08 and 1.21 g/mL) [55, 64]. Optiprep (Iodixanol) or sucrose gradients combined with a centrifugation step separate these extracellular vesicles from bigger microvesicles and extracellular proteins. In recent years many workgroups focused on subpopulations of exosomes, which cannot be analysed by the methods explained so far. Subtypes of exosomes share the same size and density, while cargo content and receptor molecules differ among subtypes. Isolation of exosomes by immunoisolation, implying magnetic beads, allows the isolation of specific exosome subgroups, which expose the desired overrepresented membrane protein [65]. Immunoisolation has been performed e.g. for MHCII containing exosomes from antigen presenting cells [66] or Her2-positive exosomes derived from breast adenocarcinoma cell lines [67].

1. Introduction

In summary, none of this method combines high purity and yield, is low time consuming and allows the study of exosome subgroups. In recent years great efforts were made to develop new technologies for vesicle isolation. Nevertheless, no common isolation protocol for exosomes, that would match the above mentioned features, is available yet.

1.4 Biogenesis of miRNAs and RNA interference (RNAi)

MiRNAs are 20-23 nt long, highly conserved non-protein coding RNA molecules. They are involved in regulation of gene expression by inhibiting translation or initiating degeneration of mRNA transcripts in a process called RNA interference (RNAi). RNAi was discovered in 1986, when Ecker *et al.* observed transcriptional inhibition by expressing antisense RNA in transgenic plants [68]. By overexpression of chalcone synthase, a key enzyme for pigmentation in plants, they wanted to darken the color of the flower. However, after overexpression they observed white instead of dark flowers due to an increased rate of mRNA degradation, which was the first observation of the RNAi mechanism [69]. In 1998 Mello and Fire reported a gene silencing effect upon injection of double stranded RNA into *C. elegans*, whereas an injection of mRNA or antisense RNA showed no outcomes on gene expression [70]. They called this phenomenon RNAi and received the Nobel Prize for this discovery in 2006. Only a few years later the first endogenous miRNAs were discovered, lin-4 in *C.elegans* [71]. In the past 20 years over 1500 miRNAs were annotated in the human genome, collected in an open available miRNA database (miRBase) [72]. The miRNA biogenesis and the RNAi pathway are summarized in Figure 4.

1. Introduction

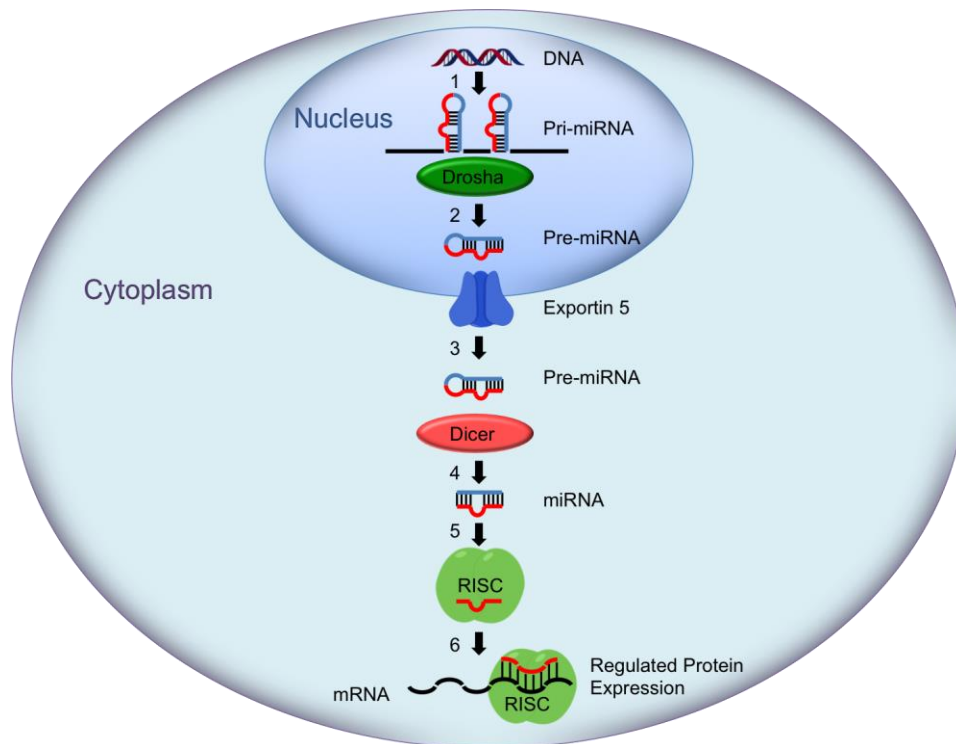


Figure 4: MiRNA biogenesis and function. MiRNAs, located in intronic regions of protein coding genes or as independent genes, are transcribed inside the nucleus by RNA polymerase II. After transcription Drosha further processes pri-miRNAs into small precursor hairpin miRNAs, also called pre-miRNAs. These are exported via Exportin 5 into the cytoplasm and further processed by Dicer, which recognized the hairpin structure of pre-miRNAs, yielding a double stranded mature miRNA. Following processing, one strand of the mature miRNA (guide) is incorporated into a miRNA-induced-silencing complex (RISC), while the other strand (passenger) is released and degraded. The miRNA/RISC complex binds to messenger RNA and stops transcription or leads to degradation of the transcript.

MiRNAs are located in introns of protein coding genes (miRtrons) or hold independent gene locations [73]. They are transcribed via polymerase II inside the nucleus and fold into hairpin structures [74]. These pri-miRNAs act as substrates for Drosha, a protein of the RNase III family, which cleaves the primary miRNA transcript (pri-miRNA) into 70 nucleotides long precursor-miRNAs (pre-miRNAs). These single stranded RNAs are exported via Exportin-5 into the cytoplasm and further processed by the bidentate endonuclease Dicer, which recognizes and removes the hairpin structure [75]. Dicer, also an RNase III enzyme, cleaves the exported pre-miRNA into 20-23 bp long double stranded mature miRNAs commonly with 2nt 3'-overhangs. Afterwards, the guide strand is incorporated into the miRNA-induced-silencing-complex (RISC), while the passenger strand is degraded. This RNA/protein complex binds complementary mRNA to stop the translation process by preventing the binding of the 60S ribosomal subunit or the eukaryotic translation initiation factor (eIF). Furthermore, the RISC complex can lead to degradation by directing an endonuclease, which belongs to the

1. Introduction

Ago family, to cleave messenger RNA [76-78]. The loading of miRNAs into EVs remains elusive at this point. Since proteins of the RISC machinery are found in exosomes (for example Ago2), recent studies suggest a possible interaction of these proteins with the ESCRT machinery leading to a direct loading into ILV in MVBs [79, 80]. The RNAi pathway combined with exosomal release is summarized in Figure 5.

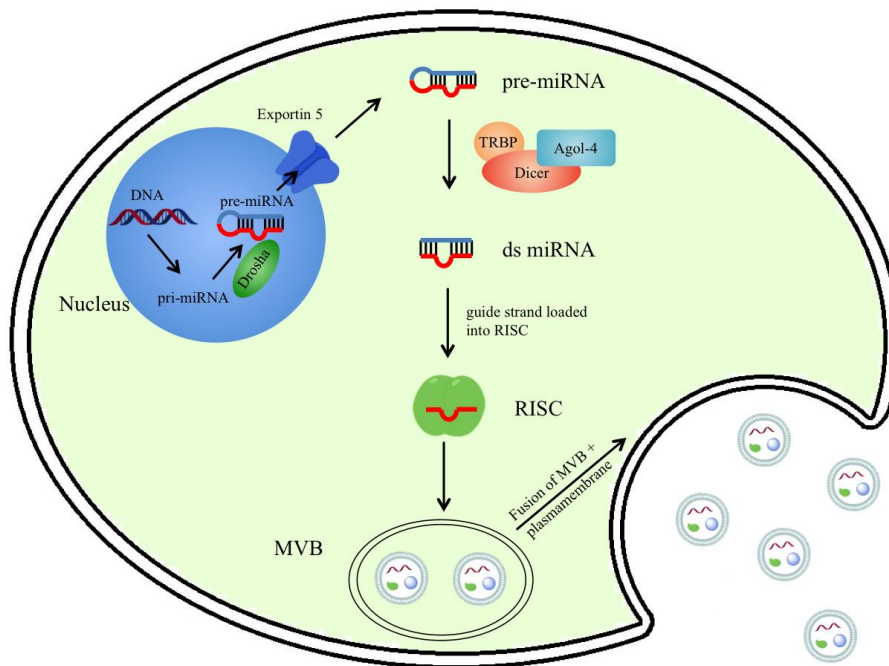


Figure 5: RNAi pathway and exosome biogenesis. All miRNAs are transcribed in the nucleus by polymerase II. After processing by Drosha pre-miRNAs are exported via Exportin 5 into the cytoplasm, where Dicer recognizes the loop structure. Further processing results in double stranded miRNAs, which are loaded into the RISC complex. They can regulate gene expression inside the cell by degradation of miRNAs or by inhibiting the translation process. However, miRNAs can be loaded into MVBs. This process is so far poorly understood. MVBs further fuse with the plasma membrane and internal vesicles are released into the extracellular space, where they are called exosomes.

In 2015 an hnRNPA2B1 dependent loading of miRNAs into EVs was discovered [40]. HnRNPs are ubiquitously expressed ribonucleoproteins that control the transport of HIV genomic RNA, e.g. in HeLa cells [81], and are involved in transport processes of specific mRNA in neurons [82]. They recognize specific EXO-motifs (GGAG) in small RNAs and provoke the loading into EVs. Furthermore, it was shown, that hnRNPA2B1 is sumoylated and this post-transcriptional modification is important for the loading process. However, the regulation of this process and interaction partners of hnRNPA2B1 are not known respectively not fully understood yet.

1. Introduction

1.5 Cell-cell communication via extracellular vesicles

First described in 1983 by Stahl and Johnstone, a key finding in interpreting the role of exosomes was made in 2007, when Valadi and co-workers discovered miRNAs and mRNAs as a cargo [37, 83]. The concept of EVs in intracellular communication implies a secretion of EVs by sending cells, a specific interaction and uptake of these vesicles by a recipient cell and a release of functional miRNAs or other signalling molecules to induce changes in gene expression (Figure 6).

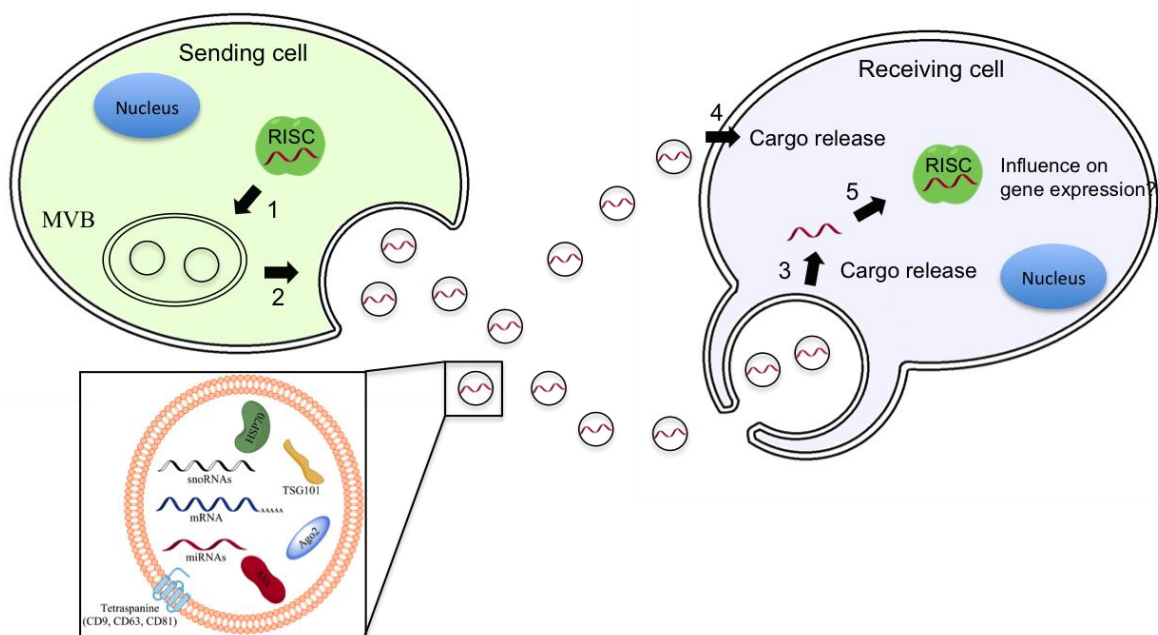


Figure 6: Cell-cell communication by exosomes. MiRNAs are loaded into MVB (1), which fuse with the plasma membrane of the sending cell (2). Exosomes can reach specific target cells by endocytosis (3) or fusion with the plasma membrane (4). In both cases the cargo (e.g. miRNAs) is released. Functionality of transferred miRNAs requires loading into RISC complex to influence the gene expression of the target cell and complete cell-cell communication.

Indeed, EVs were shown to be involved in routes of cell-cell communication beyond peptides or small molecules and with both endocrine and paracrine effects [35, 84-86]. After their release, exosomes can enter the target cell by either fusion with the plasma membrane or endocytosis. In both cases the content of exosomes including small RNAs will be disposed into the cytosol of the recipient cell [34, 87]. Recent studies showed a transfer of exosomes from oligodendrocytes to microglia cells and a fusion of these vesicles through macropinocytosis [88], while Fruhbeis *et al.* described a endocytosis dependent uptake

1. Introduction

mechanism in neurons [89]. However, the fusion of exosomes with their target cell, the release of small RNAs and the gene regulatory functions of these npcRNAs is still poorly understood and requires more analysis and examinations.

Besides their proven qualification as diagnostic tool for certain cancers, the exosome's potential to deliver functional RNAs implies putative clinical relevance, e.g. in immune system regulation or gene therapy [90]. One important part of our immune system are T-lymphocytes, which functions include elimination of viral, bacterial or parasitic infections through recognition of antigens by the T-cell receptor. The T-cell receptor recognizes specific antigenic peptides bound to MHC molecules on antigen presenting cells (like dendritic cells or B-cells). This T-cell mediated immunity is a central element of the adaptive immune response. Two important classes of T-lymphocytes are T helper cells (T_H cells, $CD4^+$) and cytotoxic T-cells (T_C cells, $CD8^+$). $CD4$ positive T-cells recognize peptide antigens on MHCII molecules presented by antigen-presenting cells (APCs). Upon presentation of antigens T_H cells get activated and secrete cytokines, assisting the active immune response. Cytotoxic T-cells recognize virus-infected or tumor-cells by binding to antigen-peptides presented in MHCI molecules. Recently, the role of exosomes influencing this process has been highlighted and exosomes were shown to affect the antigen presentation or to induce immune activation or suppression [91, 92]. In 2011, Mittelbrunn *et al.* identified a unidirectional transfer of miRNA loaded exosomes from T-cells to antigen presenting cells [35]. This exosomal transfer of regulatory small RNAs delivers new insight into the orchestration of gene expression and the cell-cell communication within the immune system.

1.6 Gene delivery via lentiviruses or virus-like particles (VLPs)

To study exosomes in more detail an efficient manipulation of cancer or recipient cells is required, which can be achieved by lentiviruses (LVs) or virus like particles (VLPs). Lentiviruses belong to the retroviridae family and have a diploid, positive strand RNA genome, which is reversely transcribed and integrated into the host genome [93]. Since the viral genome can both integrate in dividing and non-dividing cells, in particular HIV-1 based LVs became a widespread tool for gene delivery applications [94]. During the last years, lentiviral vectors were improved and optimized in regard of safety. The third and recent

1. Introduction

generation of vectors utilizes replication deficient viruses that only require three HIV-1 genes from the original genome (i.e. gag, pol and rev) [95, 96]. Another beneficial feature of LVs is the possibility of pseudotyping, a manipulation of the exposed viral surface that enables adaptations of the natural tropism by expressing foreign viral glycoproteins on its envelope. One prominent example is the vesicular stomatitis virus glycoprotein (VSVG), which facilitates LV-transduction in a wide range of cells from many different vertebrate species. In particular HIV-1 based LVs with VSVG, instead of the original HIV-GP120/GP41, have extensively been used *in vitro* and *in vivo* [97-100]. In order to create LV vectors with a high selectivity for target cells, immense efforts have successfully been devoted to engineer specific ligands, peptides or single chain antibodies that upon expression on the virus-surface would allow recognition of addressable target-cell markers. [101-109] Taken together with high GOI loading capacities of up to 10 kb, options such as integrating or non-integrating LV vectors and the high *in vitro* and *in vivo* expression levels, LVs are seen as a promising tool for research and gene therapy.

Besides LVs our workgroup established virus-like particles as a gene delivery tool for the transduction of target cells, which cannot be reached by normal transfection methods. The human polyoma JC virus (JCV) is a non-enveloped virus with 5 kb double stranded DNA genome [110]. The capsid contains a major capsid protein VP1 forming pentameric capsomers and in addition 30-60 molecules of the minor capsid proteins VP2 and VP3. However, VP1 alone is able to form viral capsids, which can be loaded *in vitro* with small DNA or RNA molecules [111, 112]. This is achieved by a specific disassembly/reassembly treatment in which the incorporation of nucleic acids occurs [113]. By removing divalent calcium ions through dialysis the VP1-VLP structure is destabilized and dissociated into VP1-pentamers. Reassociation of this pentamers by addition of calcium ions in presence of nucleic acids leads to an incorporation of this cargo inside the VP1-capsids.

The native tropism of JCV is defined by several flexible loops of the major capsid protein VP1, which bind to lactoseries tetrasaccharide c (LSTc) residues on the target cell surface [114]. After LSTc binding the 5-HT serotonin receptor is recruited and enables the cellular entry by a clathrin dependent mechanism [115].

Both virus tools (LVs and VLPs) enable an efficient transduction of recipient cells, which cannot be manipulated easily by common or commercially available methods. In figure 7 LVs are compared to exosomes and VLPs regarding size, protein and nucleic acid content

1. Introduction

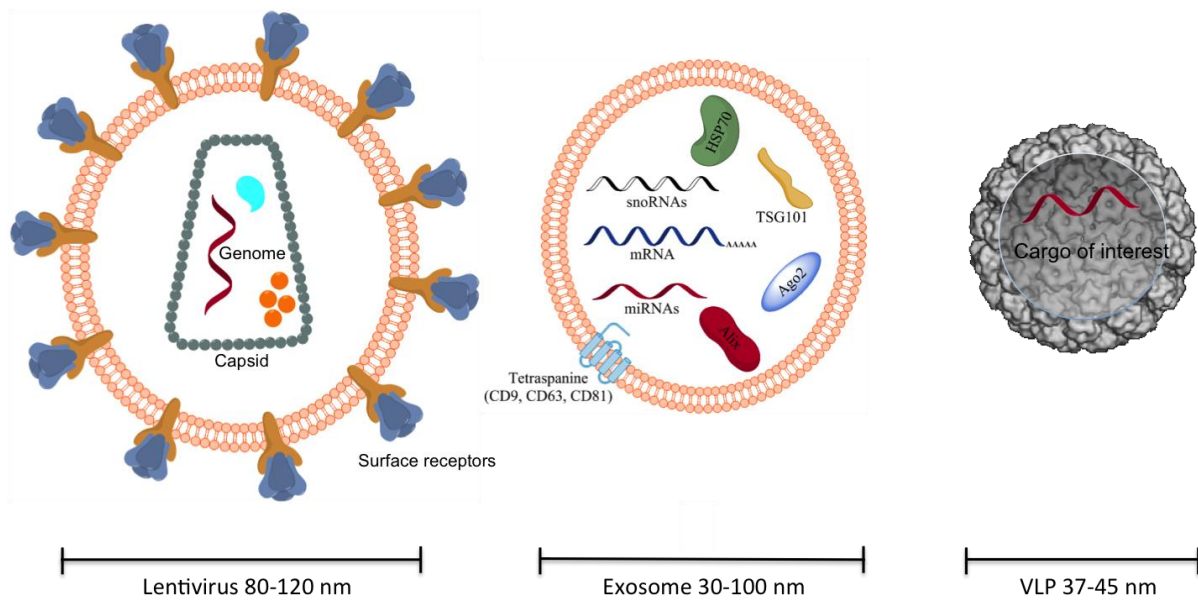


Figure 7: Comparison of lentiviruses, exosomes and virus-like particles. LVs are 80-120 nm in size and contain capsid proteins, viral genome and polymerase. These viruses are surrounded by a lipid bilayer containing receptor molecules like VSV-G. In contrast to LVs exosomes are smaller (30-100 nm) and contain RNA molecules of the host cell like snoRNAs, miRNAs and mRNAs. Furthermore, exosomes include proteins of the ESCRT machinery (TSG101 and Alix) and are as LVs surrounded by a lipid bilayer including membrane proteins like tetraspanins. Compared to LVs and exosomes VLPs contain no lipid bilayer. Their capsid (37-45 nm) consists of VP1-protein and can be filled with a cargo of interest.

As described above, lentiviruses are membranous enclosed viruses with a diameter of 80 - 120 nm. They contain a RNA genome and different proteins for reproduction and infection of target cells surrounded by capsid proteins. These proteins are enclosed by a lipid bilayer membrane containing surface receptor molecules like VSV-G. Exosomes are 30 – 100 nm sized extracellular vesicles and show similarities compared to LVs, like the lipid bilayer membrane. Exosomes contain furthermore small RNAs and mRNAs as well proteins from the ESCRT machinery like TSG101 and Alix, but also membrane proteins originally derived from the plasma membrane of the sending cell. Also the biogenesis routes of LV assembly and exosome formation are extremely similar [116]. On the other hand, VLPs are surrounded by a protein capsid. They contain no lipid bilayer and carry no genetic information, if not deliberate added as gene of interest. VLPs have a size of 37-45 nm and are the smallest gene delivery tool compared to LVs and exosomes.

1. Introduction

1.7 Aim of thesis

In the past couple of years, extracellular vesicles (EVs), mainly exosomes, have gained interest as a major research-objective. For clinical applications of exosomes a fast isolation method yielding high amounts and purity of extracellular vesicles is needed. One aim of this thesis was to isolate extracellular vesicles by three different isolation techniques and compare the amount and size profiles. Therefore, we checked the size distribution and amounts of EVs by Nanoparticle Tracking Analysis (NTA), identified exosomal proteins by western blot and analysed them by electron microscopy.

Up to now, the sorting mechanism of miRNAs into exosomes is poorly understood. To clarify this unanswered mechanism we wanted to characterize the exosomal small RNA profile of four human cell lines by next generation sequencing. We compared intracellular and exosomal small RNA candidates and tried to discover cell specific small RNA patterns and sequence motifs.

Additionally, we aimed to analyze the influence of three exosomal marker proteins on EV production and size distribution and wanted to address the fusion of exosomes with target cells by one of these proteins.

Moreover, we hypothesized a role of exosomes in cell-cell communication via a transfer of small RNAs. A discovery of secretion motif may be useful for an artificial loading of miRNAs into exosomes that opens the possibility to use engineered exosomes for gene therapy. We wanted to evaluate if exosomes can fuse with specific target cells by transwell experiments and test the functionality of transferred small RNAs by qPCR or UTA system. For the use of clinical engineered exosomes a specific modification of target cells is inevitable but, up to now, hard to achieve. To overcome this issue we wanted to use VLPs to specific modify osteoblasts in an *in vivo* rat model in cooperation with the UMG. Therefore, target specific RANKL siRNAs should be loaded into VLPs, injected into rats and the gene expression of RANKL should be analyzed by qPCR.

Taken together, the aim of this thesis should clarify the unanswered questions in the exosome field like cellular and exosomal profiles, sequence motifs, fusion with target cell and their role in cell-cell communication. The future goal of exosome research has to be the clinical application and usage as biomarkers, which should be supported by the results of this thesis.

2. Materials & Methods

2.1 Molecular biology

2.1.1 *Escherichia coli* transformation, cultivation and plasmid isolation

E. coli Top10 or Stbl3 strains were cultivated at 37 °C either on LB-plates or in LB-media at 180 rpm. Transformation was performed as described by Inoue *et al.* [117]. Positive transformed clones were selected by choosing the required antibiotic.

Table 1: Antibiotic concentrations for bacteria selection

Antibiotic	Concentration	Company
Ampicillin	100 µg/mL (H ₂ O)	Carl Roth, Germany (K029.2)
Kanamycin	50 µg/mL (H ₂ O)	Applichem, Germany (A1493)
Chloramphenicol	34 µg/mL (Ethanol)	Applichem, Germany (A1806)

For plasmid isolation 5 mL of LB-medium containing the desired clone was incubated over night at 37 °C at 180 rpm. Cells were centrifuged at 2000 xg and plasmid preparation was performed by QIAprep Spin Miniprep Kit according to manufactures condition (Qiagen, Germany). Purified plasmids were measured by Synergy2 System and stored at -20°C.

2.1.2 DNA separation by Agarose Gel Electrophoresis

For separation and size determination of DNA constructs 1% Agarose (w/v) was used. Therefore the desired DNA was mixed with loading dye (Thermo Fischer, MA, USA), while GeneRuler DNA-ladder (Thermo Fischer, MA, USA) served as size standard. Size separation was performed at 120 V for 30 min using 1x TAE buffer.

2.1.3 Polymerase chain reaction

Amplification of specific DNA fragments was achieved by polymerase chain reaction using Taq (BiothermTM, Germany) or Phusion polymerase (New England Biolabs, MA, USA). PCR reactions were performed in a total volume of 20 µL by adding the components described in table 2.

2. Materials & Methods

Table 2: Pipetting scheme for polymerase chain reaction

Volume	Component
X μ L (100ng)	DNA
1 μ L	Forward Primer (10 μ M)
1 μ L	Reverse Primer (10 μ M)
0,4 μ L	dNTPs (10 mM)
0,2 μ L	Polymerase
4 μ L	Reaction buffer (5x)
Ad to 20 μ l total volume	Water

PCR conditions were determined according to product length, GC content and melting temperature of used oligonucleotides. A standard protocol is provided in table 3.

Table 3: Standard protocol for PCR amplification

Step	Description	Time and Temperature
1	Initial denaturation	10 min at 95 °C
2	Denaturation	10 sec at 95 °C
3	Annealing	30 sec at 50-60 °C
4	Amplification	30 sec/kb at 72 °C
5	Final amplification	10 min at 72 °C

Steps 2-4 were repeated 30 times and after completion the reaction was stored at 4 °C.

2.1.4 Gel purification

PCR products were separated by agarose gel electrophoreses as described in 2.1.2. Size separated products were analysed under UV light and desired product was cutted. Excised DNA was purified by QIAquick Gel extraction Kit (Qiagen, Germany) according to manufactures condition. After purification DNA was analysed by Synergy 2 System (Biotek, Winooski, USA) to analyse concentration and salt contamination. Purified DNA was stored at -20 °C until use.

2. Materials & Methods

2.1.5 Ligation of two DNA fragments

For DNA ligation the following reaction was prepared on ice:

Table 4: Pipetting scheme for DNA ligation

Component	Volume
T4 DNA Ligase Buffer (10x)	2 μ L
T4 DNA Ligase	1 μ L
Vector DNA (4kb)	50 ng
Insert DNA (1 kb)	37.5 ng
Nuclease free water	Fill to 20 μ L

The molar ration of vector to insert was kept at 1:3. Reaction was gently mixed and incubated at 16 °C for 1 h. Enzyme was heat inactivated at 65 °C.

2.1.6 Transformation of bacteria

For transformation chemically competent E. coli were thawed on ice. For each transformation 50 μ L of E.coli and 1-5 μ L DNA were mixed and incubated for 30 min on ice. Afterwards mixture was heated up to 42 °C for 30 sec and immediately cooled down on ice. 250 μ L of prewarmed SOC medium was added and samples were incubated for 1 h at 37 °C. LB agar plates were prepared and 20-200 μ l was spread carefully. Plates were incubated at 37 °C overnight. On the next day colonies were selected and analysed by plasmid isolation, PCR or sequencing. Positive clones were stored at -80 °C in 12 % Glycerol

2.1.7 Restriction digestion of DNA

In order to confirm the insert and vector backbone a restriction digestion was performed. 5 μ g of examined plasmids were incubated with 5 units of restriction enzyme. A total volume of 20 μ L was incubated for 1 h at desired temperature and 10 μ L of this solution was separated by agarose gel electrophoresis. Restriction pattern were analysed after ethidiumbromid stain via Gel IX 20 Gel documentation system (INTAS, Germany).

2. Materials & Methods

2.1.8 Isolation of extracellular vesicles

For exosome isolation cells were seeded in 6 wells (200.000 cells/well) and cultivated three days in exosome free media (FCS was ultracentrifuged at 100.000 xg for at least 16 h). Supernatant was differential centrifuged (500 xg 5 min, 2000 xg 30 min), filtered (450 nm, Sartorius, Germany), mixed with PEG solution (1:5 PEG8000 in PBS) and incubated at 4 °C. After 16 h supernatant was centrifuged at 1500 xg for 30 min and the vesicle containing pellet resuspended in 200 µL PBS. For differential ultracentrifugation 40 mL of sequential centrifuged and filtered SN (500 xg 5 min, 2000 xg 30 min, 450 nm filter, Sartorius, Germany) were centrifuged at 10.000 xg for 2 h to remove bigger vesicles like apoptotic bodies or large microvesicles. At 100.000 xg exosome were pelleted and the pellet was washed once with PBS followed by another 100.000 xg step. The resulting pellet was resuspended in 100 µL PBS and stored at 4°C for further analysis. In contrast to the differential ultracentrifugation protocol 35 mL of differential centrifuged and filtered SN (500 xg 5 min, 2000 xg 30 min, 450 nm filter, Sartorius, Germany) was centrifuged at 10.000 xg for 2 h. Afterwards 4 mL of sucrose (20 %) was overlaid with SN of the previous step and centrifuged at 100.000 xg for 2 h. The resulting pellet dissolved in 100 µL PBS and stored at 4 °C for further analysis.

2.1.9 Extracellular vesicle characterization by Nanoparticle Tracking Analysis

EVs were analysed by NanoSight LM10 instrument. Samples were diluted 1:100 in PBS and recorded in triplicates for 30 sec. Number of particles were calculated by NTA software 2.3 and illustrated by Graphpad Prism 6.

2.1.10 RNA Isolation, size and integrity detection and cDNA synthesis

Total RNA was isolated via Phenol/Chloroform extraction according to manufacture protocol (Trizol, Thermo Fisher Scientific, CA, USA). RNA was measured by Synergy system (BioTek, Winooski, USA), 1000ng of total RNA was reverse transcribed using Sensifast cDNA Synthesis Kit (Bioline, London, UK) and diluted (1:5 or 1:10). Alternatively RNA was measured on BioAnalyzer System (Agilent, CA, USA) via RNA 6000 Pico Kit (Agilent, CA, USA) and RNA amount, size distribution and RNA integrity number (RIN) was analysed.

2. Materials & Methods

2.1.11 Quantitative PCR analysis

After reverse transcription 25ng of cDNA was used for quantitative analysis on ABI StepOnePlus system (Applied Biosystems, CA, USA). For CD9, Alix and TSG101 synthesized primers (Sigma-Aldrich, St. Louis, Missouri, USA) (Table 5) and for DNMT1 and BCL2 designed primer sets (Genecopoeia, Maryland, USA) were used for target amplification. Relative expression was calculated via $\Delta\Delta C_T$ -method using $\beta 2M$ as housekeeping gene.

Table 5: Sequence information of qPCR primers

Primer	Sequence
hB2M-fwd	TGTGCTCGCGCTACTCTCTCT
hB2M rev	CGGATGGATGAAACCCAGACA
hCD9-fwd	ATGATGCTGGTGGGCTTC
hCD9-rev	GCTCATCCTTGGTTTTTCAGC
hTSG101-fwd	CAGAGCTCAATGCCTTGAAAC
hTSG101-rev	GAACTGAGTTCTTCATCCTTC
hAlix-fwd	CAATTGTGCAGCCTTAGCTAG
hAlix-rev	GTATCTGGAGATATGTCCACG

2.1.12 NGS library preparation

RNA was isolated as described in 2.1.10. Via BioAnalyzer System quality and quantity of total RNA was measured (BioAnalyzer RNA Pico Kit, Agilent, Santa Clara, USA). 2 μ g RNA was used for RNA purification with magnetic bead cleanup module (Life Technologies, Carlsbad, USA). Purified RNA was ligated with sequencing adapters, reverse transcribed and purified (Ion Total RNA-Seq Kit v2, Life Technologies, Carlsbad, USA). Finally barcodes were added and library size and amount was detected via BioAnalyzer HS Chip (Agilent, Santa Clara, USA).

2.1.13 Next generation sequencing and data analysis

Library was prepared according to 2.1.12, diluted (18pM) and clonal amplified by emulsion PCR on IonTorrent OneTouch System according to manufacturer's protocol (Ion PGM Template OT2 200 Kit (Life Technologies, Carlsbad, USA)). Purification of amplified library was performed on OneTouch ES System. Templated ISPs are loaded onto IonTorrent 316

2. Materials & Methods

Chip and sequenced via IonTorrent PGM System. Raw reads were trimmed and high quality reads mapped to miRBase21 or snoRNABase V3 [118]. Mapped reads were further analysed by own generated R-scripts using the DEseq package [119, 120].

2.1.14 Preparing samples for electron microscopy

Exosomes were isolated as described in 2.2.8. After PEG precipitation the exosome pellet dissolved in 50 μ L Paraformaldehyd (2%) and a negative stain was performed. Therefore a copper grid (mesh = 250) was exposed to UV light for 8 min. Afterwards the grid was incubated with the exosome sample for 10 minutes and washed four times with H₂O. At the end the grid was negative stained with Uranylacetat for 3 sec and dried overnight.

For visualizing cells in electron microscopy Raji cells were cultured as described in 2.2.1. Cells were pelleted at 500 xg for 5 min and pellet was fixated with glutaraldehyd (2.5 %). Cells were embedded automatically in Agar (2%) via Lynx System (Leica, Germany) and sliced in thin pieces (1 mm). Pieces were transferred into flat embedding forms and overlaid with Epon. Samples were hardened at 60 °C for 24 h and 24 h at 24 °C. Edges of the Epon blocks were minced with a milling machine (Leica, Germany) and semi-thin slices were produced on a microtome (Leica, Germany) with a thickness of around 500 nm. Slices were stained with methylenblau according to the Richardson method [121]. After detection of cell rich regions the slices were further processed at the ultramicrotome to generate thin slices (50 nm). Slices were teased on copper grids and negative stained via uranylacetat as described above.

2.1.15 Preparation of UTA constructs and sequence information

In order to analyse miRNA efficiencies the complementary sequences for desired miRNAs were cloned into pUTA2.0 vector (Figure 8). This vector was digested using *XhoI* and *NotI* for 2 h at 37 °C. DNA was separated via agarose gel electrophoresis and extracted using QIAquick Gel Extraction Kit (Qiagen, Germany). Desired oligonucleotides were ordered (Sigma, Germany, table 6), both strands (forward and reverse) incubated at 96 °C for 90 min and cooled down to 16 °C. Ligation with linearized pUTA 2.0 plasmid was performed at 16 °C for 2 h. Ligation reaction was transformed in E.coli and mini-preps were performed as described above

2. Materials & Methods

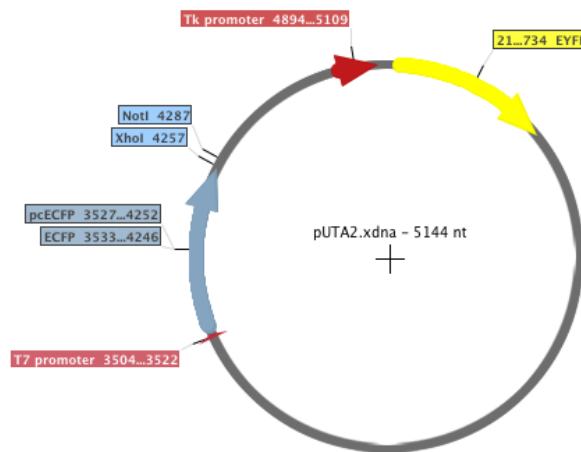


Figure 8: Generation of pUTA2.0 construct. The pUTA2.0 vector was digested with *XhoI* and *NotI* and purified by agarose electrophoresis. Full complementary miRNA target sites were ordered by Sigma. Linearized vector was ligated with complementary miRNA target sites listed in table 6.

Table 6: Generated plasmids for miRNA efficiency detection by the UTA system. Overhangs are highlighted in bold and capital letters and linker regions are marked in bold letters.

miRNA	Sequence
miR-451 F 3 copies	GGC Caaaccgttaccattactgagtt ccgga aaccgttaccattactgagtt ccgga aaccgttaccattactgagtt
miR-451 R 3 copies	TCGA aactcagtaatggtaacggtttccggaactcagtaatggtaacggtttccggaactcagtaatggtaacggttt
miR-15a-5p F 3 copies	GGCC tagcagcacataatggtttgtg ccggt tagcagcacataatggtttgtg ccggt tagcagcacataatggtttgtg
miR-15a-5p R 3 copies	TCGA cacaaaccattatgtgctgctac ccgg cacaaaccattatgtgctgctac ccgg cacaaaccattatgtgctgctac
miR-19b-3p F 3 copies	GGCC tgtgcaaatccatgcaaaactgac ccggt gtgcaaatccatgcaaaactgac ccggt gtgcaaatccatgcaaaactga
miR-19b-3p R 3 copies	TCGA tcagttttgatggattgacac ccggt tcagttttgatggattgacac ccggt tcagttttgatggattgacac
miR-21-5p F 3 copies	GGCC tagcttatcagactgatgttgac ccggt tagcttatcagactgatgttgac ccggt tagcttatcagactgatgttgac
miR-21-5p R 3 copies	TCGA tcaacatcagctctgataagctac ccggt tcaacatcagctctgataagctac ccggt tcaacatcagctctgataagctac
miR-148a-3p F 3 copies	GGCC tcagtgcactacagaactttgt ccggt tcagtgcactacagaactttgt ccggt tcagtgcactacagaactttgt
miR-148a-3p R 3 copies	TCGA acaaagttctgtagtgcactgac ccgg acaaagttctgtagtgcactgac ccgg acaaagttctgtagtgcactgac
miR-15a-5p F 3 copies	GGCC tagcagcacataatggtttgtg ccggt tagcagcacataatggtttgtg ccggt tagcagcacataatggtttgtg
miR-15a-5p R 3 copies	TCGA cacaaaccattatgtgctgctac ccgg cacaaaccattatgtgctgctac ccgg cacaaaccattatgtgctgctac

2. Materials & Methods

GL-2 F 3 copies	GGCC cacgtacgcggaataacttcgaa ccgg cacgtacgcggaataacttcgaa ccgg cacgtacgcggaataacttcgaa
GL-2 R 3 copies	TCGA tttcgaagtattccgcgtacgt ccgg tttcgaagtattccgcgtacgt ccgg tttcgaagtattccgcgtacgtg
Control 1 F	GGCC taaggctatgaagatac
Control 1 R	TCGA gtatctctcatagccta
Control 2 F	GGCC aattctccgaacgtgtcacgt
Control 2 R	TCGA acgtgacacgttcggagaatt

2.2 Cell biology

2.2.1 Cell culture

All cell lines were maintained according to manufacturing conditions at 37°C and 5% CO₂. HeLa, Raji, DG75 and Jurkat cells were cultured in RPMI (Roswell Park Memorial Institute) supplemented with 10% FCS and 1 % antibiotics (Penicillin and Streptomycin), whereas HEK293 and SW837 were maintained in DMEM (Dulbecco's modified Eagle's Medium) with 10% FCS and 1% antibiotics and SHSY-5Y were kept in DMEM with 15% FCS and 1% antibiotics.

2.2.2 Fluorescence microscopy

Fluorescence microscopy pictures were obtained by an Axio Observer microscope (Zeiss, Germany) using the filter set BP 525/50 for GFP and filter set BP 605/70 for RFP detection. Exposure time was set to 1000 msec for all fluorescence pictures.

2.2.3 Generation of lentiviral constructs

Fusion proteins were cloned from original plasmids (mEmerald-CD9-10, mCherry-hAlix and mCherry-Tsg101) into pENTR1a no CCDB. Gateway cloning with LR reaction was performed according to manufactures condition using pLENTI6.3/TO/V5-Dest as destination vector (Thermo Fisher Scientific, Woltham, MA, USA). Generated pLenti6.3-CD9_{GFP}, pLenti6.3-TSG101_{mCherry}, pLenti6.3-Alix_{mCherry} and pLemir-NS were used as GOI for LV production. Detailed information of used plasmids is provided in the appendix (9.5).

2. Materials & Methods

Table 7: Plasmids for LV generation with depositor and Addgene information

Plasmid	A gift from	Addgene number
pENTR1a no CCDB	Eric Campeau [122]	# 17398
mEmerald-CD9-10	Michael Davidson	# 54029
mCherry-hALIX	James Hurley [123]	# 21504
mCherry-TSG101	James Hurley [123]	# 21505
psPAX2	Didier Trono	# 12260
pLemir-NS	Jerry Crabtree [124]	# 32809
pLenti CMV GFP Neo	Eric Campeau [122]	#17447
pCMV-VSVG	Bob Weinberg [125]	#8454

2.2.4 Lentivirus production, concentration and titration

VSVG pseudotyped lentiviruses were generated in HEK293FT cells, whereas CD9 pseudotyped lentiviruses were produced in HEK293FT-CD9_{GFP} cells. Cells were seeded in 6-well plates at 1×10^6 cells/mL and directly transfected with according pLenti6.3 constructs for GOI delivery, psPAX2 for viral capsid proteins and pCMV-VSV-G and/or mEmerald-CD9-10 for viral envelope proteins. 16 h after transfection sodium butyrate containing media (0,01M) was added for 8 h. Afterwards media without sodium butyrate was used and collected every 24 h. After 5 days media was centrifuged 30 min at 2000 xg, filtered (450 nm) and concentrated via Vivaspin columns (100.000 MWCO, Sartorius, Germany).

2.2.5 Generation of stable CD9_{GFP}, Alix-mCherry and TSG101_{mCherry} cell lines

HEK293FT, HEK293, HeLa, SHSY-5Y, Jurkat and Raji cells were seeded in 24 well plates (50.000 cells/well) and after 24h infected with LV-VSVG-CD9_{GFP} carrying CD9_{GFP} and VSVG as envelope proteins and CD9_{GFP} as gene information. After 96h blasticidin containing media was added to cells (blasticidin concentration see table 8) and cells were selected for at least 14 days.

2. Materials & Methods

Table 8: Blastidicin concentration for selection of lentivirus transduced cell lines

Cell line	Blasticidin concentration
HEK293	5µg/mL
HEK293FT	5µg/mL
Raji	7,5µg/mL
Jurkat	3µg/mL
SHSY-5Y	5µg/mL
HeLa	3µg/mL

2.2.6 Primary cortical culture

For a co-cultivation of neurons and glia cells isolated cortices of E18 Wistar rats were prepared according to Shimada *et al.* and Fischbach with minor modifications [126, 127]. Their meninges were removed and they were cutted into small pieces in ice-cold dissection media (HBSS (Gibco, 14170-088) with 33 mM glucose (Roth, 6780.1) and 10 mM HEPES (Roth, HN78.3)). Tissue pieces were incubated in trypsin/EDTA (0.05/0.02%) (PAN Biotech, P10-023100) and afterwards washed with dissection media. The cells were singularized by trituration in DMEM (Gibco, 31966021) with 10% FCS (Gibco, 10500), 2 mM GlutaMAX (Gibco, 35050061), penicillin 10,000 U/mL and streptomycin 10 mg/mL (P06-07100, PAN Biotech), and filtered through a 100 µm cell strainer (Greiner Bio one, 542000). Using Trypan Blue (Roth, CN76.1) cells were counted and seeded in 24-well plates with PEI-treated (0.05% for 5h (Sigma, P3143)) glass cover slips. Cells were cultured at 37 °C with 5% CO₂ and a humidified atmosphere. After one day media was changed to neurobasal media (Gibco, 21103-049) with 2 mM GlutaMAX (Gibco, 35050061), penicillin 10,000 U/mL and streptomycin 10 mg/mL (P06-07100, PAN Biotech) and 2% B27 supplement (Gibco, 17504-044).

2.2.7 Immunohistochemistry and confocal microscopy

Cells were fixed with PFA (4% in PBS), permeabilized with Triton X-100 (0.2% in PBS) and blocked with BSA (5% in PBS). First antibody (NeuN, 1:500, Merck MAB377, Germany) was added over night and secondary antibody (goat anti mouse IgG/IgA/IgM Alexa Fluor 488, A-10667 Life Technologies, Carlsbad, USA) for 1h. Nuclei were stained with Hoechst 33342 (1:500 in PBS). Coverslips were mounted in Mowiol (12-15 µL) on glass slides and analysed on LSM 5 Pascal microscope (Zeiss, Germany).

2. Materials & Methods

2.2.8 Flow cytometry analysis (FACS)

Adherent cells were trypsinized by trypsin and centrifuged (300 xg, 5 min), for suspension cells this step was skipped. Cells were fixed with PFA (2% in PBS) for 30 min at 4 °C and washed three times with PBS (300 xg, 5 min). Fixed cells were analysed on BD LSR II system (BD, New Jersey, USA) using the PE 550LP- BP575/26 filterset for RFP and 505LP - BP530/30 filterset for GFP detection. Data was analysed by FACSdiva software and plots generated by Graphpad Prism 6.

2.2.9 Transfection of pUTA2.0 plasmids and data analysis

HEK293 cells were seeded in 24-well plates at a concentration of 100.000 cells/well. After 24 h the corresponding plasmid (Table 6) was transfected via Lipofectamine according to manufacturing conditions. Cells were incubated for 48 h and afterwards harvested and prepared for FACS analysis. For GL-2 exosome treatment HEK FT CD9 cells were transfected via Lipofectamine (1 µL Lipofectamine for 1000 ng DNA per 24 well with 50.000 cells). Supernatant was removed 48 h after transfection and transferred to HEK293 wildtype cells. After 30 min incubation cells were transfected with the corresponding pUTA plasmid (Control or GL-2) as described above. Fluorescence was detected 48h post transfection by flow cytometry using YFP (550LP and BP575/26) and CFP (550 LP and BP450/50) filtersets on BD LSR II instrument (BD, NJ, USA). Positive cells were selected using FACSdivaTM software and further analysed in R.

2.2.10 Virus like particle loading with DNA or RNA for *in vitro* use

JC polyoma VP1 protein was purified as described in 2.3.5. VLPs were disassembled in HEPES buffer (10 mM HEPES, 150 mM NaCl and 15 mM EGTA and DTT) at room temperature for 1 h. 25 µg VLPs were loaded with 500 ng linear DNA (CAG-GFP construct) or 2 µL of Cy3 modified siRNA (20 µM) and incubated for 30 min. Reassembly was performed in 5 L HEPES buffer containing CaCl₂ for capsid formation (10 mM HEPES, 150 mM NaCl and 1 mM CaCl₂ at 4 °C overnight. On the next day VLPs were added to human B-lymphocytes (Raji) and gene expression or red fluorescence was observed after 24-48 h via fluorescence microscopy.

2. Materials & Methods

Raji cells transduced by Cy3 siRNA loaded VLPs were transferred into transwells (Corning, NY, USA) for cocultivation with SW837 cells. Red fluorescence for SW837 was observed after 48 h to confirm vesicle transfer between this two cell lines.

2.2.11 Virus like particle loading with NanoGold particles

NanoGold solution was provided by Andrea Knauer (TU Ilmenau). 500 μ L of NanoGold stock solution (80 nM) was washed three times (21.000 xg, 15 min) with water to remove benzyldimethyl-hexadecylammonium chloride (BDAC) ligand. After wash steps the pellet was resuspended in 160 μ L nuclease free H₂O, particles were mixed with 160 μ L of thiol modified siRNA (6.25 μ M) and incubated for 2 h at room temperature at 750 rpm. After RNA hybridization the excess siRNA was removed by one wash step (13.000 xg for 15 min) and the pellet was resuspended in 80 μ L siRNA buffer (300 mM KCl, 30 mM HEPES-pH 7.5, 1.0 mM MgCl₂). UV/Vis spectra were measured on Synergy System to detect peak shift and confirm RNA hybridization [128]. Per 25 μ g VLPs 40 μ L of NanoGold-miRNA particles were used. VLPs were reassembled over night in HEPES buffer containing CaCl₂ as described above. Raji cells were treated with NanoGold loaded VLPs and Cy3 fluorescence was observed after 48 h via fluorescence microscopy. Furthermore, electron microscopy studies were performed 48 h post transduction.

siRNA	Sequence (5' \rightarrow 3')
Thiol modified miR-451a	5'-Thiol-C6-AAACCGUUACCAUUACUGAGUUU-3
Thiol and Cy3 modified miR-451a	5'-Thiol-C6-AAACCGUUACCAUUACUGAGUUU-Cy3-3

2.2.12 Virus like particle loading for *in vivo* use

For the *in vivo* use of VLPs 3 month old female Spraque-Dawley rats (Winkelmann, Germany) were used. All animal procedures were approved by the local Animal Care and Use Committee (permission number 33.9-42502-04-11/0560, district authorities of Oldenburg, Germany). All rats had approximately the same weight (289g \pm 18g) and were kept according to the german animal protection. For treatment the desired amount of VLPs were loaded as described in 2.2.10 with a ratio of 25 μ g VLPs per 7 μ L siRNA (20 μ M). SiRANKL (J-094995-09

2. Materials & Methods

and J-094995-10, GE Healthcare, UK) or control siRNA (D-001100-01, GE Healthcare, UK) were used. VLPS were injected i.p. and at the end of the experiment animals were euthanized under CO₂ anaesthesia and tibiae was removed for further analysis.

2.3 Protein biochemistry

2.3.1 Preparation of exosome or cellular samples for protein analysis

Cells were cultures in 24-well plates as mentioned above. Cell culture media was removed and 200 µL RIPA buffer was added and incubated for 5 min at room temperature. After mixing 5x up and down cell lysis was checked by microscopy and cell lysates were stored at -20 °C. Exosomes were isolated as described above with one exception. Resulting pellet at the end of the isolation procedure was dissolved in 100 µL RIPA buffer.

2.3.2 Determination of protein concentration

Before protein quantification exosomal and cellular samples were diluted 1:100 with water. Diluted protein lysate (3 µL) was mixed with Bradford reagent (297 µL) and incubated for 10 min at room temperature. Afterwards protein concentration was measured by Synergy 2 System (BioTek, VT, USA) at 595 nm. Standard curve (0 ng/µL, 200 ng/µL, 400 ng/µL, 600 ng/µL, 800 ng/µL and 1000 ng/µL) was used to calculate protein concentration.

2.3.3 Polyacrylamid gel electrophoresis

To separate proteins according to their size, sodium dodecyl sulfate (SDS-) gel electrophoresis was performed [129]. Gels were prepared in NovexTM cassettes by the following recipe.

2. Materials & Methods

Table 9: Recipe for separation gel

Component	Amount (10% gels)	Amount (12.5 % gels)
H ₂ O	2,5 mL	2.19 mL
40% Acrylamide/bis Acrylamid	1.25 mL	1.56 mL
1,5 M Tris, pH 8,8	1.25 mL	1.25 mL
10% ammonium persulfate (APS)	50 µL	50 µL
TEMED	5 µL	5 µL

Table 10: Stacking gel recipe

Component	Amount
H ₂ O	3.13 mL
40% Acrylamide/bis Acrylamid	0.62 mL
1,5 M Tris, pH 6,8	1.25 mL
10% ammoniumpersulfate (APS)	50 µL
TEMED	5 µL

After gel polymerization the prepared gel was inserted into electrophoresis chamber (Novex, Thermo Fischer, MA, USA) and the chamber was filled with 1x electrophoresis buffer. Samples were mixed with Laemmli buffer[130], incubated at 95 °C for 10 min and loaded onto the gel (10 µg total protein), while 3 µL Pageruler prestained Protein Ladder (Fermentas, MA, USA) or Magic Mark XP protein Ladder (Thermo Fischer, MA, USA) were used to detect size of proteins. Electrophoresis was performed at 35 mA for 1 h.

2.3.4 Western Blot

After size separation via SDS gel electrophoresis proteins were transferred on a nitrocellulose membrane. The gel and the membrane were assembled inside the XCell II Blot Module (Thermo Fischer, MA, USA) surrounded by 2 Whatman paper and 2 sponges soaked in transfer buffer. After 1 h transfer with 25 V the membrane was stained with Panceau to evaluate successful transfer or directly blocked with NETT-G buffer for 1h at room temperature. Afterwards membrane was incubated with primary antibody (1:1000 in NETT-G) over night at 4 °C. After three washes with TBS-T membrane was incubated with HRP coupled secondary antibody (1:10.000 in TBS-T) for 2h at room temperature. Membrane was washed three times with TBS-T and HRP substrate (Luminata Forte, Merck,

2. Materials & Methods

Germany) was added. The chemiluminescence signal was detected by ECL machine (Chemocam Imager, INTAS, Germany). Used antibodies are listed in table 11.

Table 11: Antibody information for Western Blot analysis

Antibody	Company	Description
Anti-CD9 (ab92726)	Abcam, UK	Rabbit monoclonal anti human
Anti-CD63 (10628D)	Thermo Fisher Scientific, CA, USA	Mouse monoclonal anti human
Anti-Alix (634502)	BioLegend CA, USA,	Mouse monoclonal anti human
Anti-rabbit (G-21234)	Life Technology, CA, USA	HRP labelled Goat anti human
Anti-mouse (G-21040)	Life Technology, CA, USA	HRP labelled Goat anti human
NeuN (MAB37)	Merck, Germany	Mouse monoclonal anti rat

2.3.5 VLP production and purification

The codon optimized JC VP1 DNA was ordered from GENEART for baculoviral expression. By BamHI/HindIII and SphI/NcoI the amplicon was transferred into pFBDM vector based expression system. Generation of VP1 gene containing baculovirus was performed as described elsewhere [131]. Expression of VP1 was performed in insect cells (High Five, Thermo Fischer, CA, USA) according to manufactures condition. Viral capsid supernatant was centrifuges for 30 min at 10.000 xg to remove cellular fragments. After filtration (0.45 µm filter) viral capsids were precipitated by poly ethylene glycol (7.5% (w/v) PEG8000) at room temperature. Precipitate was pelleted at 10.000 xg for 30 min and resuspended in HEPES buffer (20 mM HEPES, 150 mM NaCl, 15 mM EGTA and DTT, pH 7.4) for 2 h on a tumble shaker. Remaining precipitate was removed by a 21.000 xg centrifugation step for 30 min. VP1 particles remain in the supernatant, which is dialyzed (MWCO 6-8 kDa) over night at 4 °C against 5 L of HEPES buffer (20 mM HEPES, 150 mM NaCl, 1 mM CaCl₂, pH 7.4). Dialyzed supernatant was centrifuged at 21.000 xg for 30 min and purified by size exclusion chromatography (Sepharyl S-300 HR column using ÄKTA Avant system). Viral capsids eluted in the void volumne and were concentrated (30 kDa Vivaspin, Sartorius, Germany). Purified empty viral capsids were stored at -80 °C upon use.

2.4 Materials

2.4.1 Machines

Table 12: Used machines and manufacturer information

Machine	Model	Company
Balance	EG 620-3NM	Kern & Sohn GmbH, Germany
Chemiluminescence System	ChemoCam Imager	INTAS, Germany
Centrifuge	Heraeus Megafuge 8R	Thermo Fisher Scientific, MA, USA
Centrifuge	Heraeus Fresco21	Thermo Fisher Scientific, MA, USA
Centrifuge	Avanti J-30I	Beckman Coulter, CA, USA
E-Gel system	E-Gel iBase System	Life Technologies, CA, USA
Fluorometer	Qubit 2.0	Life Technologies, CA, USA
Freezer (-20°C)		Bosch, Germany
Freezer (-80°C)	MDF-DU500VH-PE	Panasonic, Japan
Freezer (-150°C)	ULT7150-9-D	Thermo Fisher Scientific, MA, USA
Flow Cytometer	LSR II Flow Cytometer	BD Bioscience, NJ, USA
Gel documentation system	Gel iX Imager	INTAS, Germany
Hamilton pipette	Microliter™ Syringes	Hamilton, NV, USA
Ice machine	ZBE 70-35	Ziegra, Germany
Incubator	Heracell VIOS 160i	Thermo Fisher Scientific, MA, USA
Incubator	IN75	Memmert, Germany
Incubator	Ecotron	Infors HT, Switzerland
Ion Torrent NGS	PGM	Life Technologies, CA, USA
Ion Torrent OneTouch2	OneTouch2™	Life Technologies, CA, USA
Ion Torrent OneTouch ES	OneTouch ES	Life Technologies, CA, USA
Microscope	Axio Vert. A1	Zeiss, Germany
PCR Thermocycler	Labcycler	Sensoquest, Germany
PCR Thermocycler	2720 Thermal cycler	Applied Biosystems, MA, USA
pH meter	SevenCompact™ S210	Mettler Toledo, OH, USA
Plate Reader	Synergy 2	BioTek, VT, USA
Platform Rocker	PMR-30	Grant bio, Cambridge, UK
Power supply	EV231	Consort bvba, Belgium
Rotor	JS-24.38	Beckman Coulter, CA, USA
Rotor	JA-30.50	Beckman Coulter, CA, USA

2. Materials & Methods

Safety Cabinet	Safe 2020	Thermo Fisher Scientific, MA, USA
Thermoblock	ThermoStat plus	Eppendorf, Germany
Thermoblock	CTM	HTA-BioTec, Germany
Vortexer	Vortex-Genie™ 2	Scientific Industries, NY, USA
Water bath	WNB10	Memmert, Germany
Western Blot chamber	XCell SureLock® MiniCell	Life Technologies, CA, USA

2.4.2 Buffers and Solutions

Table 13: Informations about buffers and solutions

Buffer and solutions	Recipe
Electrophoresis buffer (SDS-PAGE) (5x)	125 mM Tris 1,25 M Glycin 10 % SDS
Laemmli buffer	0,125 M Tris-HCl pH 6,8 4 % SDS 20 % Glycerol 10 % β -Mercaptoethanol 0,004 % Bromphenolblau
LB media	Yeast extract (5 g/L) Trypton (10 g/L) NaCl (5 g/L)
RIPA buffer	25 mM Tris-HCl pH 7,6 150 mM NaCl 1 % NP-40 1 % Natrium-Deoxycholat 0,1 % SDS
TAE buffer (Agarose gel electrophoreses)	40 mM Tris-HCl 20 mM acetic acid 1 mM EDTA adjust to pH 7,0
TBS	500 mM Tris 1,5 M NaCl adjust pH to 7,6
TBS-T	500 mM Tris 1,5 M NaCl 0,05 % Tween20
Western blot blockbuffer (NETT-G)	1 L NETT (1 x) 0,25 % Gelatine
Western blot transferbuffer	192 mM Tris 1,25 M Glycin 20 % Methanol

2. Materials & Methods

Western blot washbuffer (NETT, 10x)	1,5 M NaCl 0,05 M EDTA pH 8,0 0,5 M Tris-HCl pH 7,5 0,5 % Triton X-100
--	---

2.4.3 Chemicals and Materials

Table 14: Chemicals and Materials

Compounds	Provider Information
0,45 µm filter	Sigma Aldrich, MO, USA
1,4-Dithiothreitol	Carl Roth, Germany
24-well plate	Greiner, Germany
2-propanol	Merck-Millipore, Germany
6-well plate	Greiner, Germany
96-well plate	Greiner, Germany
Acetic acid	Carl Roth, Germany
Aceton	Carl Roth, Germany
Acrylamid (40%) Bis solution	Biorad Ca, USA
Acrylamid solution	Carl Roth, Germany
Agar-Agar	Carl Roth, Germany
Agarose	Biozym, Austria
Agarose (LE Agarose)	Carl Roth, Germany
Amidoblack 10B	Merck, Germany
Aminopropionic acid	Sigma Aldrich, MO, USA
Ammonium persulfate (APS)	Sigma Aldrich, MO, USA
Ammoniumchloride	Carl Roth, Germany
Ammoniumperoxodisulfat (APS)	Carl Roth, Germany
Ammoniumsulfate	Carl Roth, Germany
Ampicillin	Carl Roth, Germany
β-Mercaptoethanol	Carl Roth, Germany
Biotherm Taq	Genecraft, Germany
Biotherm Taq 10x buffer	Genecraft, Germany
Blasticidin S HCL (10mg/ml)	Gibco, CA, USA
Bordeaux Red	Sigma Aldrich, MO, USA
Boric acid	Sigma Aldrich, MO, USA
Bovine Serum albumin	Fluka, MO, USA
Brilliant Blue G	Sigma Aldrich, MO, USA
Bromphenol Sodium salt	Carl Roth, Germany
Calciumchloride (Cellpure)	Carl Roth, Germany

2. Materials & Methods

Casein Hydrolysate	Fluka, MO, USA
Chitosan	Sigma Aldrich, MO, USA
Chloramphenicol	Applichem, MO, USA
Chloroform	Merck Millipore, Germany
Complete Mini	Roche, Switzerland
Coomassie G250	Carl Roth, Germany
Coomassie R250	Carl Roth, Germany
Creatinin	Merck, Germany
Cryokonservation tubes	Sarstedt, Germany
d´NTPs	Sigma Aldrich, MO, USA
di Sodiumhydrogenphosphate	Carl Roth, Germany
Diethyl pyrocarbonate	Sigma Aldrich, MO, USA
Dimethylsulfoxid	Roth, Germany
diPotassiumhydrogenphosphate	Carl Roth, Germany
D-L-Lysine	Sigma Aldrich, MO, USA
DMSO	Carl Roth, Germany
dNTPs	Sigma Aldrich, MO, USA
D-Saccharose	Carl Roth, Germany
D-Sorbitol	Carl Roth, Germany
DTT	Carl Roth, Germany
EDTA	Applichem, MO, USA
EGTA	Sigma Aldrich, MO, USA
Ethanol	Merck-Millipore, Germany
Ethidiumbromide	Carl Roth, Germany
Epon	Serva, Germany
Falcontube 15 mL	Greiner Bio-One, Austria
Falcontube 50 mL	Greiner Bio-One, Austria
Fetal calf serum	Gibco, MA, USA
Gelatine	Sigma Aldrich, MO, USA
Geneticin	Gibco, CA, USA
Gentamycin	Carl Roth, Germany
Glas beads	Carl Roth, Germany
Glucose	Carl Roth, Germany
Glutardialdehyd 25%	Carl Roth, Germany
Glycerin	Carl Roth, Germany
Glycerol	Sigma Aldrich, MO, USA
Guanidinhydrochloride	Carl Roth, Germany
HCL solution	Merck-Millipore, Germany
HEPES	Carl Roth, Germany
HPLC-Wasser	Millipore-Merck, Germany
Hydrochloric acid(37%)	Carl Roth, Germany
Hydrogenperoxid Urea	Merck, Germany

2. Materials & Methods

Imidazol	Sigma Aldrich, MO, USA
IPTG	Carl Roth, Germany
Isopropanol	Carl Roth, Germany
Kanamycin	Applichem, MO, USA
L-Ascorbic acid	Sigma Aldrich, MO, USA
Lithiumchlorid	Carl Roth, Germany
Loading Dye (DNA)	Thermo Fischer, MA, USA
MagicMark™ XP Protein Marker	Invitrogen, CA, USA
Mealeic Acid	Sigma Aldrich, MO, USA
MES	Sigma Aldrich, MO, USA
Methanol	Carl Roth, Germany
Methyl cellulose	Sigma Aldrich, MO, USA
Methylenblue	Carl Roth, Germany
Milk powder	Carl Roth, Germany
MOPS	Carl Roth, Germany
Mowiol 4-88	Sigma Aldrich, MO, USA
Neomycin B	Carl Roth, Germany
Nickel (II)-Chloride hexahydrat	Carl Roth, Germany
Nitrocellulose membrane	Macherey-Nagel, Germany
Paraformaldehyd	Carl Roth, Germany
PBS-Dulbecco	PAA, MA, USA
PBS-Tabletten	Gibco, CA, USA
Penicillin/streptomycin	PAA, MA, USA
Pen-Strep	PAA, MA, USA
Petri dishes	Greiner Bio-one, Austria
PhenolRed	Carl Roth, Germany
Pipette tips 10µL	Eppendorf, Germany
Pipette tips 1000 µL	Eppendorf, Germany
Pipette tips 200 µL	Eppendorf, Germany
Poly(ethyleneimine) PEI solution	Sigma Aldrich, MO, USA
Polyethylenglycol 8000	Sigma Aldrich, MO, USA
Poly-L-Lysin	Sigma Aldrich, MO, USA
Ponceau Red	Sigma Aldrich, MO, USA
Potassium Hexacyanoferrat (III)	Carl Roth, Germany
Potassium hydroxyide	Carl Roth, Germany
Potassium sodium tartrate tetrahydrate	Sigma Aldrich, MO, USA
Potassiumchloride	Carl Roth, Germany
Potassium-di-Hydrogenphosphate	Carl Roth, Germany
Potassiumhydrogencarbonate	Carl Roth, Germany
Potassiumnitrate	Merck, Germany
Proteinase K	Qiagen, Germany
Puromycin Dihydrochloride	Gibco, MA, USA

2. Materials & Methods

Reaction tube 1,5 mL	Eppendorf, Germany
Reaction tube 2 mL	Eppendorf, Germany
RNA later solution	Ambion, MA, USA
RNase	Sigma Aldrich, MO, USA
Saccharose	Carl Roth , Germany
SDS-Pellets	Carl Roth, Germany
Serological pipette 10 mL	Sarstedt, Germany
Serological pipette 25 mL	Sarstedt, Germany
Serological pipette 5 mL	Sarstedt, Germany
Serva Blue R (Coomassie R250)	Serva
Shrimp alkaline phosphatase	Amersham, MA, USA
Sodium acetate	Carl Roth, Germany
Sodium butyrate	Sigma Aldrich, MO, USA
Sodium chloride	Carl Roth, Germany
Sodium hydroxid	Carl Roth, Germany
Sodiumacetate	Sigma Aldrich, MO, USA
Sodiumcarbonate	Carl Roth, Germany
Sodiumcitrate	Sigma Aldrich, MO, USA
Sodiumdihydrogenphosphate	Carl Roth, Germany
Sodiumsulfate	Merck, Germany
Sodiumthiosulfat Pentahydrate	Carl Roth, Germany
T4 DNA Ligase	Promega, WI, USA
TEMED	Sigma Aldrich, MO, USA
Tetracyclin Hydrochloride	Carl Roth, Germany
Tetramethylethylenediamine (TEMED)	Sigma Aldrich, MO, USA
Transwell (6,5 mm with 0.4 µm pores)	Corning, NY, USA
Tris acetate	Carl Roth, Germany
TRIS base	Sigma Aldrich, MO, USA
Tris-HCl	Sigma Aldrich, MO, USA
tri-Sodiumcitrate diHydrate	Carl Roth, Germany
Triton X-100	Sigma Aldrich, MO, USA
Trypanblue	PAA, MA, USA
Trypsin-EDTA	PAN, MA, USA
Trypton / Pepton	Carl Roth, Germany
Tween 20	Carl Roth, Germany
Uranylacetat	Sigma Aldrich, MO, USA
Urea	Carl Roth, Germany
Vivaspin (30 kDa)	Sartorius, Germany
Whatman Paper	Carl Roth, Germany
X-Gal	Carl Roth, Germany
Yeast	Carl Roth, Germany
Zeocin	Invitrogen, MA, USA

2. Materials & Methods

2.4.4. Bacterial strains information

Table 15: Used bacterial strains for transformation and plasmid generation

Strain	Genotype	Source
One Shot® Stbl3™ Chemically Competent <i>E.coli</i>	F-mcrB mrrhsdS20 (rB-, mB-) recA13 supE44 ara-14 galK2 lacY1 proA2 rpsL20 (StrR) xyl-5 λ-leumtl-1	Thermo Fisher Scientific, MA, USA C737303
One Shot® TOP10 Chemically Competent <i>E.coli</i>	F- <i>mcrA</i> Δ (<i>mrr-hsdRMS-mcrBC</i>) Φ80 <i>lacZ</i> ΔM15 Δ <i>lacX74</i> <i>recA1</i> <i>araD139</i> Δ (<i>araleu</i>)7697 <i>galU</i> <i>galK</i> <i>rpsL</i> (StrR) <i>endA1</i> <i>nupG</i>	Thermo Fisher Scientific, MA, USA C404010

2.4.5 Cell lines

Table 16: Cell lines for in vitro tests

Cell line	Description	Distributor information
HEK293	Human embryonic kidney	(ATCC® CRL-1573™)
HEK293 FT	Human embryonic kidney	Thermo Fisher Virapower™ System
HeLa	Human cervix carcinoma	(ATCC® CCL-2™)
Jurkat	Human Lymphocyte	(ATCC® TIB-152™) Clone E6-1
Raji	Human B-Lymphocyte	(ATCC® CCL-86™)
SH-SY5Y	Human neuroblastoma	(ATCC® CRL-2266™)
DG75	Human B-Lymphocyte	(ATCC® CRL-2625™)
SW837	Human rectal adenocarcinoma	(ATCC® CRL-235™)

2.4.6 Cell culture media and additives

Table 17: Different media for cell culture use.

Medium	Additives	Company
DMEM	+ L-Glutamine, + phenol red, high glucose	Gibco
Optimem	+ L-Glutamine, + phenol red	Gibco
DPBS	No Ca, no Mg, no phenol red	PAN
Fetal calf serum	Heat inactivated	Gibco
RPMI	+ L-Glutamine, + phenol red	Gibco
Trypsin	0,05 % in PBS, no Mg2+, no Ca2+	PAN

3. Results

2.4.7 Software

Diverse online databases and software were used to generate graphs or analyse RNA or DNA sequences.

ChemDraw Professional 15.1 (University of Göttingen licence)

Flowing software

Graphpad Prism 6 (DPZ licence)

miRBase21

Microsoft Excel

Microsoft Word

Microsoft PowerPoint

Multialign

NCBI Blast

Bioconductor R software and DESeq package [120]

3. Results

3.1. Comparison of three isolation techniques for exosomes

Extracellular vesicles (EVs) display a diversity of approved and putative cellular functions and are accepted markers in diagnosis and prognosis of disease. However, limited information is available when it comes to the most efficient isolation method for high yields combined with high purity of EVs [58].

3.1.1 Different isolation techniques yield various size profiles of EVs

To address the problem of EV isolation a comparison of three different techniques with cell culture supernatants (CCSN) of four human cell lines was performed. Both yields and size distributions of isolated EVs were examined. The three individual isolation techniques are summarized in Figure 9.

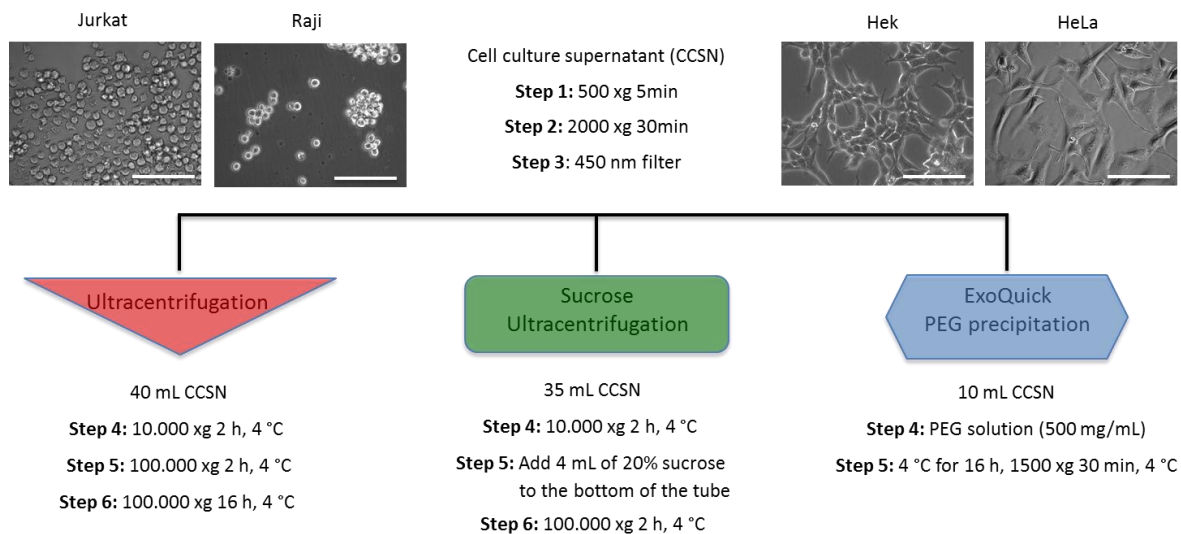


Figure 9: Comparison of three exosome isolation techniques. For all techniques cell culture supernatant (CCSN) harvested after 72 hours was differentially centrifuged (500 xg 5 min, 2000 xg 30 min) and filtered through a 450 nm filter. For the ultracentrifugation protocol 40 mL of filtered CCSN were differentially centrifuged (10.000 xg 2 h, 100.000 xg 2 h and 100.000 xg 16 h). For sucrose cushion ultracentrifugation 35 mL of CCSN were centrifuged at 10.000 xg for 2 h followed by a 100.000 xg centrifugation step through a 20 % sucrose cushion. For the PEG precipitation technique only 10 mL of CCSN were used and mixed (1:5) with PEG solution (500mg/mL in PBS), incubated over night at 4 °C and centrifuged at 1500 xg for 30 min. Resulting pellets of all isolation methods were dissolved in 100 µL PBS. All centrifugation steps were performed at 4 °C. Scale bar = 100 µm

3. Results

All four cell lines were cultured under the same conditions for the different isolation protocols. Cells were seeded in same densities and cultured for three days in exosome free media with supplements. Living cells were separated by a 500 xg centrifugation step, while cell debris and fragments were removed during a 2000 xg centrifugation for 30 min. Subsequently a 450 nm cellulose acetate filter was used to remove residual fragments. To perform ultracentrifugation (UC), 40 mL of pre-purified supernatant were centrifuged at 10.000 xg for 2 h to remove bigger vesicles including apoptotic bodies and large microvesicles. At 100.000 xg exosomes were pelleted and the pellet was washed once with PBS followed by a second 100.000 xg step. The resulting pellet was resuspended in 100 µL PBS and stored at 4 °C for further analysis. In contrast to the UC protocol only 35 mL of differential CCSN were centrifuged at 10.000 xg for sucrose isolation. In order to separate larger microvesicles from exosomes a 20 % sucrose cushion was used during one centrifugation step at 100.000 xg. The exosome containing pellet was resuspended in 100 µL PBS and stored at 4 °C. For the PEG precipitation workflow 10 mL of CCSN were mixed with the PEG solution, incubated overnight at 4 °C and subsequently centrifuged at 1500 xg for 30m. The resulting pellet was diluted in 100µL PBS and stored at 4 °C. The EV-PBS solutions were diluted 1:100 and were analysed by Nanoparticle Tracking Analysis (NTA) to determine size distribution and yield (Figure 10).

EVs from HEK293 isolated by Sucrose UC yields the smallest mean size of EVs (mean: 149 nm, Figure 10a), while UC and PEG precipitation isolated slightly bigger vesicles (mean: 168 nm, respectively 156 nm). The same general trend was observed for Jurkat cells, upon sucrose UC with the smallest vesicle size profile (mean: 65 nm) compared to UC (mean: 150 nm) and PEG precipitation (mean: 188 nm). Size distributions were similar for HeLa and Raji cells. Sucrose UC and UC resulted in almost the same size distributions of extracellular vesicles. The detected mean particle size for HeLa sucrose UC (mean: 96 nm) was slightly higher compared the vesicles isolated by differential UC (mean: 87 nm). Raji EVs displayed a mean size of 88 nm after sucrose UC and 86 nm after differential UC. In contrast PEG precipitation yields EVs with higher diameters (mean size for HeLa 188 nm and Raji 174 nm).

3. Results

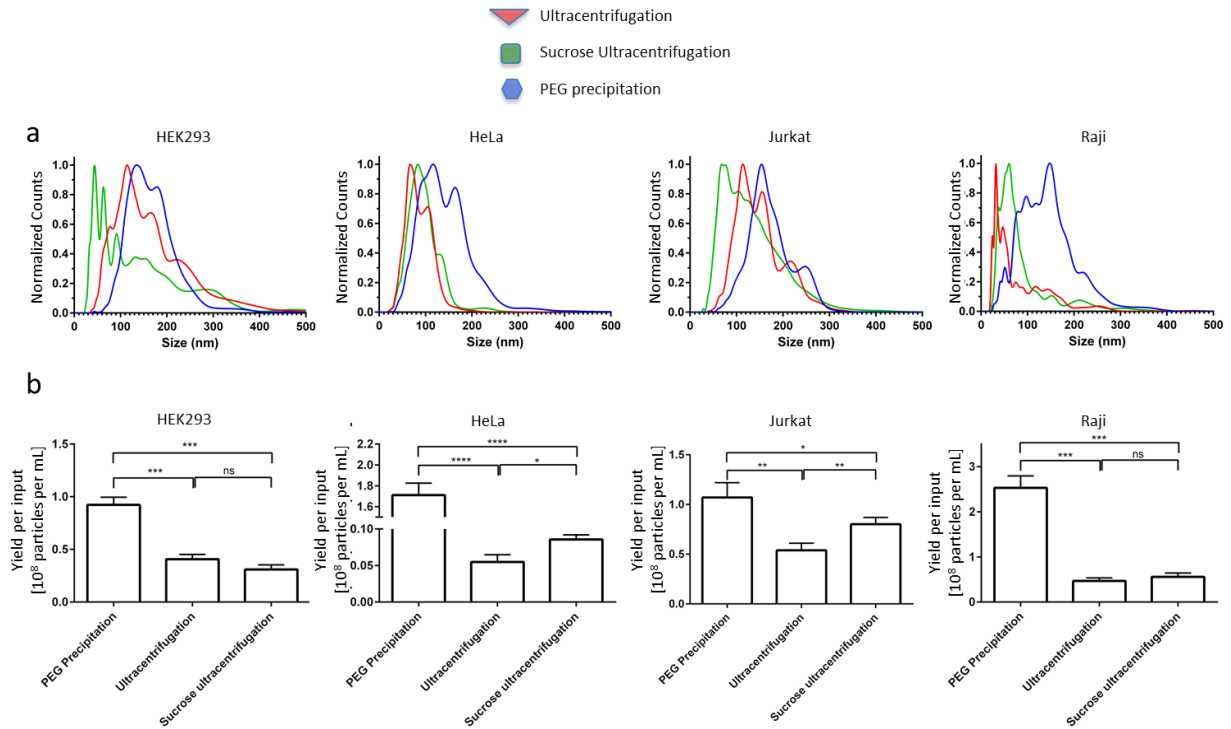


Figure 10: Comparing size and yield of extracellular vesicles (EVs) isolated by three different techniques. EVs of four human cell lines were isolated by the three isolation techniques described in Figure 1. Size profiles of isolated EVs were measured by Nanoparticle Tracking Analysis and are depicted in (a). Nanoparticle Tracking Analysis of extracellular vesicles showed significantly enlarged particle concentrations (yield per input) for PEG precipitation compared to ultracentrifugation and sucrose ultracentrifugation (b). The two ultracentrifugation isolation techniques displayed only minor differences in the individual yields of particles for all tested cell lines.

Analysis of the yield per input revealed different values for the purification protocols. PEG precipitation displayed improved performance in all cell lines. From HEK293 cells $0.92 \pm 0.04 \cdot 10^8$ particles/mL input material (CCSN) were isolated by PEG precipitation, while UC yielded $0.41 \pm 0.02 \cdot 10^8$ and sucrose UC $0.31 \pm 0.02 \cdot 10^8$ particles/mL. An even bigger effect was observed for HeLa cells, in which PEG precipitation resulted in $1.71 \pm 0.07 \cdot 10^8$ particles/mL compared to only $0.05 \pm 0.005 \cdot 10^8$ particles for UC and $0.08 \pm 0.003 \cdot 10^8$ particles/mL for sucrose UC. Studying Jurkat EVs from CCSN using PEG precipitation indicated the double amount of particles ($1.07 \pm 0.09 \cdot 10^8$ particles/mL) compared to the UC techniques ($0.54 \pm 0.04 \cdot 10^8$ particles/mL for UC and $0.80 \pm 0.04 \cdot 10^8$ particles/mL for Sucrose UC). For Raji EVs similar trends were observed. Via PEG precipitation $2.53 \pm 0.15 \cdot 10^8$ particles/mL were isolated, while UC and sucrose UC yielded only $0.47 \pm 0.04 \cdot 10^8$ respectively $0.56 \pm 0.05 \cdot 10^8$ particles/mL. The NTA analysis results were summarized in table 18.

3. Results

Table 18: Mean particle size and yield of different EV isolated from four different human cell lines by three isolation methods.

	HEK293 mean particle size	HEK293 yield per input
PEG Precipitation	156.2 [nm]	0.92 *10 ⁸ [particles per mL]
Ultracentrifugation	168.1 [nm]	0.41 *10 ⁸ [particles per mL]
Sucrose ultracentrifugation	149.6 [nm]	0.31 *10 ⁸ [particles per mL]
	HeLa mean particle size	HeLa yield per input
PEG Precipitation	188.3 [nm]	1.71 *10 ⁸ [particles per mL]
Ultracentrifugation	86.8 [nm]	0.05 *10 ⁸ [particles per mL]
Sucrose ultracentrifugation	96.4 [nm]	0.08 *10 ⁸ [particles per mL]
	Jurkat mean particle size	Jurkat yield per input
PEG Precipitation	188.1 [nm]	1.07 *10 ⁸ [particles per mL]
Ultracentrifugation	150.4 [nm]	0.54 *10 ⁸ [particles per mL]
Sucrose ultracentrifugation	65.8 [nm]	0.80 *10 ⁸ [particles per mL]
	Raji mean particle size	Raji yield per input
PEG Precipitation	174.5 [nm]	2.53 *10 ⁸ [particles per mL]
Ultracentrifugation	85.9 [nm]	0.47 *10 ⁸ [particles per mL]
Sucrose ultracentrifugation	88.1 [nm]	0.56 *10 ⁸ [particles per mL]

3.1.2 All tested isolation techniques show exosomal marker protein expression like CD9, CD63 or Alix

In addition to the examination of the size profiles and EVs amounts of by the NTA technique, a verification of particle identities by detecting three exosomal marker proteins was performed in western blot analysis (Figure 11).

Alix (Ensembl: PDCD6IP) is a class E VPS protein that functions within the ESCRT machinery and is present in the exosomal lumen, was the first exosomal marker protein to be detected. No signal was detected inside the cell (500 xg pellet), in cell debris (2000 xg pellet) and in bigger microvesicles (10.000 xg pellet). A specific signal with the expected molecular weight of 90 kDa was observed after the first UC step (100.000 xg P1) with even increased signal intensity after washing (100.000 xg P2). Furthermore, a strong signal was detected after PEG precipitation and sucrose UC.

3. Results

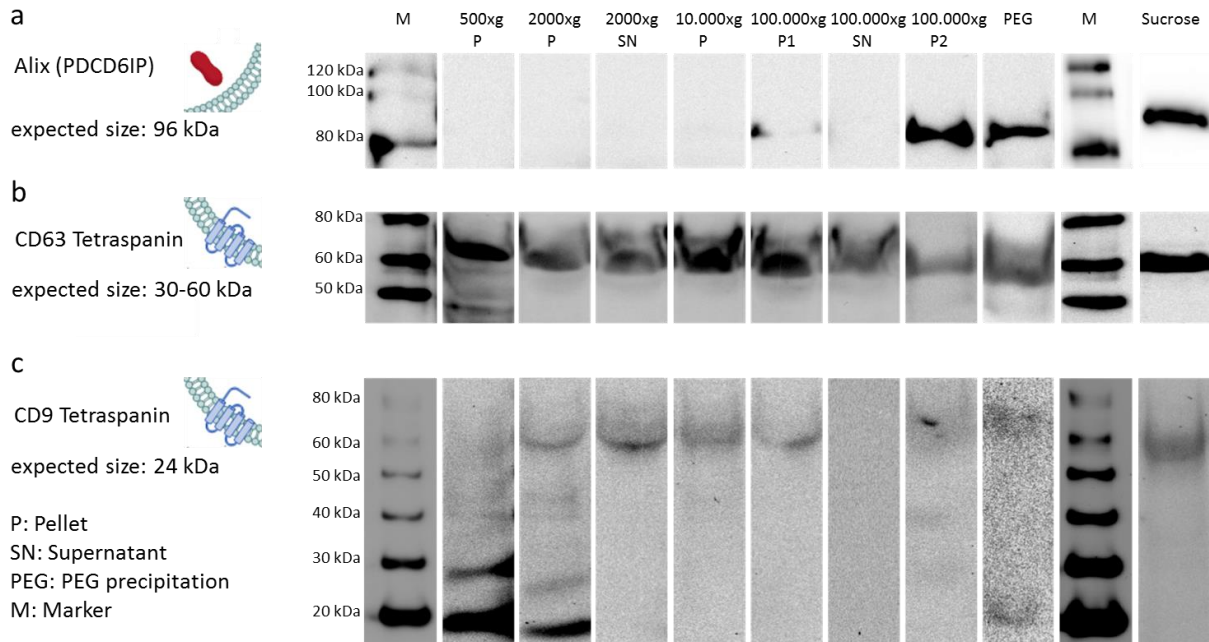


Figure 11: Detection of three different exosome marker proteins via Western Blot. Exosomes of Raji cells were isolated by three different isolation techniques and equal amounts of protein (10 µg total protein) were separated via SDS PAGE. Presence of Alix (a), CD63 (b) and CD9 (c) for all three techniques was confirmed using specific antibodies (Table 11). Alix was detectable in ultracentrifugation pellets, after PEG precipitation and in the sucrose cushion pellet, while CD63 was detectable after all differential centrifugation steps. Intracellular CD9 gave a signal around 20 kDa, which increased in higher centrifugation speeds to 60 kDa.

Secondly the expression of tetraspanin CD63 (Ensembl: TSPAN-30) was tested. CD63 was advised in virtually all cellular membranes including cell membrane, lysosomal membrane, late endosomal membrane and exosomal membrane. This tetraspanin was detected in all samples, i.e. the cell pellet (500 xg), cell debris (2000 xg), the microvesicle pellet (10.000 xg) and exosome pellets (100.000 xg P1 and P2, PEG and Sucrose) at around 60 - 65 kDa.

Finally, the tetraspanin CD9 (TSPAN29) was analysed. This tetraspanin is detectable in cell membranes and in extracellular space for example in exosome membranes. For CD9 a broad cellular signal was observed at 20 kDa, 30 kDa and weak signals at 40-60 kDa. In the 2000 xg fraction the same pattern was observed, whereas the 10.000 xg, 100.000 xg fractions and sucrose UC show a single signal at 60 kDa. For PEG precipitation 2 signals at 20 kDa and 60 kDa were detected. In summary all three isolation techniques revealed a positive signal for CD9, CD63 and Alix.

3. Results

3.1.3 Confirmation of EV isolation by electron microscopy

To further confirm successful EV isolation electron microscopy studies were performed (Figure 12). Exosomes were isolated as described before and fixed with PFA. Afterwards samples were negative stained with uranylacetate and immobilized on copper grids. In theory exosomes appear as 30 – 100 nm membranous vesicles in EM microscopy.

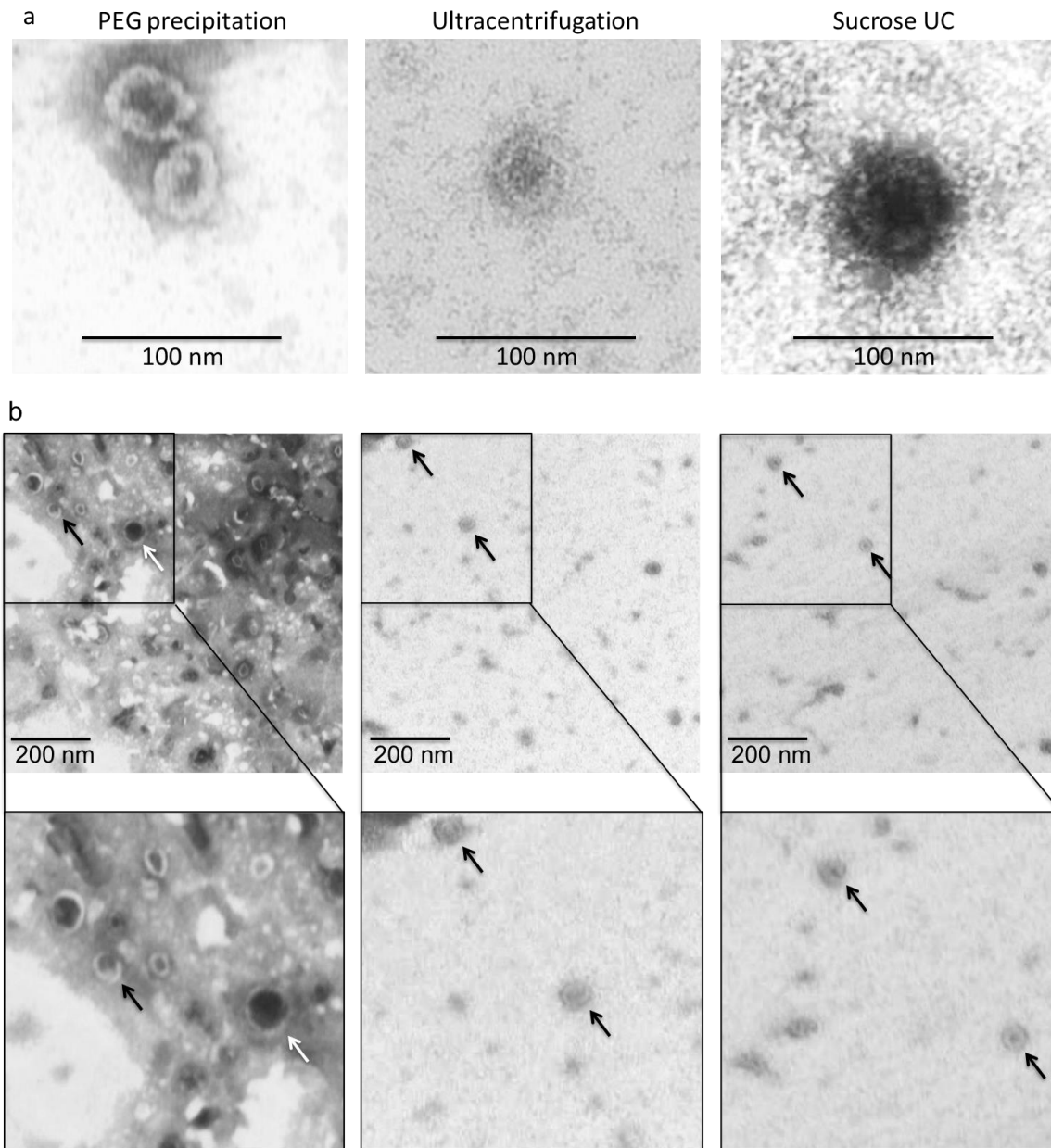


Figure 12: Detection of extracellular vesicles by electron microscopy. Exosomes of Raji cells were isolated using the three different techniques and visualized by electron microscopy. Spherical particles with a diameter of around 50 nm were observed in all samples (a). Additionally, PEG precipitation showed also vesicles larger than 100 nm (white arrow). After ultracentrifugation only vesicles with a diameter smaller than 100 nm (black arrows) were observed. Furthermore, a higher background compared to the ultracentrifugation techniques was observed (b) for PEG-precipitated samples.

3. Results

In figure 12a high-resolution pictures of EVs are illustrated for PEG-precipitated samples, while overview pictures are depicted in Figure 12b. PEG precipitation yielded a high number of vesicles with a broad size range (50-150 nm) with the majority of vesicles at around 100nm diameter. In addition, a relatively high background level was detected. For the ultracentrifugation techniques a different pattern was observed. Both techniques gave rise of homogenous vesicles with sizes smaller than 100 nm and also the background levels were reduced when compared to the PEG precipitation.

3.2. Small RNA profiles of cellular and exosomal RNA

3.2.1 Cellular and exosomal RNA differ in size distribution

Following the analysis of exosome isolation techniques, cellular and exosomal RNAs from four different human cell lines were isolated and prepared for Next Generation Sequencing (NGS) of their small RNA content. Size profiles of isolated RNAs from Raji cells and Raji EVs are shown in Figure 13.

Profiles of the cellular Raji RNA displayed two main peaks with approximately 2000 and 4000 nucleotides corresponding to 18S and 28S ribosomal RNAs. The RNA integrity number (RIN) was calculated by the ratio of these 2 peaks reached 9.8, indicating good quality RNA (10 is maximum). Furthermore, small RNAs between 50 and 300 nucleotides were detectable, while the marker peak showed the expected signal at 25 nucleotides. The pool of cellular RNAs included mainly long RNAs (56.6 %) with sizes larger than 1000 nucleotides, while the small RNA fraction up to 200 nucleotides showed a share of 40.4 %. To use cellular RNA for small RNA sequencing a purification of the small RNA fraction was necessary to be performed. After small RNA refinement (Figure 13 b) size distribution altered to a majority of small RNAs with 25 and 200 nt in size (76.1 %) and only 23.0 % of RNAs larger than 1000 nt. The portion of RNAs between 200 and 1000 nt was reduced from 3.0 % to 0.9 %.

When comparing cellular (Figure 13a) and exosomal RNA (Figure 13c) different size patterns were observed. Due to the limited RNA amount after exosomal RNA isolation no smallRNA purification was performed. Mainly small RNAs (66.7 %) were detected inside exosomes and

3. Results

only 5.0 % of RNAs longer than 1000 nucleotides were visible. The fraction of 200-1000 nt RNAs was more dominant (28.3 %) compared to cellular RNA (3.0 %).

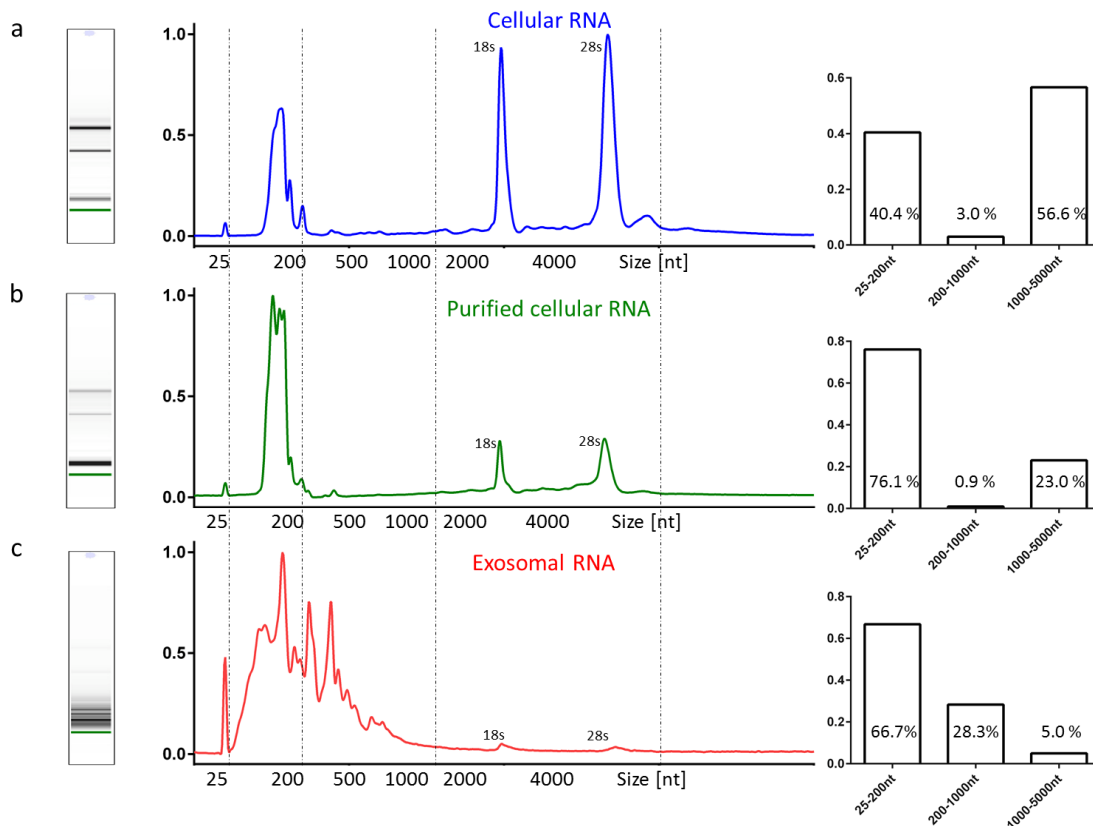


Figure 13: RNA size-profile of cellular (purified / total RNA) and exosomal RNA. RNA was extracted from Raji cells and their EVs. Total RNA was purified by magnetic beads. Cellular RNA showed 40.4 % small RNAs and 56.6 % large RNA. After purification the small RNA content increased to 76.1% and the large RNA content decreased to 23,0 %. Exosomal RNA showed high portion of small RNAs (66.7 %), while the large RNAs were underrepresented (5.0 %).

3.2.2 Next generation sequencing workflow

After evaluation of the RNA quality on Bioanalyzer System, small RNAs were subjected to library preparation and next generation sequencing (Figure 14). The RNA quality was analysed (Step 1) by Bioanalyzer system (RIN >9) and small RNAs were purified and ligated to adapters (Step 2). In a second PCR step the adapters were completed or barcode sequences for sample identification were added. Completed libraries were clonally amplified (Step 3) and sequenced on the IonTorrent PGM platform. Shortly, the PCIM system recognized inserted by the pH drop upon proton release (Step 4). After sequencing raw signals were processed, adapters trimmed, low quality reads deleted and fastq files generated (Step 5).

3. Results

Quality checked reads were aligned against miRBase21 and snoRNABase V3 and analysed by Bioconductor DESeq package in R [120].

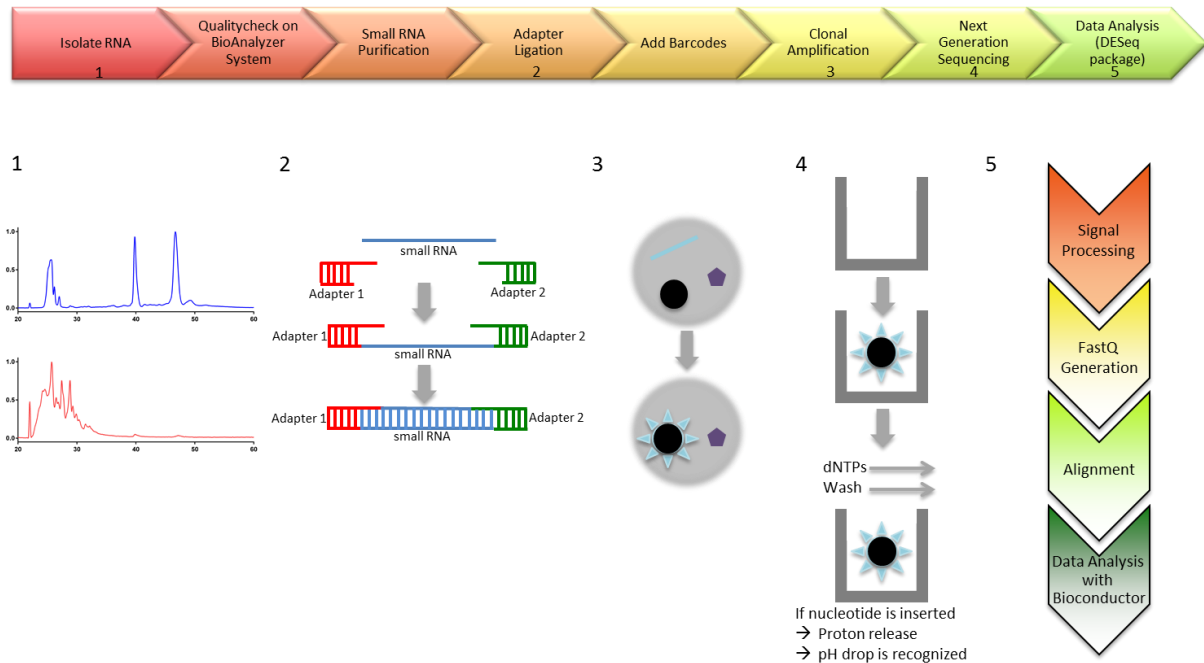


Figure 14: Illustration of the next generation sequencing workflow. RNA was isolated (1) and the RNA integrity number (RIN) was checked for RNA samples on BioAnalyzer system. Cellular RNA (RIN \geq 9) was purified and the small RNAs were ligated to sequence adapters and barcodes (2). Because of the high small RNA content in exosomes the small RNA purification step was skipped. Completed libraries were clonally amplified (3) and sequenced on the IonTorrent PGM system (4). Afterwards sequences were processed, quality checked, trimmed and analysed by the Bioconductor DESeq software package on R.

3.2.3 Reproducibility of NGS data on the IonTorrent system

The reproducibility of the NGS workflow was confirmed by three different biological replicas of each cellular and exosomal RNAs isolated from Raji cells (Figure 15). Detailed sequence information is listed in table 19.

Table 19: Sequencing information for Raji libraries

	Bases	Reads	Mean Read Length
Raji cell1	23.564.413	1.328.741	30 bp
Raji cell2	9.482.133	519.690	18 bp
Raji cell3	4.203.270	229.203	18 bp
Raji exo1	36.856.068	1.489.896	25 bp
Raji exo2	14.711.571	487.422	30 bp
Raji exo3	5.833.148	266.501	22 bp

3. Results

Having a more detailed look at the distribution of small RNAs unique patterns were observed in cellular and exosomal (Figure 15a). Using the sequence cluster algorithms included in DESeq package cellular samples cluster together, whereas exosomal samples cluster apart (Figure 15b). Raji exo1 and exo2 are more similar compared to Raji exo3, while all the cellular samples displayed only minor differences. The same tendencies were observed in a PCA plot (Figure 15c).

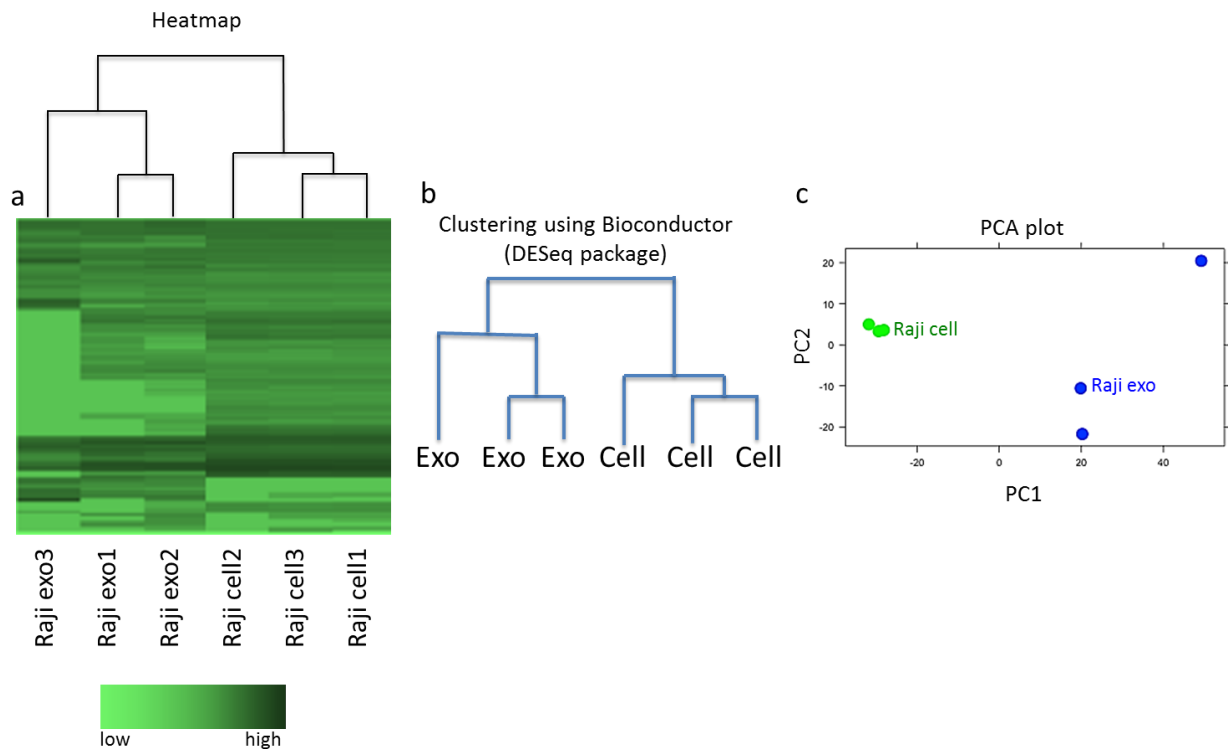


Figure 15: Reproducibility of NGS data generated by IonTorrent System. Exosomal and cellular RNA of three different biological replicates from Raji cells were utilized for the NGS workflow. Raw reads were quality checked, trimmed and aligned against miRBase21 and snoRBase V3. Data analysis was performed with Bioconductor DESeq package to generate the heatmap (a), clustering (b) and PCA plot (c). Distinct exosomal and intracellular patterns were observed after cluster analysis. Cellular pattern showed only minor differences after cluster analysis, whereas exosome samples comprise higher deviation, especially between Raji exo1/exo2 and Raji exo3. Trends were confirmed by principle component calculations.

3.2.4 Exosomal and intracellular small RNA profiles of human B-lymphocytes (Raji)

To visualize the different expression patterns and clustering of samples a log₂ fold change plot was generated for small RNA profiles from Raji (Figure 16b). A list of candidates that appeared enriched in either exosomes or intracellular is provided in table 20.

3. Results

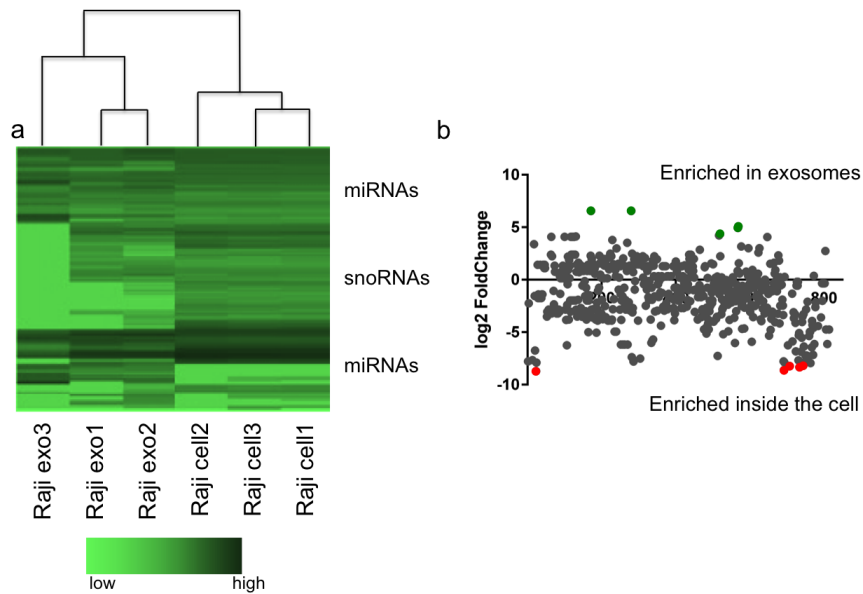


Figure 16: Cellular and exosomal small RNA distribution of Raji small RNA libraries. Heatmap and log2foldchange were calculated and generated by Bioconductor DESeq package. Top five cellular (red) and exosomal (green) overexpressed miRNAs were highlighted and listed in table 20.

Both strands (5p and 3p) of miR-3607 were overrepresented in the intracellular small RNA population and only barely detectable in extracellular vesicles. The same is true for the snoRNA U104 and miR-130b-5p and miR-20a-3p, which showed a 40-170 fold cellular overexpression. In contrast the miRNA miR-1246 showed the highest extracellular overrepresentation (140 fold) followed by miR-223-3p (82 fold), miR-222-3p (78 fold), miR-145-5p (43 fold) and miR-27b-3p with 19 fold higher abundance in extracellular vesicles.

Table 20: MiRNA candidates of Raji and distribution in cells compared to exosomes

small RNA	Log2foldchange	Basemean cell	Basemean exo
hsa-miR-3607-5p	-9,53	313,28	0,42
hsa-miR-3607-3p	-7,63	83,96	0,42
U104	-7,40	419,25	2,48
hsa-miR-130b-5p	-6,60	75,57	0,78
hsa-miR-20a-3p	-5,39	44,44	1,06
hsa-miR-1246	7,20	1,30	191,33
hsa-miR-223-3p	6,36	4,71	386,16
hsa-miR-222-3p	6,29	3,12	244,37
hsa-miR-145-5p	5,44	3,60	156,26
hsa-miR-27b-3p	4,26	12,94	247,31

Furthermore, I detected exclusively intracellular or extracellular small RNA candidates (Table 21). MiR-218-5p showed the highest extracellular only expression followed by miR-

3. Results

451a and miR-367-3p. However I detected some miRNAs only in cell extracts, e.g. miR-4284, miR-582-5p or miR-664a-3p, too. Moreover two snoRNAs (U57 and U73a) were identified, which showed high levels in cellular small RNA samples but were not detectable in EV samples.

Table 21: MiRNA candidates exclusively present in exosomes (log2 foldchange = Inf) or intracellular (log2foldchange = -Inf)

small RNA	Log2foldchange	Basemean exo
hsa-miR-218-5p	Inf	4986,27
hsa-miR-451a	Inf	434,19
hsa-miR-367-3p	Inf	222,65
hsa-miR-486-5p	Inf	110,99
hsa-miR-122-5p	Inf	89,17

small RNA	Log2foldchange	Basemean cell
hsa-miR-4284	-Inf	549,45
hsa-miR-582-5p	-Inf	73,77
U57	-Inf	65,61
hsa-miR-664a-3p	-Inf	37,01
U73a	-Inf	32,85

Taken together, the IonTorrent System displayed a high level of reproducibility with three different small RNA-libraries, each for cellular and exosomal samples as was analysed by cluster calculations and PCA plots. Furthermore, distinct cellular and exosomal small RNA patterns were observed for human Raji B-cells and distinct expressed small RNAs were described.

3.2.5 Exosomal and intracellular small RNA profiles of human T-lymphocytes (Jurkat)

After confirming the reproducibility and reliability of the IonTorrent System and analysing intra- and extracellular small RNA distribution of human B-cells I examined exosomal and intracellular RNAs of human T-cells (Jurkat). The heatmap and foldchange plot were generated by the DESeq package in R and are depicted in Figure 17.

3. Results

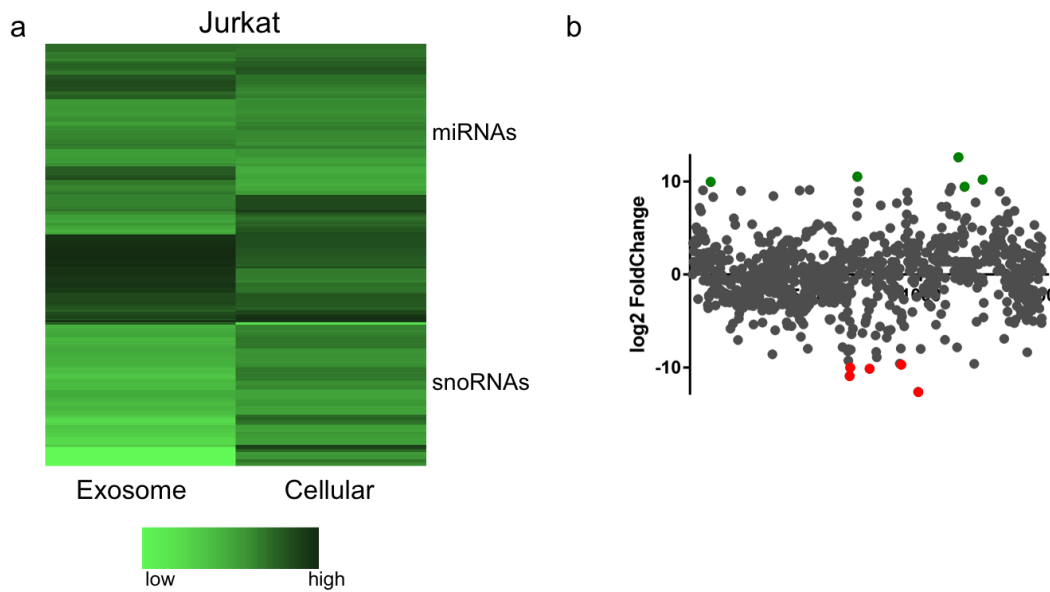


Figure 17: Small RNA distribution in cells and exosomes of Jurkat. Exosomal and cellular human T-lymphocytes (Jurkat) were utilized for the NGS workflow. Raw reads were quality checked, trimmed and aligned to miRBase21 and snoRBase V3. Data analysis was performed with Bioconductor DESeq package to generate the heatmap (a) and log₂foldchange (b). Top five cellular (red) and exosomal (green) enriched miRNAs were highlighted.

Both for human B-cells and for human T-cells (Jurkat) I detected distinct small RNA distributions in cellular and extracellular RNA samples. The top5 cellular (red) or exosomal (green) enriched small RNAs were highlighted in a log₂foldchange plot (Figure 17b) and are summarized in table 22.

Table 22: MiRNA candidates of Jurkat and distribution in cells compared to exosomes

small RNA	Log2foldchange	Basemean cell	Basemean exo
hsa-miR-378f	-9.69	2238.37	2.69
hsa-let-7e-5p	-8.83	3696.45	8.08
hsa-miR-378g	-8.11	2240.23	8.08
U24	-7.41	459.78	2.69
U48	-6.86	314.94	2.69
hsa-miR-143-3p	8.09	0.74	201.94
hsa-miR-486-5p	7.84	1.11	255.79
hsa-miR-122-5p	7.32	0.37	59.24
hsa-miR-145-5p	7.04	2.60	341.96
hsa-miR-130a-3p	6.56	0.37	35.00

MiR-378f was almost 1000 fold more frequently found intracellular, whereas let-7e-5p and miR-378g represent a 280-462 fold cellular overrepresentation. I also detected two snoRNAs

3. Results

among the top5 candidates, while U24 was 170 fold and U48 117 fold enriched inside the cell. The top 5 small RNAs overrepresented in exosomes consist of miR-143-3p (272 fold), miR-486-5p (230 fold), miR-122-5p (160 fold), miR-145-5p (132 fold) and miR130a-3p (94 fold). A full list of mapped small RNA reads and previewed in the supplements of this thesis. Similar to human B-cell profiles small RNAs only present in one of the groups were identified. Top 5 exclusively exosomal or cellular candidates are summarized in table 23.

Table 23: MiRNA candidates exclusively present in Jurkat exosomes (log2foldchange = Inf) or intracellular (log2foldchange = -Inf)

small RNA	Log2foldchange	Basemean exo
hsa-miR-451a	Inf	651.60
hsa-miR-494-3p	Inf	166.94
hsa-miR-376c-3p	Inf	72.70
hsa-miR-214-3p	Inf	61.93
hsa-miR-526b-5p	Inf	53.85

small RNA	Log2foldchange	Basemean cell
hsa-miR-378b	-Inf	2324.16
hsa-miR-378i	-Inf	2015.16
hsa-miR-181c-5p	-Inf	572.68
hsa-miR-196b-5p	-Inf	237.32
hsa-miR-4318	-Inf	121.07

Analogous to Raji cells miR-451a was only detectable extracellular together with miR-494-3p, miR-376c-3p, miR-214-3p and miR-526b-5p. On the other hand the top 5 exclusively intracellular miRNAs consisted of miR-378b, followed by miR-378i, miR181c-5p, miR186b-5p and miR-4318.

3.2.6 Exosomal and intracellular small RNA profiles of human B-lymphocytes (DG75)

In order to check a second human B-cell line I analysed human DG75 cells. This cell line was established in 1975 from a pleural effusion of a patient with Burkitt's lymphoma [132]. Heatmap and log2foldchange plot were generated via DESeq package and are shown in Figure 18.

3. Results

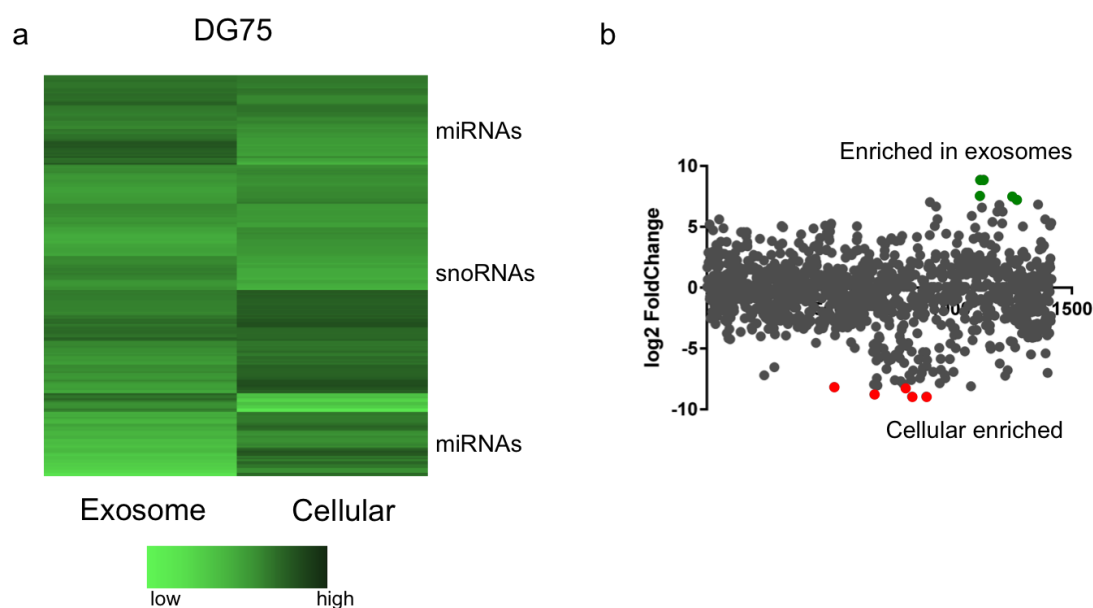


Figure 18: Cellular and exosomal small RNA expression of human B-lymphocytes (DG75). Exosomal and cellular small RNA libraries of human B-lymphocytes (DG75) were utilized for the NGS workflow. Raw reads were quality checked, trimmed and aligned against miRBase21 and snoRBase V3. Data analysis was performed with Bioconductor DESeq package to generate the heatmap (a) and PCA plot (b). Top five cellular (red) or exosomal (green) enriched small RNAs were highlighted.

Distinct small RNA pattern were observed for cellular and exosomal DG75 small RNAs. Top 5 intracellular (red) and extracellular (green) small RNAs were highlighted in a log2foldchange plot (Figure 18b) and are listed in table 24.

Table 24: MiRNA candidates of DG75 and distribution in cells compared to exosomes

small RNA	Log2foldchange	Basemean cell	Basemean exo
U29	-6,92	197,80	1,63
HBII-429	-6,67	333,74	3,26
hsa-miR-4521	-6,63	10374,20	104,51
hsa-miR-3607-5p	-5,43	2527,26	58,79
hsa-miR-20a-5p	-4,65	10153,13	404,98
hsa-miR-451a	10,79	0,61	1085,94
hsa-miR-125a-5p	7,82	0,61	138,80
hsa-miR-126-3p	7,57	3,06	581,34
hsa-miR-130a-3p	6,744	0,61	65,32
hsa-miR-223-3p	6,07	26,94	1817,52

Surprisingly two snoRNAs (U29 and HBII-429) showed the highest foldchange (102-121 fold) comparing DG75 cells and extracellular vesicles followed by miRNAs miR-4521 (99 fold), miR3607-5p (43 fold) and miR-20a-5p (25 fold). Additionally miR-451a was 1780 fold

3. Results

enriched inside exosomes followed by miR-125a-5p (228 fold), miR-126-3p (190 fold), miR-130a-3p (107 fold) and miR-223-3p (67 fold).

Furthermore, I identified small RNAs only present intracellular or in extracellular vesicles (Table 25). More detailed analyses and comparisons of the two human B-cell derived cell lines Raji and DG75 is provided in 3.2.8.

Table 25: MiRNA candidates exclusively present in DG75 exosomes (log2foldchange = Inf) or intracellular (log2foldchange = -Inf)

small RNA	Log2foldchange	Basemean exo
hsa-miR-145-5p	Inf	357,63
hsa-miR-494-3p	Inf	311,90
hsa-miR-203b-5p	Inf	153,50
hsa-miR-203a-3p	Inf	145,34
hsa-miR-143-3p	Inf	133,91
small RNA	Log2foldchange	Basemean cell
hsa-miR-33a-5p	-Inf	179,43
hsa-miR-590-3p	-Inf	137,17
U36B	-Inf	100,43
hsa-miR-1275	-Inf	59,40
snR38A	-Inf	53,89

Mir-145-5p and miR-494-3p showed strong extracellular presence without being detectable inside the cell. Similar observations were made for miR-203-3p, miR-203b-5p and miR143-3p, which displayed a weaker expression in extracellular vesicles compared to miR-145-5p and miR-494-3p.

In contrast miR-33a-5p, miR-590-3p and miR-1275 showed only intracellular expression, together with two snoRNAs (U36B and SnR38A).

3. Results

3.2.7 Exosomal and intracellular small RNA profiles of human cervical cancer cells (HeLa)

After checking three human suspension cell lines of B- and T-cell origins I analysed intracellular and extracellular small RNAs of the adherent growing HeLa cells. This cell line derived from cervical cancer cells and is the oldest and commonly used human cell line [133]. Heatmap and log₂foldchange plot were generated via DESeq package in R and are depicted in Figure 19. Five cellular (red) and exosomal (green) overrepresented small RNAs are highlighted. A summary of overrepresented small RNAs is provided in table 26.

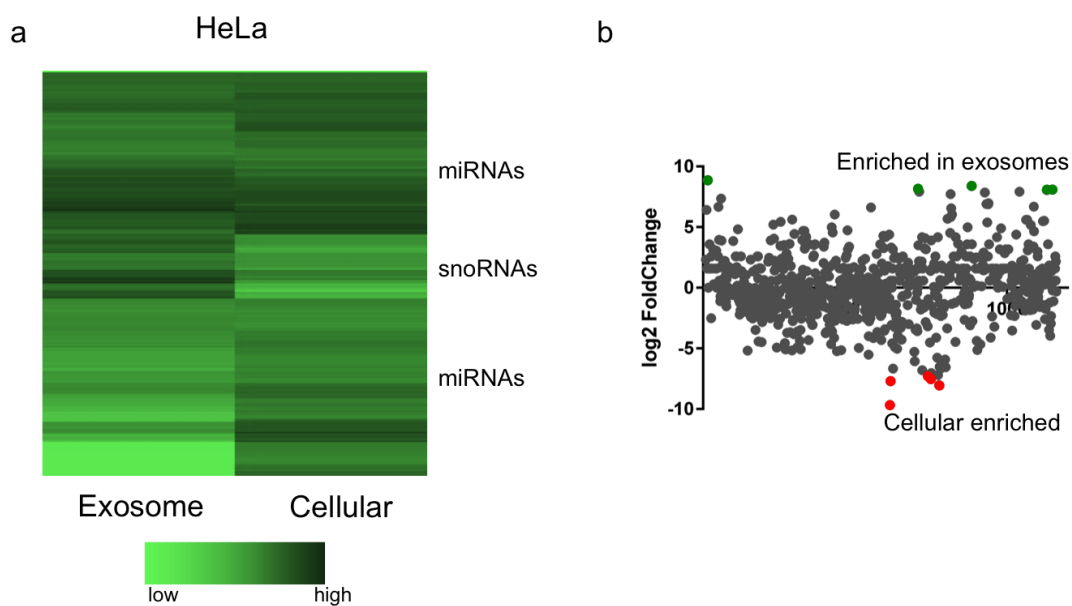


Figure 19: Cellular and exosomal small RNA expression of human cervical cancer cells (HeLa). Exosomal and cellular small RNA libraries of HeLa cells were utilized for the NGS workflow. Raw reads were quality checked, trimmed and aligned against miRBase21 and snoRBase V3. Data analysis was performed with Bioconductor DESeq package to generate the heatmap (a) and PCA plot (b). Top five cellular (red) and exosomal (green) enriched miRNAs were highlighted.

Diverging profiles of extracellular and intracellular small RNAs were detected for human cervical cancer cells. The top 5 cell-enriched small RNAs included four miRNAs and one snoRNA. MiR-204-5p displayed the highest cellular enrichment (187 fold) followed by miR-4284 (135 fold) and miR-95-3p (15 fold). U74 belongs to small nucleolar RNAs and showed a 14 fold overexpression and miR-454-3p was 12 fold enriched comparing cellular and exosomal small RNAs of HeLa (Table 26).

3. Results

Table 26: Top 5 cellular and exosomal miRNAs in HeLa

small RNA	Log2foldchange	Basemean cell	Basemean exo
hsa-miR-204-5p	-7,55	423,09	2,26
hsa-miR-4284	-7,08	917,80	6,79
hsa-miR-95-3p	-3,91	34,04	2,26
U74	-3,86	131,75	9,05
hsa-miR-454-3p	-3,60	27,41	2,26
hsa-miR-376c-3p	8,74	0,88	377,74
hsa-miR-1246	7,95	8,84	2194,06
hsa-miR-340-3p	7,41	2,65	450,12
hsa-miR-320d	7,32	7,96	1275,72
hsa-miR-150-5p	7,19	0,88	128,93

Vice versa miR-376c-3p was 429 fold enriched in exosomes, ensuing miR-1246 (248 fold), miR-340-3p (170 fold), miR-320d (160 fold) and miR-150-5p with 146 fold enrichment in extracellular vesicles compared to intracellular appearance.

Moreover, I detected several small RNAs exclusively detectable intracellular or extracellular (Table 27). Equally to Raji and Jurkat small RNA distributions miR-451a was solely detectable in extracellular vesicles. Besides miR-451a the small RNAs miR-223-3p, miR-486-5p, miR-134-5p and miR-494-3p are expressed extracellular but not detectable intracellular.

On the other hand the snoRNAs U63 and U81 are only expressed inside the cell and not detectable extracellular, which is also true for miR-324-5p, miR-28-5p and miR-4521.

Table 27: Exclusively extracellular (log2foldchange = Inf) or intracellular (log2foldchange = -Inf) HeLa miRNA candidates

small RNA	Log2foldchange	Basemean cell
U63	-Inf	26,53
U81	-Inf	18,57
hsa-miR-324-5p	-Inf	13,26
hsa-miR-28-5p	-Inf	11,94
hsa-miR-4521	-Inf	11,94

3. Results

small RNA	Log2foldchange	Basemean exo
hsa-miR-223-3p	Inf	531,55
hsa-miR-451a	Inf	484,05
hsa-miR-486-5p	Inf	217,14
hsa-miR-134-5p	Inf	104,05
hsa-miR-494-3p	Inf	81,43

3.2.8 Cluster analysis of cellular and exosomal small RNAs

In addition to the comparison of cellular and exosomal RNA profiles a cluster analysis of all samples was performed to evaluate sequencing data and workflow. The focus was set to extracellular smallRNA profiles and the comparison to intracellular small RNAs.

Clustering of small RNA profiles from the various samples was performed in DESeq software using preset standard parameters. In the cluster analysis of Raji und Jurkat cells (Figure 20) different distributions of small RNAs were detected. Four main groups we identified. The Raji cellular RNA samples clustered closely together, which was already seen in Figure 15 and Figure 16. A similar outcome was detected for exosomal small RNA profiles of Raji cells, whereas the samples "Raji exo1" and "Raji exo2" showed more similarities compared to "Raji exo3". Small RNA profiles of Jurkat cells and exosomes cluster apart showing low resemblances to each other and forming two separate cluster-groups.

3. Results

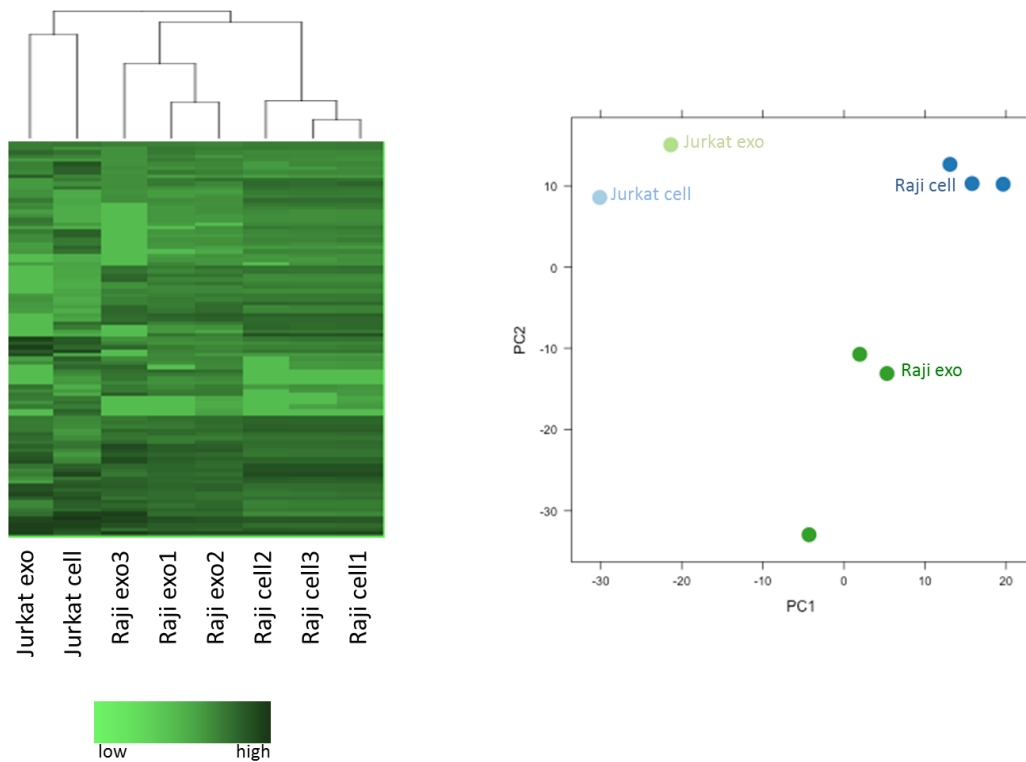


Figure 20: Cellular and exosomal small RNA expression of Raji and Jurkat. Exosomal and cellular small RNA libraries of human T- and B-cells were utilized for the NGS workflow. Raw reads were quality checked, trimmed and aligned against miRBase21 and snoRBase V3. Heatmap (a) and PCA plot (b) were generated via Bioconductor DESeq package in R. Distinct exosomal and intracellular small RNA profiles were detected for each cell line. Principle component analysis shows separate clustering for extracellular and intracellular samples and for different cell lines as well.

Comparable trends were observed in a principal component analysis. Raji cellular samples clustered in one group shown in blue, while exosomal samples (depicted in green) showed a broader distribution. Jurkat exosome (light green) and cellular samples (light blue) show low similarities to Raji cells and exosomes.

When analysing HeLa and DG75 NGS datasets similar trends were observed (Figure 21). No changes in clustering were seen for Raji and Jurkat datasets. The exosome NGS datasets of HeLa and DG75 clustered together, although the PCA plot showed a larger difference. For the cell-derived datasets of HeLa and DG75 an identical clustering behaviour was observed, but the samples plotted closer in the principle component analysis.

In summary, distinct cell and exosome RNA profiles of the four different human cell lines were detected and compared in clustering and principal component analysis. The next step is the analysis of exosomal RNAs and the distribution among the four cell lines.

3. Results

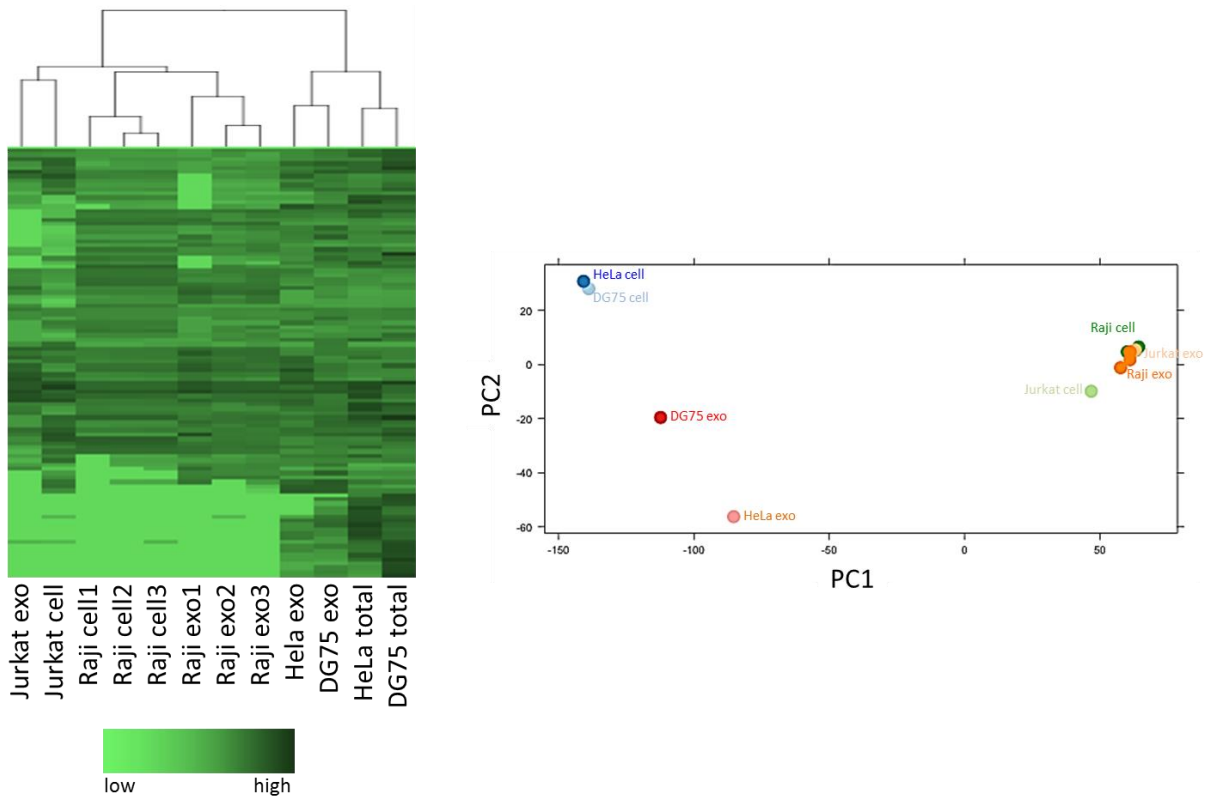


Figure 21: Cellular and exosomal small RNAs of Raji, Jurkat, DG75 and HeLa. Exosomal and cellular small RNA libraries of four different human cell lines were utilized for the NGS workflow. Raw reads were quality checked, trimmed and aligned against miRBase21 and snoRBase V3. Heatmap (a) and PCA plot (b) were generated via Bioconductor DESeq package in R. Raji cells could be clearly distinguished from Raji exosomes by cluster calculations. Jurkat show differences in small RNA expression and build a second group. Nevertheless Jurkat cellular and extracellular profiles show a low resemblance to each other, which leads to a formation of two separate cluster-groups. Extracellular and intracellular datasets of HeLa and DG75 build a third cluster group, whereas extracellular and intracellular datasets were distinguishable.

3.2.9 Comparison of miRNA distribution in exosomes and sequence motifs

In order to exclude misleading cell culture artefacts by RNA remains or contaminations in exosome free cell culture media and to detect cell specific exosomal miRNAs I investigated the extracellular miRNA profiles of HeLa, Jurkat, Raji and DG75. NGS datasets were analysed by Bioconductor DESeq package and aligned to miRBase 21. Discovered miRNAs were represented in a VENN diagram [134] and identified sequence motifs were depicted in Figure 22.

3. Results

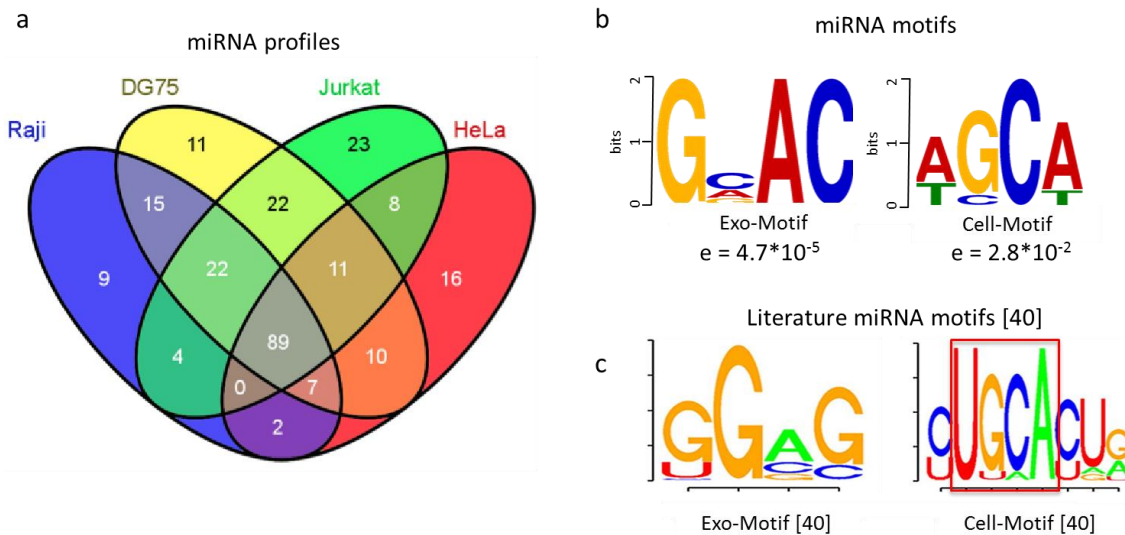


Figure 22: Expression pattern and sequence motifs of exosomal miRNAs in HeLa, Jurkat, DG75 and Raji exosomes. Exosomal miRNAs (a) showed a common pool with 89 miRNAs upon all four tested cell lines, nevertheless distinct small RNAs for all tested cell lines were detected too and are listed in table 28. Totally 249 miRNAs were compared. Sequence motif analysis revealed distinct extracellular and intracellular (b) patterns, which match with the literature (c).

Analysis of the extracellular miRNA distributions of four human cell lines revealed a common pool of 89 miRNAs. MiR451a was present in the extracellular fractions of all human cell lines but in Raji, Jurkat and HeLa it was not detectable in cell samples. Besides miR-451a, miR-148a, miR-21, miR-93 and miR-16 were found to be common extracellular RNAs in all four tested cell lines. In general the two B-cell lines show an overlap of 111/249 miRNAs. Similar values were reached when comparing DG75 and Jurkat cells, whereas Raji and Jurkat only displayed an overlap of 93 miRNAs. Comparison of Raji and HeLa extracellular miRNA profiles indicated only 91 similar common miRNAs.

In the distinct exosomal miRNA datasets I discovered miR140-5p, miR-10b, miR-369-3p, miR-376b and miR-136 as specific extracellular small RNAs for human B-lymphocytes (Raji). Additionally I analysed a second human B-lymphocyte (DG75) cell line and checked for specific extracellular RNAs. MiR203, miR-1295, miR-598, miR-195 and miR-330-3p were exclusively detectable within DG75 exosomes. Besides B-lymphocytes I studied the extracellular RNA content of human T-Lymphocytes (Jurkat). Specific extracellular miRNAs for human T-lymphocyte consists of miR-1274a, miR-363, miR-20b, miR-326 and miR-182. The cervix carcinoma cell line HeLa was selected as representative. Mir-100, miR-31, miR-452, miR-224 and miR-134 were only detectable inside exosomes of HeLa cells. A summary of specific miRNA profiles of each cell line and a common pool is illustrated in table 28.

3. Results

In addition I succeeded with the identification of specific intracellular and extracellular miRNA motifs using the DESeq package and the online motif-based sequence analysis tool (MEME). The exosomal sequence motif contains a set of four bases with the following sequence: GNAC (wherein N is G, A or C), frequently flanked by T (or better U) residues at 3' and 5'. The intracellular sequence motif is also composed of four bases but shows a diverging sequence with PGCA (wherein P is A or T). These sequence motifs match well with sequence motifs generated by microarray analysis as previously reported (Figure 22c).

Table 28: Exosomal miRNA distribution among four human cell lines

Common pool	Raji exosomes	DG75 exosomes	Jurkat exosomes	HeLa exosomes
hsa-miR-451a	hsa-miR-140-5p	hsa-miR-203	hsa-miR-1274a	hsa-miR-100
hsa-miR-148a	hsa-miR-10b	hsa-miR-1295	hsa-miR-363	hsa-miR-31
hsa-miR-21	hsa-miR-369-3p	hsa-miR-598	hsa-miR-20b	hsa-miR-452
hsa-miR-93	hsa-miR-376b	hsa-miR-195	hsa-miR-326	hsa-miR-224
hsa-miR-16	hsa-miR-136	hsa-miR-330-3p	hsa-miR-182	hsa-miR-134

Cellular and exosomal miRNA profiles of Raji, Jurkat and DG75 are summarized in figure 23. Cellular profiles of B-cells, i.e. of Raji and DG75 cells, revealed similarities like the sequence AGGAGCAT were observed, whereas human T-Lymphocytes showed distinct cellular profiles. Furthermore, I identified specific extracellular miRNA profiles of human B- and T-lymphocytes, whereas Raji and Jurkat profiles show more similarities (ACT sequence) compared to DG75 cells.

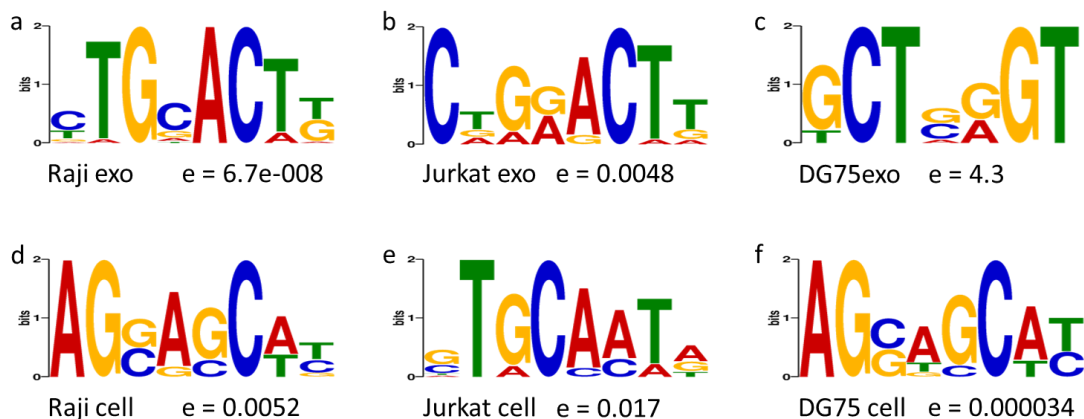


Figure 23: Distinct small RNA sequence motifs of three different human B- and T-lymphocytes. NGS datasets of exosomal small RNAs of Raji, Jurkat and DG75 were analysed quality checked, trimmed and aligned against miRBase 21 by Bioconductor DESeq package in R. Annotated miRNAs were checked via the online available motif-based sequence analysis tool (MEME) and best matching motifs are depicted in a-f. The cellular Raji motif shows high similarities with DG75 cellular motif, whereas the Jurkat cellular motif differs. For exosomal motifs Raji and Jurkat are more equivalent, when the DG75 exosomal profile shows more alteration.

3.3 Comparison of exosome isolation techniques

Although being research topic for many years the isolation of extracellular vesicles is still a challenging procedure. Ultracentrifugation techniques are time consuming and require specific materials and machines, which is not present in basic equipped laboratories or clinics. To overcome this issue I evaluated two different exosome isolation techniques, i.e. by PEG precipitation and the gold standard differential ultracentrifugation. Multiple analyses were performed in the context of extracellular vesicle size profiles and small RNA contents. Raji cells were cultured for three days in exosome free media and exosomes were harvested. After exosome isolation I checked the size profiles of isolated particles via Nanoparticle Tracking Analysis (NTA) and performed RNA isolation. Size profiles of isolated RNA were checked on a BioAnalyzer System and are depicted together with particle size profiles measured by NTA in Figure 24.

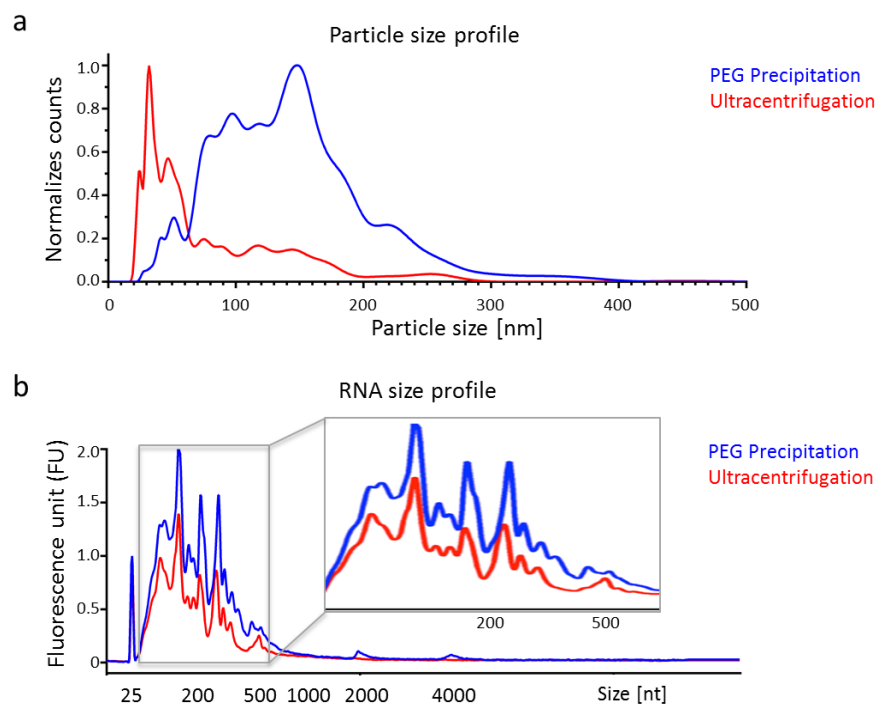


Figure 24: RNA- and vesicle size-profiles of EVs isolated from Raji cells. Human B-lymphocytes (Raji) were cultured for 3 days in exosome free media and exosomes were isolated by PEG precipitation (blue) or differential ultracentrifugation (red). Size profiles of extracellular vesicles were analysed by Nanoparticle Tracking Analysis (NTA) system (a) and subsequently RNA was isolated by phenol-chloroform extraction. Size profiles of RNA (b) show minor differences comparing both isolation techniques, whereas size profiles of vesicles differ strongly. Extracellular vesicles isolated by differential ultracentrifugation show smaller sized vesicles compared to particles isolated by PEG precipitation. Marker peaks at 25 nt were normalized to 1 FU.

3. Results

As described before extracellular vesicles isolated by PEG precipitation showed a broader size distribution and bigger mean vesicle sizes compared to particles isolated by differential ultracentrifugation (Figure 10 and Figure 24a). Comparing small RNA profiles by BioAnalyzer system I detected only minor differences (Figure 24b). Both isolation methods revealed small RNAs up to 500 nucleotides. After PEG precipitation a small leftover of 18S and 28S ribosomal RNAs was detected, while in differential ultracentrifuged particles no ribosomal RNA was detectable. The main RNA peak after PEG precipitation was observed at 152 nt followed by two peaks at 224 and 343 nt. Exosomes isolated by ultracentrifugation showed a similar pattern of RNA sizes with a main group around 150 nt followed by two peaks at 217 nt and 327 nt.

After similar small RNA size profiles were confirmed, I prepared small RNA libraries for NGS with samples from both isolation techniques to compare their small RNA contents. NGS datasets were analysed by Bioconductor DESeq package and aligned against miRBase 21 and snoRNABaseV3 (Figure 25).

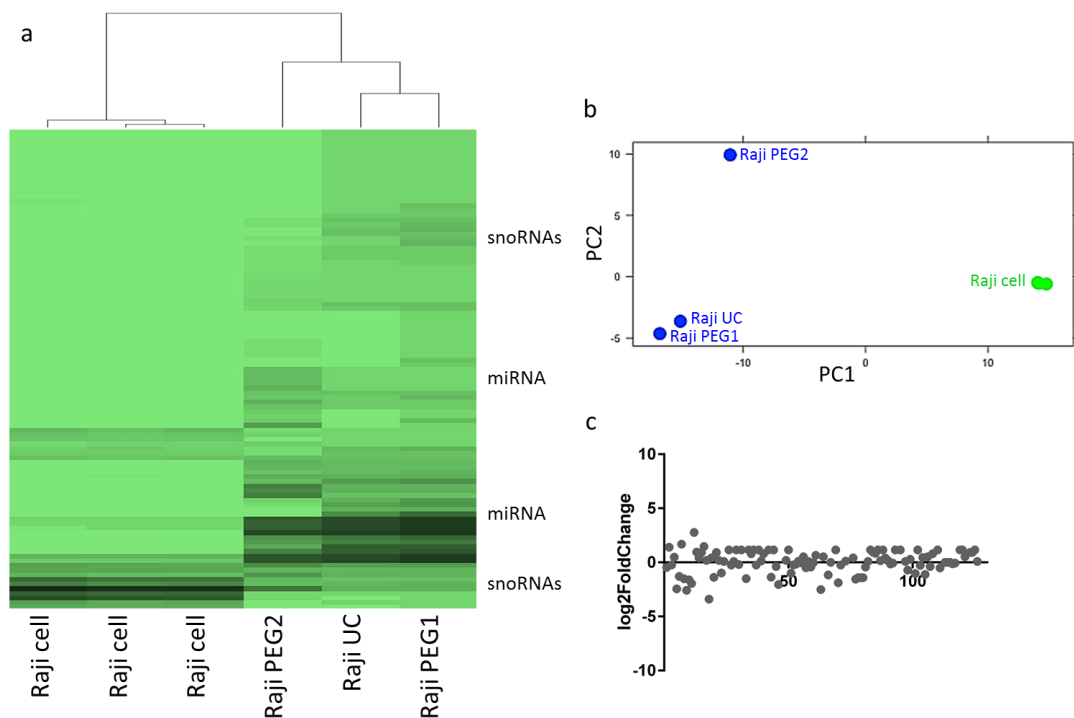


Figure 25: Small RNA profiles of cellular and exosomal RNA isolated by ultracentrifugation or PEG precipitation, principle component analysis and foldchange analysis. NGS datasets were analysed by DESeq package and aligned against miRBase 21 and snoRNABase V3. According to a cluster analysis Raji ultracentrifugated smallRNAs cluster closely to PEG precipitated small RNA profiles (a). Cellular RNA profiles were added to assess exosomal small RNA datasets. Principle component analysis revealed a close clustering of Raji UC and PEG1 sample, whereas Raji PEG2 shows a different profile (b). Nevertheless Raji PEG and UC profiles look more similar compared to cellular small RNA distributions. This trend was confirmed checking the log2fold scatter plot, which demonstrates only minor differences comparing PEG and UC samples.

3. Results

Principle component and cluster analysis revealed a close relation between ultracentrifugation and PEG precipitated samples, whereas cellular samples showed a different small RNA profile. Raji PEG1 and Raji UC showed more overlap compared to Raji PEG2, while an obvious difference to cellular samples was observed. Having a closer look at differentially expressed miRNAs (Figure 25c and table 29) only minor differences in expression was detected. Most small RNAs show a log2 foldchange between -2 and 2, while miR-378a-3p was enriched in PEG precipitated samples. The same is true for miR-19a-3p, miR-301a-3p, miR-16-5p and miR-142-5p. Also ultracentrifugation samples contained enriched miRNAs including miR-218-5p, miR-186-5p, miR-3591-3p, miR-122-5p and miR-27b-3p.

However equal distributed extracellular miRNAs comparing both isolation techniques were also detected, mentioning miR-451a, miR-367-3p and miR-486-5p. Expression patterns of miRNAs isolated by different isolation procedures were summarized in table 29.

Table 29: Small RNA content of PEG precipitated or ultracentrifuged extracellular vesicles

smallRNA	Log2foldchange	Basemean PEG	Basemean UC
hsa-miR-378a-3p	-3,395724874	1139,420477	108,2602376
hsa-miR-19a-3p	-2,578352317	646,5920531	108,2602376
hsa-miR-301a-3p	-2,504593013	21,88057725	3,855681498
hsa-miR-16-5p	-2,449318078	689,8171318	126,3036105
hsa-miR-142-5p	-2,043601659	5,298650755	1,285227166
hsa-miR-218-5p	2,782730118	1767,227197	12161,23336
hsa-miR-186-5p	1,691231583	27,93677652	90,21686465
hsa-miR-3591-3p	1,479923227	32,34345774	90,21686465
hsa-miR-122-5p	1,400481621	34,1743886	90,21686465
hsa-miR-27b-3p	0,964081601	46,24558201	90,21686465
hsa-miR-451a	0,847086794	37,86668023	68,11703979
hsa-miR-367-3p	0,426068819	2,869734089	3,855681498
hsa-miR-486-5p	0,163034413	1,147893636	1,285227166

No exclusively extracellular miRNAs were detected in samples isolated by ultracentrifugation. However, some small RNAs were only detectable in PEG precipitated extracellular vesicles, for example the snoRNA U24, miR146a-5p and miR-744-5p (Table 30).

3. Results

Table 30: miRNAs only detectable after PEG precipitation

smallRNA	Log2foldchange	Basemean PEG
U24	-Inf	10.33
miR-146a-5p	-Inf	3.55
miR-744-5p	-Inf	1.83

Only minor differences on small RNA expression were observed, when comparing both exosomal isolation techniques. PEG precipitation and ultracentrifugation showed similar outcome after cluster analysis and principle component calculations. However, overrepresented miRNA candidates for each isolation technique were observed.

3.4 Overexpression of exosomal marker proteins and influence on EVs and LVs

3.4.1 Overexpression of TSG101, Alix or CD9 alters both amount and mean sizes of EVs

Relatively little is known about exosomal marker proteins and their influence on EV assembly and secretion. To pursue this question human HEK293 were transduced by lentiviruses to generate stable expressing cell lines for the exosomal marker proteins CD9, Alix and TSG101. Afterwards the expression of target proteins was analysed by qPCR (Figure 26).

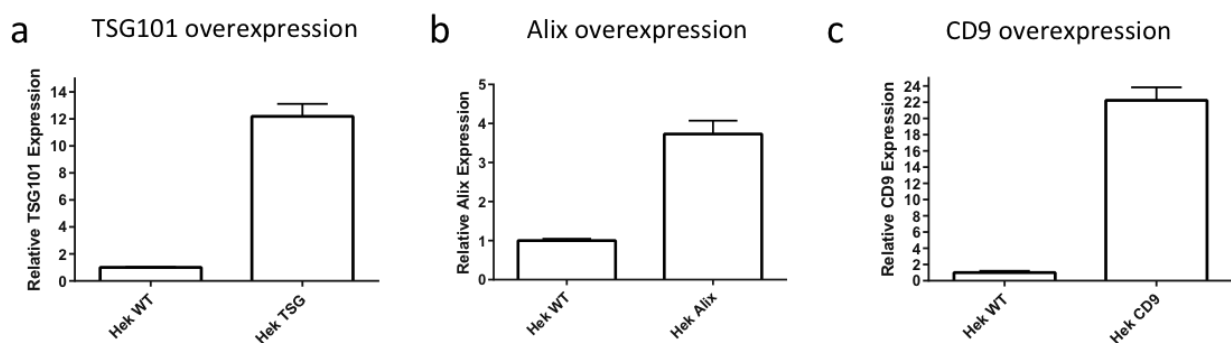


Figure 26: Overexpression of exosomal marker proteins CD9, Alix and TSG101 in HEK293 cells affects vesicle amounts and sizes. QPCR analyses were performed and displayed a 12-fold increase of TSG101 expression after lentiviral transduction. In stable expressing HEK-Alix cells a 4-fold increase was detected, whereas CD9 showed a 23-fold overexpression after stable cell line generation.

3. Results

QPCR analysis revealed a 12-fold increase of expression in stably TSG101 expressing HEK293 cells when compared to wildtype HEK293. The expression of Alix was 4-fold and the CD9 expression 23-fold increased in the respective stable cells.

To analyse the influence of overexpression on extracellular vesicles I measured size profiles of secreted vesicles by Nanoparticle Tracking Analysis (Figure 27). Reduced average-size of extracellular vesicles for HEK293-CD9_{GFP} cells with diameters of 160.9 nm (± 2.16 nm) compared to wildtype cells with 170.5 nm (± 2.46 nm) were observed. In contrast, an increased size was detected both for HEK293-TSG101 (197.2 nm ± 4.99) and HEK293-Alix cells (186.4 nm ± 4.92). Furthermore, CD9_{GFP} expressing cells produced significantly more extracellular vesicles ($6.27 \pm 0.54 \cdot 10^8$) in contrast to HEK293 WT ($4.86 \pm 0.15 \cdot 10^8$). However, the lowest EV concentrations were observed in HEK293-TSG101 ($2.24 \pm 0.25 \cdot 10^8$), and HEK293-Alix ($2.78 \pm 0.24 \cdot 10^8$) cell culture supernatants. By examining only vesicles in the size range of exosomes (i.e. 30-100nm) [6, 22, 60, 135] this trend was confirmed and for HEK293-CD9_{GFP} cell supernatants the effect was even stronger, I detected $68.76 \pm 8.45 \cdot 10^8$ particles for HEK293-CD9_{GFP} compared to $28.98 \pm 2.74 \cdot 10^8$ for HEK293 WT cells, reflecting a CD9 mediated 2.5-fold increase of secreted exosomes. Besides the reduced concentration of extracellular vesicles in HEK293-TSG101 and HEK293-Alix supernatants I also detected lower concentrations of exosome-sized vesicles ($8.65 \pm 1.15 \cdot 10^8$ particles for HEK293-TSG101 and $17.66 \pm 2.79 \cdot 10^8$ vesicles for HEK293-Alix cells).

In summary, I observed an increased amount of extracellular vesicles in response to CD9-overexpression, while both TSG101 and Alix overexpression resulted in a reduced abundance of extracellular vesicles. This observation was confirmed and even more obvious for vesicles within the exosome size-range of 30-100nm. The size of EVs increased, however, on the course of TSG101 and Alix overexpression but decreased after CD9 overexpression.

3. Results

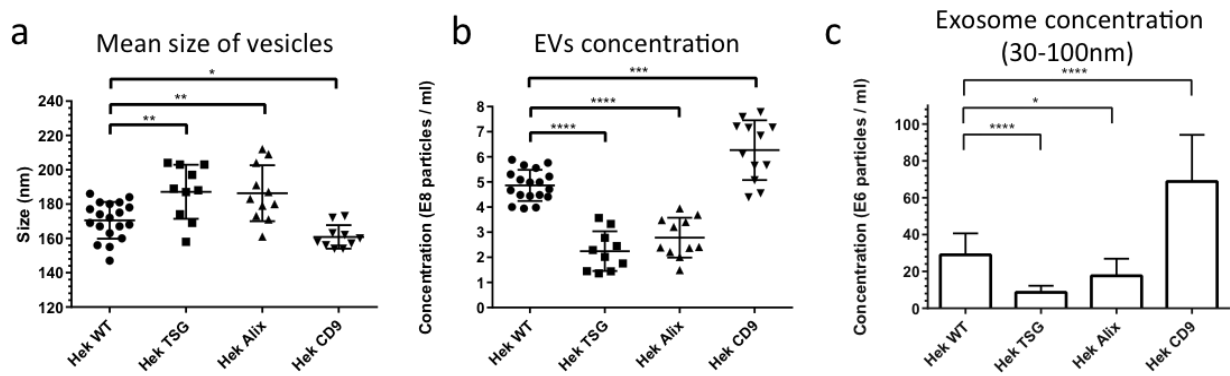


Figure 27: 19: Overexpression of exosomal marker proteins CD9, Alix and TSG101 in HEK293 cells affects vesicle amounts and sizes. Nanoparticle Tracking analysis of extracellular vesicles (a-c) showed significantly enlarged particles for HEK293-TSG101 and HEK293-Alix compared to the wildtype. The overexpression of CD9 led to a decreased average size of secreted vesicles (a). Total extracellular vesicle amount was decreased upon TSG101 and Alix overexpression, but the extracellular vesicle amount was significantly increased upon CD9 overexpression (b). For vesicles within the size range of exosomes (30-100nm) these trends were even more robust (c).

3.4.2 CD9 overexpression affects size and amount of extracellular vesicles in different cell types

To further investigate and to prove the significantly increased number of extracellular vesicles upon CD9 overexpression different stable CD9_{GFP} expressing cell lines were generated by LV transduction (HeLa CD9_{GFP}, Jurkat CD9_{GFP}, Raji CD9_{GFP} and HEKFT CD9_{GFP}). Secreted vesicles were examined in respect to their abundance and size distribution by NTA (Figure 28 and table 31).

A 22-fold overexpression of CD9 in HEK293FT cells (commonly used for the production of lentiviral vectors), resembled the observations made with HEK293 wild type cells. Human HeLa cells only reached a 2-fold increase of CD9 as seen in qPCR analysis, while the B-cell line Raji cells displayed the highest transgene expression level of CD9 (920-fold), and the human T-cell line Jurkat reached a 55-fold overexpression.

3. Results

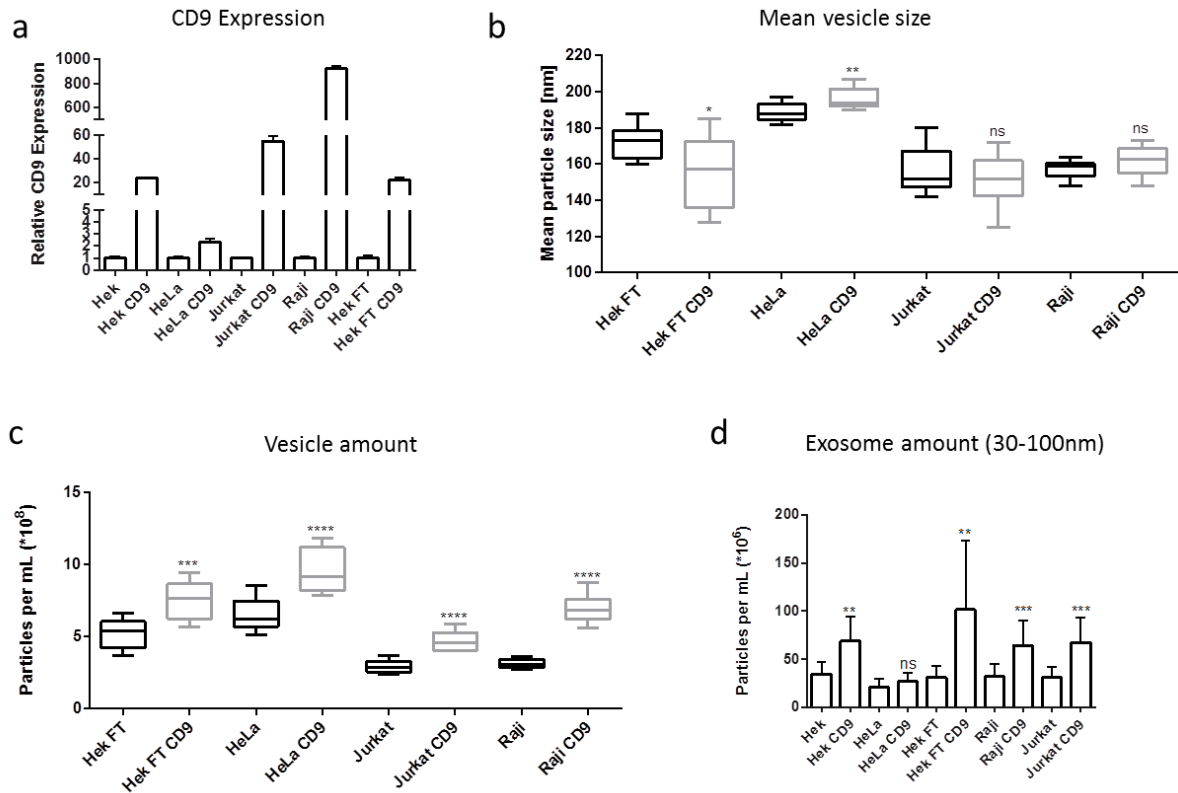


Figure 28: CD9 overexpression in HEK293 FT, HeLa, Jurkat and Raji cells. CD9 overexpression increases the amount of extracellular vesicles in all tested cell lines (a) Furthermore, the vesicle size was significant lower in HEK293 FT cells due to CD9 overexpression. Opposite effects were observed in HeLa cells and suspension cells like Raji and Jurkat, these extracellular vesicles show no change in size distribution compared to wildtype cells (b). Exosome amount was significant increased in all cell lines except HeLa and CD9 expression was quantified by qPCR (d).

The amounts of cell-free vesicles were increased in all cell culture supernatants of CD9 overexpressing cells when compared to the original cells. HEK293FT cells increased their particle concentration from $5.18 \pm 0.33 \cdot 10^8$ to $7.59 \pm 0.36 \cdot 10^8$ vesicles per mL, while HeLa cells increased their extracellular vesicles from $6.5 \pm 0.35 \cdot 10^8$ to $9.66 \pm 0.5 \cdot 10^8$ per ml. Both B- and T- cells exhibited in general a lower vesicle amount ($2.92 \pm 0.13 \cdot 10^8$ vesicles for Jurkat cells and $3.12 \pm 0.10 \cdot 10^8$ particles produced by Raji wild type cells). Nevertheless both suspension cell lines increased their extracellular vesicle production to $4.73 \pm 0.2 \cdot 10^8$ for Jurkat- CD9GFP cells respectively $6.99 \pm 0.31 \cdot 10^8$ particles detected in Raji- CD9GFP cells, indicating an approximately 2-fold higher concentration.

3. Results

Table 31: Summary of CD9, Alix and TSG overexpression and influence on EVs

Cell line	CD9 overexpression	Mean vesicle size	Vesicle amount	Exosome Amount
HEK293	-	170,5±2,46 nm	4,86±0,15*10 ⁸	28,98±2,74 *10 ⁶
HEK293 CD9 _{GFP}	23-fold	160,9±2,16 nm	6,27±0,54 *10 ⁸	68,76±8,45*10 ⁶
HEK293 FT	-	171,7±3,11 nm	5,18±0,33 *10 ⁸	30,96±3,80 *10 ⁶
HEK293 FT CD9 _{GFP}	22-fold	156,2±5,76 nm	7,59±0,36 *10 ⁸	101,5±19,32 *10 ⁶
HeLa	-	188,8±1,68 nm	6,50±0,35 *10 ⁸	20,66±2,83 *10 ⁶
HeLa CDP _{GFP}	2-fold	196.4±1,94 nm	9,66±0,50 *10 ⁸	26,98±3,02 *10 ⁶
Jurkat	-	155.8 ±3.71 nm	2,92±0,13 *10 ⁸	30,74±3,32 *10 ⁶
Jurkat CD9 _{GFP}	55-fold	151.8±3.79 nm	4,73±0,20 *10 ⁸	67,14±8,72 *10 ⁶
Raji	-	157.0 ±1.65 nm	3,12±0,10 *10 ⁸	32,01±3,89 *10 ⁶
Raji CD9 _{GFP}	920-fold	161.4 ±2.31 nm	6,99±0,31 *10 ⁸	64,37±7,37 *10 ⁶

Cell line	Alix overexpression	Mean vesicle size	Vesicle amount	Exosome Amount
HEK293	-	170,5±2,46 nm	4,86±0,15*10 ⁸	28,98±2,74 *10 ⁶
HEK293-Alix _{mCherry}	4-fold	186,4±4,92 nm	2,78±0,24 *10 ⁸	17,66±2,79 *10 ⁸

Cell line	TSG101 overexpression	Mean vesicle size	Vesicle amount	Exosome Amount
HEK293	-	170,5±2,46 nm	4,86±0,15*10 ⁸	28,98±2,74 *10 ⁶
HEK293-TSG101 _{mCherry}	12-fold	197,2±4,99 nm	2,24±0,25 *10 ⁸	8,65±1,15 *10 ⁸

Additionally reduced extracellular vesicle sizes in HEK293FT upon CD9 overexpression were detected (171.70 nm ±3.11 in HEK293FT and 156.20 nm ±5.76 in HEK293FT-CD9_{GFP}), which confirm the observations in HEK293. However opposite effects were observed in HeLa, where extracellular vesicle size was increased from 188.8 nm ±1.68 to 196.4 nm ±1.94 caused by CD9 overexpression. In suspension cells no significant change of extracellular vesicle size was detected.

Focussing on secreted vesicles with exosomal size (30-100nm) revealed a confirmation of the previously described trend and HEK293FT cells show an >3-fold increase of exosomes (from 30.96±3.80 *10⁶ to 101.5±19.32 *10⁶ particles/ml), whereas the suspension cell lines double their exosome production from 32.01±3,89 *10⁶ to 64.37±7.37 *10⁶ particles per mL for Raji cells, and, respectively from 30.74±3.32 *10⁶ to 67.14±8.72 *10⁶ particles per mL for Jurkat

3. Results

cells. Only for HeLa cells the amount of vesicles with exosomal size was not significantly changed ($20.66 \pm 2.83 * 10^6$ to $26.98 \pm 3.02 * 10^6$ particles per mL).

Taken together in HEK293FT, Jurkat and Raji cell culture supernatant an increased amount of extracellular vesicles after CD9_{GFP} overexpression was detected by NTA. However, HeLa cells displayed no significant increase of vesicles with exosome size, but at the same time the foreign CD9 expression was also the lowest in cell lines studied.

3.4.3 Cellular localization of CD9_{GFP}, Alix_{mCherry} and TSG101_{mCherry}

The CD9_{GFP} expression was also monitored by fluorescence microscopy (Figure 29). CD9_{GFP} was visualized mainly in the membranes of the adherently growing cells as well as suspension cells. The CD9_{GFP} overexpressing cell lines did not show any visible changes of their phenotype and displayed no increased mortality compared to the respective wildtype cells. Some accumulation of CD9_{GFP} as indicated by increased GFP fluorescence intensities was observed in cell-cell contact regions.

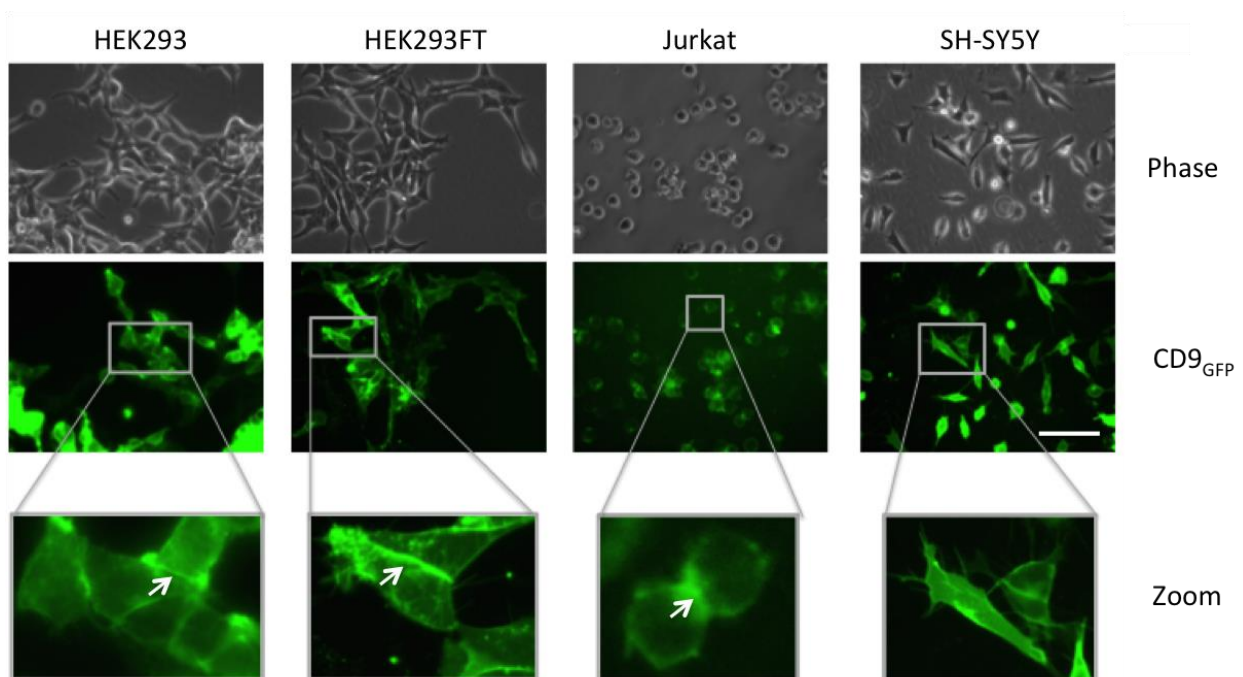


Figure 29: CD9 locate to the plasma membrane and cell-cell-contact surfaces in stably CD9-GFP expressing cell lines. Cell membrane localization of CD9_{GFP} was observed via fluorescence microscopy. Green fluorescence was detected with a fixed exposure time (1000 msec) after at least two weeks of Blasticidin selection. Membrane expression of CD9_{GFP} was detected in every tested cell line. White arrows indicate increased CD9_{GFP} expression on cell-cell contact areas. Scale bar = 100 μ m.

3. Results

Furthermore, I was able to generate stable expressing HEK293 TSG101_{mCherry} and Alix_{mCherry} cell lines by lentivirus transduction. In contrast to CD9_{GFP} overexpression an increased mortality rate was observed after lentiviral transduction. Cells with high TSG101_{mCherry} or Alix_{mCherry} expression (indicated by fluorescence microscopy) showed a round phenotype, whereas cells with lower TSG101_{mCherry} or Alix_{mCherry} expression presented cytoplasmic fluorescence with local accumulations (Figure 30).

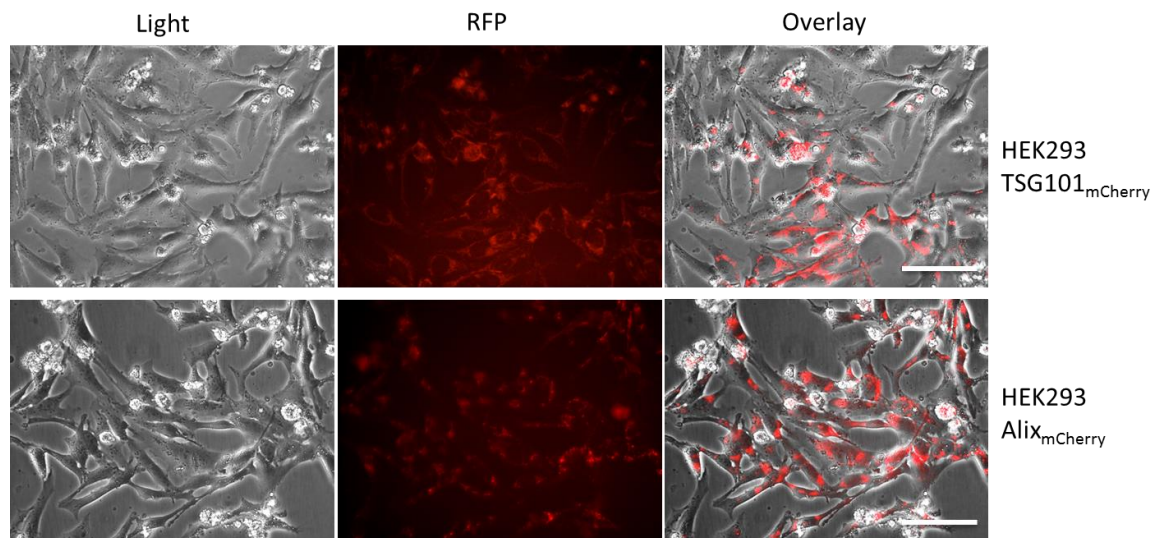


Figure 30: Alix and TSG101 overexpression in HEK293 cells visualized by fluorescence microscopy. HEK293 cells were transduced with VSVG LVs carrying Alix_{mCherry} or TSG101_{mCherry} as gene of interest. Cells were selected via Blasticidin and fluorescence microscopy was performed with a fixed exposure time (1000msec). Scale bar 100 μ m.

3.4.4 LV production workflow and produced LVs

Previous studies reported some positive influence of increased extracellular vesicle amounts on the transduction efficiency of recombinant adeno-associated viruses (AAV) and HIV [136, 137]. To examine these effects in response to increased levels of CD9 the HEK293FT-CD9_{GFP} cell line was utilized for LV production and the resulting virus titers and the transduction efficiency were compared. The general workflow is shown in Figure 31a. Three variants of lentiviral vectors were generated, i.e. a pseudotyped variant exposing the vesicular stomatitis virus glycoprotein (VSVG), the CD9_{GFP} variant and a combined VSVG-CD9_{GFP} lentiviral vector (Figure 31c). All three LV deliver RFP coding genetic information into the host cell, which can be detected by fluorescence microscopy or FACS analysis.

3. Results

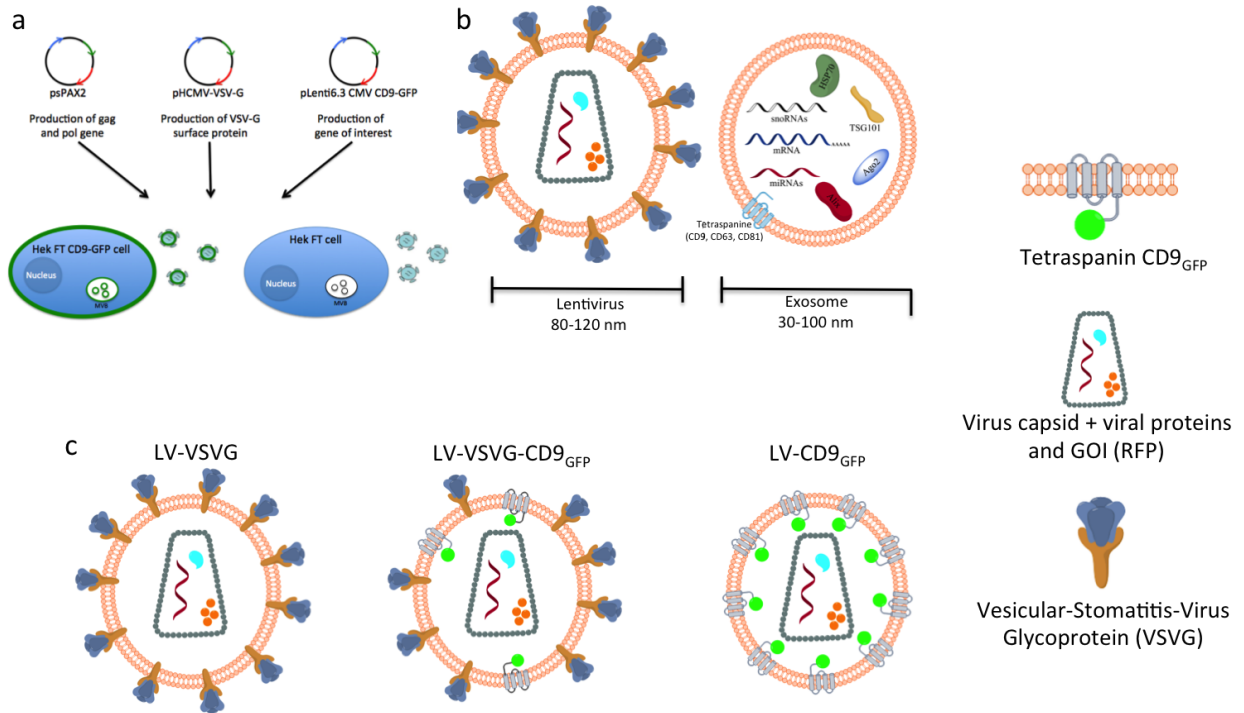


Figure 31: Procedure of Lentivirus production and comparison between exosomes and LVs. HEK293FT or HEK293FT-CD9 cells were transfected with three different plasmids encoding for envelope glycoproteins (i.e. CD9 and/or VSVG), viral capsid proteins and the gene of interest, here a red fluorescent protein (RFP) (a). LVs are shed from the cell membrane, and LVs produced in HEK293FT-CD9 cells carry additional CD9-GFP and/or VSVG within their envelope. Exosomes and LVs are depicted in (b) and show similar characteristics including in particular their size and partially the lipid contents. Three different kinds of LVs, i.e. exposing VSVG, CD9 or VSVG and CD9, were produced and are schematically shown in (c).

3.4.5 The CD9 mediated increase of extracellular vesicles boosts the transduction efficiency of lentiviral vectors

The putative effect of high CD9 expression and the resulting increase of EV release on LV performance were examined. The modified recombinant LVs were generated with VSVG as envelope protein (LV-VSVG) in standard HEK293FT and viruses carrying CD9_{GFP} and VSVG (LV-VSVG-CD9_{GFP}) on the virus envelope produced in HEK293FT-CD9_{GFP}. The incorporation of membrane proteins, in this case CD9_{GFP} and/or VSVG, into the envelope of the recombinant lentivirus is directly linked to virus budding. With an increased expression level and a higher abundance of specific proteins in membranous cell compartments the chances of incorporation into the envelope are dramatically increased. Surprisingly I detected in our previous experiments a higher infectivity of LV-VSVG-CD9_{GFP} on Jurkat and Raji cells compared to LV-VSVG. Lentiviruses with CD9 and VSVG as envelope proteins transduced 97% of Jurkat and 80% of Raji cells, whereas LV-VSVG LVs infected 45% of Jurkat and only

3. Results

6 % of Raji cells. Both viruses delivered the GFP reporter as GOI, which was examined by FACS analysis (Figure 32).

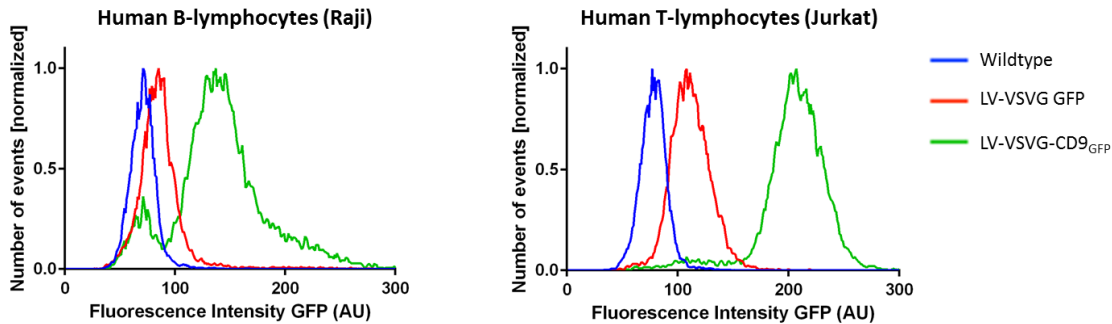


Figure 32: Lentiviral transduction of Raji and Jurkat. Raji and Jurkat cells were transduced with two different LVs and transduction efficiency was analysed after 72h by FACS analysis. LV-VSVG-CD9_{GFP} showed higher efficiency compared to LV-VSVG-GFP.

In order to undock the GOI (GFP) expression from the CD9_{GFP} expression LV-VSVG and LV-VSVG-CD9_{GFP} viruses carrying RFP as GOI were designed. Subsequently, the transduction efficiencies of the recombinant LVs and a set of negative controls lacking viral capsid or viral envelope proteins were analysed by fluorescence microscopy and FACS analysis (Figure 33-34). Equal amount of viruses (physical titer of $1 \cdot 10^7$ lentivirus particles according to p24 Elisa titration) were used for infections of equal amount of HeLa, HEK293 or SH-SY5Y.

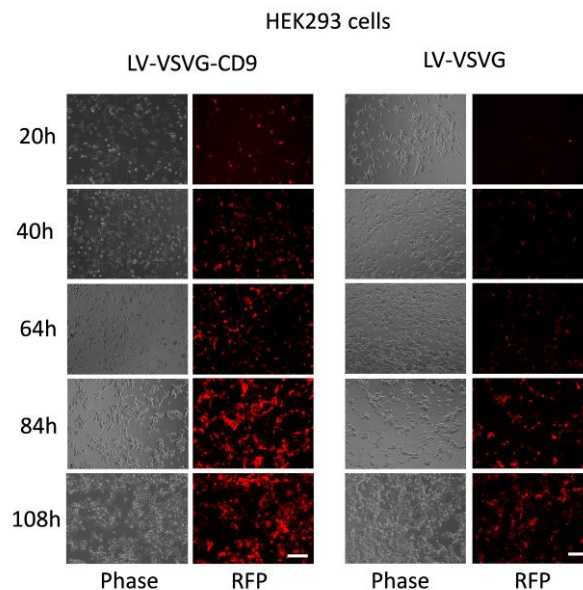


Figure 33: Transduction efficiency of LV-VSVG and LV-VSVG-CD9. Comparison of transduction efficiency was evaluated with LV-VSVG as a standard control and LV-VSVG-CD9 on HEK293. Successful transduction was confirmed via fluorescence microscopy in regular intervals from 20 to 108 hours after transduction. Scale bar 200 μ m.

3. Results

On HEK293 cells LV-VSVG-CD9_{GFP} revealed a faster and more efficient transduction, once after 40 hours 45% of the treated cells were transduced with a physical titer of $1 \cdot 10^7$, while at this stage the control LV-VSVG only reached 15% of the cells under the same conditions. Besides the faster onset of transgene (RFP) expression also increased transduction efficiency after 116 hours were observed. LV-VSVG-CD9_{GFP} transduced 85% of HEK293, while the maximum for LV-VSVG was 75% of cells. In HeLa similar observations were detected, since after 40 hours 22% of cells were transduced, whereas LV-VSVG only reached 8%. At the peak time 116 hours after infection the differences between transduction efficiencies was even more obvious than it was shown in HEK293 cells. LV-VSVG-CD9 transduced 48% of HeLa, while LV-VSVG led to RFP expression in only 20%. Additionally the influence of CD9 on LV transduction efficiency was tested on SH-SY5Y. 40 hours after transduction no remarkable differences in virus transduction was detected due to a low amount of RFP expression. The increased efficiency of LV-VSVG-CD9_{GFP} got more evident after 72h, since LV-VSVG-CD9_{GFP} infected 12% of SH-SY5Y while LV-VSVG remained at 4%. After 160 hours the general tendency from the experiments with HEK293 and HeLa was confirmed in SH-SY5Y. LV-VSVG transduced a maximum of 12% of cells and LV-VSVG-CD9_{GFP} transduced 23% with the same physical titer. Our findings were graphically summarized in figure 34.

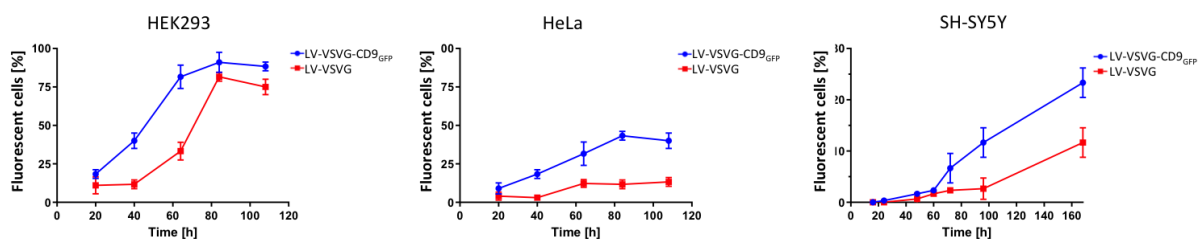


Figure 34: Transduction efficiency of LV-VSVG and LV-VSVG-CD9. Comparison of transduction efficiency was evaluated with LV-VSVG as a standard control and LV-VSVG-CD9 on HEK293. Successful transduction was confirmed via fluorescence microscopy in regular intervals from 20 to 108 hours after transduction. In the fluorescence microscopy analysis positive cells were quantified by manual counting and the transduction efficiency was calculated.

The transduction efficiency was further examined with a second method, i.e. FACS analysis, where the number of cells expressing RFP was quantified 108 hours post infection (Figure 35). The overall observation of increased efficiency of LV-VSVG-CD9_{GFP} as seen by fluorescence microscopy was confirmed. LV-VSVG-CD9_{GFP} was more efficient on HEK293 cells with transducing $46.53\% \pm 2.14\%$ of HEK293 cells compared to LV-VSVG, which infected only

3. Results

31.22%±0.25% of target cells. The same tendency was observed for HeLa and SHSY-5Y cells, where LV-VSVG-CD9_{GFP} transduced 10.81%±0.13% and 12.12%±0.67%, while LV-VSVG only infected 7.81%±0.25% of HeLa and 6.88%±1.11% of SHSY-5Y cells.

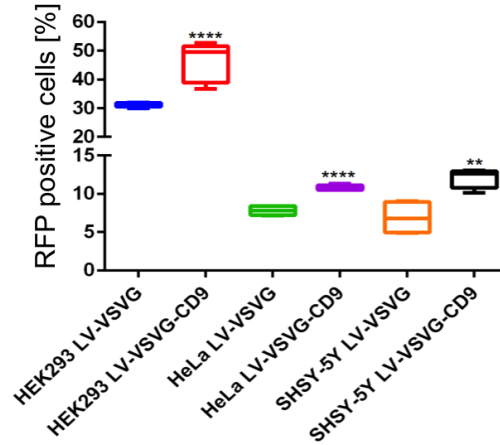


Figure 35: Transduction efficiency of LV-VSVG and LV-VSVG-CD9 determined by FACS analysis. Comparison of transduction efficiency was evaluated with LV-VSVG as a standard control and LV-VSVG-CD9 on HEK293, HeLa and SH-SY5Y cells. End-point analysis was performed by detecting virus encoded RFP in flow cytometry analysis 108 h after transduction.

Thus, LV-VSVG-CD9_{GFP} showed remarkably higher transduction rates and transgene expression efficiencies when compared to LV-VSVG. Cells transduced with LV-VSVG-CD9_{GFP} displayed higher RFP intensities, a faster onset of expression (Figure 33 and 34) and reached an increased amount of cells after 108 hours (Figure 35). The obtained results were summarized in table 32.

Table 32: Comparison of LV-VSVG and LV-VSVG-CD9_{GFP} transduction efficiency

Cell line	LV-VSVG Microscopy	LV-VSVG-CD9 _{GFP} Microscopy	LV-VSVG 108h FACS	LV-VSVG-CD9 _{GFP} 108h FACS
HEK293	75%	85%	31.22%±0.25%	46.53%±2.14%
HeLa	20%	48%	7.81%±0.25%	10.81%±0.13%
SH-SY5Y	12%	23%	6.88%±1.11%	12.12%±0.67%

3. Results

3.4.6 Overexpression of CD9 yields transduction competent LVs in absence of viral envelope proteins

To further investigate the beneficial effects of the tetraspanin CD9 on lentiviral transductions its capability to mediate membrane fusion in absence of VSVG was examined. Therefore three different LVs (LV-CD9, LV-VSVG and LV-VSVG-CD9_{GFP}) were used and checked for successful transduction events on HEK293 cells by RFP detection per fluorescence microscopy 72h post infection (Figure 36).

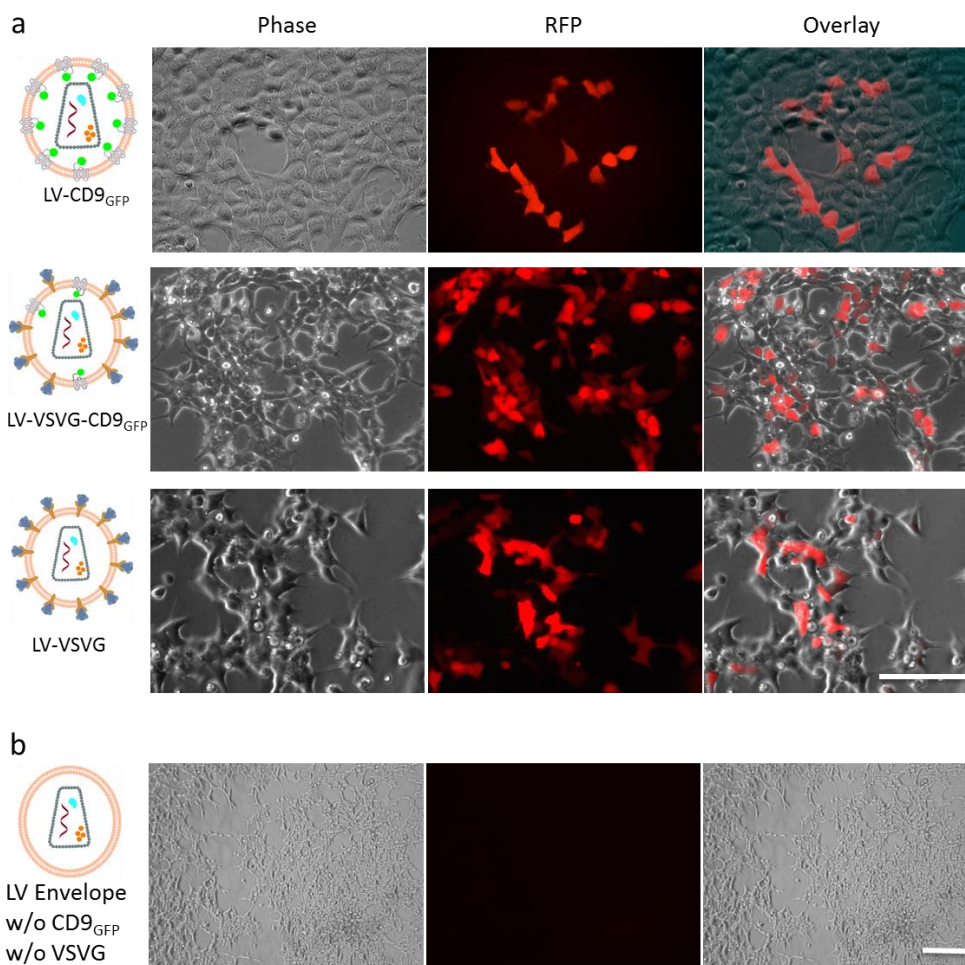


Figure 36: CD9 mediates fusion with target cell membrane. HEK293 cells were transduced with CD9, VSVG and VSVG-CD9 LVs. All tested LVs show expression after 72h. The highest efficiency was observed with LV-VSVG-CD9_{GFP} followed by LV-VSVG, but also the virus without any viral glycoprotein (LV-CD9_{GFP}) successfully infected a minor proportion of cells. Negative control without viral envelope proteins or CD9_{GFP} shows no transduction (b). Scale bar 100 μ m (a) respectively 200 μ m (b).

Indeed RFP positive cells were observed after 72h for all three tested viruses, including LV-CD9_{GFP} without VSVG on the virus envelope. To access whether the tested envelope

3. Results

glycoproteins can drive RFP expression by themselves, a set of control experiments in which all relevant virus components were omitted were designed and the putative transductions on HEK293 cells was analysed (Figure 36b and Figure 37). All negative controls like virus capsids lacking envelope proteins to drive tropism or envelope proteins without capsid did not lead to any RFP expression in the target cells.

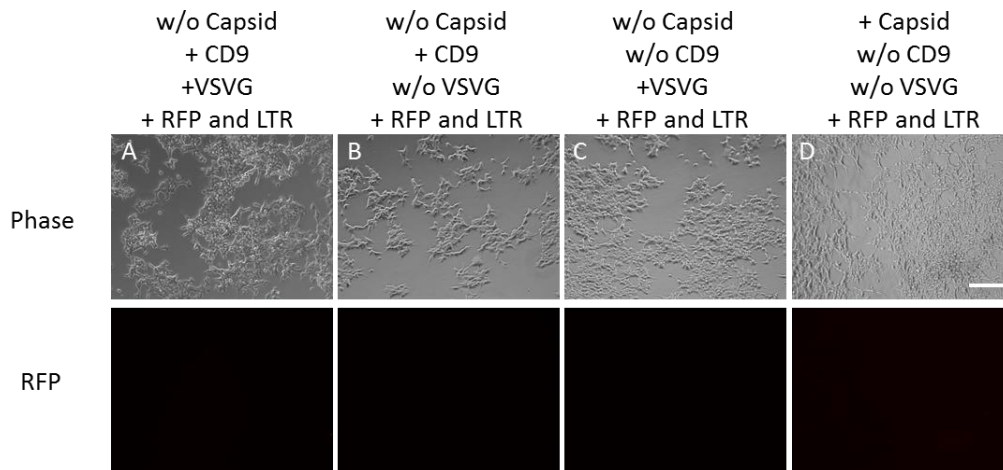


Figure 37: Negative control setup for transduction efficiency comparison of CD9, VSVG and CD9-VSVG virus. HEK293 cells treated with described negative controls show no expression of RFP after 72h. Scale bar 200 μm .

3.4.7 Influence of CD9 on LV production and amount tested by ELISA

The influence of different surface proteins on the productive amount of viruses was examined by determining the physical titer by p24-ELISA measurement (Figure 38). When only CD9_{GFP} was present on the virus surface the physical titer ($\text{TU}=4.13 \cdot 10^8 \pm 2.66$) did not significantly change when compared to the VSVG virus ($\text{TU}=3.43 \cdot 10^8 \pm 3.24$). Upon co-expression of CD9_{GFP} and VSVG a moderate increase of the virus amount was observed ($\text{TU}=4.70 \cdot 10^8 \pm 2.61$).

3. Results

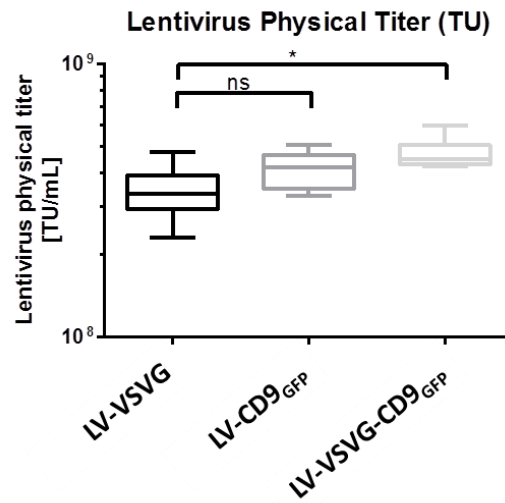


Figure 38: Physical titer of tested lentiviruses measured by Elisa. LV-CD9_{GFP} (TU= $4.13 \times 10^8 \pm 2.66$) show no increased physical titer compared to VSVG virus (TU= $3.43 \times 10^8 \pm 3.24$). If CD9 together with VSVG is present on viral surface a mild increase of physical titer (TU= $4.70 \times 10^8 \pm 2.61$) was observed.

3.4.8 Performance of CD9 LVs on primary cell material

Three recombinant and pseudotyped LVs were tested on primary rat central nervous system (CNS) material (E18 Wistar rat dissociated cortex cultures, Figure 39) to exclude misleading cell culture artefacts of CD9 fusion. These viruses (physical titer TU = 10^7 viral particles) were added to fresh isolated neuronal rat cells and incubated for 96 hours. All three viruses led to expression of the transgene (RFP) on primary rat CNS primary cells.

3. Results

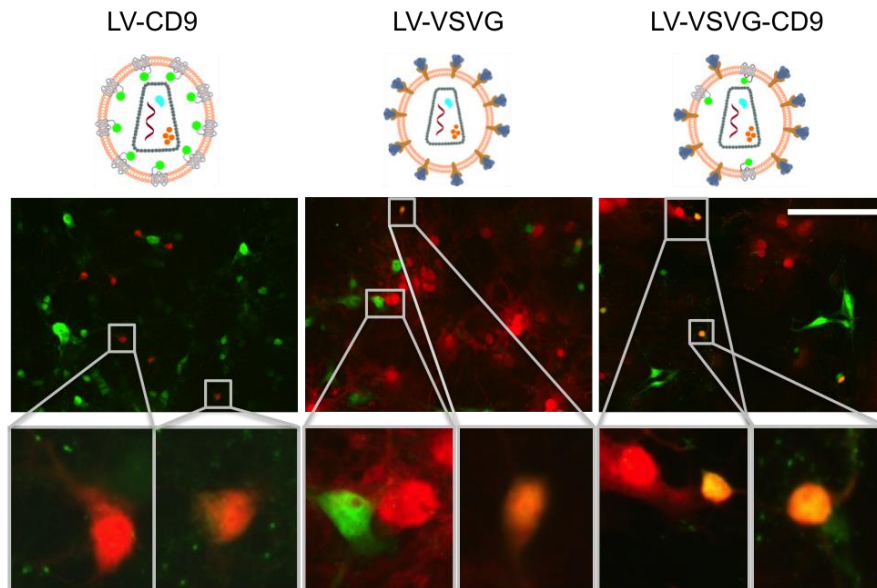


Figure 39: Lentivirus function on primary rat brain culture. Lentiviruses were tested on E18 Wistar rat dissociated cultures. After 96h cells were fixed and stained for NeuN (green). Transduced cells (red) partially show neuronal shape and NeuN expression (right side) for all tested viruses.

3.4.9 Cytoplasmic relocalization of CD9 during lentivirus production

During production of LVs in HEK293FT-CD9_{GFP} cells a change of CD9_{GFP} localization from the plasma membrane towards cytoplasmic speckles was observed (Figure 40). This observation was made both in confocal microscopy as well as in standard fluorescence microscopy 24, 48 and 72h after transfection with lentiviral plasmids (data not shown). With the increased resolution in confocal microscopy the focal CD9-containing accumulations were detected in the cytoplasm (speckles) as well, which was not as clearly detectable in fluorescence microscopy.

To examine the putative re-localization of CD9_{GFP} in HEK293FT-CD9_{GFP} cells during production of recombinant lentivirus, cells not showing signs of virus production (no RFP expression), and those during LV production (detected by RFP expression) were quantified by manual counting. Localizations of CD9_{GFP} was analysed by microscopy. Without virus production 86.5% of all cells displayed membranous localization of CD9_{GFP} and only 13.5% displayed a partially cytoplasmic localization, which was visible as diffuse stain or speckles. In contrast to this observation, upon virus production, which was confirmed by RFP expression, 98% of all cells exhibited cytoplasmic localization of the CD9_{GFP} tetraspanin, while only in 2% of the cells CD9_{GFP} remained in the plasma membrane.

3. Results

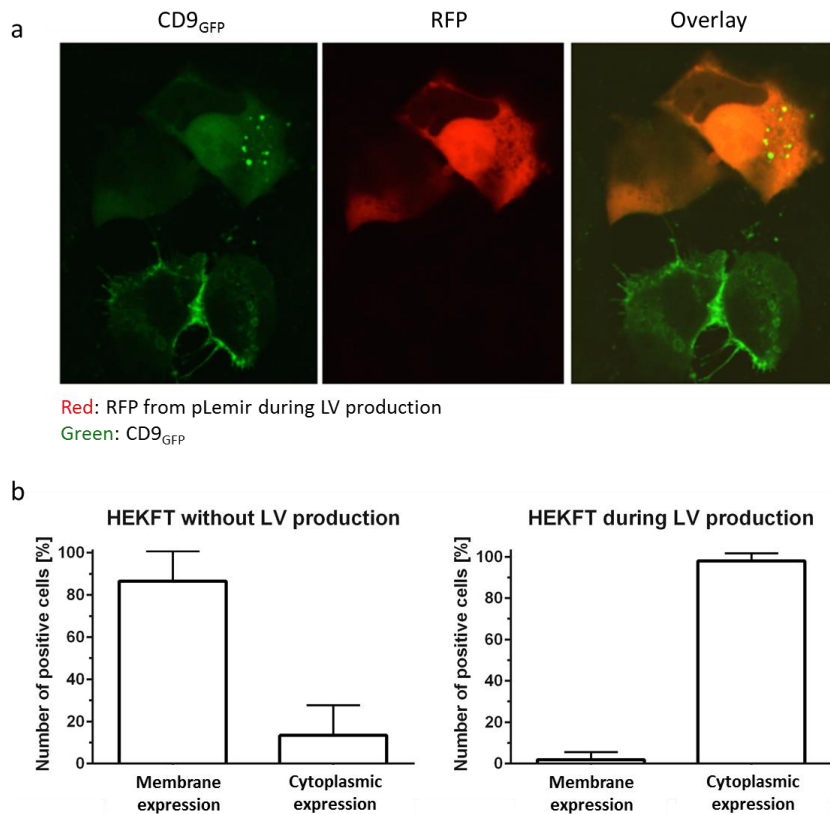


Figure 40: Localization of CD9_{GFP} in HEK293FT-CD9_{GFP} cells. Cellular localization of CD9_{GFP} was analysed by fluorescence and confocal microscopy. Confocal pictures of lentivirus producing cells (red and green) and HEK293FT-CD9_{GFP} wildtype cells (green) are depicted in (a). In addition fluorescence microscopy and cell quantification was performed and cellular localization of CD9 was analysed (b).

Taken together we showed that raised expression of the ESCRT proteins TSG101 and Alix lead to an overall decrease of secreted vesicles with enlarged average sizes. In contrast, enhanced levels of the tetraspanin CD9 resulted in significantly increased numbers of extracellular vesicles with smaller and more exosome-like size that were secreted from four different human cell lines. Intriguingly, exosomes and their biogenesis route display similarities to lentivirus and we studied the impact of CD9 expression on release and infectivity of recombinant lentiviral vectors. Although the titers of released particles were not increased upon production in high-CD9 cells we observed improved performance in terms of speed and efficiency of lentiviral gene delivery into numerous human cell lines including HEK293, HeLa, SHSY-5Y and also B- and T-lymphocytes. Furthermore, we demonstrate that enhanced CD9 enables lentiviral transduction in absence of any pseudotyping viral glycoprotein or fusogenic molecule. Our findings indicate an important role of CD9 for lentiviral vector and exosome

3. Results

biogenesis and point out a remarkable function of this tetraspanin in membrane fusion, viral infectivity and exosome mediated horizontal information-transfer [138].

3.4.10 CD9 influence on exosomal small RNA content

Since CD9 influenced the extracellular vesicle size and secretion, the CD9 overexpression effects on extracellular small RNA content of Raji cells were examined. Therefore extracellular vesicles of wildtype and CD9 overexpressing Raji were isolated and small RNA libraries were prepared. After next generation sequencing on the IonTorrent System and subsequent data analysis I generated heatmap, PCA plot and foldchange scatter plot with my own scripts in R (Figure 41).

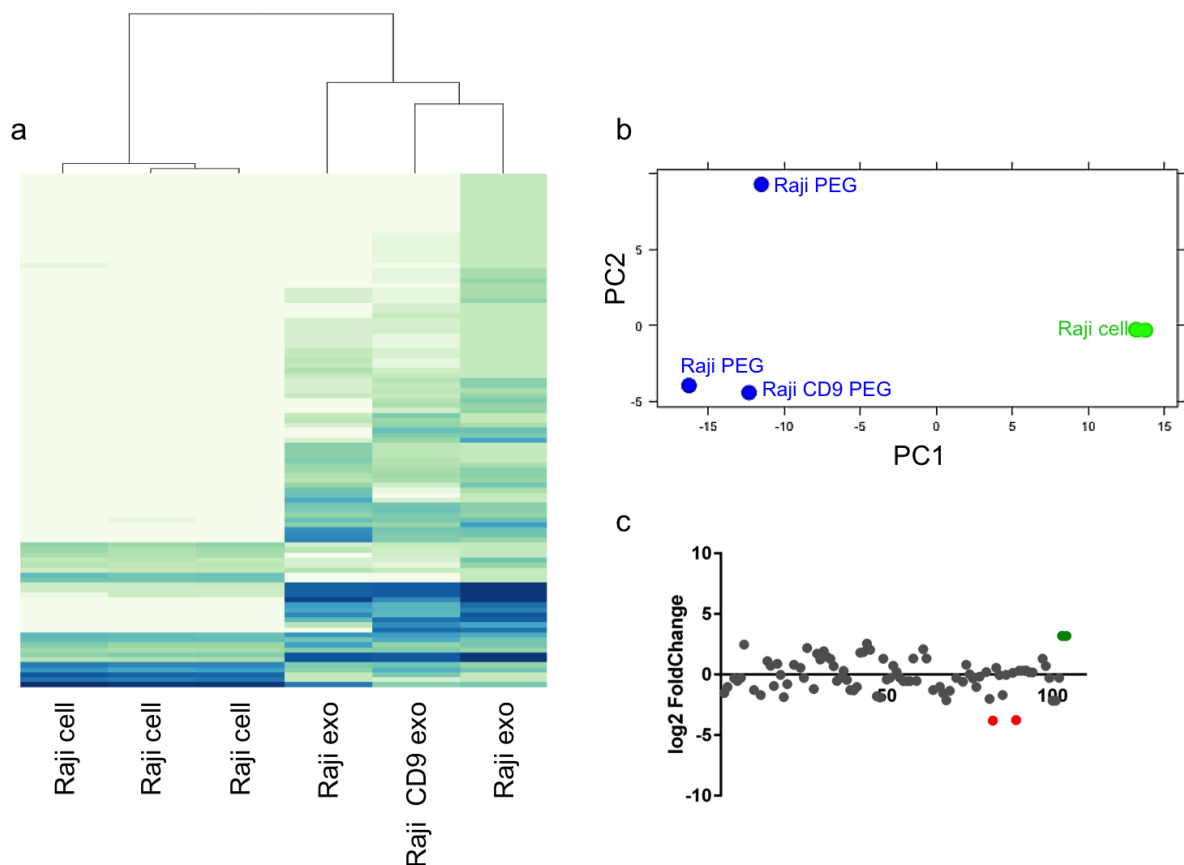


Figure 41: CD9 influence on exosomal miRNA content. Extracellular vesicles were isolated from wildtype and CD9 overexpressing Raji cells by PEG precipitation. After small RNA workflow and NGS sequencing heatmap (a), PCA plot (b) and foldchange scatter plot (c) were generated with DESeq package in R. Extracellular RNAs of wildtype and CD9 overexpressing Raji cells cluster together and both differ from cell samples. Principle component analysis revealed a greater consistency of Raji CD9 PEG and Raji PEG compared to Raji PEG2. Small RNA candidates with log₂foldchange higher than 3 were highlighted in green (enriched in wildtype extracellular vesicles) or red (enriched in extracellular vesicles of CD9 overexpressing Raji).

3. Results

The cluster analysis of all samples displayed differences between cellular and exosomal samples. However, the exosomal samples exhibited many parallels. Raji PEG samples showed high similarities with Raji CD9 PEG, whereas Raji PEG2 had a more distinct profile but still different compared to cellular samples. Two snoRNAs, i.e. U73a and U78, comprised the highest enrichment (9 fold) inside CD9 overexpressed extracellular vesicles followed by miR-30d-5p (6 fold), HBII-429 (5.5 fold) and miR-155-5p (4.5 fold). However, I detected four snoRNAs that were enriched in the PEG precipitated samples, mgU6-47 (14 fold), U24 (13.5 fold), U58B (4.5 fold) and U61 (4.5 fold). MiR-5585-3p was ranking fifth among the overrepresented small RNAs with 4-fold enrichment.

Table 33: Top5 overrepresented extracellular small RNA candidates of wildtype and CD9 overexpressing B-lymphocytes

smallRNA	Log2foldchange	Basemean PEG	Basemean CD9 PEG
U73a	3,18	1,81	16,38
U78	3,18	1,81	16,38
hsa-miR-30d-5p	2,57	12,23	72,44
HBII-429	2,47	2,05	11,34
hsa-miR-155-5p	2,19	29,70	135,44
mgU6-47	3,81	8,85	0,63
U24	3,75	16,99	1,26
U58B	2,16	2,81	0,63
U61	2,16	2,81	0,63
hsa-miR-5585-3p	2,12	8,23	1,89

Furthermore, I detected specific wildtype exosomal small RNA candidates, which were not detected in extracellular vesicles of CD9 overexpressing Raji cells. MiR-142-5p showed the highest expression of exclusively wildtype exosomal candidates followed by miR-1303, whereas the miRNAs miR-107, miR-15a-5p and miR-93-3p were only expressed on low level.

Table 34: MiRNAs exclusively present in exosomes of wildtype Raji

smallRNA	Log2foldchange	Basemean PEG
hsa-miR-142-5p	-Inf	8,61
hsa-miR-1303	-Inf	1,52
hsa-miR-107	-Inf	0,76
hsa-miR-15a-5p	-Inf	0,76
hsa-miR-93-3p	-Inf	0,76

3. Results

3.5. Role of EVs in cell-cell communication

3.5.1 Sequence motifs of secreted miRNAs of Jurkat and Raji

Although exosomes were already described in 1987 these EVs have only been recognized as a potent vehicles of intercellular communication over the past couple of years [27]. Since I detected specific patterns of extracellular small RNAs with specific sequence motifs in four human cell lines and recently published studies share these observations [40]. Increasing evidence suggests that small RNAs are actively loaded into EVs to modify target cells. To clarify these findings samples of Jurkat and Raji exosome small RNA sequence motifs were analysed (Figure 42).

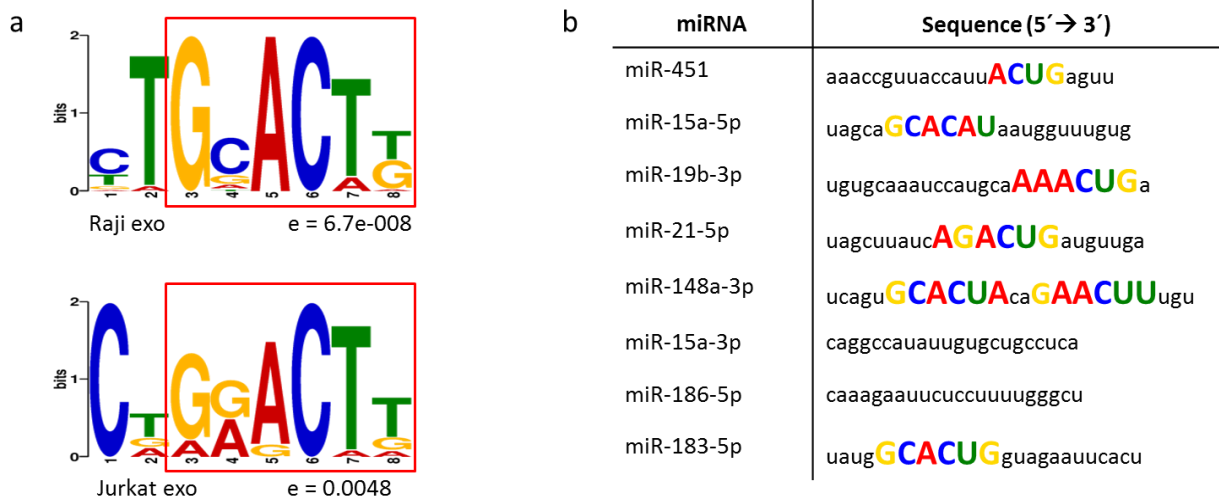


Figure 42: Exosomal miRNAs of Raji and Jurkat and their sequence motifs. Exosomes of Raji and Jurkat cells were isolated by PEG precipitation and the NGS workflow for small RNA sequences was performed. Raw reads were aligned to miRBase21 and sequence motifs were discovered by a motif-based sequence analysis tool (MEME). Because of the reverse transcription step during library syntheses DNA motifs were presented (T=U). Raji and Jurkat cells show high similarities to the discovered motifs (a). Some exosomal miRNAs discovered in Raji and Jurkat exosomes carry the observed motif, whereas miRNAs without this sequence (miR-15a-3p and miR-186-5p) were discovered too (b).

Sequence motifs of extracellular miRNAs showed high similarities in both studied cell lines. Nevertheless not all miRNAs found in extracellular vesicles contained this sequence motif, for example miR-15a-3p and miR-186-5p. However miR-148a-3p contains the motif twice.

3. Results

3.5.2 Cell-cell communication between Raji and Jurkat cells

In order to analyse the influence of EVs on the intracellular Raji miRNA content we treated Raji cells with Jurkat supernatant (including exosomes) and performed a comparative analysis via next generation sequencing. Therefor we analysed three biological replicas of untreated Raji cells and compared the small RNA content with two biological replicas of exosome treated Raji cells (Figure 43).

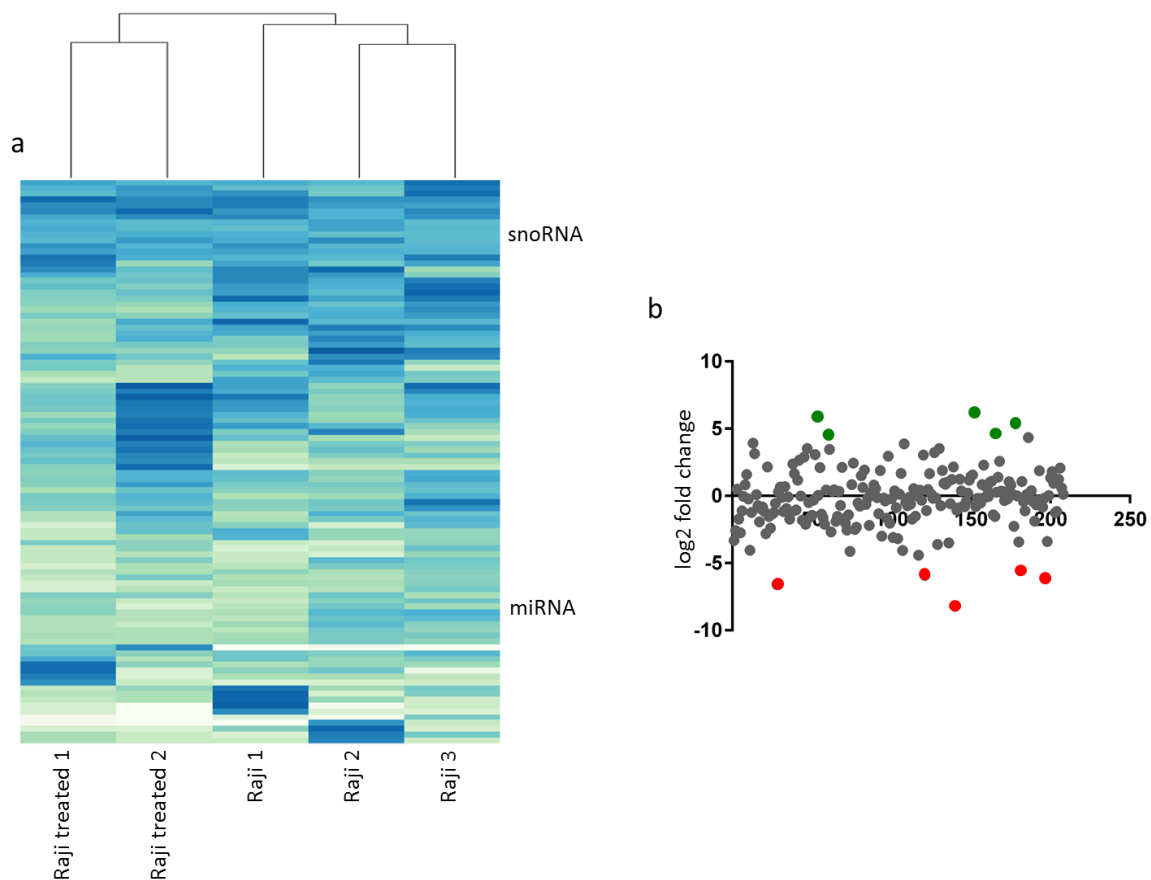


Figure 43: Co-cultivation of Raji cells with Jurkat cell culture supernatant and the resulting change of intracellular miRNA composition. Raji cells were co-cultures with Jurkat cell culture supernatant and small RNA was sequenced by NGS. Data was trimmed, aligned and analysed by DESeq package in R. Heatmap shows clustering of treated sample compared to wildtype Raji cells. Five top overrepresented (green) and underrepresented (red) miRNAs after Jurkat SN treatment were highlighted in a Log2 foldchange plot.

Cluster analysis revealed a different pattern of miRNAs in treated Raji cells compared to the wildtype. Foldchange calculation showed that miR-19b-1-5p was overrepresented after

3. Results

treatment with Jurkat supernatant together with miR-320a, miR-766-3p, miR-1307-5p and miR-193-3p (Table 35). However, candidates with decreased abundance were observed too, e.g. miR-106a-5p, miR-182-5p, miR-27b-3p, miR-9-3p and miR-146b-5p.

Table 35: Increased and decreased miRNA candidates after Jurkat exosome treatment

miRNA	Basemean Raji WT	Basemean Raji treated	Fold change
hsa-miR-19b-1-5p	15,79	48,15	0,335
hsa-miR-320a	20,09	57,04	0,35
hsa-miR-766-3p	18,66	51,69	0,36
hsa-miR-1307-5p	37,33	102,10	0,36
hsa-miR-193b-3p	66,02	171,01	0,38

miRNA	Basemean Raji WT	Basemean Raji treated	Fold change
hsa-miR-106a-5p	66,02	2,33	28,25
hsa-miR-182-5p	14,35	1,68	8,54
hsa-miR-27b-3p	20,09	2,63	7,64
hsa-miR-9-3p	15,78	3,50	4,50
hsa-miR-146b-5p	97,60	32,88	2,96

After the comparative analysis between exosome treated and untreated Raji cells we picked five miRNA candidates, carrying the exosomal secretion motif (Figure 42 and table 36). All candidates were high abundant in Jurkat exosomes and increased (miR-21-5p and miR-19b-3p) or unaffected (miR-15a-5p, miR-148a-3p) by exosome treatment insight Raji cells. For miR-451a no intracellular expression, neither in wildtype Raji cells nor in exosome treated cells, was detected. All miRNA candidates are listed in table 36.

3. Results

Table 36: High represented miRNAs in Jurkat exosomes and change in Raji cells upon treatment with Jurkat exosomes

miRNA	Basemean Raji WT	Basemean Raji treated	Fold change	Jurkat exosome
hsa-miR-21-5p	2428.55	4419.44	0,55	608,52
hsa-miR-19b-3p	3423.23	4790.87	0,71	2250,99
hsa-miR-15a-5p	241.13	210,33	1.146	153,48
hsa-miR-148a-3p	134.92	121,93	1.147	395.81
hsa-miR-451a	-	-	-	651.60

Further experiments focussed on high abundant exosomal miRNAs carrying the exosomal secretion motif and to investigate the putative cell-cell communication between Raji and Jurkat cells. For these miRNA candidates I performed an *in silico* analysis by checking the current literature and using and miRNA target database “miRTarBase” (Table 37).

Table 37: *In silico* analysis of miRNA targets

miRNA	<i>In silico</i> analysis of regulated genes	miRNA Databases (miRTarBase)
hsa-miR-15a-5p	Bcl-2[139]	BCL-2
hsa-miR-19b-3p	Bcl-2 [140]	DNMT1
hsa-miR-21-5p	DNMT1 [141]	BCL-2
hsa-miR-148a-3p	DNMT1 [142], Bcl-2 [143]	DNMT1, BCL-2
hsa-miR-451a		BCL-2

The miRNA target database revealed for all identified miRNA candidates B-cell lymphoma 2 (BCL-2) and/or DNA methyltransferase 1 (DNMT1) as common target genes. This observation was confirmed by several recent publications [139-143].

In the next experiment I cultivated Raji cells and treated them with Raji or Jurkat exosomes (isolated by PEG precipitation). Afterwards the expression of DNMT1 and BCL2 was tested via quantitative PCR analysis (Figure 44).

3. Results

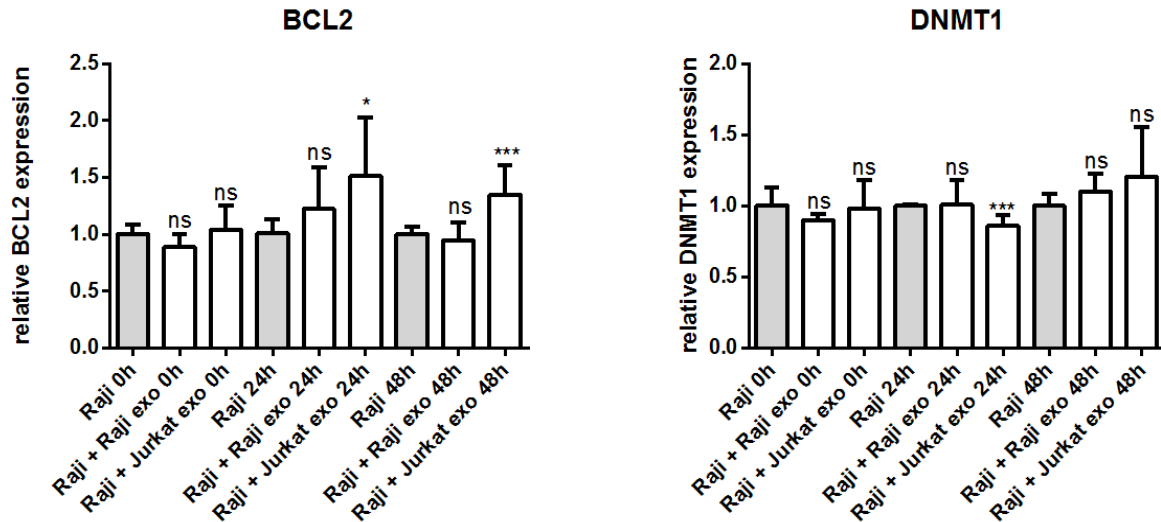


Figure 44: QPCR analysis of BCL2 and DNMT1 in Raji cells. Raji cells were treated with Jurkat or Raji exosomes and gene expression of BCL2 and DNMT1 was analyzed after 0h, 24h and 48h. For BCL2 no change in gene expression was observed after 0h. After one day the gene expression of BCL2 was non significant increased by Raji exosomes, while a treatment with Jurkat exosomes showed a significant increase on mRNA level. After 48h no change in gene expression by Raji exosomes was observed, whereas Jurkat exosomes lead to a significant increase in gene expression. For DNMT1 no significant change compared to wildtype Rajis was observed with any treatment. After 24h a significant reduction of DNMT1 gene expression was detected by Jurkat exosomes, however this effect dissappeared after 48h.

Immediately after adding the exosomes to Raji cells no effect on gene expression of BCL2 and DNMT1 was detected. After 24 h the BCL2 expression was 51% increased upon treatment with Jurkat exosomes, while Raji exosomes show no effect. 48 h post treatment the effects remains stable, we observed a 35 % increase of Bcl-2 expression upon Jurkat exosome treatment ($p < 0.05$).

In contrast I observed a 15 % reduction ($p < 0.05$) of DNMT1 after 24h upon treatment with Jurkat exosomes, whereas Raji exosomes lead to no effect. 48 h post treatment with Jurkat exosomes no change in gene expression was observed.

In summary I analysed exosomal miRNAs of Raji and Jurkat and selected candidates by their sequence motif and expression change in Raji cells after treatment with Jurkat exosomes. In an *in silico* analysis I discovered two target genes and analysed their expression after treatment with extracellular vesicles of Raji or Jurkat cells, where I observed an significant decrease of DNMT1 expression upon Jurkat EV treatment and a significant increase of BCL2 expression due to treatment with Jurkat exosomes.

3. Results

3.5.3 Cell-cell communication analysis by a novel dual reporter gene toolbox

After candidate selection and gene expression analysis small effects on gene expression of BCL2 and DNMT1 were observed (see 3.5.2). A key role for exosomes is postulated for intracellular communication, however the exact mechanisms remain elusive. In order to analyse putative cell-cell communication on a single cell level, I used a novel reporter gene toolbox [144]. This reporter gene assay is based on a construct with two different fluorescence proteins, cyan fluorescent protein (CFP) and yellow fluorescent protein (YFP). While CFP carries a complete complementary miRNA sequence at the 3'UTR region, YFP is unaffected and is not influenced by miRNAs. CFP and YFP intensities of each cell were measured 48 h post treatment by flow cytometry. We designed "non cognate" controls to test the unaffected expression of both proteins inside HEK293 cells. In Figure 45a a proportional increase of YFP and CFP was detected for this control. Using constructs with a miRNA target site (e.g. miR-23a-3p or miR-27a-3p) inserted into the 3'UTR region of CFP a reduction of CFP/YFP ratio was observed (Figure 45 a/b), indicating a miRNA binding and translational repression of CFP. The reduction of CFP expression is more pronounced for the miR-27a-3p construct, reflecting the observed effects after luciferase assay analysis (data not shown).

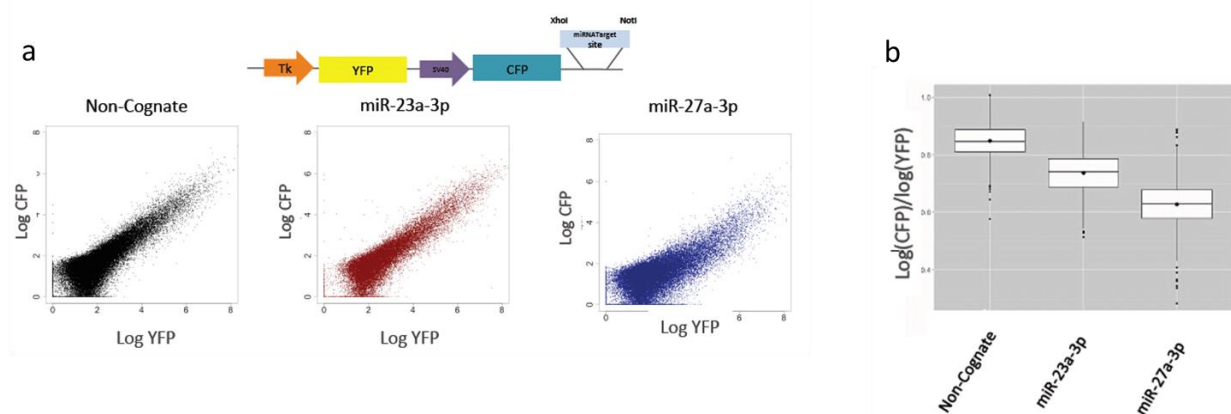


Figure 45: Principle of the dual fluorescence reporter gene toolbox and miRNA characterization. Two different fluorescent proteins (CFP and YFP) were expressed from one plasmid under two different promoters (a). Furthermore, CFP contains a perfect target region for a miRNA within its 3'UTR region. HEK293 cells were transfected with the plasmid-miRNA target combination and fluorescence intensity was evaluated after 72 h. A non-cognate control, miR.23a-3p and miR-27a-3p were studied. The CFP/YFP ratio was reduced for miR-23a-3p and miR-27a-3p but remains for the negative control plasmid (b), indicating a miRNA binding followed by transcriptional repression of CFP for miR-23 and miR-27. CFP repression was more pronounced for miR-27a, reflecting the results obtained by luciferase assays (data not shown).

3. Results

For the following experiments I used two controls with non-human complementary miRNA sequence sites. Both controls show a proportional increase of YFP and CFP, even after treatment with Jurkat or Raji exosomes (Figure 46). MiRNAs show no effect on CFP expression, confirming the complementary non-human miRNA sequence sites. For every performed experiment I used at least two controls to confirm the reliability of the reporter gene assay.

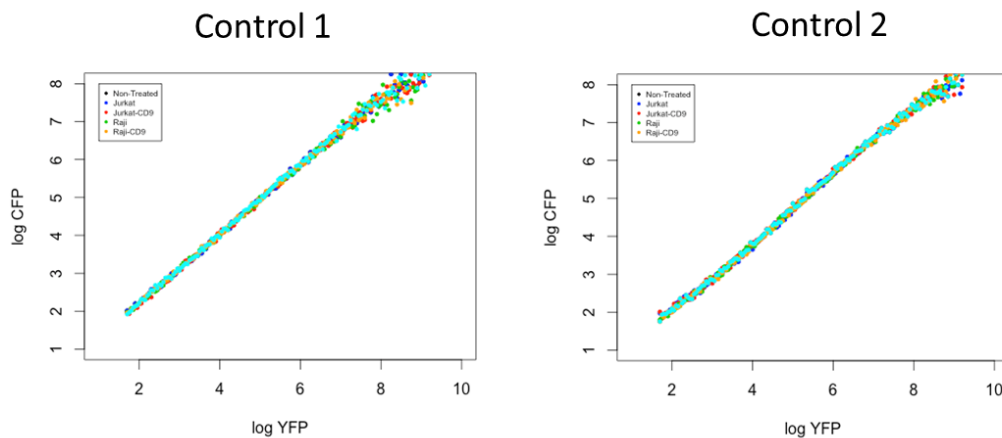


Figure 46: Non cognate controls for dual reporter gene assay. Two negative controls containing a non human miRNA target site were used. Transfected HEK293 were directly used for FACS analysis or further treated with Jurkat, Jurkat-CD9, Raji or Raji-CD9 exosomes. All samples show a linear behaviour, indicating a constant expression of both proteins without any miRNA influence.

For candidate miRNAs, which were selected in accordance to their high abundance in exosomes (i.e. miR-451a miR-148a-3p), no effects on CFP expression was detected. Furthermore, I tested a third non cognate control (GL-2), which also showed a proportional behaviour of CFP and YFP expression. To elucidate an uptake of exosomes we performed an exosome treatment and analysed the CFP and YFP expression. All candidates showed a linear YFP/CFP expression indicating no influence of exosomal treatment on the intracellular miRNA content (Figure 47).

3. Results

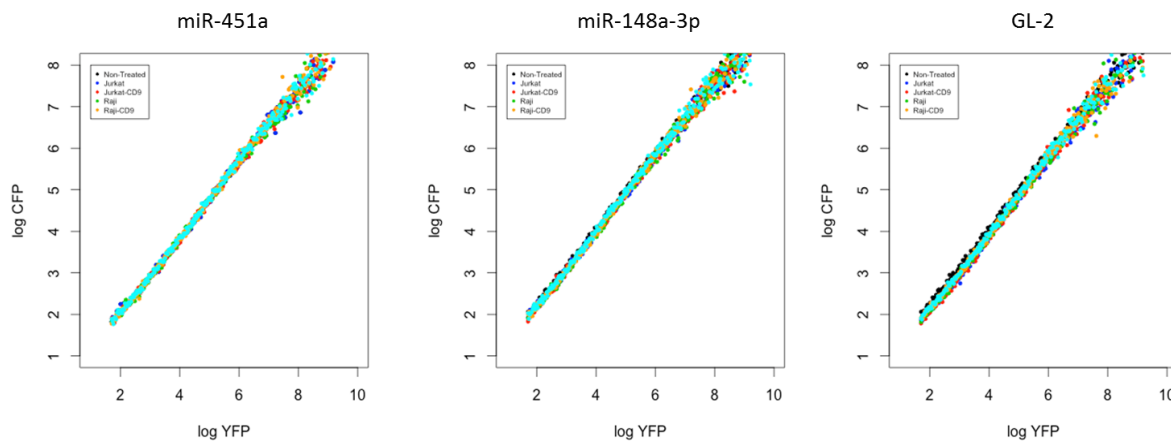


Figure 47: Functional characterization of miR-451a, miR-148a-3p and GL-2. MiRNA target sites were inserted in the 3'UTR site of CFP and transfected into HEK293 cells. Cells were treated with exosomes and fluorescence intensities were analysed by flow cytometry. No change in YFP/CFP ratio was observed for the tested candidates and treatment with Raji or Jurkat exosomes show no effect.

Besides miR-451a and miR-148a-3p I tested a construct containing the complementary sequence of miR-15a-5p (Figure 48). A non-cognate control (black) was used to identify efficient and successful transfection. The used construct lead to a CFP reduction in untreated HEK293 cells, indicating miRNA binding to the complementary miRNA sequence. To analyse an exosomal uptake HEK293 cells were treated with Raji and Jurkat exosomes and CFP and YFP expression was compared to untreated cells. None of the exosome treatments led to a reduction of CFP expression, indicating no exosomal uptake and miRNA release insight HEK293 cells.

3. Results

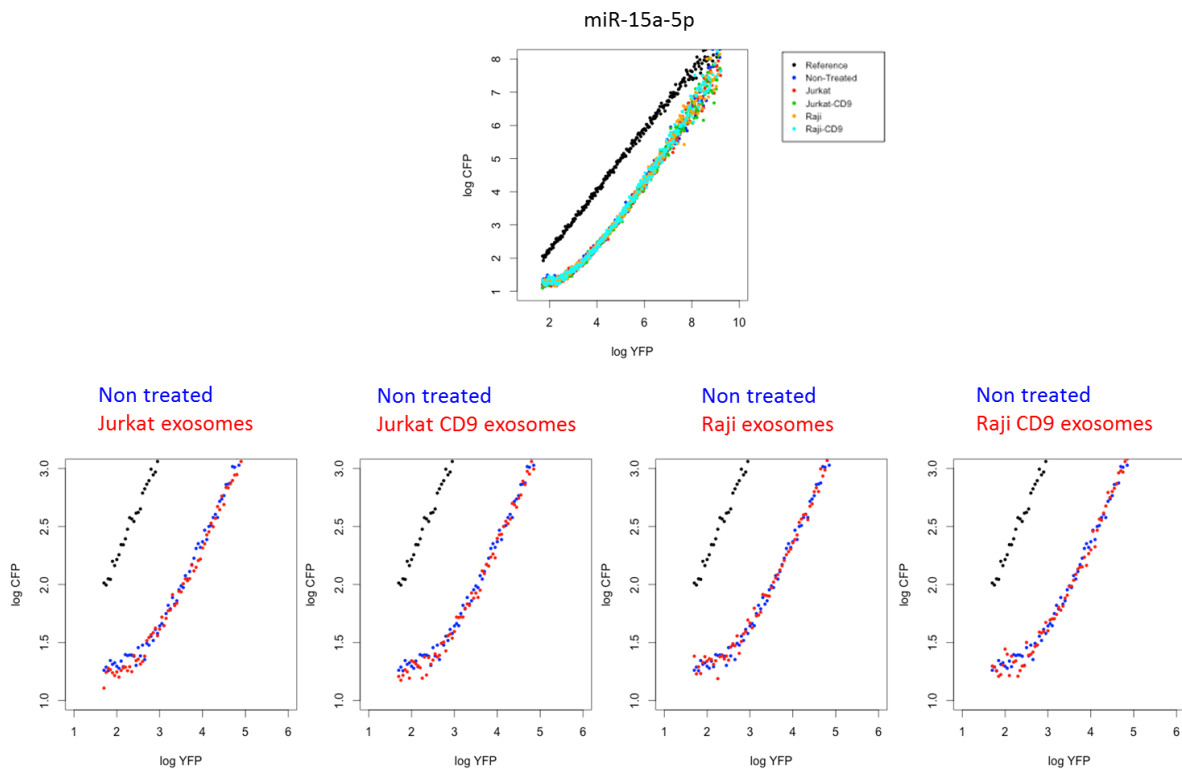


Figure 48: Functional characterization of miR-15a-5p and influence of exosome treatment. MiR-15a-5p target site was inserted into 3'UTR site of CFP and construct was transfected into HE293 cells. Non-cognate control (black) showed proportional YFP/CFP ratio indicating a successful transfection. CFP/YFP ratio was reduced for miR-15a-5p target site (blue), indicating miRNA binding to the full complementary miRNA sequence at the 3'UTR of CFP. To analyze a putative exosome uptake cells were treated with Raji or Jurkat exosomes (red). All treatments lead to a comparable reduction compared to wildtype cells, indicating no exosomal uptake and miRNA release.

For a miR-21-5p construct stronger silencing effects on CFP expression (blue) compared to the miR-15a-5p construct were observed (Figure 49). Non cognate control was used for identification of efficient and successful transfection. Treatment with Jurkat or Raji exosomes (red) lead to no further reduction of CFP expression, indicating no efficient exosomal uptake and miRNA release.

3. Results

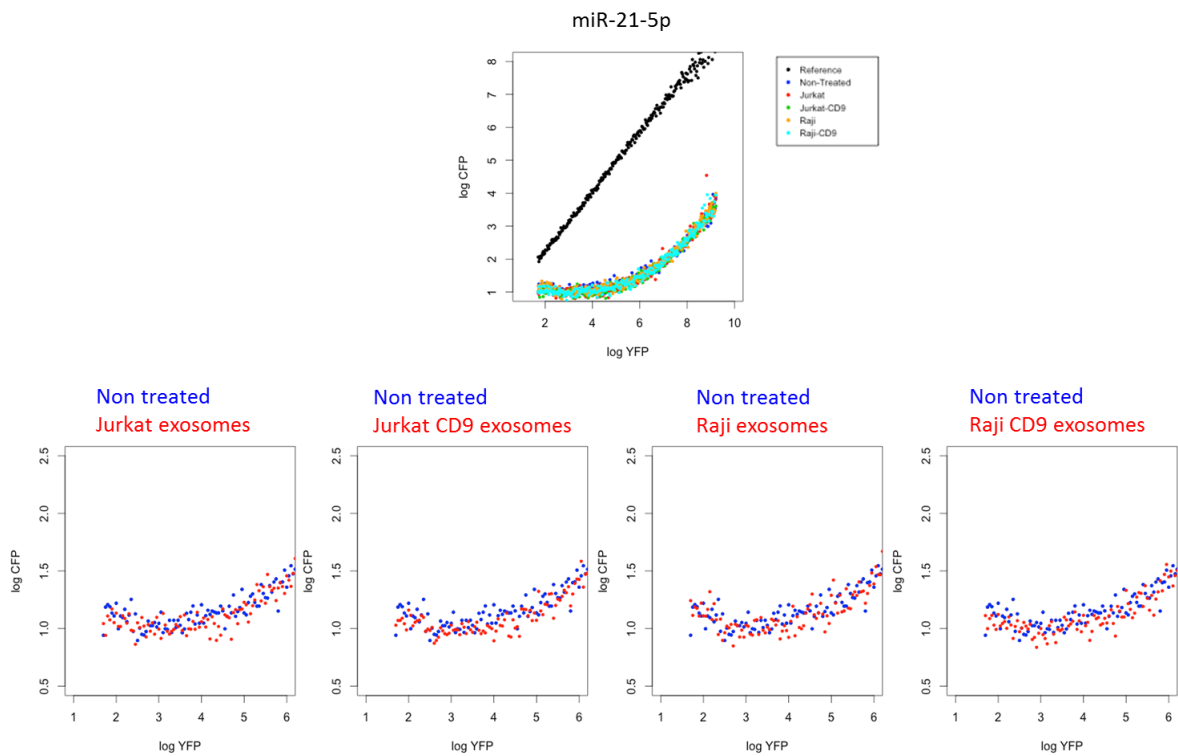


Figure 49: Functional characterization of miR-21-5p and influence of exosome treatment. MiR-21-5p target site was inserted into 3'UTR site of CFP and construct was transfected into HE293 cells. Non-cognate control (black) showed proportional YFP/CFP ratio indicating a successful transfection. Strong reducing effects on CFP/YFP ratio compared to non cognate control was observed for the miR-21-5p construct, indicating an efficient miRNA binding to the complementary miR-21-5p sequence. To confirm an exosomal uptake and miRNA release HEK293 cells were treated with Jurkat and Raji exosomes. No exosome treatment led to an increased CFP reduction, indicating no exosomal uptake and miRNA release in HEK293 cells.

Eventually I tested the functionality of miR-19b-3p in HEK293 cells and the influence of exosome from B- and T-lymphocytes (Figure 50). MiR-19b-3p showed a weaker silencing functionality compared to miR-21-5p but acted stronger compared to miR-15a-5p. Upon exosome treatment the functionality was slightly increased in low fluorescent cells (log YFP between 2 and 4). CFP fluorescence was reduced for a minor extend all tested exosome treatments, indicating a functional transfer of exosomes, successful release and functionality of miR-21-5p.

3. Results

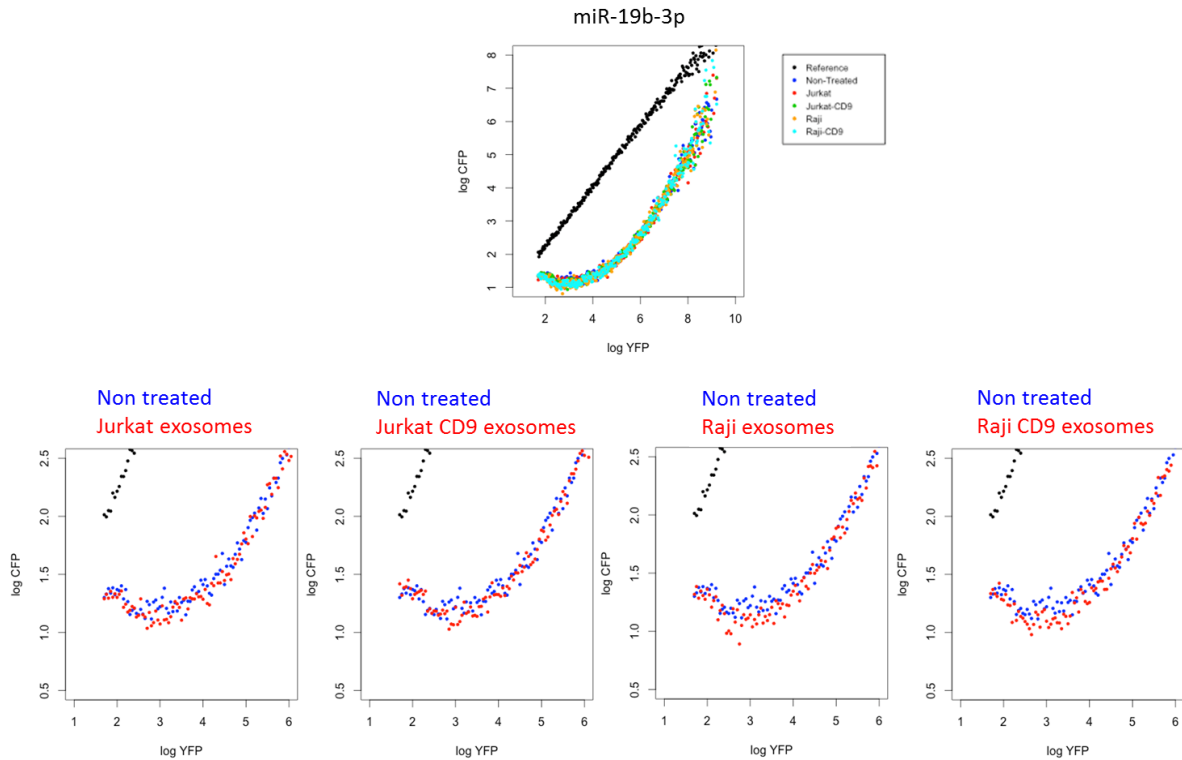


Figure 50: Functional characterization of miR-19b-3p and influence of exosome treatment. MiR-19b-3p target site was inserted into 3'UTR site of CFP and construct was transfected into HE293 cells. Non-cognate control (black) showed proportional YFP/CFP ratio indicating a successful transfection. MiR-19b-3p led to a strong reduction of CFP, indicating a miRNA binding to the complementary region in HEK293. Exosome treatment shows small effects on CFP expression, CFP showed a stronger downregulation between log2 and log4 YFP expression for all exosome treatments.

In order to use the reporter gene system with a non-endogenous miRNA I designed a construct containing a GL-2 target sequence in the 3' region of CFP. GL-2 contains a secretion motif (Figure 51) and should theoretically be exported into exosomes.

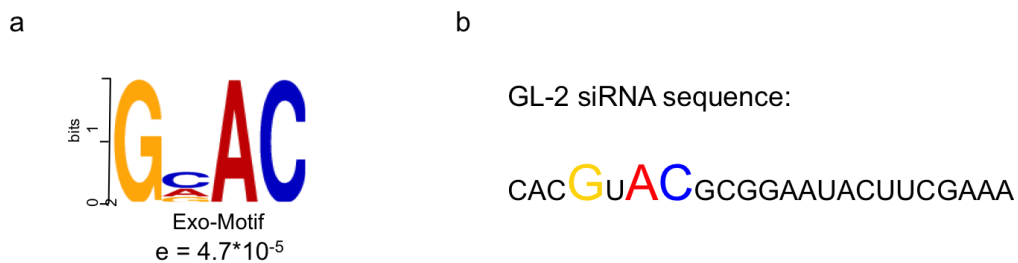


Figure 51: Exosomal secretion motif and comparison to GL-2 siRNA sequence. The secretion motif of our generated next generation sequencing data of 4 human cell lines was analyzed by DESeq package in R in combination with the online motif tool MEME (a). GL-2 siRNA contains 3 of 4 nucleotides of the secretion motif (b). The second nucleotide differs from the secretion motif, nevertheless this nucleotide is highly variable.

3. Results

HEK293 FT CD9 cells were transduced with a GL-2 siRNA and the supernatant including the exosomes was transferred to HEK293 wildtype cells. After transfection of the control plasmid or GL-2 plasmid the influence on CFP expression was analysed by flow cytometry (Figure 52).

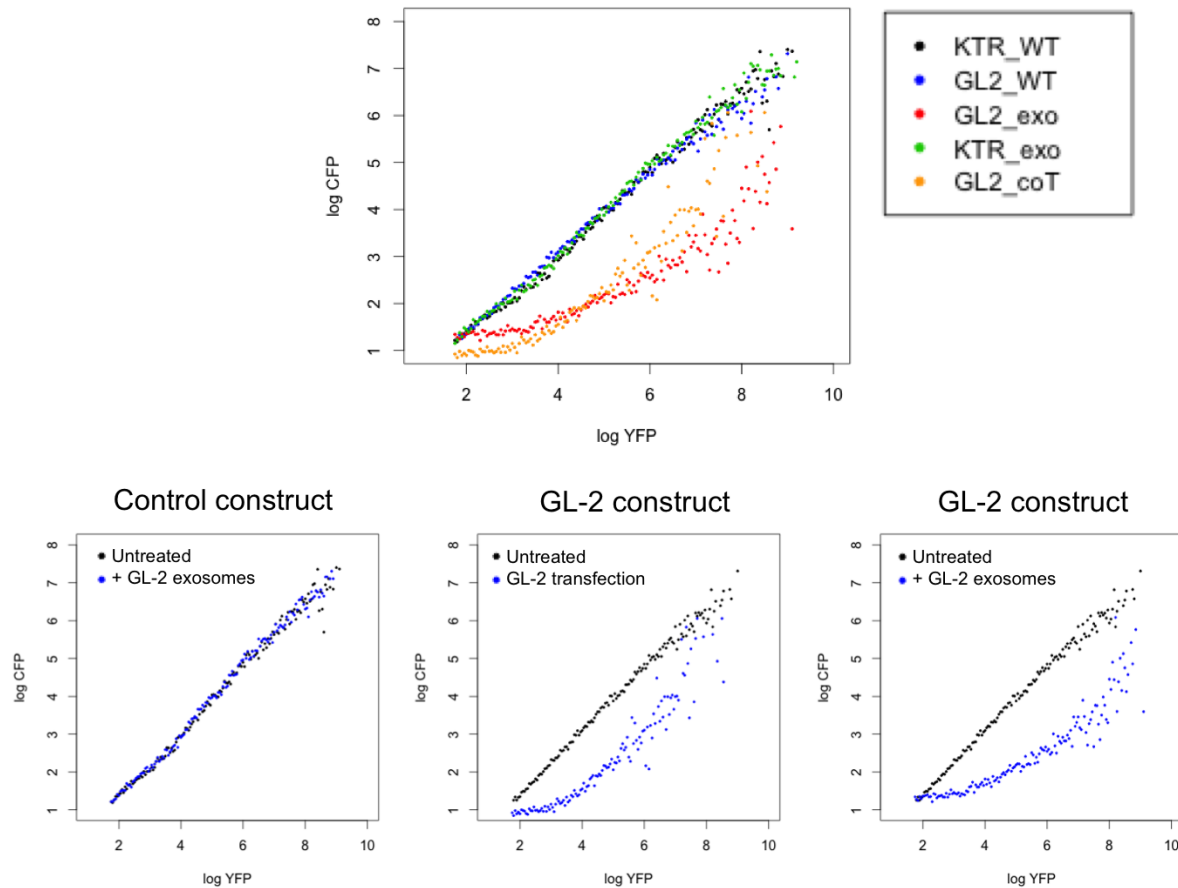


Figure 52: Functional characterization of non-endogenous GL-2 transferred by lipofection or extracellular vesicles. HEK FT CD9 cells were transfected with GL-2 siRNA and supernatant was transferred 48h post transfection to HEK293 wildtype cells. The functionality of GL-2 was analyzed by flow cytometry. The negative control showed no influence upon exosome treatment, while analyzing the GL-2 construct a reduction of the CFP signal was observed after exosome treatment. As a positive control a cotransfection with GL-2 construct and GL-2 siRNA was performed and reduction of CFP expressions was observed. Comparing the GL-2 cotransfection and GL-2 exosome treatment stronger effects were seen at lower fluorescence intensities (log YFP between 2 and 4) in the cotransfection, while at higher fluorescence intensities the effect appeared stronger for the exosome treatment.

The control plasmid with a non-human miRNA target sequence at the 3' end of CFP exhibited a linear behavior for CFP and YFP expression which also remained unaffected by treatment with GL-2 loaded exosomes. As a positive control I used a construct with a GL-2 target sequence at the 3' end of CFP. Using this control a linear behavior of CFP and YFP expression

3. Results

was observed in HEK293 wildtype cells. However after exosome treatment a reduction of CFP expression was observed, indicating an uptake of GL-2 loaded exosomes and activity of the transferred GL-2 siRNA inside the cell and the corresponding inhibition of CFP expression. As a positive control I used a cotransfection of GL-2 siRNA and GL-2 sensor construct. Similar effects compared to the exosome treatment were observed. Nevertheless the GL2 cotransfection showed stronger target repression at low fluorescence intensities (log YFP 2-4), while a stronger effect at high fluorescence intensities (log YFP > 4) was observed for the exosome treatment.

Nevertheless free Lipofectamine complexes or free-floating siRNAs can influence the obtained results. To check the effect of free siRNAs and Lipofectamine I transfected HEKFT-CD9 and HEKFT wildtype cells with GL-2 siRNA by lipofection. The supernatant of transfected cells was harvested 48h post transfection and was used as a positive control due the effects observed before (Figure 52). Additionally cells were washed 6h post transfection to remove residual Lipofectamine complexes and siRNAs and supernatant was harvested after 48h to allow exosome production. As controls HEKFT-CD9 and wildtype cells were treated with GL-2 siRNAs without Lipofectamine to analyze the effect of free siRNAs. Additionally we used Lipofectamine complexes, which were cocultivated for 48h with GL-2 siRNAs at 37 °C in cell free media. All supernatants were transferred to HEK293, which were incubated for 30 min and afterwards transfected with desired constructs for functional analysis (Control-1a and GL-2). All controls, except of cell free Lipofectamine with siRNA, showed no effects on CFP expression in flow cytometry analysis after 48h incubation. Cell-free Lipofectamine had toxic effects on HEK293 cells, leading to a small reduction of CFP expression at high fluorescence intensities (logYFP>6). GL2-loaded exosomes led to CFP reduction in HEK293 target cells. This effect was less pronounced, when cells were washed 6 h after GL-2 transfection to remove free-floating siRNAs and Lipofectamine complexes (Figure 53). However, the observed effects were less dominant compared to the experiment before, where we observed stronger CFP repression.

3. Results

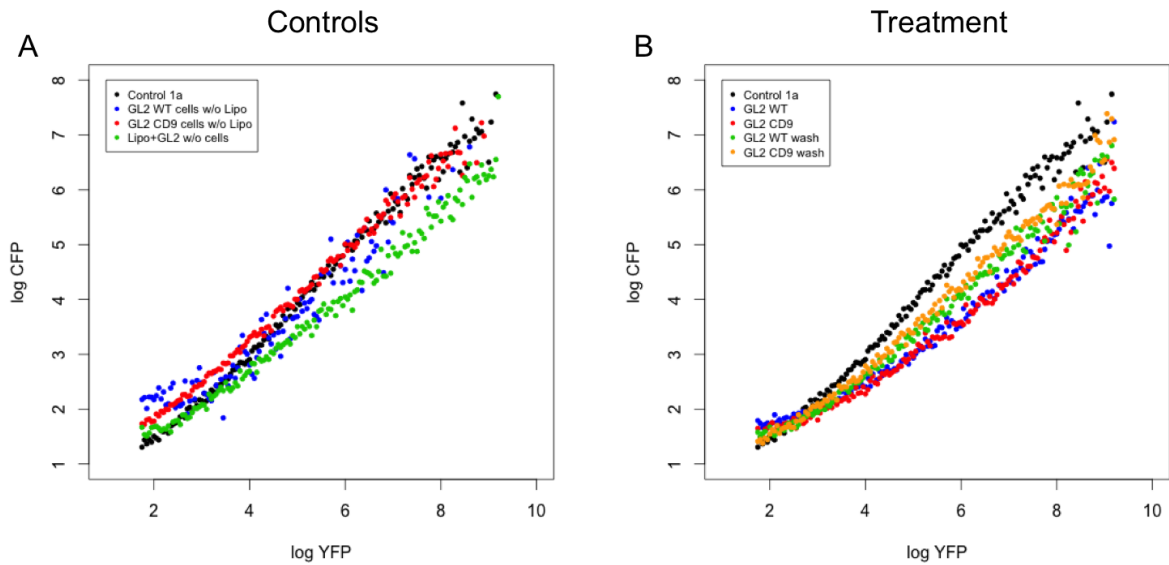


Figure 53: Functional characterization of non-endogenous GL-2 transferred by CD9 or WT exosomes. HEKFT-CD9 or wildtype cells were transfected with GL-2 siRNA and supernatant was collected after 48 h. Additionally, to avoid contaminations of free siRNA and Lipofectamine complexes, cells were washed 6h after transfection and exosomes were collected 54h post transfection. Supernatant was transferred to HEK293 and incubated for 30 min. Constructs for control siRNA (Control_1a) and GL-2 were transfected into HEK293 and functionality was analyzed 48h post transfection by flow cytometry. Supernatant of HEK FT cells treated with GL-2 siRNA without Lipofectamine (red and blue) show a control like behavior in FACS analysis (A). Cells treated with cell free Lipofectamine and siRNA, which were incubated for 48h at 37 °C, showed toxic effects and low reduction of CFP at high intensities ($\log YFP > 5$). For cells treated with GL-2 supernatant of washed CD9 and WT cells reduced intensities of CFP were detected. If unwashed supernatant was used this effect was even increased and reflects the results gained before (Figure 52).

In summary we detected several upregulated miRNAs in Raji cells treated with Jurkat supernatant by NGS sequencing, which were also present in Jurkat exosomes. *In silico* analysis revealed two targets for these miRNA candidates, DNMT1 and BCL-2. Raji cells treated with PEG precipitated exosomes showed significant reduction of DNMT1 detected by qPCR studies. Furthermore, I verified the cell-cell communication between HEKFT and HEK293 cells via our own generated UTA system. We demonstrate a transfer of GL-2 loaded vesicles and confirmed the functionality of a non-human siRNA inside HEK293 cells, which opens new insights into the role of exosomes in cell-cell communication.

3. Results

3.6 Manipulation of human B-lymphocytes and *in vivo* studies

3.6.1 Transduction of human B-lymphocytes via virus-like particles (VLPs)

Since suspension cells are hard to transfect with commercial kits I used JC polyomavirus derived virus-like particles, which were produced and purified in our lab. This tool was chosen, because JCV is known to infect human B-lymphocytes [145]. Furthermore, VLPs have been defined as suitable tool for delivery of genetic material like siRNAs or shRNAs in cell culture as well as *in vivo* [110, 146-150].

In order to test virus-like particles on human B-lymphocytes (Raji) we used a GFP expression cassette containing a CAG-promoter and GFP as GOI with a SV40 poly-A signal. This cassette was loaded into VLPs, added to Raji cells and GFP expression as analysed 72 h post transduction (Figure 54).

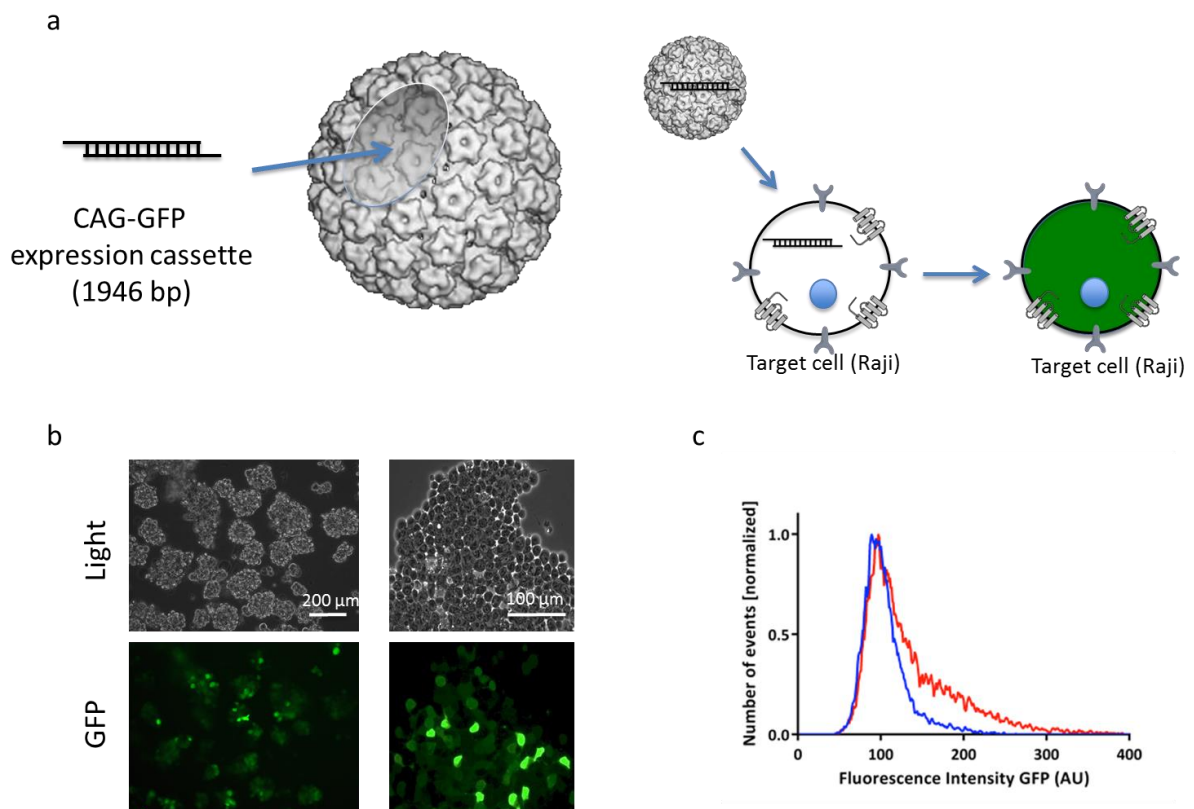


Figure 54: CAG-GFP expression cassette supply into B-lymphocytes via VLP transduction. The linearized expression cassette was obtained by amplification from the pAAV-CAG-GFP plasmid and contains a CAG promoter as well as a SV40 poly-A signal. This cassette was loaded into virus like particles to transduce Raji cells. GFP expression was observed 72h post transduction via fluorescence microscopy(b, scale bar 200 μm, exposure time 1 sec). or flow cytometry (c). FACS analysis revealed 30 % GFP positive cells.

3. Results

After 72h green fluorescence was detected by fluorescence microscopy. Approximately 50% of all cells showed green fluorescence, while the intensities varied among the cell population. To quantify the transduction efficiency we performed FACS analysis, which revealed 30 % of positive transduced Raji cells.

3.6.2 Tracking of miR-451a inside human B-lymphocytes via NanoGold particles

After successful transduction of human B-lymphocytes I designed a thiol and Cy3 modified miR-451a sequence. Thiol groups were covalently attached to NanoGold particles, which allow a saturation of the NanoGold particle surface with the designed miRNAs. Since I detected miR-451a mainly in exosomes of four human cell lines I selected this miRNA (sequence and modifications in Table 38), covalently attached it to NanoGold particles, transduced them into human B-lymphocytes and tracked the NanoGold particle inside the cell via electron microscopy (Figure 55). Because of the high electron density of NanoGold spherical particles electron microscopy is the preferable method to analyse these particles [151, 152].

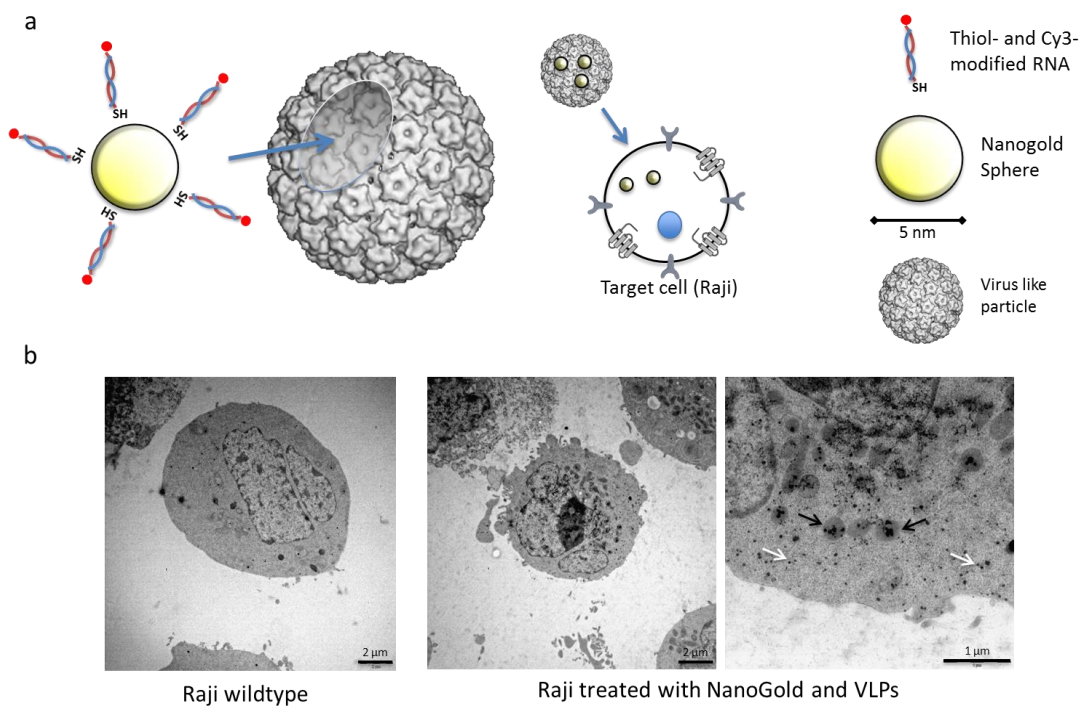


Figure 55: Delivery of NanoGold particles via virus-like particles into human B-lymphocytes (Raji). Thiol- and Cy3- modified miR-451a was coupled to NanoGold particles and loaded into VLPs to transduce human B-cells (a). Raji cells were prepared for electron microscopy by negative staining. Due to the high electron density NanoGold particles appear as dark spots in EM images. Wildtype cells showed no dark spots, while NanoGold-VLP treated cells contained locally dark spots inside the cytoplasm (white arrows) or inside intraluminal vesicles (dark arrows) (b).

3. Results

Electron microscopy demonstrated a successful transduction of Raji cells with NanoGold loaded VLPs. VLP treated cells show locally dark accumulations of NanoGold particles which are not visible in untreated cells (Figure 55 b). Furthermore, miR-451a coupled particles were visible inside the cytoplasm (white arrows), while a large proportion was visible inside intraluminal vesicles (black arrows) with a diameter around 500 nm. Many dark accumulations were visible inside the nucleus, too.

Table 38: Sequence and modification of miR-451a

MiRNA	Sequence and modifications
MiR-451a	5'- Thiol-aug cgg aaa ccg uua cca uua cug agu uu -Cy3 -3'

3.6.3 Studying cell-cell communication between Raji and SW837

After successful transduction of Raji cells with DNA expression constructs and miRNA modified NanoGold particles I transduced these cells with a Cy3-modified non-cognate siRNA containing the Raji secretion motif, which was detected by analysis of small RNA sequence data (compare Figure 22). The aim was to study the cell-cell communication between human B-lymphocytes and human colorectal carcinoma cells SW837 [153]. Raji cells were transduced with Cy3-modified RNA and after washing and centrifugation steps co-cultivated with SW837 cells. Since the Cy3-modified siRNA contained a secretion motif for Raji cells a transfer of this siRNA by extracellular vesicles was studied (Figure 56).

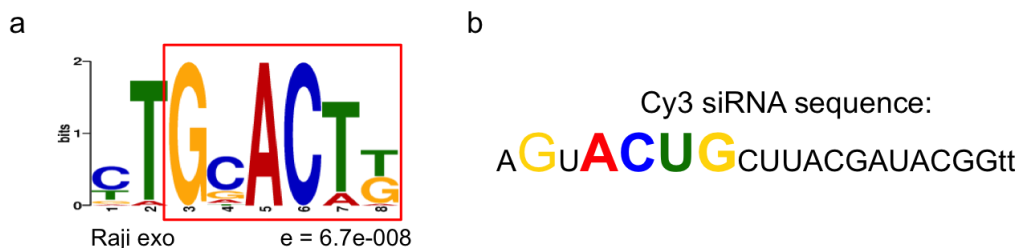


Figure 56: Raji secretion motif and comparison to Cy3 siRNA sequence. Raji secretion motif of own generated next generation sequencing data was analyzed by DESeq package in R in combination with the online motif tool MEME. The Cy3 siRNA sequence shows the secretion motif at the 5' end

3. Results

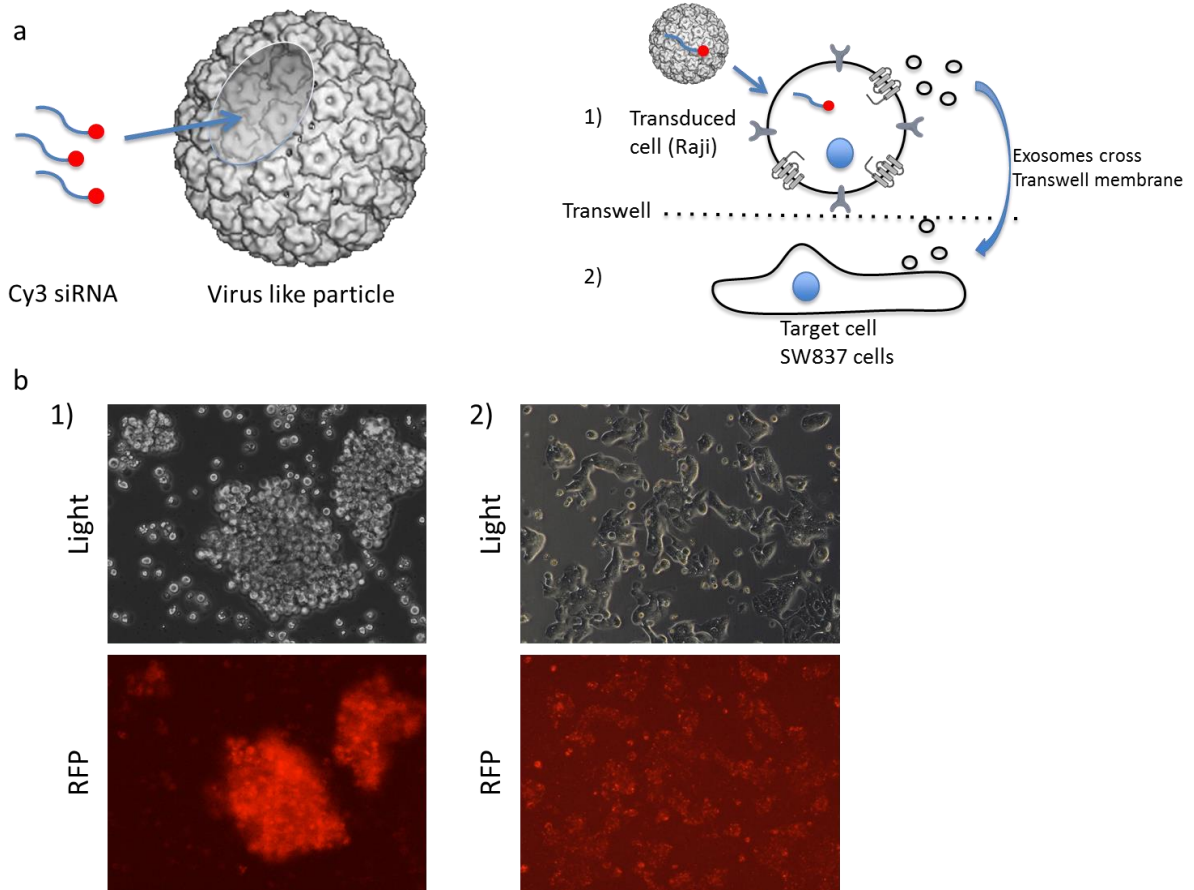


Figure 57: Analysis of cell-cell communication between Rajhi and SW837 cells. Cy3-modified siRNAs were delivered via virus like particles into Raji cells. After 24h Raji cells show red fluorescence due to the Cy3-modified siRNA (b). Subsequently cells were washed and transferred into transwells for cocultivation with SW837 (a). Fluorescence microscopy was performed after 48h to detect positive cell-cell communication via EVs between Raji and SW837 cells. Indeed most of SW837 showed red fluorescence with local accumulations inside the cytoplasm, indicating a positive transfer of Cy3-labelled siRNA via EVs (b).

Raji cells showed red fluorescence 24 h post transduction with Cy3-modified siRNA loaded VLPs, indicating positive transduction by virus-like particles (Figure 57). Furthermore, I detected red fluorescent SW837 cells after 48 h co-cultivation, presuming an intracellular transport of this modified siRNA, carrying the secretion motif of Raji cells, by extracellular vesicles.

3. Results

3.6.4 *In vivo* siRNA delivery by virus-like particles (VLPs)

Because of the recent research on exosomes as biomarkers and the *in vivo* use of modified exosomes in clinical use its getting more important to modify cells and their released vesicles *in vivo* [154, 155]. However, all *in vivo* studies facing the same issue, the delivery of the desired cargo and off target effects. To tackle these issues we used virus-like particles as a gene delivery vehicle to study and modify RANKL expression level during osteoporosis in a rat model. Virus-like particles enter cells through binding of specific glycolipids and glycoproteins. Furthermore, a specific interaction with serotonin receptors HTR2a (5-hydroxytryptamine receptor 2a) is needed. Due to the high expression of HTR2a in cultured osteoblasts as well as in rat tibiae (data not shown) we selected this model system to perform first *in vivo* tests of virus like particles. Therefore virus-like particles were loaded *in vitro* with siRNAs against RANKL by disassembling and reassociation in the presence of the desired nucleic acid. Different amounts of virus-like particles were intraperitoneal injected into female Sprague-Dawley rats and RANKL expression was analysed by qPCR (Figure 58). Beta-2-microglobulin served as housekeeping gene for normalization of RANKL levels by $\Delta\Delta CT$ -method. Two animals were used for every treatment, except for the injection of 105 μg siRANKL-VLPs, where we used five animals.

For the first *in vivo* test of siRNA loaded virus-like particles we chose three different doses of siRNA loaded virus like particles summarized in table 39.

Table 39: Three different doses of siRNA loaded virus-like particles.

Dose	Virus like particles amount	siRNA amount	Ratio (VLP/siRNA)
Low	40 μg	3 μg	1:13.3
Medium	105 μg	7.8 μg	1:13.4
High	150 μg	11.2 μg	1:13.4

To compare the different treatments the VLP/siRNA ratio was kept constant.

3. Results

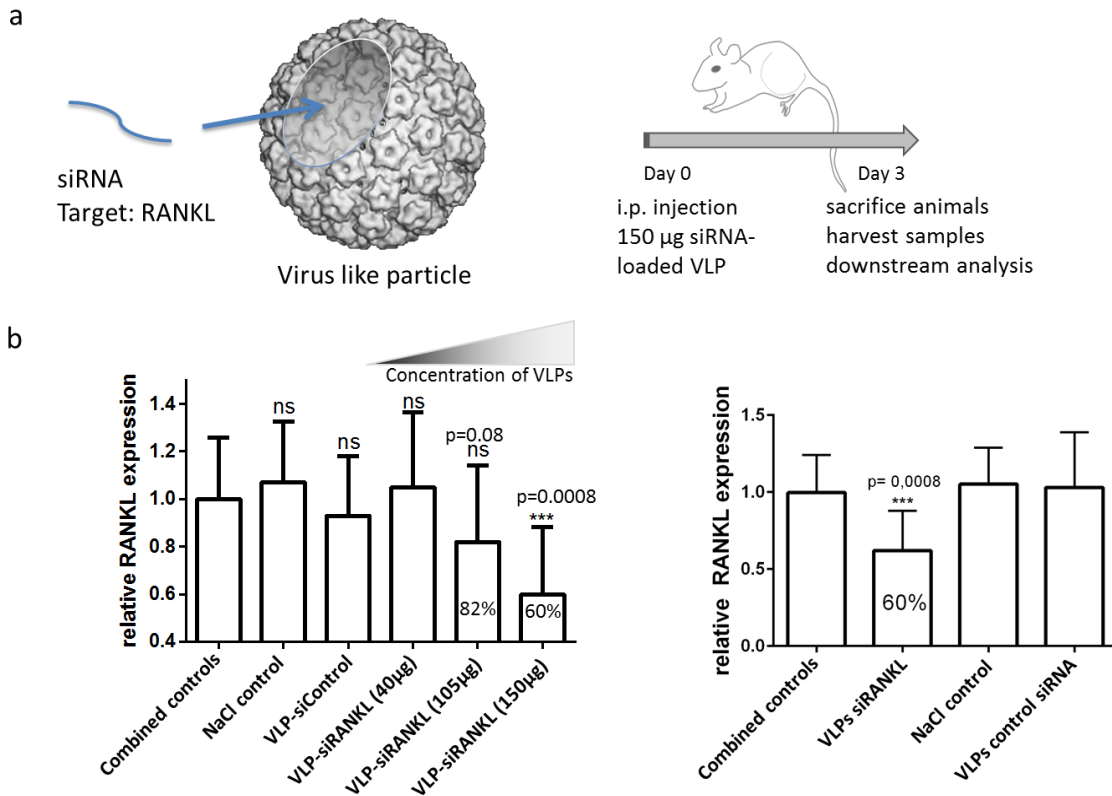


Figure 58: *In vivo* siRNA delivery against RANKL in rat tibiae via virus-like particles. VLPs were intraperitoneal injected into female Sprague-Dawley rats and tibiae was removed 72 h post transduction. After total RNA isolation and qPCR analysis no significant changes on RANKL mRNA level were observed due to control treatment (NaCl injection and VLP + control siRNA injection). Furthermore, low doses of VLPs show no significant silencing effects. Nevertheless injecting 105 µg of VLPs resulted in 18% knockdown of RANKL mRNA without reaching significance ($p=0.08$). Strongest effects were observed using 150 µg of VLPs, reaching a knockdown of 40% ($p=0.0008$).

No significant silencing effects were observed for the control setup, meaning animals injected with NaCl or 120 µg of control siRNA (siControl) loaded VLPs. This control siRNA was designed to not target any known rat gene and is used to distinguish sequence-specific silencing from non-specific effects caused by the treatment. Furthermore, we observed no silencing effects for 40 µg VLPs loaded with siRANKL. Nevertheless injections of 105 µg and 150 µg siRANKL-VLPs reduced the RANKL mRNA by 18% respectively 40 %, while treatment with 150 µg VLPs reached significance (b). Therefore this condition was used for further experiments. Because of the high fluctuations in the RANKL mRNA level in all treatment groups we increased the number of treated animals. Animals were treated with NaCl, 150 µg VLP-siControl and 150 µg VLP-siRANKL (10 animals each). Rats were euthanized after three

4. Discussion

days and tibia was extracted for qPCR analysis. We observed 40 % reduction of endogenous RANKL expression on mRNA level with $P < 0.001$. Control animals showed no significant change upon treatment with NaCl or VLP-siControl.

Summarizing we reduced the endogenous RANKL mRNA level by injecting RANKL specific siRNAs using virus-like particles as a delivery system.

4. Discussion

In the following paragraph I want to summarize the results of this work:

In this thesis I was able to isolate extracellular vesicles of four human cell lines by three different isolation techniques (chapter 4.1). The small RNA content of EVs from four cell lines was detected by next generation sequencing and analysed by own generated scripts by the open source R-software. Sequence motif analysis revealed cellular retention and secretion motifs for miRNAs as well as distinct miRNA patterns for all cell lines (chapter 4.2). Comparison of EVs isolated by the UC-protocol and PEG precipitation revealed no difference in small RNA content (chapter 4.3). Through generation of LVs a role in vesicle fusion was discovered for CD9. Furthermore, CD9 overexpression raises the transduction efficiency of generated LV constructs. An increased EV production was detected for CD9 overexpressing cell lines. However the extracellular small RNA content was not changed upon CD9 overexpression (chapter 4.4). Moreover, I was able to detect a cell-cell communication between several cell lines by qPCR analysis, fluorescent labelled siRNAs and our own generated reporter gene construct (chapter 4.5). With our VLP technology we were able to adapt the *in vitro* manipulation of cells by small RNAs to an *in vivo* rat model, which opens new perspectives for future exosome analysis and manipulation thereof (chapter 4.6). More details are provided in the indicated paragraphs.

4.1 Comparison of exosome isolation techniques

In the last decade extracellular vesicles, in particular exosomes, have gained interest because of their potential application in gene therapy diagnosis and prognosis of diseases. However, no common isolation technique for extracellular vesicle, which can be performed

4. Discussion

fast and yields high amounts of pure exosomes, is established and accepted so far. To study exosomes for clinical purpose, e.g. diagnosis of cancers, a fast, easy and efficient isolation method is necessary. In our screening we include three different isolation techniques (Figure 9) and analysed the size distribution, amount and purity of extracellular vesicles. All cell lines were cultured in exosome free FCS (100.000 xg for 16 h) to avoid contamination of bovine vesicles [156]. Polyethylene glycol is often used for enveloped virus purification and concentration [157, 158]. Since exosomes share size properties of enveloped viruses, i.e. lentiviruses, I choose PEG precipitation to compare with common ultracentrifugation protocols. Furthermore, commercially available exosome isolation kits like ExoQuick (System Bioscience, CA, USA) or "Total Exosome Isolation" (Life Technologies, MA, USA) use this precipitation technique. PEG Precipitation is, when compared to the two tested ultracentrifugation protocols, faster and easier to perform; a hands on time of less than 30 min is needed. In total the process of PEG precipitation requires only 75 min including centrifugation time, which is compared to ultracentrifugation techniques, because of the more laborious procedure (ultracentrifugation steps, compensate weights etc.), much faster. In NTA analysis PEG precipitated vesicles displayed higher mean sizes compared to ultracentrifugation techniques (Figure 10). PEG is a polymer, which displays water and increases the local protein concentration until precipitation. Since the NTA cannot distinguish between 200 nm vesicles and two 100 nm particles sticking together this results have to be evaluated carefully. For the four tested cell lines I observed a size distribution between 156.2 – 174.5 nm. This size distribution reflects the current literature, where vesicles between 50-250 nm were observed after PEG precipitation [58, 159]. In HEK293 no differences in mean sizes between the tested isolation techniques were observed. Probably the microvesicle amount differs from other cell lines and not all microvesicles were removed during the purification steps.

Furthermore, I performed a comparative analysis regarding the yield of extracellular vesicles. Increased yield per input values were observed for the PEG precipitation protocol, while the two ultracentrifugation techniques show similar yields. PEG precipitation requires less input material and yields more particles compared to the ultracentrifugation techniques. Thus this technique is suitable for extracellular vesicle isolation for limited material e.g. in clinical approaches. However, after PEG precipitation many vesicles with sizes of microvesicles were

4. Discussion

detected, suggesting a mixed population of exosomes and microvesicles, while microvesicles were less abundant in samples from both UC-protocols [32].

To further elucidate the presence of exosomes and their purity I checked for exosomal marker proteins via western blot analysis (Figure 11). For all isolation techniques a positive Alix signal was observed, while Alix was at the same protein concentration not detectable inside the cell. After increasing the protein concentration from 10 to 20 μg total protein concentration Alix was detectable in cell extracts (data not shown). Alix is a component of the ESCRT machinery and a well characterized exosome marker protein [160-162]. Besides Alix I studied the two tetraspanins CD9 and CD63. Both proteins have been described as exosomal marker proteins and are often used to detect or identify exosomes. Escola *et al.* showed in 1998 a seven fold enrichment of CD63 in exosomes compared to cellular extracts [163]. Nevertheless tetraspanins are also expressed on the plasma membrane and therefore these proteins are also detectable in microvesicle fractions [164]. This fact was confirmed by our comparative protein analysis via western blot. CD63 was detected intracellular, in microvesicles and in exosomes with a molecular weight of 60 kDa. In contrast CD9 displayed a shift from 20 kDa (intracellular) to 60 kDa in microvesicles and exosomes. Both signals, for CD9 and CD63, were detected at higher molecular weight compared to their expected size. CD63 and also CD9 are known to be posttranscriptional modified by glycosylation, lipidation or palmitoylation [165]. Furthermore, traces of membrane fragments influence the migration in PAGE and in turn increase the size visualized by western blotting. Posttranscriptional modified CD63 was observed by other workgroups too [58], for instance Gallo *et al* reported a signal around 60 kDa for CD63 [166]. To overcome this issue a TCA precipitation and several wash steps to remove membrane fragments will be a suitable approach [167].

In addition we confirmed successful EV isolation by electron microscopy (Figure 12). All isolation techniques showed vesicle in the expected size range of 30 – 100 nm. Nevertheless bigger vesicles (>100 nm) were observed in PEG precipitated samples which is also described in literature [58]. No difference in vesicle size was obtained for the two ultracentrifugation techniques, in both samples vesicles between 30 – 100 nm were observed. Ultracentrifuged exosomes were also reported to have diameters between 50-100 nm by several groups, matching our observations [57, 166].

4. Discussion

Taken together I performed a comparative analysis of three different exosome isolation techniques yielding different size profiles and yields, while PEG precipitation contains to some extent larger vesicles but also increased amounts of EVs. All isolation techniques showed presence of exosomal marker proteins like CD9, CD63 and Alix and existence of vesicles with exosomal size in electron microscopy.

4.2 Cellular and extracellular small RNA profiles of four human cell lines

After confirming successful exosome isolation by detecting size profiles of EVs, exosomal protein marker and visualization in electron microscopy I compared exosomal and cellular small RNA profiles of four human cell lines by next generation sequencing. Therefore total RNA was directly isolated from PEG precipitated exosomes or from cell pellets. Analysis of extracted RNA was performed on BioAnalyzer System to detect size, purity and amount of isolated RNA (Figure 13). Cellular RNA shows two main peaks at 2000 and 4000 nucleotides, representing the 18S and 28S ribosomal RNA. The ratio of the integral of both peaks leads to the RNA Integrity Number (RIN) number, which reveals the quality of isolated RNA. RNA is rapidly degraded in presence of ubiquitous RNase enzymes. No degradation occurred at RIN of 10, whereas the RNA is completely degraded at RIN=1 [168, 169]. For total RNA samples RIN values above 9 were accepted for NGS. Since the main proportion of intracellular RNA is composed of ribosomal RNA [169] a purification step was performed for cellular RNA samples to remove rRNA and increase the amount of small RNAs. Nevertheless the BioAnalyzer system combined with the RNA Pico chip is not capable of recognizing small RNAs like miRNAs with a size of 21-23 nt, since the range of detectable RNAs is limited from 25-5000 nucleotides. At this point we can't evaluate the presence or purification of miRNAs. For exosomal RNA only low amounts of 18S and 28S ribosomal RNA were detected and the small RNA content (25-200 nt) was higher compared to cellular samples. Due to the absence of rRNA and the high amount of small RNAs the small RNA purification was skipped. Same distributions of cellular RNAs and small RNAs of PEG precipitated exosomes were described before [157], indicating a successful workflow.

After RNA isolation the next generation sequencing workflow was performed as described in Figure 14. For Raji intracellular and exosomal triplicates were analysed and unique miRNA

4. Discussion

patterns were observed (Figure 15). Cellular triplicates showed high similarities in hierarchical clustering, even though differences in sequence depth and mean sequence length were detected (229.203 reads and 18 bp mean read length for the lowest and 1.328.741 reads and 30 bp mean read length for the deepest sequenced library), concluding an efficient and reproducible sequencing workflow. Close clustering was also observed for exosomal samples, however bigger differences in hierarchical clustering were detected for the third exosomal library (Raji exo3). Raji exo3 had 266.501 total reads, 5.6 times less compared to Raji exo1 (1.489.896 reads). Mean read length was consistent for all three replicates (between 22 - 30 bp). SnoRNAs showed in general low abundance inside exosomes. All candidates belong to the C/D box snoRNA family responsible for methylation of ribosomal RNA and are localized inside the nucleolus [170]. These npcRNAs are not processed by Dicer and Drosha and no studies observed snoRNAs in exosomes, indicating a cellular remaining of snoRNA candidates. Having a closer look at the heatmap the region of snoRNAs is underrepresented in Raji exo3, most likely because of the lowest sequence depth of all exosome replicas. An overview of identified intracellular or extracellular miRNA of all tested human cell lines and their relevance and occurrence described in literature is provided in table 41.

Table 41: Identified miRNAs, description in the literature and motif (c= cellular, e= extracellular, n= neutral)

MiRNAs	Cell type	Tissue/Cell line [Literature]	Motif
miR-3607	Raji cell	Prostate cancer [171]	c
miR-4284	Raji cell	B-cell lymphoma [172]	n
miR-218-5p	Raji exo	Pericardial fluid[173]	e
miR-451a	Raji exo	B- and T-cell exosomes [40]	n
miR-378b/f/g/i	Jurkat cell	Colon carcinom [174]	c
miR-451a	Jurkat exo	B- and T-cell exosomes [40]	n
miR-494-3p	Jurkat exo	Melanoma exosomes [175]	e
miR-143-3p	Jurkat exo	Smooth muscle cells exosomes [176]	c
miR-4521	DG75 cell	Whole blood [177]	n
miR-33a-5p	DG75 cell	Human plasma [178]	c
miR-590-3p	DG75 cell	Monocytes [179]	c
miR-125a-5p	DG75 exo	Plasma exosomes [180]	n
miR-451a	DG75 exo	B- and T-cell exosomes [40]	n
miR-204-5p	HeLa cell	Colorectal cancer [181]	c

4. Discussion

miR-451a	HeLa exo	B- and T-cell exosomes [40]	n
miR-223-3p	HeLa exo	Exosomes of whole blood samples [182]	n

For all tested cell lines a differential expression pattern of miRNAs was observed. MiR-4284 showed the highest cellular expression combined with absence in extracellular vesicles in Raji cells and recent studies suggested this miRNA as a putative biomarker for B-cell lymphoma [172], matching perfectly our observations in human B-lymphoma cells. Moreover we detected miR-218-5p and miR-451a as strong expressed miRNAs in EVs. MiR-218-5p was found in pericardial fluid from patients with heart failure [173], indicating an extracellular appearance of this miRNA. Maturation of miR-451 is Dicer independent and requires Ago catalysis, opening a complete new miRNA processing pathway [183]. This miRNA is known to be highly expressed in exosomes of Hek293T cells, primary T-lymphocytes and Epstein-Barr virus transformed B-Lymphocytes [40, 184-186], confirming our sequence workflow and data analysis. Furthermore, miR-451a is a frequently described exosomal miRNA and used as biomarker for several diseases [187, 188]. Some differential expressed candidates contain a secretion or retention motif, which will be discussed in the next paragraph in more detail.

In addition to the distinct small RNA profiles of four human cell lines cluster analysis from various samples were performed via DESeq package in R. As described before, Raji cells showed comparable small RNA profiles, which differ from extracellular profiles. We compared Raji and Jurkat intracellular RNA, which identified differences in small RNA expression (Figure 20). Adding DG75 and HeLa datasets (Figure 21) has no influence on Raji and Jurkat clustering. Surprisingly both cell lines show more similarities compared to DG75 and HeLa. Raji and DG75 belong to B-lymphocytes and are of hematopoietic origin [189], while Raji cells were infected by Epstein-Barr virus. Surprisingly DG75 and HeLa showed similar small RNA patterns, which were unexpected, since DG75 is a suspension cell line of B-cells and HeLa an adherent cervical cancer cell line. Nevertheless both cell lines (HeLa and DG75) were only sequenced once. For a statistical analysis at least triplicates are needed to compare different cell lines.

Analysis of extracellular miRNAs of four human cell lines revealed 89 common miRNAs. As described before miR-451a was detectable in all exosomal samples and is already known as an exosomal miRNA [187]. Besides miR-451a I identified miR-148a as a common extracellular

4. Discussion

miRNA. It is known to be present in exosomes of MSC [190] and functions as a critical regulator of B-cell autoimmunity [191]. MiR-203 is known to be present in B-Lymphocytes but downregulated upon Epstein-Bar virus infection, which explains the presence only in DG75 cells [192].

Due to the extracellular miRNA analysis I searched for sequence motifs enriched in extracellular RNAs. Indeed I found a motif of four nucleotides (GNAC) enriched in exosomes with an e value of $e = 0.000047$, confirming statistical significance. So far no extracellular miRNA motif identified by NGS is available, nevertheless Villarroya-Beltri published 2013 an extracellular miRNA motif analysed by microarrays (GGAG/C) looking similar to our motif [40]. Furthermore, an intracellular sequence motif was published too, matching complete with our intracellular motif (Figure 22). Since statistical power increases with the number of miRNAs, the motif search was performed with combined samples of all four cell lines, Nevertheless sequence motifs were analysed also for single cell lines, however only for Raji exosomes (UGNACU, e-value $6.7e-008$) and intracellular DG75 miRNAs (AGG/CAGC, e-value 0.000034) confident e-values were reached (Figure 23).

Summarizing a high reproducibility of the IonTorrent PGM system was achieved and intracellular and exosomal small RNA profiles of four different human cell lines were generated. A common pool of 89 miRNAs was identified and sequence motifs of cellular and exosomal miRNAs were discovered.

4.3 Comparison of PEG precipitation and Ultracentrifugation

Research on extracellular vesicles, in special exosomes, gained interest in recent years. Currently research is focusing on exosomes as biomarkers and for diagnosis in of diseases [155]. In particular for clinical application an efficient exosome isolation is needed, since patient material is complex (like human plasma) and limited. However, until today no general isolation protocol for exosomes is available. The isolation of EVs is still a challenging and time consuming procedure not adapted to clinical use yet.

An efficient and fast isolation method is needed for clinical applications of exosomes. Therefore I compared i) the “golden standard” technique ultracentrifugation, which is most frequently used in research environments to isolate pure exosomes, and ii) the fast PEG

4. Discussion

precipitation method in regards of vesicle yield, size distribution and small RNA content. For the comparative analysis exosomes were isolated from Raji cells after 72 h incubation and EVs were isolated by PEG precipitation or ultracentrifugation as described in 2.1.8. Smaller size profiles of exosomes isolated by ultracentrifugation were observed as already described above (chapter 4.1). Both isolation techniques revealed similar small RNA size profiles after separation on BioAnalyzer system. Recent studies compared small RNA profiles of ExtraPEG (PEG precipitation followed by one ultracentrifugation step) isolated exosomes with differential ultracentrifuged exosomes and detected similar size profiles of small RNAs [157]. Our protocol of PEG precipitation lacks an ultracentrifugation step and still yields similar size profiles of small RNAs, providing a promising method for clinical research (Figure 24). Since size profiles of small RNAs give no evidence of present small RNAs, I performed NGS sequencing and compared exosomes isolated by ultracentrifugation and PEG precipitation. All exosomal samples were distinct to cellular samples after hierarchical clustering and PCA plot analysis (Figure 25). Ultracentrifuged exosomes were similar to PEG precipitated sample. Small difference observed in cluster analysis can be explained by regular variances in biological replicates because of slightly different procedure during PEG precipitation or small technical variations during library preparation and sequencing procedure. After small RNA analysis via R-software using the DESeq package I detected several small RNAs enriched in PEG precipitation or ultracentrifugation. For miR-378a-3p and miR-19a-3p, both known miRNA enriched in exosomes, an enrichment in PEG samples was detected [193]. Besides these candidates we identified miR-301a-3p, also known as circulating miRNA and suggested biomarker for Alzheimer's disease [194]. Besides PEG enriched candidates we also detected miRNA candidates enriched after ultracentrifugation, for example miR-218-5p. As described in chapter 4.2 this miRNA found in pericardial fluid from patients with heart failure [173], indicating an extracellular appearance of this miRNA. Furthermore, miR-186-5p was overrepresented in exosomes isolated by ultracentrifugation. This miRNA is also identified extracellular after myocardial infarction. Interestingly, also miR-122-5p, overrepresented in UC exosomes, was detected in patients after acute myocardial infarction. These findings indicate a specific isolation of miRNAs after cell damage processes like myocardial infarction or in cell culture after apoptosis.

For miRNA candidates, which were solely detectable in Raji exosomes (compare Figure 16 and table 21) no drastically changes were observed comparing both isolation techniques.

4. Discussion

However, three small RNA candidates were solely detected in PEG precipitated samples. Surprisingly we detected one snoRNA (U24). C/D box snoRNAs are transcribed and processed inside the nucleus. However, studies showed an interaction of U8 with nuclear export proteins (like PHAX, CRM1 and Ran) and suggested an export of U8 during biogenesis [195]. This export process is unknown for other snoRNA candidates (like U24) and needs further investigation. Besides U24 we identified miR-146a-5p and miR-744-5p as exclusively present small RNAs in PEG samples. MiR-146a-5p was already observed in EVs of human serum [196], while miR-744-5p was found in plasma samples and is proposed as a biomarker for pancreatic cancer [197]. All identified miRNAs isolated by PEG precipitation or ultracentrifugation are described as extracellular miRNAs in literature, suggesting a successful isolation of extracellular miRNAs by both isolation techniques.

Taken together both methods yield vesicles in exosomal size range (30 – 100 nm), while UC revealed smaller particles compared to PEG precipitation. Nevertheless both isolation techniques disclosed similar small RNA patterns and similarities after principle component analysis and cluster calculations. For miRNAs overrepresented in exosomes isolated by UC three candidates are known to be released after myocardial infarctions, indicating a specific enrichment of miRNAs released after cell damage processes. This phenomenon was not observed for PEG precipitated exosomes. Since both techniques revealed known extracellular miRNAs with similar frequency and PEG precipitation showed no specificity for miRNAs released after cell damage, we suggest to use this method for clinical applications of exosomes. PEG precipitation uncovers similar miRNA amounts compared to ultracentrifugation techniques and needs less hands-on-time and no specific lab equipment.

4.4 Overexpression of exosomal marker proteins and influence on EVs and LVs

The influence of extracellular vesicles and their biogenesis pathways on virus production as well as on virus infection has been discussed during the last decade [198, 199]. Although the precise mode of action of extracellular vesicles for example in HIV infection has not been characterized in very detail, increasing evidence suggests that EVs facilitate the enhancement of infection and replication [135]. However, contributions of intraluminal vesicles like exosomes to viral pathogenesis are currently unravelling and the utilization of the cellular vesiculation machinery was identified as an enhancer for virus transduction e.g.

4. Discussion

in HIV or AAV pathogenesis. Positive effects on virus efficiency and stability were observed [136, 137].

In this chapter new functional connections of the vesiculation machinery of intraluminal vesicles (ILVs) in particular with HIV-1 based LV transduction were identified. We overexpressed three exosomal marker proteins (i.e. CD9, TSG101 and Alix) and investigated the influence on extracellular vesicles (Figure 26). Only CD9 overexpression increased the overall level of microvesicles and exosome production with some emphasis towards the latter, supporting the previously proposed contribution of tetraspanins on ILV biogenesis [41, 200]. Both TSG101 and Alix are responsible for trafficking of the ESCRT machinery and led upon overexpression to a decreased amount of extracellular vesicles upon constitutive overexpression. In particular exosomes were affected by increased expression of all the marker proteins, whereas CD9 increased both total vesicle amount and the proportion of exosomes in conditioned medium. Increased expression of the ESCRT related Alix and TSG101 resulted in the exact opposite effect with an overall decreased amount of cell free vesicles and a size range indicating an increase of membrane shedding microvesicles (average > 150 nm). Phenotypic changes of expressing cells were not observed for CD9, but TSG101 and Alix overexpressing Hek293 cells developed increased mortality rates (Figure 30). This finding indicates that too high levels of TSG101 or Alix induce cytotoxic effect and thus the surviving cells displayed less pronounced expression when compared to the average of CD9 overexpression. The toxicity of high TSG101 levels, and also its role in regulation of cell growth, proliferation and cell survival were previously reported [201, 202]. Overexpression of Alix was linked to an increased rate of neuronal death by caspase activation [203], fitting our observations.

The increased levels of extracellular vesicles and the shift towards a higher proportion of exosomes were consistent for the overexpression of CD9 in four different human cell lines. These findings strongly indicate a role of CD9 in ILV biogenesis and thus extracellular vesicle production. This direct connection between CD9 expression alone and the production of extracellular vesicles was not reported far, although a general role of tetraspanins in microdomain formation and ILV assembly has been discussed [41, 200].

Extracellular vesicles were reported to positively influence viral transduction, accordingly we investigated whether LVs produced in pro-exosome conditions (i.e. increased CD9 levels) will differ from standard LVs [52, 137]. Expecting more efficient LVs from CD9-overexpressing

4. Discussion

producer cells in the context of accelerated extracellular vesicle secretion we indeed observed faster transduction with LV-VSVG-CD9_{GFP} and a quicker onset of transgene expression (GFP or RFP) compared to standard LV-VSVG viruses (Figure 33-34).

Unexpectedly, we also observed transduction competent LV-CD9_{GFP} virus that delivered its genomic content into minor portions of target cells in absence of any additional and known fusogen (Figure 36). This, however, indicated a direct contribution of producer cell provided increased levels of CD9 to facilitate membrane fusion between the LV envelope and the target cell membrane. We confirmed this finding *in vitro* in HEK293 cells as well as *ex vivo* with primary rat CNS tissue. In 2000 Miyado *et al.* showed that CD9 is capable of fusing membranes of sperm and eggs *in vitro*, gathering some insights into functions of tetraspanins [52]. Recently an interaction of CD9 was shown to interact with growth factors and integrins, indicating a role in cell fusion [48, 204]. To figure out if CD9-overexpression also had a boosting effect on recombinant LV-production, we determined their physical titer after production in standard HEK293FT and pro-exosomal HEK293FT-CD9_{GFP} cells. LV-VSVG and LV-CD9_{GFP} did not display significant differences and only the LV-VSVG-CD9_{GFP} production was slightly increased. The influence of tetraspanins on virus production, efficiency and stability is recently controversial discussed in the literature. Kremetsow *et al.* neglected effects of CD9 overexpression on subsequent virus release, while others described a supporting role of tetraspanins in uptake, trafficking and spread of viruses [205, 206]. Other studies reported that extracellular domains of CD9, CD53, CD63 and CD81 are involved in HIV-1 infection [207]. Thus, our findings of positive influence of the tetraspanin CD9 on LV performance is partially explained by increased exosome biogenesis and also by CD9 assisted transduction of target cells. Kadiu *et al.* described that HIV is “entrapped” by exosomes, forming heterogeneous aggregates of cell derived and viral particles that in turn facilitate infection events [136]. Our negative controls (Figure 37) indicate that specific proteins on the LV envelope are substantial for transduction. Viral capsids without either viral glycoproteins (e.g. VSV-G) or high levels of CD9_{GFP} were not capable of transducing HEK293 cells, although exosomes and endogenous CD9 were present during the production process. Reflecting our observations, we are convinced that increased CD9 expression has supportive effects on the performance of LV-VSVG-CD9_{GFP} and furthermore, that CD9_{GFP} promotes the fusion with target cell membranes.

4. Discussion

Furthermore, we observed a cytoplasmic relocalization of CD9_{GFP} during virus production already 24h after transfection with lentiviral plasmids (Figure 40). In 2007 Deneka *et al.* already observed a HIV-1 assembly in intracellular vesicular structures containing tetraspanins like CD53, CD81 and CD9 [208], which supports our observations. These findings together with the increased efficiency and the feature of membrane fusion of CD9 deliver novel and in part unexpected insights into the influence of tetraspanins on virus production and performance and open new prospects of using tetraspanins in the context of future therapeutic interventions with LV based delivery strategies.

Since CD9 influenced the extracellular vesicle amount and size distribution the impact on extracellular small RNAs in Raji cells was examined by high throughput sequencing via IonTorrent system. Cluster analysis revealed only minor differences between CD9 and WT exosomes. Surprisingly we observed an increased abundance of U73a, U78 and HBII-429 in exosomes of CD9 overexpressing cells. So far there is no evidence of CD9 interaction with snoRNAs or miRNAs. However, tetraspanins can interact with membrane molecules and organize supramolecular clusters, called tetraspanin enriched microdomains (TEM). These microdomains are a putative key to understand how genetic information is transported into EVs [48, 209]. Nevertheless, further research is needed to understand this complex process. Furthermore, miR-30d-5p and miR-155-5p were more dominant in exosomes produced by CD9 overexpressing cells. Both are known extracellular miRNAs and no connection to CD9 was observed so far [175, 196]. On the other hand we observed four snoRNA candidates overrepresented in wildtype exosomes (mgU6-47, U24, U58B and U61). U24 was already observed in PEG precipitated samples and was overrepresented in PEG precipitated exosomes compared to ultracentrifuged exosomes. The overrepresentation of snoRNAs in PEG precipitated samples can be explained by a possible contamination of MVs. Still the function of snoRNAs inside EVs and their biogenesis route is unknown. Besides snoRNA candidates we found increased miR-5585-3p amounts in PEG precipitated exosomes. Little is known about this miRNA. A recent study detected this miRNA in extracellular vesicles of glioblastoma cells. However, all candidates enriched in WT exosomes displayed low basemean values, allowing only careful conclusions.

Taken together CD9 and WT exosomes show many similarities and only few deregulated small RNA candidates, indicating no active role of CD9 in exosomal sorting of small RNAs into exosomes.

4. Discussion

4.5 Role of EVs in cell-cell communication

Although exosome research is developing since 30 years little is known about their role in cell-cell communication. Previous findings indicate a direct transfer of genetic material by exosomes [19, 35, 86, 210]. These findings have increased the interest in exosomes and their role in communication between cells and support the idea that exosomes transfer proteins and genetic information. However, only little is known about the functionality of miRNAs inside the target cell after exosomal transfer. To address this mechanism, I treated Raji cells with Jurkat supernatant (including exosomes) and analysed the change in small RNA expression by next generation sequencing (Figure 41). We identified several differentially expressed miRNA candidates after Jurkat exosome treatment. We focussed on miRNAs, which were increased after treatment but at the same time strong abundant in Jurkat exosomes, like miR-21-5p, miR-19b-3p, miR-15a-5p and miR-148a-3. Since miR-451a is high abundant in Jurkat exosomes and beyond the detection threshold within Raji cells we chose this miRNA as a fifth candidate. All selected miRNAs carry the secretion motif of Jurkat cells at least partially, for miR-148a-3p it was even detected twice (Figure 42). *In silico* analysis via miRNA target databases and literature research revealed two different targets for all candidate, B-cell lymphoma 2 (BCL-2) and DNA methyltransferase 1 (DNMT1) (Table 38) [139-143]. DNMT1 is a known target for miR-148a-3p and miR-21-5p. The promoter of miR-148a is silenced by DNMT1-depending methylation and DNMT1 itself is a target of miR-148a, revealing a feedback loop insight this gene regulatory network [211]. Indeed we detected a DNMT1 reduction 48 h post treatment with Jurkat exosomes (PEG precipitated) but no effects were caused by Raji exosomes. These findings represent a functional transfer of miRNAs via exosomes between T- and B-cells (Figure 44). The reduction in DNMT1 gene expression vanished after 48h. This indicates only short time effects for exosome treatment upon absorption of exosomes. However, the effect of silencing was weak but significant, giving evidence for a fine-tuning effect on gene expression by extracellular vesicles. For the target Bcl-2 opposing effects were observed. Increased gene expression of Bcl-2 was detected 24 h post treatment with Jurkat exosomes. This effect was still detected after 48 h. Treatment with Raji exosomes leads to no effect, suggesting a specific uptake of exosomes from a different cell type and the omission of own generated exosomes. A transfer of EVs between human T-lymphocytes and B-lymphocytes was published in 2011, however no

4. Discussion

functionality of transferred miRNAs was shown in this study [35]. To elucidate the functionality of transferred small RNAs in recipient cells we used our own designed dual reporter gene toolbox. We used a reporter gene construct containing two fluorescent proteins under constitutive promoters. One reporter gene (CFP) contains a full complementary miRNA target site at the 3'UTR region. Upon small RNA binding the expression of CFP will be reduced while the second reporter gene (YFP) stays unaffected, which can be detected via flow cytometry (Figure 45). The manuscript for our dual reporter gene assay was submitted for publication and is currently under review [144]. To check the reliability of the system we used several negative controls, transfect them into HEK293 WT, performed a treatment with exosomes of different origin and analysed the gene expression of YFP and CFP by flow cytometry (Figure 46). All negative controls contain a non-human miRNA target site at the 3'UTR of CFP and show no influence on CFP expression after flow cytometry analysis, indicating no influence of miRNAs and exosome treatment. To test the functionality of the selected miRNA candidates we designed constructs containing the full complementary target site of the desired miRNA (miR-15a-5p, miR-19b-3p, miR-21-5p, miR-148-3p and miR-451a) at the 3'UTR of CFP and tested the functionality in cell culture experiments followed by FACS analysis. MiR-451a, miR-148a-3p and GL-2 did not affect the target (CFP) expression (Figure 47). Since GL-2 is a synthetic siRNA with no known human target we expected this outcome. MiR-451a and miR-148a-3p are low expressed inside HEK293 cells (data not shown) but high abundant in exosomes. Nevertheless we could not detect a reduction of CFP in wildtype and exosome treated cells, confirming the NGS data and presuming inefficient exosomes transfer or too low concentrations of the respective miRNAs. For miR-15a-5p and miR-21-5p a reduction of CFP intensity was observed in HEK293 WT cells (Figure 48-49). Both miRNAs are strong expressed intracellular, confirming the results of our reporter gene system. However the exosome treatment showed no effect on CFP expression, indicating no effect of exosomal transferred miRNAs. Eventually we tested the functionality of miR-19b-3p (Figure 50). We observed a stronger CFP reduction upon exosome treatment at low YFP intensities (log YFP 2-4). Low effects after exosome treatment were expected since we observed a low reduction of DNMT1 before.

Based on our previous results we wanted to drastically increase the small RNA content in exosomes by siRNA transduction in high-exosome producing cells (HEKFT CD9). For the siRNA candidate we choose GL-2, since it contains the secretion motif for small RNAs

4. Discussion

(Figure 51). As a positive control we cotransfected GL-2 siRNA and a construct with a complementary GL-2 target site in recipient cells and observed a reduction of CFP after FACS analysis (Figure 52). Furthermore, we treated recipient HEK293 cells with exosomes produced in GL-2 transfected HEK293FT cells. We observed a strong reduction of CFP after exosome treatment, proposing a sufficient transfer of GL-2 loaded HEKFT CD9 exosomes in HEK293 cells. Compared to the GL-2 co-transfection we observed weaker reduction of CFP in low fluorescent cells ($\log \text{YFP} < 4$) but stronger effects at high fluorescent cells ($\log \text{YFP} > 5$), which can be explained by a low transfection efficiency for the cotransfection of reporter gene plasmid and effector GL-2 siRNA.

To confirm a transfer of GL-2 loaded exosomes and to rule out an effect of free-floating GL-2 siRNA or Lipofectamine-complexes we analysed several negative controls (Figure 53). All controls showed no effect on fluorescent expression except of 48h-incubated Lipofectamine-complexes with GL-2. Here we observed after treatment an increased mortality rate induced by the toxicity of Lipofectamine, an often overseen but very critical factor for non-viral gene delivery [212, 213]. Moreover we compared the effect of GL-2 loaded exosomes of wildtype HEKFT and HEKFT CD9 cells. CD9 overexpressing cells should produce an increased amount of exosomes without affecting the extracellular RNA content. However, the reducing effect on CFP expression was comparable between WT and CD9 exosomes. The amount of wildtype exosomes seems to be sufficient to load the transfected GL-2 siRNA into these vesicles since an increased amount of exosomes showed no effect. To exclude the effect of free-floating siRNAs and Lipofectamine complexes, we included several negative controls leading to no or very weak effects on target gene expression. Nevertheless the effect of samples treated with exosomes is more pronounced. These findings reveal new prospects using exosomes as a drug delivery system. There is huge interest in using exosomes as therapeutics by influencing the cargo transported within these vesicles [214]. Although exosomal content can vary between different cell types we were able to boost the exosomal loading by a desired siRNA. Furthermore, we were able to verify the transport of artificial loaded exosomes and demonstrate the functionality of the artificial siRNA inside the target cell.

In summary we identified differentially expressed miRNAs after exosome treatment in Raji cells and selected five candidates containing an exosome secretion motif. Furthermore, we observed a repressing effect of Jurkat exosomes on DNMT1 in Raji cells, proposed by a

4. Discussion

miRNA transfer via exosomes. Moreover we solidified these assumptions by an dual reporter assay, which indicated an increased functionality of miR-19b-3p in exosome treated samples. Finally, we exhausted the loading of exosomes by a GL-2 transfection in high-producing exosome cells and detected an efficient transfer of GL-2 loaded vesicles. These findings support the proposed mechanism of cellular communication via exosomes and confirmed the functionality of transferred small RNAs.

4.6 Manipulation of human B-lymphocytes and *in vivo* studies

In this thesis I focused in the extracellular RNA content and cell-cell communication between suspension cells (B- and T-lymphocytes). Since this cell lines are in general hard to transfect with commercial methods, we used JC polyomavirus derived VLPs. VLPs are known to be a suitable tool for transferring genetic material in different human cell lines and also lead to an efficient transfer of siRNAs *in vivo* [215].

We confirmed the transduction of human B-lymphocytes by transferring an expression cassette, containing a GFP-coding sequence under control of a constitutive promoter, and analyzed the fluorescence by microscopy or flow cytometry (Figure 54). Native JC polyomavirus requires 5-HT2a receptors combined with lactoseries tetrasaccharide c (LSTc) for infection [114][205, 206]. B-lymphocytes are susceptible for native JCV infection and LSTc was detected on their surface [145, 216, 217]. Thus, VLPs represent an alternative delivery tool to transfer genetic material into desired target cells without transferring viral genetic material and avoiding viral integration into the host genome. These results were submitted for publication and are currently under review [218].

After approving the successful transduction of B-lymphocytes we wanted to track miRNAs with a secretion motif inside the cytoplasm of Raji cells (Figure 55). Therefore, I used a thiol-modified miRNA, which is highly enriched in exosomes (miR-451a). NanoGold particles are attractive biocompatible materials often used to label proteins or nucleic acids [219, 220]. However, these particles aggregate under physiological conditions without ligands. To prevent aggregation and to track the miRNA within Raji cells, we linked the thiol-modified miRNA to the NanoGold surface, enabling solubility particles under physiological conditions. Through transduction of these NanoGold-miRNA particles into B-lymphocytes we were able

4. Discussion

to pursue the complexes within the cell by electron microscopy. NanoGold particles are recognized by electron microscopy due to their high electron density [221]. Indeed we observed dark spots in electron microscopy images, reflecting the NanoGold complexes. NanoGold was mainly localized inside the nucleus and inside ILVs, reflecting the size of multivesicular bodies of approximately 500 nm [222]. Since we used the exosome enriched miR-451a for covering the NanoGold particles, these observations may deliver first insights into the trafficking pathway of exosomal miRNAs and support our next generation sequencing data.

For exosomes a role in cell-cell communication is postulated. So far we confirmed the communication between B and T-lymphocytes via qPCR analysis and proved a transfer of siRNA-loaded vesicles between embryonic kidney cells by our reporter gene assay. The local communication via exosomes, for example in the tumor microenvironment, is well studied [223]. In 2009 a study reported, that the acidic microenvironment of tumors increases the rate of exosomal uptake [224]. Since B- and T-lymphocytes are both high abundant cell populations in the tumor environment [225], we choose human B-lymphocytes (Raji) and a colon carcinoma cell line (SW837) and checked for a communication via EVs between these two cell lines. Therefore, we modified a siRNA, carrying the exosome secretion motif (Figure 56), with a fluorescent label for easy and fast identification via fluorescent microscopy. VLPs were loaded with the labeled siRNA and transferred to Raji cells. We were able to transduce a high amount of B-lymphocytes, perceptible by the red fluorescence (Figure 57). After wash steps B-cells were transferred into transwells and cocultured with SW837. Transwells provide a physical separation between both cell lines, allowing only particles smaller than 400 nm to pass. Indeed we observed after 48h co-cultivation a transfer of labeled siRNA, leading to red fluorescent SW837 cells. Since both cell lines have no physical contact and free-siRNA added to the supernatant lead to no fluorescent cells (data not shown), we propose a transfer of labeled siRNA via extracellular vesicles between Raji and SW837 cells. So far we focused on the cell-cell communication *in vitro* using several cancer cell lines. We were able to identify a communication between human B- and T-lymphocytes by qPCR, among B-lymphocytes and colon carcinoma cells via fluorescence microscopy and among HEK293 cells by our own generated reporter gen assay.

The restriction to *in vitro* analysis was based on the absence of an efficient and selective manipulation of cells *in vivo*. However, this is a future goal for exosomal research. To

4. Discussion

overcome the issue of manipulating cells *in vivo* we used our VLP technology. The cellular uptake of VLPs is mediated by 5-hydroxytryptamine (5-HT) receptors, a subgroup of the serotonin receptor family, highly expressed on osteoblasts [226]. Since the primary amino acid sequence of 5-HT_{2a} receptors is highly conserved between rats and human, we used rats as a model for testing *in vivo* siRNA delivery by VLPs. Indeed we were able to reduce the endogenous RANKL level by RANKL-siRNA loaded VLPs. Injection of 40 or 105 µg lead to no significant effects after qPCR analysis, but reproducible and significant silencing effects were achieved by injecting 150 µg (0.5 mg/kg) of siRNA-loaded VLPs (Figure 58). For our studies 0.04 mg/kg siRNAs were used, however the amounts of VLPs and injected siRNA is low compared to previous studies using chemically modified siRNAs (2.5–5 mg/kg) or lipid-based technologies (0.3 mg/kg) [227, 228]. These findings report for the first time an efficient transfer of siRNAs by VLPs *in vivo*. With these observations the basics for *in vivo* cell manipulation were established. We showed an efficient transfer of siRNA loaded VLPs *in vivo* and proved the functionality of transferred siRNAs by qPCR analysis. Further studies will focus on the manipulation of selective cell types (e.g. cancer cells) and the modification of their exosomal small RNA content to study cell-cell communication *in vitro*.

In Figure 59 the key findings of this thesis are summarized and will be summed up in the next chapter (5. Summary).

4. Discussion

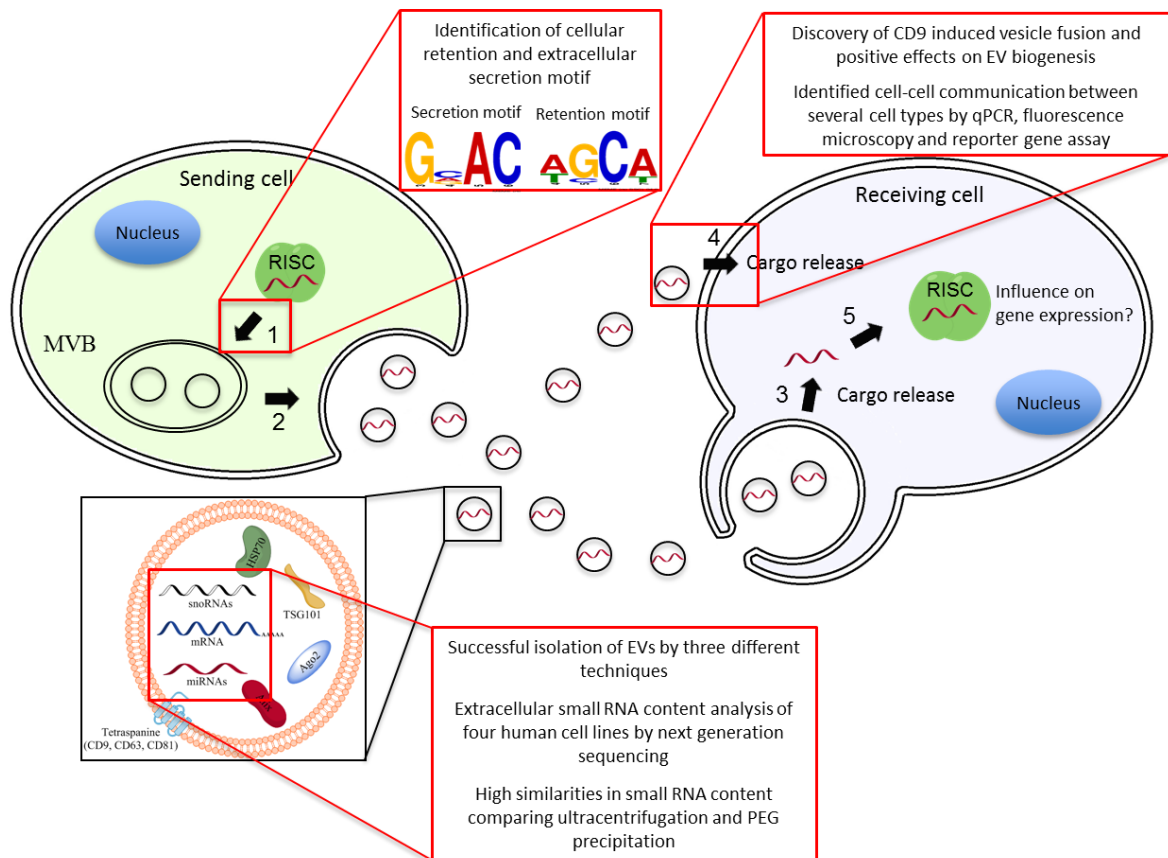


Figure 59: Key findings evaluated in this thesis. Three EV isolation methods were compared in regards of yield and particle size distribution. Via next generation sequencing comparative analysis of intracellular and extracellular small RNAs were performed for four human cell lines. Motif searches revealed an intracellular retention and an exosome secretion motif. Comparison of PEG precipitation and ultracentrifugation revealed only minor differences in extracellular small RNA content. Furthermore, we discovered a role of CD9 in vesicle fusion and on EV production. Cell-cell communication between various cell lines was confirmed by qPCR, fluorescence microscopy and a dual reporter gene assay.

5. Summary

Exosomes are small extracellular vesicles (EVs) of endocytic origin and get released by a multitude of cell types. These vesicles have been found in a variety of body fluids and more recently an important role in exchanging genetic information between cells was postulated for exosomes.

The aims of this thesis were to investigate the npcRNA content of exosomes and analyse their putative role in cell-cell communication. I established three different exosome isolation techniques yielding EVs in the appropriate size range determined by nanoparticle tracking analysis (NTA) and detected three exosomal marker proteins, i.e. Alix, TSG101 and CD9, by immunoblot. Furthermore, the identity of exosomes was confirmed by electron microscopy. Stable cell lines were generated to investigate the effect of the individual marker proteins on exosome production and characteristics. The tetraspanin CD9 positively influenced exosome and microvesicle production, while overexpression of Alix or TSG reduced the amount of EVs. In the context of lentiviral vector production a role in membrane fusion was identified for CD9, indicating a direct participation in fusion of exosomes with target cell membranes. However, extracellular CD9-enriched and WT vesicles comprise similar npcRNA content, suggesting no active role of CD9 in sorting of npcRNAs to exosomes.

The extracellular npcRNA content of four human cell lines was successfully examined via Next Generation Sequencing. Data analysis was performed using the DESeq package in R with self-made, question-adjusted, scripts. NGS data analysis revealed secretion (exosome) and retention (cell) motifs for miRNAs, an important finding for further cell-cell communication studies. Furthermore, I identified differentially expressed miRNAs after Jurkat exosome treatment in Raji cells by NGS and *in silico* analysis revealed two target genes (DNMT1 and Bcl-2) for these candidates. Extracellular vesicles derived from T-lymphocytes transferred sufficient amounts of functional miRNAs to induce a significant knockdown of DNMT1 as was confirmed by qPCR analysis. We generated a reporter gene assay that enabled detection of the horizontal transfer of synthetic siRNA (siGL-2) in exosomes. The results indicated a direct and functional communication via extracellular vesicles. In contact-inhibiting co-cultures we were able to confirm an EV mediated transfer of fluorescent labelled siRNAs between human B-lymphocytes and colon carcinoma cells, reflecting the cellular communication in the tumor microenvironment. Modification of cells with npcRNAs to study EV-functions is difficult in some cell types and hard to adapt for *in vivo* research. We utilized a gene delivery technology based on virus-like particles (VLP) that facilitates modification of cells *in vivo*. Feasibility was confirmed in a rat animal model by systemic delivery of functional siRNAs. The directed *in vivo* manipulation of cells opens new prospects for the exosome research and has to be expanded in the future.

6. Reference

1. Wehman, AM, Poggioli, C, Schweinsberg, P, Grant, BD, and Nance, J (2011). The P4-ATPase TAT-5 inhibits the budding of extracellular vesicles in *C. elegans* embryos. *Curr Biol* **21**: 1951-1959.
2. Silverman JMC, CJ, de'Oliveira CC, Shirvani O, Fang Y (2010). An exosome-based secretion pathway is responsible for protein export from *Leishmania* and communication with macrophages. *Journal of cell science* **123**: 842-852.
3. Pope, SM, and Lasser, C (2013). *Toxoplasma gondii* infection of fibroblasts causes the production of exosome-like vesicles containing a unique array of mRNA and miRNA transcripts compared to serum starvation. *Journal of extracellular vesicles* **2**.
4. Rodrigues, ML, Nakayasu, ES, Almeida, IC, and Nimrichter, L (2014). The impact of proteomics on the understanding of functions and biogenesis of fungal extracellular vesicles. *J Proteomics* **97**: 177-186.
5. Kulp, A, and Kuehn, MJ (2010). Biological functions and biogenesis of secreted bacterial outer membrane vesicles. *Annu Rev Microbiol* **64**: 163-184.
6. Jenjaroenpun, P, Kremenska, Y, Nair, VM, Kremenskoy, M, Joseph, B, and Kurochkin, IV (2013). Characterization of RNA in exosomes secreted by human breast cancer cell lines using next-generation sequencing. *PeerJ* **1**: e201.
7. Aatonen, MT, Ohman, T, Nyman, TA, Laitinen, S, Gronholm, M, and Siljander, PR (2014). Isolation and characterization of platelet-derived extracellular vesicles. *Journal of extracellular vesicles* **3**.
8. Gould, S, Raposo, G. As we wait: coping with an imperfect nomenclature for extracellular vesicles. *J Extracell Vesicles* **2**.
9. Kerr, JF, Wyllie, AH, and Currie, AR (1972). Apoptosis: a basic biological phenomenon with wide-ranging implications in tissue kinetics. *British journal of cancer* **26**: 239-257.
10. Hristov, M, Erl, W, Linder, S, and Weber, PC (2004). Apoptotic bodies from endothelial cells enhance the number and initiate the differentiation of human endothelial progenitor cells in vitro. *Blood* **104**: 2761-2766.
11. Thery, C, *et al.* (2001). Proteomic analysis of dendritic cell-derived exosomes: a secreted subcellular compartment distinct from apoptotic vesicles. *Journal of immunology* **166**: 7309-7318.
12. Casciola-Rosen, LA, Anhalt, G, and Rosen, A (1994). Autoantigens targeted in systemic lupus erythematosus are clustered in two populations of surface structures on apoptotic keratinocytes. *J Exp Med* **179**: 1317-1330.
13. Majno, G, and Joris, I (1995). Apoptosis, oncosis, and necrosis. An overview of cell death. *Am J Pathol* **146**: 3-15.
14. Bilyy, RO, *et al.* (2012). Macrophages discriminate glycosylation patterns of apoptotic cell-derived microparticles. *The Journal of biological chemistry* **287**: 496-503.
15. Minciocchi, VR, Freeman, MR, and Di Vizio, D (2015). Extracellular vesicles in cancer: exosomes, microvesicles and the emerging role of large oncosomes. *Semin Cell Dev Biol* **40**: 41-51.
16. Palmisano, G, *et al.* (2012). Characterization of membrane-shed microvesicles from cytokine-stimulated beta-cells using proteomics strategies. *Mol Cell Proteomics* **11**: 230-243.

6. Reference

17. Hugel, B, Martinez, MC, Kunzelmann, C, and Freyssinet, JM (2005). Membrane microparticles: two sides of the coin. *Physiology (Bethesda)* **20**: 22-27.
18. Ratajczak, J, *et al.* (2006). Embryonic stem cell-derived microvesicles reprogram hematopoietic progenitors: evidence for horizontal transfer of mRNA and protein delivery. *Leukemia* **20**: 847-856.
19. Ratajczak, J, Wysoczynski, M, Hayek, F, Janowska-Wieczorek, A, and Ratajczak, MZ (2006). Membrane-derived microvesicles: important and underappreciated mediators of cell-to-cell communication. *Leukemia* **20**: 1487-1495.
20. Thery, C, *et al.* (1999). Molecular characterization of dendritic cell-derived exosomes. Selective accumulation of the heat shock protein hsc73. *J Cell Biol* **147**: 599-610.
21. Raposo, G, and Stoorvogel, W (2013). Extracellular vesicles: exosomes, microvesicles, and friends. *J Cell Biol* **200**: 373-383.
22. Thery, C, Zitvogel, L, and Amigorena, S (2002). Exosomes: composition, biogenesis and function. *Nature reviews Immunology* **2**: 569-579.
23. Gould, GW, and Lippincott-Schwartz, J (2009). New roles for endosomes: from vesicular carriers to multi-purpose platforms. *Nature reviews Molecular cell biology* **10**: 287-292.
24. Stoorvogel, W, Strous, GJ, Geuze, HJ, Oorschot, V, and Schwartz, AL (1991). Late endosomes derive from early endosomes by maturation. *Cell* **65**: 417-427.
25. Harding, C, Heuser, J, and Stahl, P (1983). Receptor-mediated endocytosis of transferrin and recycling of the transferrin receptor in rat reticulocytes. *J Cell Biol* **97**: 329-339.
26. Vidal, MJ, and Stahl, PD (1993). The small GTP-binding proteins Rab4 and ARF are associated with released exosomes during reticulocyte maturation. *Eur J Cell Biol* **60**: 261-267.
27. Johnstone, RM, Adam, M, Hammond, JR, Orr, L, and Turbide, C (1987). Vesicle formation during reticulocyte maturation. Association of plasma membrane activities with released vesicles (exosomes). *The Journal of biological chemistry* **262**: 9412-9420.
28. Chiba, M, Kimura, M, and Asari, S (2012). Exosomes secreted from human colorectal cancer cell lines contain mRNAs, microRNAs and natural antisense RNAs, that can transfer into the human hepatoma HepG2 and lung cancer A549 cell lines. *Oncology reports* **28**: 1551-1558.
29. Caby, MP, Lankar, D, Vincendeau-Scherrer, C, Raposo, G, and Bonnerot, C (2005). Exosomal-like vesicles are present in human blood plasma. *Int Immunol* **17**: 879-887.
30. Zlotogorski-Hurvitz, A, *et al.* (2015). Human saliva-derived exosomes: comparing methods of isolation. *The journal of histochemistry and cytochemistry : official journal of the Histochemistry Society* **63**: 181-189.
31. Palanisamy, V, Sharma, S, Deshpande, A, Zhou, H, Gimzewski, J, and Wong, DT (2010). Nanostructural and transcriptomic analyses of human saliva derived exosomes. *PloS one* **5**: e8577.
32. Cheng, L, Sun, X, Scicluna, BJ, Coleman, BM, and Hill, AF (2014). Characterization and deep sequencing analysis of exosomal and non-exosomal miRNA in human urine. *Kidney international* **86**: 433-444.
33. Keller S, RC, Stoeck A, Runz S, Fogel M, Lugert S, Hager HD, Abdel-Bakky MS, Gutwein P, Altevogt P. (2007). CD24 is a marker of exosomes secreted into urine and amniotic fluid. *Kidney Int* **72**: 1095-1102.

6. Reference

34. Thery, C (2011). Exosomes: secreted vesicles and intercellular communications. *F1000 Biol Rep* **3**: 15.
35. Mittelbrunn, M, *et al.* (2011). Unidirectional transfer of microRNA-loaded exosomes from T cells to antigen-presenting cells. *Nature communications* **2**: 282.
36. Llorente, A, *et al.* (2013). Molecular lipidomics of exosomes released by PC-3 prostate cancer cells. *Biochimica et biophysica acta* **1831**: 1302-1309.
37. Valadi H., EK, Bossios A., Sjöstrand M., Lee J.J., Lötvall J.O. (2007). Exosome-mediated transfer of mRNAs and microRNAs is a novel mechanism of genetic exchange between cells. *Nature cell biology* **9**: 654-659.
38. Miranda, KC, *et al.* (2010). Nucleic acids within urinary exosomes/microvesicles are potential biomarkers for renal disease. *Kidney international* **78**: 191-199.
39. Chen, TS, Lai, RC, Lee, MM, Choo, AB, Lee, CN, and Lim, SK (2010). Mesenchymal stem cell secretes microparticles enriched in pre-microRNAs. *Nucleic acids research* **38**: 215-224.
40. Villarroya-Beltri, C, *et al.* (2013). Sumoylated hnRNP A2B1 controls the sorting of miRNAs into exosomes through binding to specific motifs. *Nature communications* **4**: 2980.
41. Andreu, Z, and Yanez-Mo, M (2014). Tetraspanins in extracellular vesicle formation and function. *Frontiers in immunology* **5**: 442.
42. Conde-Vancells, J, *et al.* (2008). Characterization and comprehensive proteome profiling of exosomes secreted by hepatocytes. *J Proteome Res* **7**: 5157-5166.
43. Epple, LM, *et al.* (2012). Medulloblastoma exosome proteomics yield functional roles for extracellular vesicles. *PloS one* **7**: e42064.
44. Szala, S, Kasai, Y, Stepkowski, Z, Rodeck, U, Koprowski, H, and Linnenbach, AJ (1990). Molecular cloning of cDNA for the human tumor-associated antigen CO-029 and identification of related transmembrane antigens. *Proceedings of the National Academy of Sciences of the United States of America* **87**: 6833-6837.
45. Jankowski, SA, Mitchell, DS, Smith, SH, Trent, JM, and Meltzer, PS (1994). SAS, a gene amplified in human sarcomas, encodes a new member of the transmembrane 4 superfamily of proteins. *Oncogene* **9**: 1205-1211.
46. Takagi, S, Fujikawa, K., Imai, T., Fukuhara, N., Fukudome, K., Minegishi, M., Tsuchiya, S., Konno, T., Hinuma, Y., Yoshie, O. (1995). Identification of a highly specific surface marker of T-cell acute lymphoblastic leukemia and neuroblastoma as a new member of the transmembrane 4 superfamily. *International journal of cancer* **61**: 706-715.
47. Boucheix, C, *et al.* (1991). Molecular cloning of the CD9 antigen. A new family of cell surface proteins. *The Journal of biological chemistry* **266**: 117-122.
48. Hemler, ME (2005). Tetraspanin functions and associated microdomains. *Nature reviews Molecular cell biology* **6**: 801-811.
49. Si, Z, and Hersey, P (1993). Expression of the neuroglandular antigen and analogues in melanoma. CD9 expression appears inversely related to metastatic potential of melanoma. *International journal of cancer* **54**: 37-43.
50. Sauer, G, Windisch, J., Kurzeder, C., Heilmann, V., Kreienberg, R., Deissler, H. (2003). Progression of Cervical Carcinomas Is Associated with Down-Regulation of CD9 But Strong Local Re-expression at Sites of Transendothelial Invasion. *Clinical Cancer Research* **9**: 6426-6431.
51. Wang JC, BL, Bérubé NG, Chevalier S, Aprikian AG, Gourdeau H, Chevrette M. (2007). Down-regulation of CD9 expression during prostate carcinoma progression is associated with CD9 mRNA modifications. *Clinical Cancer Research* **13**: 2354-2361.

6. Reference

52. Miyado, K, *et al.* (2000). Requirement of CD9 on the egg plasma membrane for fertilization. *Science* **287**: 321-324.
53. Miyado, K, *et al.* (2008). The fusing ability of sperm is bestowed by CD9-containing vesicles released from eggs in mice. *Proceedings of the National Academy of Sciences of the United States of America* **105**: 12921-12926.
54. Hanson, PI, and Cashikar, A (2012). Multivesicular body morphogenesis. *Annual review of cell and developmental biology* **28**: 337-362.
55. Raposo, G, *et al.* (1996). B lymphocytes secrete antigen-presenting vesicles. *J Exp Med* **183**: 1161-1172.
56. Blanchard, N, *et al.* (2002). TCR activation of human T cells induces the production of exosomes bearing the TCR/CD3/zeta complex. *Journal of immunology* **168**: 3235-3241.
57. Vlassov, AV, Magdaleno, S, Setterquist, R, and Conrad, R (2012). Exosomes: current knowledge of their composition, biological functions, and diagnostic and therapeutic potentials. *Biochimica et biophysica acta* **1820**: 940-948.
58. Lobb, RJ, *et al.* (2015). Optimized exosome isolation protocol for cell culture supernatant and human plasma. *Journal of extracellular vesicles* **4**: 27031.
59. Thery, C, Amigorena, S, Raposo, G, and Clayton, A (2006). Isolation and characterization of exosomes from cell culture supernatants and biological fluids. *Curr Protoc Cell Biol Chapter 3*: Unit 3 22.
60. Lasser, C, Eldh, M, and Lotvall, J (2012). Isolation and characterization of RNA-containing exosomes. *Journal of visualized experiments : JoVE*: e3037.
61. Schageman, J, *et al.* (2013). The complete exosome workflow solution: from isolation to characterization of RNA cargo. *BioMed research international* **2013**: 253957.
62. Atha, DH, and Ingham, KC (1981). Mechanism of precipitation of proteins by polyethylene glycols. Analysis in terms of excluded volume. *The Journal of biological chemistry* **256**: 12108-12117.
63. Trawis, J, Kevin, K. (2014). Methods for microvesicle isolation and selective removal. *Patent WO 2013188832 A1*.
64. Mignot, G, Roux, S, Thery, C, Segura, E, and Zitvogel, L (2006). Prospects for exosomes in immunotherapy of cancer. *J Cell Mol Med* **10**: 376-388.
65. Tauro, BJ, *et al.* (2012). Comparison of ultracentrifugation, density gradient separation, and immunoaffinity capture methods for isolating human colon cancer cell line LIM1863-derived exosomes. *Methods* **56**: 293-304.
66. Clayton, A, *et al.* (2001). Analysis of antigen presenting cell derived exosomes, based on immuno-magnetic isolation and flow cytometry. *J Immunol Methods* **247**: 163-174.
67. Koga, K, *et al.* (2005). Purification, characterization and biological significance of tumor-derived exosomes. *Anticancer Res* **25**: 3703-3707.
68. Ecker, JR, and Davis, RW (1986). Inhibition of gene expression in plant cells by expression of antisense RNA. *Proceedings of the National Academy of Sciences of the United States of America* **83**: 5372-5376.
69. Van Blokland R, VdGN, Mol JN, Kooter JM (1994). Transgene-mediated suppression of chalcone synthase expression in *Petunia hybrida* results from an increase in RNA turnover. *Plant J* **6**: 861-877.
70. Fire, A, Xu, S, Montgomery, MK, Kostas, SA, Driver, SE, and Mello, CC (1998). Potent and specific genetic interference by double-stranded RNA in *Caenorhabditis elegans*. *Nature* **391**: 806-811.

6. Reference

71. Wightman, B, Ha, I, and Ruvkun, G (1993). Posttranscriptional regulation of the heterochronic gene *lin-14* by *lin-4* mediates temporal pattern formation in *C. elegans*. *Cell* **75**: 855-862.
72. Kozomara, A, and Griffiths-Jones, S (2011). miRBase: integrating microRNA annotation and deep-sequencing data. *Nucleic acids research* **39**: D152-157.
73. Carthew, RW, and Sontheimer, EJ (2009). Origins and Mechanisms of miRNAs and siRNAs. *Cell* **136**: 642-655.
74. Kim, VN, Han, J, and Siomi, MC (2009). Biogenesis of small RNAs in animals. *Nature reviews Molecular cell biology* **10**: 126-139.
75. Bohnsack MT, CK, Gorlich D. (2004). Exportin 5 is a RanGTP-dependent dsRNA-binding protein that mediates nuclear export of pre-miRNAs. *Rna*: 185-191.
76. Hutvagner, G, and Simard, MJ (2008). Argonaute proteins: key players in RNA silencing. *Nature reviews Molecular cell biology* **9**: 22-32.
77. Liu J, CM, Rivas FV, Marsden CG, Thomson JM, Song JJ, Hammond SM, Joshua-Tor L, Hannon GJ. (2004). Argonaute2 is the catalytic engine of mammalian RNAi. *Science* **305**: 1437-1441.
78. Song, JJ, Smith, SK, Hannon, GJ, and Joshua-Tor, L (2004). Crystal structure of Argonaute and its implications for RISC slicer activity. *Science* **305**: 1434-1437.
79. Melo, SA, *et al.* (2014). Cancer exosomes perform cell-independent microRNA biogenesis and promote tumorigenesis. *Cancer Cell* **26**: 707-721.
80. Zhang, J, *et al.* (2015). Exosome and exosomal microRNA: trafficking, sorting, and function. *Genomics, proteomics & bioinformatics* **13**: 17-24.
81. Lévesque K, HM, Abrahamyan L, Chatel-Chaix L, Poupon V, Gordon H, DesGroseillers L, Gatignol A, Mouland AJ (2006). RNA is mediated by heterogeneous nuclear ribonucleoprotein A2 expression and impacts on viral assembly. *Traffic* **7**: 1177-1193.
82. Hoek, KS, Kidd, GJ, Carson, JH, and Smith, R (1998). hnRNP A2 selectively binds the cytoplasmic transport sequence of myelin basic protein mRNA. *Biochemistry* **37**: 7021-7029.
83. Pan, BT, and Johnstone, RM (1983). Fate of the transferrin receptor during maturation of sheep reticulocytes in vitro: selective externalization of the receptor. *Cell* **33**: 967-978.
84. Regev-Rudzki, N, *et al.* (2013). Cell-cell communication between malaria-infected red blood cells via exosome-like vesicles. *Cell* **153**: 1120-1133.
85. Umezū, T, Ohyashiki, K, Kuroda, M, and Ohyashiki, JH (2013). Leukemia cell to endothelial cell communication via exosomal miRNAs. *Oncogene* **32**: 2747-2755.
86. Simons, M, and Raposo, G (2009). Exosomes--vesicular carriers for intercellular communication. *Current opinion in cell biology* **21**: 575-581.
87. Record M, CK, Poirot M, Silvente-Poirot S. (2014). Exosomes as new vesicular lipid transporters involved in cell-cell communication and various pathophysiological processes. *Biochim Biophys Acta* **1841**: 108-120.
88. Fitzner, D, *et al.* (2011). Selective transfer of exosomes from oligodendrocytes to microglia by macropinocytosis. *Journal of cell science* **124**: 447-458.
89. Fruhbeis, C, *et al.* (2013). Neurotransmitter-triggered transfer of exosomes mediates oligodendrocyte-neuron communication. *PLoS Biol* **11**: e1001604.
90. O'Loughlin, AJ, Woffindale, CA, and Wood, MJ (2012). Exosomes and the emerging field of exosome-based gene therapy. *Curr Gene Ther* **12**: 262-274.
91. Anand, PK (2010). Exosomal membrane molecules are potent immune response modulators. *Commun Integr Biol* **3**: 405-408.

6. Reference

92. Chalmin F, LS, Mignot G, Vincent J, Bruchard M, Remy-Martin JP, Boireau W, Rouleau A, Simon B, Lanneau D, De Thonel A, Multhoff G, Hamman A, Martin F, Chauffert B, Solary E, Zitvogel L, Garrido C, Ryffel B, Borg C, Apetoh L, Rébé C, Ghiringhelli F. (2010). Membrane-associated Hsp72 from tumor-derived exosomes mediates STAT3-dependent immunosuppressive function of mouse and human myeloid-derived suppressor cells. *J Clin Invest* **120**: 457-471.
93. Anderson, JL, and Hope, TJ (2005). Intracellular trafficking of retroviral vectors: obstacles and advances. *Gene therapy* **12**: 1667-1678.
94. Bukrinsky MI, HS, Dempsey MP, Sharova N, Adzhubel A, Spitz L, Lewis P, Goldfarb D, Emerman M, Stevenson M. (1993). A nuclear localization signal within HIV-1 matrix protein that governs infection of non-dividing cells. *Nature* **14**: 666-669.
95. Dull, T, *et al.* (1998). A third-generation lentivirus vector with a conditional packaging system. *Journal of virology* **72**: 8463-8471.
96. Zufferey, R, *et al.* (1998). Self-inactivating lentivirus vector for safe and efficient in vivo gene delivery. *Journal of virology* **72**: 9873-9880.
97. Burns J, FT, Driever W, Burrascano M, Yee J (1993). Vesicular stomatitis virus G glycoprotein pseudotyped retroviral vectors: concentration to very high titer and efficient gene transfer into mammalian and nonmammalian cells. *Proc Nat Acad Sci USA* **90**: 8033-8037.
98. Cronin J, ZX, Reiser J (2005). Altering the tropism of lentiviral vectors through pseudotyping. *Curr Gene Ther* **5**: 387-398.
99. Mastromarino P, CC, Goldoni P, Hauttecoeur B, Orsi N (1987). Characterization of membrane components of the erythrocyte involved in vesicular stomatitis virus attachment and fusion at acidic pH. *J Gen Virol* **68**: 2359-2369.
100. Hall, MP, Burson, KK, and Huestis, WH (1998). Interactions of a vesicular stomatitis virus G protein fragment with phosphatidylserine: NMR and fluorescence studies. *Biochimica et biophysica acta* **1415**: 101-113.
101. Nguyen T, PJ, Farge D, Briand P, Weber A (1998). Amphotropic retroviral vectors displaying hepatocyte growth factor-envelope fusion proteins improve transduction efficiency of primary hepatocytes. *Hum Gene Ther* **17**: 2469-2474.
102. Somia N, ZM, Verma I (1995). Generation of targeted retroviral vectors by using single-chain variable fragment: an approach to in vivo gene delivery. *Proc Nat Acad Sci USA* **92**: 7570-7574.
103. Jiang A, DR (1999). In vivo cell type-specific gene delivery with retroviral vectors that display single chain antibodies. *Gene therapy* **6**: 1982-1987.
104. Valsesia-Wittmann, S, *et al.* (1994). Modifications in the binding domain of avian retrovirus envelope protein to redirect the host range of retroviral vectors. *Journal of virology* **68**: 4609-4619.
105. Kasahara N., DA, Kan Y. (1994). Tissue-specific targeting of retroviral vectors through ligand-receptor interactions. *Science* **266**: 1373-1376.
106. Jiang A., CT, Nocken F., Cichutek K., Dornburg. R. (1998). Cell-type-specific gene transfer into human cells with retroviral vectors that display single-chain antibodies. *Journal of virology* **72**: 10148-10156.
107. Maurice M., VE, Salmon P., Trono D., Russell SJ., Cosset FL. (2002). Efficient gene transfer into human primary blood lymphocytes by surface-engineered lentiviral vectors that display a T cell-activating polypeptide. *Blood* **99**: 2342-2350.
108. Gollan, TJ, and Green, MR (2002). Selective targeting and inducible destruction of human cancer cells by retroviruses with envelope proteins bearing short peptide ligands. *Journal of virology* **76**: 3564-3569.

6. Reference

109. Fielding, AK, Chapel-Fernandes, S, Chadwick, MP, Bullough, FJ, Cosset, FL, and Russell, SJ (2000). A hyperfusogenic gibbon ape leukemia envelope glycoprotein: targeting of a cytotoxic gene by ligand display. *Hum Gene Ther* **11**: 817-826.
110. C. Goldmann, NS, T. Nisslein, G. Hunsmann, W. Luke, H. Petry (2000). Packaging of small molecules into VP1-virus-like particles of the human polyomavirus JC virus. *Journal of virological methods*: 85-90.
111. Salunke, DM, Caspar, DL, and Garcea, RL (1986). Self-assembly of purified polyomavirus capsid protein VP1. *Cell* **46**: 895-904.
112. Salunke, DM, Caspar, DL, and Garcea, RL (1989). Polymorphism in the assembly of polyomavirus capsid protein VP1. *Biophys J* **56**: 887-900.
113. Brady, JN, Winston, V.D., Consigli, R.A (1977). Dissociation of polyoma virus by the chelation of calcium ions found associated with purified virions. *J Virol* **23**: 717-724.
114. Neu U, MM, Palma AS, Ströh LJ, Nelson CD, Feizi T, Atwood WJ, Stehle T. (2010). Structure-function analysis of the human JC polyomavirus establishes the LSTc pentasaccharide as a functional receptor motif. *Cell host & microbe* **8**: 309-319.
115. Querbes W, BA, Tosoni D, Di Fiore PP, Atwood WJ. (2004). A JC virus-induced signal is required for infection of glial cells by a clathrin- and eps15-dependent pathway. *Journal of virology* **78**: 250-256.
116. Johnson, EL, Chu, H, Byrareddy, SN, Spearman, P, and Chakraborty, R (2015). Placental Hofbauer cells assemble and sequester HIV-1 in tetraspanin-positive compartments that are accessible to broadly neutralizing antibodies. *Journal of the International AIDS Society* **18**: 19385.
117. Inoue, H, Nojima, H, and Okayama, H (1990). High efficiency transformation of Escherichia coli with plasmids. *Gene* **96**: 23-28.
118. Lestrade, L, and Weber, MJ (2006). snoRNA-LBME-db, a comprehensive database of human H/ACA and C/D box snoRNAs. *Nucleic acids research* **34**: D158-162.
119. Anders, S, and Huber, W (2010). Differential expression analysis for sequence count data. *Genome biology* **11**: R106.
120. Team, RC (2014). A language and environment for statistical computing. *R Foundation for Statistical Computing, Vienna, Austria*.
121. Richardson KC, JL, Finke EH (1960). Embedding in epoxy resins for ultra-thin sectioning in electron microscopy. *Stain Technol* **35**: 313-325.
122. Campeau, E, et al. (2009). A versatile viral system for expression and depletion of proteins in mammalian cells. *PLoS one* **4**: e6529.
123. Lee, HH, Elia, N, Ghirlando, R, Lippincott-Schwartz, J, and Hurley, JH (2008). Midbody targeting of the ESCRT machinery by a noncanonical coiled coil in CEP55. *Science* **322**: 576-580.
124. Yoo, AS, et al. (2011). MicroRNA-mediated conversion of human fibroblasts to neurons. *Nature* **476**: 228-231.
125. Stewart, SA, et al. (2003). Lentivirus-delivered stable gene silencing by RNAi in primary cells. *Rna* **9**: 493-501.
126. Fischbach, G (1972). Synapse formation between dissociated nerve and muscle cells in low density cell cultures. *Developmental Biology* **28**: 407-429.
127. Shimada, Y, Fischman, DA, and Moscona, AA (1969). Formation of neuromuscular junctions in embryonic cell cultures. *Proceedings of the National Academy of Sciences of the United States of America* **62**: 715-721.
128. Mulvaney, P (1996). Surface Plasmon Spectroscopy of Nanosized Metal Particles. *Langmuir* **12**: 788-800.

6. Reference

129. Weber K, PJ, Osborn M (1972). Measurement of molecular weights by electrophoresis on SDS-crylamide gel. *PtC:3-27* **26**.
130. Cleveland, DW, Fischer, SG, Kirschner, MW, and Laemmli, UK (1977). Peptide mapping by limited proteolysis in sodium dodecyl sulfate and analysis by gel electrophoresis. *The Journal of biological chemistry* **252**: 1102-1106.
131. Fitzgerald, D, Berger, P, Schaffitzel, C, Yamada, K, Richmond, TJ and Berger, I (2006). Protein complex expression by using multigene baculoviral vectors. *Nat Methods* **3**: 1021-1032.
132. Ben-Bassat H, GN, Mitrani S, Goldblum T, Yoffey JM, Cohen MM, Bentwich Z, Ramot B, Klein E, Klein G. (1977). Establishment in continuous culture of a new type of lymphocyte from a "Burkitt like" malignant lymphoma (line D.G.-75). *International journal of cancer* **19**: 27-33.
133. Rahbari, R, Sheahan, T, Modes, V, Collier, P, Macfarlane, C, and Badge, RM (2009). A novel L1 retrotransposon marker for HeLa cell line identification. *Biotechniques* **46**: 277-284.
134. Oliveros, JC (2007-2015). Venny. An interactive tool for comparing lists with Venn's diagrams. .
135. Chahar, HS, Bao, X, and Casola, A (2015). Exosomes and Their Role in the Life Cycle and Pathogenesis of RNA Viruses. *Viruses* **7**: 3204-3225.
136. Kadiu, I, Narayanasamy, P., Dash, P. K., Zhang, W., Gendelman, H. E. (2012). Biochemical and Biologic Characterization of Exosomes and Microvesicles as Facilitators of HIV-1 Infection in Macrophages. *Journal of immunology* **189**: 744-754.
137. Hudry, E, *et al.* (2016). Exosome-associated AAV vector as a robust and convenient neuroscience tool. *Gene therapy* **23**: 380-392.
138. Böker, KO, Lemus, N., Rinaldi Ferreira, R., Schiller, L. T., Schneider, S., Gruber, J. (2016). The impact of the CD9 tetraspanin on exosome secretion and lentivirus infectivity. *Molecular Therapy (in review)*.
139. Druz, A, Chen, Y., Guha, R., Betenbaugh, M., Martin, S., Shiloach, J. (2013). Large-scale screening identifies a novel microRNA, miR-15a-3p, which induces apoptosis in human cancer cell lines. *RNA biology* **10**: 287-300.
140. Scherr, M, Elder, A., Battmer, K., Barzan, D., Bomken, S., Ricke-Hoch, M., Schröder, A., Venturini, L., Blair, H. J., Vormoor, J., Ottmann, O., Ganser, A., Pich, A., Hilfiker-Kleiner, D., Heidenreich, O., Eder, M. (2014). Differential expression of miR-17~92 identifies BCL2 as a therapeutic target in BCR-ABL-positive B-lineage acute lymphoblastic leukemia. *Leukemia* **28.3**: 554-565.
141. Pan, W, *et al.* (2010). MicroRNA-21 and microRNA-148a contribute to DNA hypomethylation in lupus CD4+ T cells by directly and indirectly targeting DNA methyltransferase 1. *Journal of immunology* **184**: 6773-6781.
142. Braconi, C, Huang, N, and Patel, T (2010). MicroRNA-dependent regulation of DNA methyltransferase-1 and tumor suppressor gene expression by interleukin-6 in human malignant cholangiocytes. *Hepatology* **51**: 881-890.
143. Zhang, H, *et al.* (2011). MiR-148a promotes apoptosis by targeting Bcl-2 in colorectal cancer. *Cell Death Differ* **18**: 1702-1710.
144. Lemus-Diaz, N, Böker, K. O., Rodriguez-Polo, I., Mitter, M., Preis, J., Gruber, J. (2016). Dissecting the gene regulatory activity of miRNAs at the single cell level. *Scientific Reports (in review)*.
145. Chapagain, ML, and Nerurkar, VR (2010). Human polyomavirus JC (JCV) infection of human B lymphocytes: a possible mechanism for JCV transmigration across the blood-brain barrier. *J Infect Dis* **202**: 184-191.

6. Reference

146. Goldmann, C, *et al.* (1999). Molecular cloning and expression of major structural protein VP1 of the human polyomavirus JC virus: formation of virus-like particles useful for immunological and therapeutic studies. *Journal of virology* **73**: 4465-4469.
147. Hoffmann, DB, *et al.* (2016). In Vivo siRNA Delivery Using JC Virus-like Particles Decreases the Expression of RANKL in Rats. *Molecular therapy Nucleic acids* **5**: e298.
148. Chang, D, *et al.* (1997). Self-assembly of the JC virus major capsid protein, VP1, expressed in insect cells. *J Gen Virol* **78 (Pt 6)**: 1435-1439.
149. C.N. Chao, MCL, C.Y. Fang, P.L. Chen, D. Chang, C.H. Shen, M. Wang (2016). Gene Therapy for Human Lung Adenocarcinoma Using a Suicide Gene Driven by a Lung-Specific Promoter Delivered by JC Virus-Like Particles. *PloS one*.
150. Lin, MC, Wang, M, Fang, CY, Chen, PL, Shen, CH, and Chang, D (2014). Inhibition of BK virus replication in human kidney cells by BK virus large tumor antigen-specific shRNA delivered by JC virus-like particles. *Antiviral Res* **103**: 25-31.
151. Renard, HF, *et al.* (2015). Endophilin-A2 functions in membrane scission in clathrin-independent endocytosis. *Nature* **517**: 493-496.
152. Ren, D, Wang, J. and You, Z. (2014). Long-term monitoring of capase-3 activity in living cells based on the FRET probe composed of quantum dot, nanogold and EGF. *RSC Adv* **4**: 54907-54918.
153. Leibovitz, A, Stinson, JC, McCombs, WB, 3rd, McCoy, CE, Mazur, KC, and Mabry, ND (1976). Classification of human colorectal adenocarcinoma cell lines. *Cancer Res* **36**: 4562-4569.
154. Ohno, S, *et al.* (2013). Systemically injected exosomes targeted to EGFR deliver antitumor microRNA to breast cancer cells. *Molecular therapy : the journal of the American Society of Gene Therapy* **21**: 185-191.
155. Lin, J, *et al.* (2015). Exosomes: novel biomarkers for clinical diagnosis. *ScientificWorldJournal* **2015**: 657086.
156. Shelke, GV, Lasser, C, Gho, YS, and Lotvall, J (2014). Importance of exosome depletion protocols to eliminate functional and RNA-containing extracellular vesicles from fetal bovine serum. *Journal of extracellular vesicles* **3**.
157. Rider, MA, Hurwitz, SN, and Meckes, DG, Jr. (2016). ExtraPEG: A Polyethylene Glycol-Based Method for Enrichment of Extracellular Vesicles. *Sci Rep* **6**: 23978.
158. Albertsson, PA, and Frick, G (1960). Partition of virus particles in a liquid two-phase system. *Biochimica et biophysica acta* **37**: 230-237.
159. Taylor DD, SS (2015). Methods of isolating extracellular vesicles impact downstream analyses of their cargoes. *Methods* **87**: 3-10.
160. Mathivanan, S, Ji, H, and Simpson, RJ (2010). Exosomes: extracellular organelles important in intercellular communication. *J Proteomics* **73**: 1907-1920.
161. Johnstone, RM (2006). Exosomes biological significance: A concise review. *Blood Cells Mol Dis* **36**: 315-321.
162. Bobrie, A, Colombo, M., Krumeich, S., Raposo, G., Thery, C. (2012). Diverse subpopulations of vesicles secreted by different intracellular mechanisms are present in exosome preparations obtained by differential ultracentrifugation. *Journal of extracellular vesicles* **1**.
163. Escola, JM, Kleijmeer, MJ, Stoorvogel, W, Griffith, JM, Yoshie, O, and Geuze, HJ (1998). Selective enrichment of tetraspan proteins on the internal vesicles of multivesicular endosomes and on exosomes secreted by human B-lymphocytes. *The Journal of biological chemistry* **273**: 20121-20127.

6. Reference

164. Fritzsching, B, Schwer, B, Kartenbeck, J, Pedal, A, Horejsi, V, and Ott, M (2002). Release and intercellular transfer of cell surface CD81 via microparticles. *Journal of immunology* **169**: 5531-5537.
165. Charrin, S, Manie, S, Oualid, M, Billard, M, Boucheix, C, and Rubinstein, E (2002). Differential stability of tetraspanin/tetraspanin interactions: role of palmitoylation. *FEBS letters* **516**: 139-144.
166. Gallo A, TM, Alevizos I, Illei GG (2012). The majority of microRNAs detectable in serum and saliva is concentrated in exosomes. *PloS one* **7**.
167. Rajalingam, D, Loftis, C, Xu, JJ, and Kumar, TK (2009). Trichloroacetic acid-induced protein precipitation involves the reversible association of a stable partially structured intermediate. *Protein Sci* **18**: 980-993.
168. Mueller, O, *et al.* (2000). A microfluidic system for high-speed reproducible DNA sizing and quantitation. *Electrophoresis* **21**: 128-134.
169. Imbeaud S, GE, Boulanger V, Barlet X, Zaborski P, Eveno E, Mueller O, Schroeder A, Auffray C. (2005). Towards standardization of RNA quality assessment using user-independent classifiers of microcapillary electrophoresis traces. *Nucleic acids research* **33**.
170. Samarsky, DFMSRBE (1998). The snoRNA box C/D motif directs nucleolar targeting and also couples snoRNA synthesis and localization. *The EMBO journal* **17**: 3747-3757.
171. Saini, S, *et al.* (2014). Regulation of SRC kinases by microRNA-3607 located in a frequently deleted locus in prostate cancer. *Mol Cancer Ther* **13**: 1952-1963.
172. Tamaddon, G, Geramizadeh, B., Hossein, M. K., Mowla, S. J., Abroun, S. (2016). miR-4284 and miR-4484 as Putative Biomarkers for Diffuse Large B-Cell Lymphoma. *IJMS* **41**: 334-339.
173. Kuosmanen, SM, Hartikainen, J, Hippelainen, M, Kokki, H, Levonen, AL, and Tavi, P (2015). MicroRNA profiling of pericardial fluid samples from patients with heart failure. *PloS one* **10**: e0119646.
174. Zhang GJ, ZH, Xiao HX, Li Y, Zhou T. (2014). MiR-378 is an independent prognostic factor and inhibits cell growth and invasion in colorectal cancer. *BMC Cancer* **14**.
175. Lunavat, TR, *et al.* (2015). Small RNA deep sequencing discriminates subsets of extracellular vesicles released by melanoma cells--Evidence of unique microRNA cargos. *RNA biology* **12**: 810-823.
176. Deng L, BF, Stevens H, Lu R, Caudrillier A, McBride M, McClure JD, Grant J, Thomas M, Frid M, Stenmark K, White K, Seto AG, Morrell NW, Bradshaw AC, MacLean MR, Baker AH (2015). MicroRNA-143 Activation Regulates Smooth Muscle and Endothelial Cell Crosstalk in Pulmonary Arterial Hypertensio. *Circ Res* **117**: 870-883.
177. Sarachana T, DN, Simhadri VL, Pandey GS, Saini S, Guelcher C, Guerrero MF, Kimchi-Sarfaty C, Sauna ZE, Atreya CD. (2015). Small ncRNA Expression-Profiling of Blood from Hemophilia A Patients Identifies miR-1246 as a Potential Regulator of Factor 8 Gene. *PloS one* **10**: doi: 10.1371/journal.pone.0132433. eCollection 0132015.
178. Jørgensen, S, Tholstrup, D., Hansen, J. W., Keld, H. M., Hjalgrim, H., de Nully Brown, P. Troelsen, J (2014). Plasma Microrna Predicts B-Cell Lymphoma up to 12 Months before Diagnosis – Data from the Danish Blood Donor Study. *Blood* **124**.
179. Favreau, AJ, and Sathyanarayana, P (2012). miR-590-5p, miR-219-5p, miR-15b and miR-628-5p are commonly regulated by IL-3, GM-CSF and G-CSF in acute myeloid leukemia. *Leuk Res* **36**: 334-341.

6. Reference

180. Yuan, T, *et al.* (2016). Plasma extracellular RNA profiles in healthy and cancer patients. *Sci Rep* **6**: 19413.
181. Sumbul, AT, *et al.* (2014). miR-204-5p expression in colorectal cancer: an autophagy-associated gene. *Tumour Biol* **35**: 12713-12719.
182. Leidinger, P, Backes, C, Meder, B, Meese, E, and Keller, A (2014). The human miRNA repertoire of different blood compounds. *BMC genomics* **15**: 474.
183. Cheloufi, S, Dos Santos, CO, Chong, MM, and Hannon, GJ (2010). A dicer-independent miRNA biogenesis pathway that requires Ago catalysis. *Nature* **465**: 584-589.
184. Ekstrom K, VH, Sjostrand M, Malmhall C, Bossios A, Eldh, M., Lötval, J. (2012). Characterization of mRNA and microRNA in human mast cell-derived exosomes and their transfer to other mast cells and blood CD34 progenitor cells. *Journal of extracellular vesicles* **1**: 1-12.
185. Koppers-Lalic, D, *et al.* (2014). Nontemplated nucleotide additions distinguish the small RNA composition in cells from exosomes. *Cell Rep* **8**: 1649-1658.
186. Guduric-Fuchs, J, O'Connor, A, Camp, B, O'Neill, CL, Medina, RJ, and Simpson, DA (2012). Selective extracellular vesicle-mediated export of an overlapping set of microRNAs from multiple cell types. *BMC genomics* **13**: 357.
187. Mohan A, SR, Kumari M, Garg D, Upadhyay A, Ecelbarger CM, Tripathy S, Tiwari S. (2016). Urinary Exosomal microRNA-451-5p Is a Potential Early Biomarker of Diabetic Nephropathy in Rats. *PloS one* **11**: doi: 10.1371/journal.pone.0154055.
188. Hannafon, BN, and Ding, WQ (2013). Intercellular communication by exosome-derived microRNAs in cancer. *Int J Mol Sci* **14**: 14240-14269.
189. Karpova, MB, Schoumans, J, Ernberg, I, Henter, JI, Nordenskjold, M, and Fadeel, B (2005). Raji revisited: cytogenetics of the original Burkitt's lymphoma cell line. *Leukemia* **19**: 159-161.
190. Eirin, A, *et al.* (2014). MicroRNA and mRNA cargo of extracellular vesicles from porcine adipose tissue-derived mesenchymal stem cells. *Gene* **551**: 55-64.
191. Gonzalez-Martin A, AB, Lai M, Shepherd J, Salvador-Bernaldez M, Salvador JM, Lu J, Nemazee D, Xiao C. (2016). The microRNA miR-148a functions as a critical regulator of B cell tolerance and autoimmunity. *Nat Immunol* **17**: 433-440.
192. Haibo Yu, JL, Lielian Zuo, Qijia Yan, Zhengyuan Yu, Xiayu Li, Jin Huang, Lian Zhao, Hailin Tang, Zhaohui Luo, Qianjin Liao, Zhaoyang Zeng, Junyi Zhang and Guiyuan Li (2012). Epstein-Barr Virus Downregulates MicroRNA 203 through the Oncoprotein Latent Membrane Protein 1: a Contribution to Increased Tumor Incidence in Epithelial Cells. *J Virol* **86**: 3088-3099.
193. Ji, H, *et al.* (2014). Deep sequencing of RNA from three different extracellular vesicle (EV) subtypes released from the human LIM1863 colon cancer cell line uncovers distinct miRNA-enrichment signatures. *PloS one* **9**: e110314.
194. Kumar, P, *et al.* (2013). Circulating miRNA biomarkers for Alzheimer's disease. *PloS one* **8**: e69807.
195. Watkins, NJ, Lemm, I, and Luhrmann, R (2007). Involvement of nuclear import and export factors in U8 box C/D snoRNP biogenesis. *Mol Cell Biol* **27**: 7018-7027.
196. Rodosthenous, RS, Coull, BA, Lu, Q, Vokonas, PS, Schwartz, JD, and Baccarelli, AA (2016). Ambient particulate matter and microRNAs in extracellular vesicles: a pilot study of older individuals. *Part Fibre Toxicol* **13**: 13.
197. Miyamae M, KS, Ichikawa D, Kawaguchi T, Hirajima S, Okajima W, Ohashi T, Imamura T, Konishi H, Shiozaki A, Morimura R, Ikoma H, Ochiai T, Okamoto K, Taniguchi H, Otsuji E. (2015). Plasma microRNA profiles: identification of miR-

6. Reference

- 744 as a novel diagnostic and prognostic biomarker in pancreatic cancer. *British journal of cancer* **113**: 1467-1476.
198. Meckes, DG, Jr., and Raab-Traub, N (2011). Microvesicles and viral infection. *Journal of virology* **85**: 12844-12854.
199. Gould, SJ, Booth, AM, and Hildreth, JE (2003). The Trojan exosome hypothesis. *Proceedings of the National Academy of Sciences of the United States of America* **100**: 10592-10597.
200. Charrin, S, Jouannet, S, Boucheix, C, and Rubinstein, E (2014). Tetraspanins at a glance. *Journal of cell science* **127**: 3641-3648.
201. Wagner, KU, *et al.* (2003). Tsg101 Is Essential for Cell Growth, Proliferation, and Cell Survival of Embryonic and Adult Tissues. *Molecular and Cellular Biology* **23**: 150-162.
202. Oh, KB, Stanton, MJ, West, WW, Todd, GL, and Wagner, KU (2007). Tsg101 is upregulated in a subset of invasive human breast cancers and its targeted overexpression in transgenic mice reveals weak oncogenic properties for mammary cancer initiation. *Oncogene* **26**: 5950-5959.
203. Trioulier, Y, *et al.* (2004). Alix, a protein regulating endosomal trafficking, is involved in neuronal death. *The Journal of biological chemistry* **279**: 2046-2052.
204. Stipp CS, KT, Hemler ME. (2001). EWI-2 is a major CD9 and CD81 partner and member of a novel Ig protein subfamily. *The Journal of biological chemistry* **276**: 40545-40554.
205. Kremontsov, DN, Weng, J, Lambele, M, Roy, NH, and Thali, M (2009). Tetraspanins regulate cell-to-cell transmission of HIV-1. *Retrovirology* **6**: 64.
206. Monk, PN, and Partridge, LJ (2012). Tetraspanins: gateways for infection. *Infect Disord Drug Targets* **12**: 4-17.
207. Tippett, E, Cameron, PU, Marsh, M, and Crowe, SM (2013). Characterization of tetraspanins CD9, CD53, CD63, and CD81 in monocytes and macrophages in HIV-1 infection. *J Leukoc Biol* **93**: 913-920.
208. Deneka, M, Pelchen-Matthews, A, Byland, R, Ruiz-Mateos, E, and Marsh, M (2007). In macrophages, HIV-1 assembles into an intracellular plasma membrane domain containing the tetraspanins CD81, CD9, and CD53. *The Journal of cell biology* **177**: 329-341.
209. Yanez-Mo, M, Barreiro, O, Gordon-Alonso, M, Sala-Valdes, M, and Sanchez-Madrid, F (2009). Tetraspanin-enriched microdomains: a functional unit in cell plasma membranes. *Trends Cell Biol* **19**: 434-446.
210. They, C, Ostrowski, M., Segura, E. (2009). Membrane vesicles as conveyors of immune responses. *Nat Rev Immunol* **9**: 581-593.
211. Xu Q., JY, Yin Y., Li Q., He J., Jing Y. (2012). A regulatory circuit of miR-148a/152 and DNMT1 in modulating cell transformation and tumor angiogenesis through IGF-IR and IRS1. *J Mol Biol* **5**: 3-13.
212. Maurisse, R, De Semir, D., Enamekhoo, H., Bedayat, B., Abdolmohammadi, A., Parsi, H., Gruener, D. (2010). Comparative transfection of DNA into primary and transformed mammalian cells from different lineages. *BMC Biotechnology* **10**: DOI: 10.1186/1472-6750-1110-1189.
213. Bauer, M, *et al.* (2006). Toxic effects of lipid-mediated gene transfer in ventral mesencephalic explant cultures. *Basic Clin Pharmacol Toxicol* **98**: 395-400.
214. Salido-Guadarrama, I, Romero-Cordoba, S., Peralta-Zaragoza, O., Hidalgo-Miranda, A., Rodriguez-Dorantes, M. (2014). Micrornas transported by exosomes in body fluids as mediators of intercellular communication in cancer. *OncoTargets and therapy* **7**: 1327-1338.

6. Reference

215. Hoffmann, DB, *et al.* (2016). In Vivo siRNA Delivery Using JC Virus-like Particles Decreases the Expression of RANKL in Rats. *Molecular therapy Nucleic acids* **5**: e298.
216. R. Komagome, HS, T. Suzuki, Y. Suzuki, S. Tanaka, W.J. Atwood, K. Nagashima (2002). Oligosaccharides as receptors for JC virus. *Journal of virology* **76**: 12992-13000.
217. C.K. Liu, GW, W.J. Atwood, (1998). Infection of glial cells by the human polyomavirus JC is mediated by an N-linked glycoprotein containing terminal alpha(2-6)-linked sialic acids. *Journal of virology* **72**: 4643-4649.
218. Schneider, S, Schiller, L. T., Böker, K. O., Lemus-Diaz, N., Gruber, J. (2016). Retargeted JC polyoma derived virus-like particles as efficient and specific cell transduction tool. *Journal of controlled release* **(in review)**.
219. Zhang, L, *et al.* (2016). Three-dimensional structural dynamics and fluctuations of DNA-nanogold conjugates by individual-particle electron tomography. *Nature communications* **7**: 11083.
220. Ackerson, CJ, Powell, RD, and Hainfeld, JF (2010). Site-specific biomolecule labeling with gold clusters. *Methods Enzymol* **481**: 195-230.
221. Horisberger, M, and Rosset, J (1977). Colloidal gold, a useful marker for transmission and scanning electron microscopy. *The journal of histochemistry and cytochemistry : official journal of the Histochemistry Society* **25**: 295-305.
222. Gruenberg, JaS, H. (2004). The biogenesis of multivesicular endosomes. *Nature Reviews Molecular Cell Biology* **5**: 317-323.
223. Milane L, SA, Mattheolabakis G, Suresh M, Amiji MM. (2015). Exosome Mediated Communication within the Tumor Microenvironment. *J Control Release* **10**: 276-294.
224. I. Parolini, CF, C. Raggi, L. Lugini, S. Palleschi, A. De Milito, C. Coscia, E. Iessi, and M. Logozzi, AM, M. Colone, M. Tatti, M. Sargiacomo, S. Fais, (2009). Microenvironment pH is a key factor for exosome traffic in tumor cells. *The Journal of biological chemistry* **284**: 34211-34222.
225. Quail, DF, and Joyce, JA (2013). Microenvironmental regulation of tumor progression and metastasis. *Nat Med* **19**: 1423-1437.
226. Dai, SQ, *et al.* (2014). Serotonin regulates osteoblast proliferation and function in vitro. *Braz J Med Biol Res* **47**: 759-765.
227. Liang C, GB, Wu H, Shao N, Li D, Liu J, Dang L, Wang C, Li H, Li S, Lau WK, Cao Y, Yang Z, Lu C, He X, Au DW, Pan X, Zhang BT, Lu C, Zhang H, Yue K, Qian A, Shang P, Xu J, Xiao L, Bian Z, Tan W, Liang Z, He F, Zhang L, Lu A, Zhang G. (2015). Aptamer-functionalized lipid nanoparticles targeting osteoblasts as a novel RNA interference-based bone anabolic strategy. *Nat Med* **21**: 288-294.
228. Hu, YB, Li, DG, and Lu, HM (2007). Modified synthetic siRNA targeting tissue inhibitor of metalloproteinase-2 inhibits hepatic fibrogenesis in rats. *J Gene Med* **9**: 217-229.

7. Acknowledgements

First of all I would like to express my gratitude towards my supervisor Dr. Jens Gruber for providing this interesting project. Thank you for your patience, support and always open mind for new ideas.

Furthermore, I would like to thank Prof. Dr. Lutz Walter for his great support during my PhD and the always helpful discussions.

Prof. Dr. Reinhard Jahn and Prof. Dr. Mika Simons I would like to thank for being part of my thesis committee, for the nice atmosphere during my committee meetings and all the tips and suggestions provided there.

Prof. Dr. Uwe Groß and Dr Julia Gross I want to thank for taking part in my extended thesis committee.

Prof Dr Anja Schneider and Dr. Anne Stündl I would like to thank for providing the NTA machine and for the nice introduction and patience.

I want to thank Larissa Hummel and Nadine Schminke for explaining every detail for negative staining and electron microscopy in general.

Special thanks go to Angelina Schuder, Astrid Backhaus and Ellen Eckermann-Felkl for the outstanding technical supervision, support during several cloning steps and animating words.

Dr. Stefan Schneider, the “one and only” Postdoc, I want to thank for the nice ideas and discussions during our coffee breaks and for providing the remarkably VLP material.

Especially I want to thank Nicolas Lemus for the support during my thesis, all the discussions even late at night in the lab and for inventing the awesome UTA system. Your always open mind and honesty were very important for promoting my thesis.

An enormous amount of gratitude goes to Rafael Rinaldi, who was always a great help in performing Elisa experiments or during the last weeks of my PhD. You (sometimes your “grumpiness”) and your cat Nikita always conjure a smile on my lips.

I want to thank Lara Timantra Schiller together with all the present and former members of the DPZ institute for the last years of my PhD.

Nina Schindler receives my thanks for proofreading and sustaining my expandable english.

Special thanks go to Pascal and Marco for all the good times, the evenings and nights in Vlotho or Koblenz and the always supporting words.

Very big and special thanks go to Annika and Lars Felix, the loves of my life, for putting me up during the hard times and for the excellent catering.

Last, but not least, I would like to thank my family, especially my parents and my sister Andrea for supporting me during my thesis

8. Abbreviations

8. Abbreviations

aa	amino acid
ab	antibody
APS	ammoniumperoxodisulfate
Amp	ampicillin
ATP	adenosine triphosphate
β -ME	beta mercaptoethanol
BSA	bovine serum albumin
bp	base pair
Ca	calcium
Da	dalton
DAPI	4'-6'-diamidin-2'-phenylindol-dihydrochlorid
DMEM	Dulbecco's modified Eagle's medium
DMSO	dimethylsulfoxide
DNA	deoxyribonucleic acid
dNTP	desoxynucleotide triphosphate
E. coli	Escherichia coli
ECL	enhanced chemiluminescence
EDTA	ethylendiamine tetraacetate
h	hour(s)
HRP	horse radish peroxidase
IPTG	isopropyl- β -D-thiogalactopyranosid
k	kilo
kDa	kilo Dalton
MCS	multiple cloning site
min	minute(s)
m	milli
μ	micro
Mg	magnesium
mRNA	messenger RNA
MW	relative molecular weight

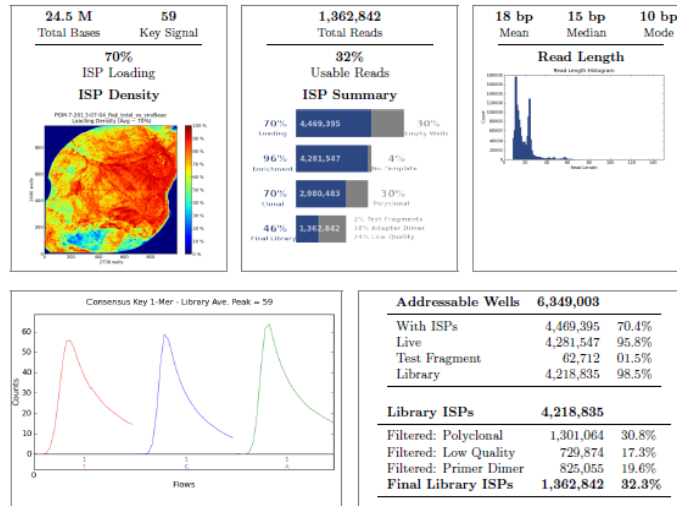
PAGE	polyacrylamide gel electrophoresis
PBS	phosphate buffered saline
PCR	polymerase chain reaction
RNA	ribonucleic acid
rRNA	ribosomal ribonucleic acid
ss	single stranded
ds	double stranded
rpm	revolutions per minute
s	second(s)
SDS	sodium dodecyl sulphate
siRNA	small interfering RNA
Tris	Tris(hydroxymethyl)-aminomethane
U	unit
wt	wild type
x g	x-fold gravity double stranded
rpm	revolutions per minute
s	second(s)
SDS	sodium dodecyl sulphate
siRNA	small interfering RNA
Tris	Tris(hydroxymethyl)-aminomethane
U	unit
wt	wild type
x g	x-fold gravity

9. Appendix

9. Appendix

9.1 Raji sequencing reports

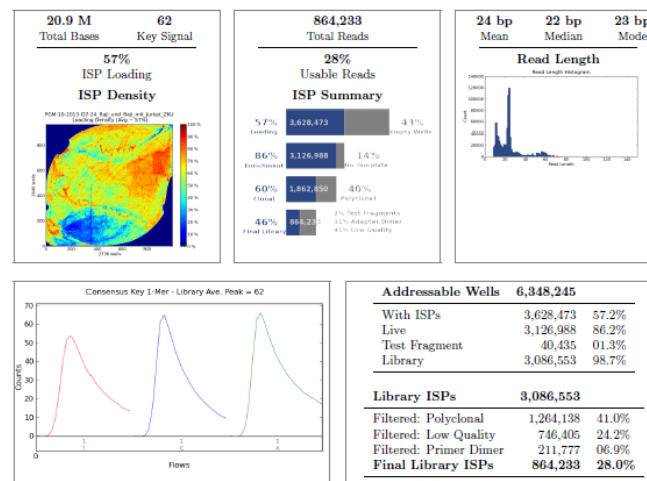
9.1.1 Intracellular Raji library (Raji cell1)



Barcode Name	Sample	Bases	≥ Q20	Reads	Mean Read Length
No barcode	none	995,503	687,144	33,475	30 bp
IonXpressRNA_001	Raji total	23,564,413	17,603,849	1,328,741	18 bp

Test Fragment	Reads	Percent 50AQ17	Read Length Histogram
TF_A	61,149	89%	

9.1.2 Intracellular Raji library (Raji cell3)

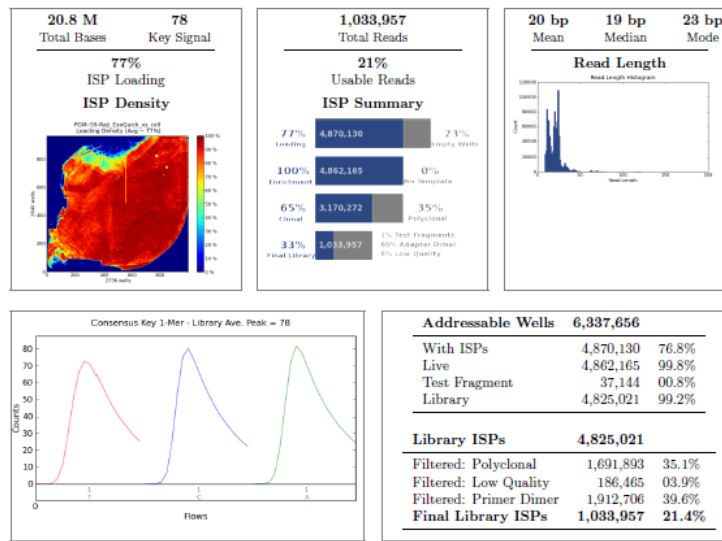


Barcode Name	Sample	Bases	≥ Q20	Reads	Mean Read Length
No barcode	None	1,376,323	728,078	48,584	28 bp
IonXpressRNA_001	Raji	4,203,270	3,523,460	229,203	18 bp
IonXpressRNA_008	Raji mit Jurkat_ZKU	15,339,630	12,987,431	586,308	26 bp

Test Fragment	Reads	Percent 50AQ17	Read Length Histogram
TF_A	39,563	92%	

9. Appendix

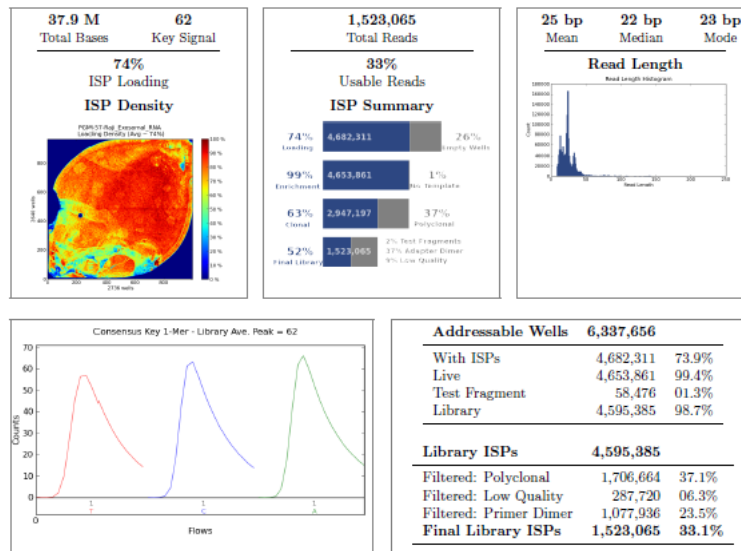
9.1.3 Intracellular Raji (Raji cell2) and exosomal Raji library (Raji exo3)



Barcode Name	Sample	Bases	≥ Q20	Reads	Mean Read Length
No barcode	none	5,444,778	2,866,358	247,669	22 bp
IonXpressRNA.001	Raji cell	9,482,133	7,795,966	519,690	18 bp
IonXpressRNA.014	Raji EQ	5,883,148	4,844,129	266,501	22 bp

Test Fragment	Reads	Percent 50AQ17	Read Length Histogram
TF_A	35,640	75%	

9.1.4 Exosomal Raji library (Raji exo1)

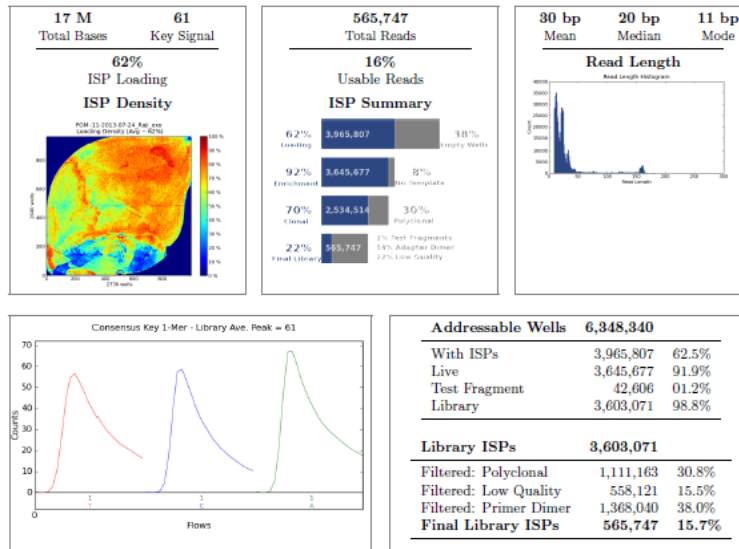


Barcode Name	Sample	Bases	≥ Q20	Reads	Mean Read Length
No barcode	none	1,069,999	773,252	33,160	32 bp
IonXpressRNA.007	Raji Exosomal RNA	36,856,068	29,874,693	1,489,896	25 bp

Test Fragment	Reads	Percent 50AQ17	Read Length Histogram
TF_A	57,597	92%	

9. Appendix

9.1.4 Exosomal Raji library (Raji exo2)

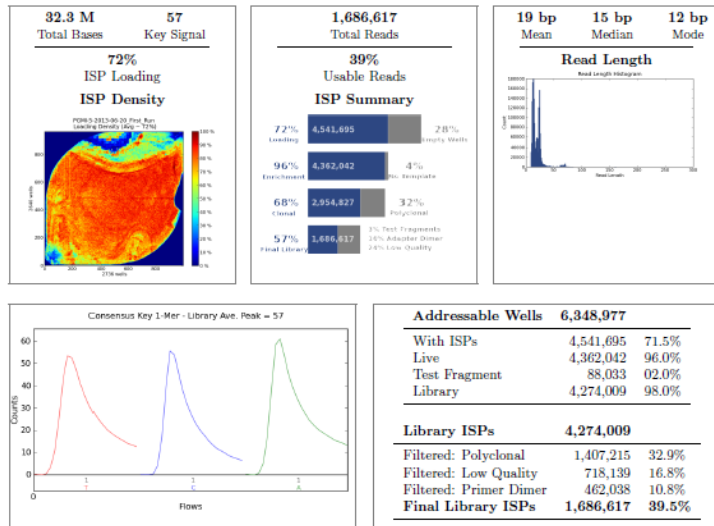


Barcode Name	Sample	Bases	$\geq Q20$	Reads	Mean Read Length
No barcode	none	2,291,211	1,824,734	77,209	30 bp
IonXpressRNA_004	Raji Exo	14,711,571	12,258,368	487,422	30 bp

Test Fragment	Reads	Percent 50AQ17	Read Length Histogram
TF_A	42,008	94%	

9.2 Jurkat sequencing run reports

9.2.1 Intracellular Jurkat library



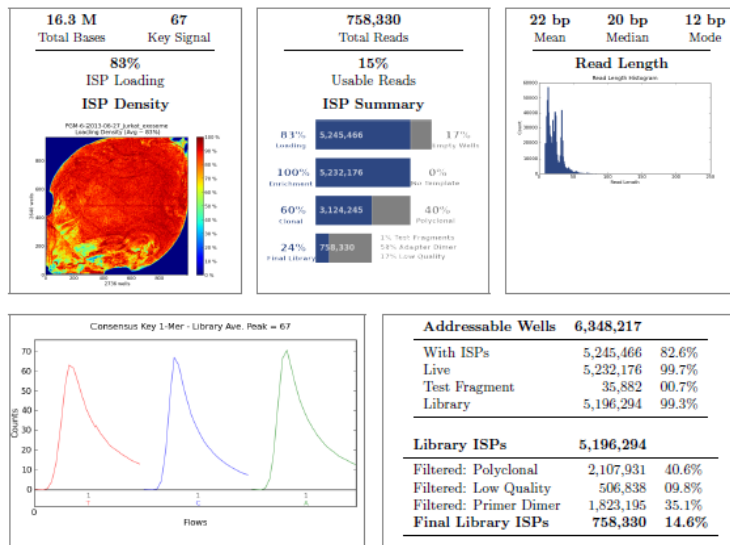
Notes: Primer Dimere

Barcode Name	Sample	Bases	$\geq Q20$	Reads	Mean Read Length
No barcode	Jurkat_total	402,178	253,022	12,734	32 bp
IonXpressRNA.003	Jurkat total	31,949,436	25,181,216	1,668,966	19 bp

Test Fragment	Reads	Percent 50AQ17	Read Length Histogram
TF_A	86,814	90%	

9. Appendix

9.2.2 Exosomal Jurkat library



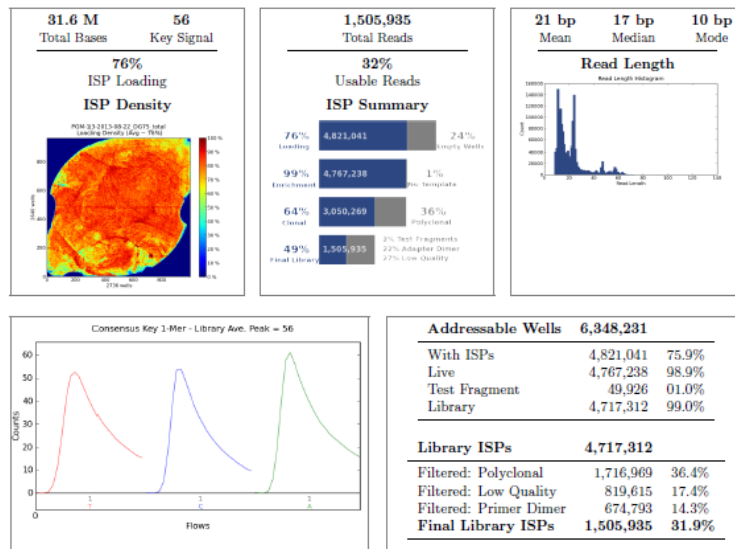
Notes: Primerdimer, Peak bei 50bp

Barcode Name	Sample	Bases	$\geq Q20$	Reads	Mean Read Length
No barcode	Jurkat_exosome	540,232	373,248	21,437	25 bp
IonXpressRNA_006	Jurkat_exosome	15,812,274	12,065,515	736,620	21 bp

Test Fragment	Reads	Percent 50AQ17	Read Length Histogram
TF_A	35,155	10%	

9.3 DG75 sequencing reports

9.3.1 Intracellular DG75 library

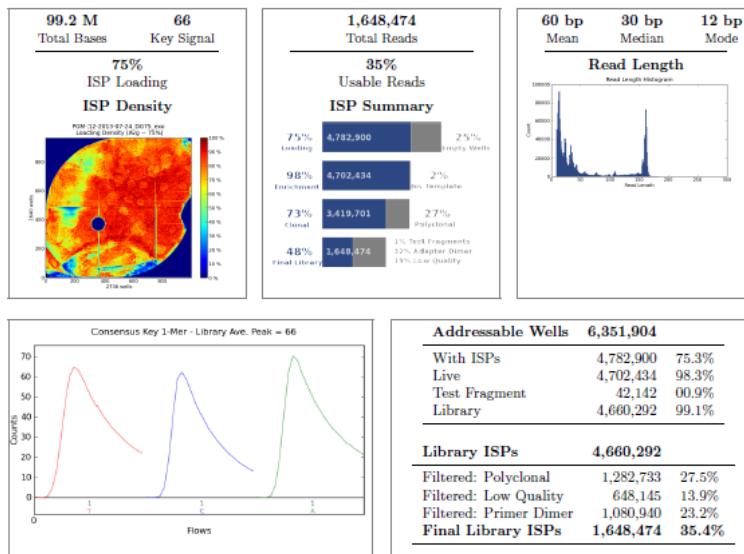


Barcode Name	Sample	Bases	$\geq Q20$	Reads	Mean Read Length
No barcode	None	406,890	271,547	14,620	28 bp
IonXpressRNA_002	DG75 total	31,247,445	24,188,657	1,491,225	21 bp

Test Fragment	Reads	Percent 50AQ17	Read Length Histogram
TF_A	49,038	88%	

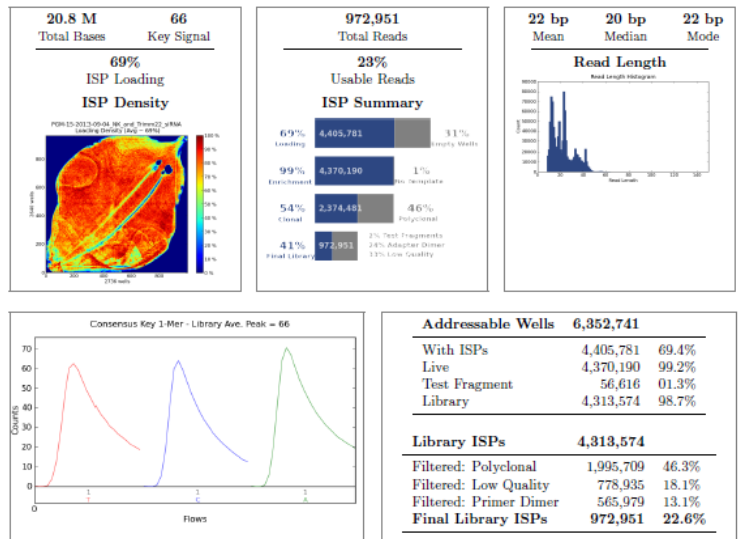
9. Appendix

9.3.2 Exosomal DG75 library



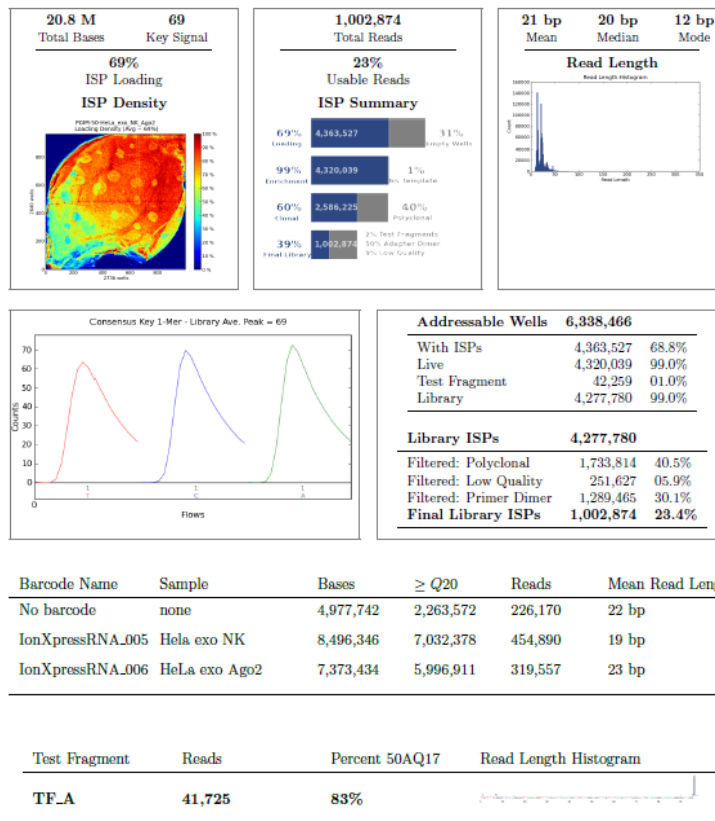
9.4 HeLa sequencing reports

9.4.1 Intracellular HeLa library



9. Appendix

9.4.2 Exosomal HeLa library



9.5 Raji small RNA sequencing results

id	baseMean cell	baseMean exo	foldChange	log2FoldChange
hsa-miR-3607-5p	313,280829	0,42463986	0,00135546	-9,527001
hsa-miR-3607-3p	83,9653381	0,42463986	0,00505732	-7,6274103
U104	419,253362	2,47706583	0,00590828	-7,4030463
hsa-miR-130b-5p	75,572145	0,77850641	0,0103015	-6,6010019
hsa-miR-20a-3p	44,4430407	1,06159964	0,02388675	-5,3876458
U37	28,6202996	0,7077331	0,02472836	-5,3376896
hsa-miR-33a-5p	36,2775353	0,92005302	0,02536151	-5,3012156
U74	286,158361	7,93256811	0,0277209	-5,1728819
U49A	11,7669666	0,35386655	0,03007288	-5,0553933
hsa-miR-582-3p	10,2957857	0,35386655	0,03437004	-4,8627047
snR39B	252,822842	10,3517684	0,04094475	-4,6101777
U52	23,3935402	0,99082633	0,0423547	-4,5613342
U45B	13,2417636	0,56618648	0,04275763	-4,5476742
U80	138,969281	6,30478199	0,04536817	-4,4621757
hsa-let-7a-5p	4314,22095	195,760055	0,04537553	-4,4619417
hsa-miR-155-3p	62,5667129	2,97744353	0,0475883	-4,3932493
hsa-miR-590-3p	34,7039905	1,91087936	0,05506224	-4,182793
hsa-let-7a-3p	14,3390376	0,84927971	0,0592285	-4,0775646
hsa-let-7f-5p	3746,70638	228,883626	0,06108929	-4,0329368
U38B	134,999042	8,29636371	0,06145498	-4,0243262

9. Appendix

hsa-miR-1306-5p	5,67102304	0,35386655	0,06239907	-4,0023317
hsa-miR-183-5p	6,17962929	0,42463986	0,06871607	-3,8632086
hsa-miR-29b-3p	4082,15575	281,119853	0,06886554	-3,860074
U58C	85,6032162	5,95687288	0,06958702	-3,8450379
U33	17,991849	1,27391957	0,07080537	-3,8199974
hsa-miR-28-5p	11,9103026	0,84927971	0,07130631	-3,8098265
hsa-miR-92a-1-5p	78,8255426	6,08650462	0,07721488	-3,6949773
U18A	10,5410822	0,84927971	0,08056855	-3,6336394
hsa-let-7g-3p	5,22421164	0,42463986	0,08128305	-3,6209016
hsa-let-7d-5p	1107,62105	97,3029425	0,08784859	-3,5088371
U31	140,533911	12,6115498	0,08974026	-3,4781008
U79	36,2897213	3,33230299	0,09182498	-3,4449695
hsa-miR-7-1-3p	32,1344007	3,04325231	0,09470388	-3,4004327
hsa-miR-4454	84,1675835	8,21764716	0,09763435	-3,3564674
hsa-miR-1260b	202,006143	21,4920504	0,10639305	-3,2325241
U47	3,91142879	0,42463986	0,10856387	-3,203384
U42A	29,5519517	3,39711886	0,11495413	-3,1208698
hsa-miR-18a-3p	13,6796017	1,62778612	0,11899368	-3,0710432
hsa-let-7f-1-3p	9,610843	1,20314626	0,12518634	-2,9978509
hsa-miR-4286	262,823428	33,0031095	0,12557141	-2,99342
hsa-miR-1307-5p	233,797963	29,6120377	0,12665653	-2,9810067
hsa-miR-625-3p	95,3113941	12,112165	0,12707993	-2,9761919
U76	41,827853	5,44954484	0,13028507	-2,9402563
hsa-miR-361-3p	33,6882495	4,39290972	0,13039887	-2,9389967
U96a	18,7375102	2,48203036	0,13246319	-2,9163366
hsa-miR-19b-1-5p	115,894404	15,5162342	0,13388251	-2,9009605
hsa-miR-877-3p	4,57194103	0,63695979	0,13931934	-2,8435326
hsa-miR-598-3p	3,02604762	0,42463986	0,14032821	-2,833123
hsa-miR-551a	6,03414875	0,84927971	0,14074557	-2,8288386
U26	21,5516732	3,18479893	0,14777502	-2,7585257
hsa-miR-324-5p	16,9958624	2,54783914	0,14990938	-2,7378375
U61	2,34685728	0,35386655	0,15078316	-2,7294528
hsa-miR-505-5p	18,287091	3,11402562	0,17028546	-2,5539729
U45A	26,6501587	4,81854249	0,18080727	-2,4674754
hsa-miR-625-5p	127,613561	23,3112273	0,18267046	-2,4526848
U20	17,4160988	3,26053677	0,18721396	-2,4172401
hsa-miR-148a-5p	4,11542477	0,77850641	0,18916793	-2,4022605
hsa-miR-21-5p	8754,3285	1765,85034	0,20171168	-2,3096334
hsa-let-7g-5p	1655,69778	356,219149	0,21514745	-2,2166024
hsa-miR-545-3p	1,93667048	0,42463986	0,21926283	-2,1892668
hsa-miR-99a-5p	162,705394	37,3392362	0,22948985	-2,1234978
hsa-let-7b-5p	137,369481	34,3837459	0,2503012	-1,9982629
hsa-miR-92b-3p	6,89041534	1,76933274	0,25678173	-1,9613856
U50B	2,17875429	0,56618648	0,25986706	-1,9441543
hsa-miR-505-3p	86,3786815	22,8885733	0,26497942	-1,9160478
U25	42,1453891	11,4133681	0,27080941	-1,8846502
hsa-miR-365a-3p	383,666195	103,944454	0,27092419	-1,8840389
hsa-miR-365b-3p	383,666195	103,944454	0,27092419	-1,8840389
hsa-miR-33a-3p	31,8603764	8,64427283	0,27131735	-1,8819468
hsa-miR-98-5p	47,0251531	13,0391684	0,27728072	-1,8505808

9. Appendix

hsa-miR-95-3p	5,54998113	1,55701281	0,2805438	-1,8337021
hsa-miR-454-3p	28,654713	8,14588094	0,28427718	-1,8146298
hsa-miR-28-3p	7,04345619	2,05242598	0,29139472	-1,7789533
hsa-miR-101-3p	453,44853	132,983211	0,29327079	-1,7696947
U75	44,6233297	13,2604244	0,29716349	-1,7506712
hsa-miR-181a-3p	16,9911783	5,37877153	0,3165626	-1,6594373
hsa-miR-151a-5p	122,770758	39,0417672	0,31800543	-1,6528767
hsa-miR-148b-5p	4,22749343	1,34469288	0,31808278	-1,6525258
HBII-276	4,17219071	1,34469288	0,322299	-1,6335284
hsa-miR-3618	1,08937714	0,35386655	0,32483383	-1,6222262
hsa-miR-15b-3p	48,8925269	16,0844065	0,32897474	-1,6039513
hsa-miR-17-3p	346,037622	113,871992	0,32907402	-1,6035159
hsa-miR-29c-3p	389,946498	129,012955	0,33084784	-1,5957603
hsa-miR-25-5p	4,46060399	1,4862395	0,33319243	-1,5855725
hsa-miR-103a-3p	2023,77682	685,726512	0,33883505	-1,561345
hsa-miR-103b	2023,77682	685,726512	0,33883505	-1,561345
hsa-miR-151b	123,739094	43,2243428	0,34931841	-1,5173854
hsa-miR-106b-5p	889,873402	319,555643	0,35910237	-1,4775329
hsa-miR-191-5p	5067,04896	1873,3135	0,36970503	-1,4355534
U21	8,78905647	3,25557224	0,37041203	-1,4327971
hsa-miR-628-5p	2,27214484	0,84927971	0,37377886	-1,4197431
ACA45	95,3286757	36,1939555	0,37967543	-1,3971615
hsa-miR-3613-3p	2,41186485	0,92005302	0,38146956	-1,3903602
U83A	20,61601	7,86576642	0,3815368	-1,3901059
hsa-miR-629-3p	2,03006103	0,77850641	0,38348916	-1,3827423
hsa-miR-20a-5p	4329,40744	1778,10283	0,41070351	-1,2838308
hsa-miR-107	880,012167	371,543919	0,42220316	-1,2439907
hsa-miR-182-5p	5,85707252	2,54783914	0,43500215	-1,2009056
hsa-miR-454-5p	3,14708953	1,41546619	0,44976992	-1,1527409
hsa-miR-3940-3p	1,08937714	0,49541317	0,45476736	-1,1367994
hsa-let-7i-5p	170,566743	78,2399747	0,45870592	-1,1243586
U42B	19,3804207	9,07487012	0,46824939	-1,094651
hsa-miR-15b-5p	379,118241	178,990526	0,47212322	-1,0827646
U83B	27,7758239	13,1797221	0,47450337	-1,0755098
hsa-miR-29a-3p	1257,60972	614,2612	0,48843548	-1,0337601
U62A	5,33554868	2,61861245	0,49078597	-1,0268341
U62B	5,33554868	2,61861245	0,49078597	-1,0268341
hsa-miR-98-3p	0,84729333	0,42463986	0,50117219	-0,9966217
U17a	4,08777341	2,05242598	0,50208898	-0,993985
hsa-miR-19a-3p	3580,82292	1807,10183	0,50466104	-0,9866134
hsa-miR-19b-3p	8696,78788	4706,95034	0,5412286	-0,88569
hsa-miR-196a-5p	5,18685542	2,83093238	0,54578972	-0,8735829
hsa-miR-185-5p	158,926579	90,7709002	0,5711499	-0,8080586
hsa-miR-296-5p	60,1423173	34,3827374	0,5716896	-0,806696
hsa-miR-944	3,78068203	2,26474591	0,59903105	-0,7392973
hsa-miR-3184-5p	8,05450492	4,95413167	0,61507588	-0,7011637
hsa-miR-374b-5p	51,809382	32,3741826	0,62487104	-0,6783696
hsa-miR-374c-3p	51,809382	32,3741826	0,62487104	-0,6783696
hsa-miR-577	34,1059463	21,5918168	0,63308071	-0,6595386
hsa-miR-21-3p	20,0118686	13,04314	0,65177022	-0,6175647

9. Appendix

hsa-miR-1285-3p	1,90901912	1,27391957	0,6673163	-0,5835574
hsa-miR-425-5p	372,946481	251,292128	0,67380212	-0,5696031
hsa-miR-378a-5p	78,3823472	53,0398837	0,67668149	-0,5634512
hsa-miR-106b-3p	44,0623051	29,9220174	0,67908425	-0,5583375
hsa-miR-186-5p	116,891458	81,5793217	0,69790661	-0,5188941
hsa-miR-769-5p	24,4351164	17,2786166	0,70712234	-0,4999683
hsa-miR-193b-3p	306,244135	222,908021	0,72787686	-0,4582337
hsa-miR-766-3p	82,0901166	60,2716847	0,73421366	-0,4457281
hsa-miR-590-5p	173,311609	131,588157	0,7592576	-0,3973386
hsa-miR-142-5p	7,35590485	5,88212794	0,7996471	-0,3225647
hsa-miR-589-3p	0,96833524	0,77850641	0,80396372	-0,3147977
hsa-miR-18a-5p	4430,99514	3716,77303	0,83881226	-0,2535802
U55	1,93667048	1,62778612	0,84050753	-0,2506674
hsa-miR-138-5p	415,309279	352,641552	0,84910588	-0,2359836
hsa-miR-18b-5p	13,0423933	11,2618924	0,86348358	-0,2117594
hsa-miR-181a-5p	211,24423	183,870147	0,870415	-0,2002247
hsa-miR-301a-3p	49,2624813	43,9261185	0,89167491	-0,1654103
hsa-let-7c-5p	52,997507	47,9880338	0,90547719	-0,1432498
hsa-miR-4524a-3p	0,84729333	0,77850641	0,91881568	-0,1221526
hsa-miR-4524b-5p	0,84729333	0,77850641	0,91881568	-0,1221526
hsa-miR-140-5p	23,8475168	22,4779122	0,94256825	-0,085331
hsa-miR-93-3p	19,1598911	18,5844028	0,96996391	-0,043997
hsa-miR-26b-5p	60,1188883	59,9956314	0,99794978	-0,0029609
hsa-miR-576-3p	0,84729333	0,84927971	1,00234438	0,00337827
hsa-miR-484	189,096986	192,345084	1,01717689	0,02457059
hsa-miR-22-3p	20,9636703	21,3973692	1,02068812	0,02954211
hsa-miR-324-3p	10,7286031	10,9778062	1,02322792	0,03312753
hsa-miR-181b-5p	107,191842	110,2692	1,02870888	0,04083476
hsa-miR-1307-3p	38,9583955	41,1032231	1,05505431	0,07731726
hsa-miR-30e-3p	2,29979619	2,48203036	1,07923927	0,11001475
hsa-miR-296-3p	22,209301	24,0778188	1,08413222	0,11654072
hsa-miR-1180-3p	1,33146095	1,4862395	1,11624715	0,1586565
hsa-miR-30d-5p	661,800191	739,006292	1,11666074	0,15919094
hsa-miR-26a-5p	244,297408	275,451522	1,12752536	0,17315988
hsa-miR-148a-3p	195,833695	227,026613	1,15928269	0,21323241
hsa-miR-378c	281,706908	340,033513	1,20704712	0,271482
hsa-miR-423-3p	211,957086	256,550365	1,21038824	0,27546988
hsa-miR-140-3p	129,991291	160,83342	1,23726304	0,30715225
hsa-miR-155-5p	349,189008	434,270153	1,24365356	0,31458465
hsa-miR-210-3p	23,9549013	30,2011391	1,26074988	0,33428209
U3	377,321853	476,018673	1,26157197	0,33522251
U3-3	377,321853	476,018673	1,26157197	0,33522251
hsa-miR-30c-5p	178,948422	226,120407	1,2636066	0,33754738
hsa-miR-629-5p	21,3706444	27,3542421	1,27999145	0,35613417
hsa-miR-128-3p	136,596909	174,854999	1,28008021	0,35623421
hsa-miR-197-3p	82,2582278	113,822074	1,38371659	0,46854848
hsa-miR-30b-5p	126,41172	178,129441	1,40912125	0,49479575
hsa-miR-339-5p	74,635742	106,032828	1,42067092	0,50657241
hsa-miR-744-5p	44,5888496	63,7684648	1,43014376	0,51616017
hsa-miR-342-3p	76,8579496	112,327782	1,46149855	0,5474484

9. Appendix

hsa-miR-1270	0,72625143	1,06159964	1,46175222	0,54769879
hsa-miR-32-5p	11,9716942	17,7141784	1,4796718	0,56527722
hsa-miR-545-5p	0,60520952	0,92005302	1,52022231	0,60428232
U3-2	302,760823	471,135314	1,55613038	0,63796294
U3-2B	302,760823	471,135314	1,55613038	0,63796294
U3-4	302,760823	471,135314	1,55613038	0,63796294
hsa-miR-192-5p	22,1532667	34,6628675	1,56468425	0,64587155
hsa-miR-671-5p	10,8668517	17,1271409	1,57609042	0,65635031
hsa-miR-16-5p	1224,72157	1938,90303	1,58313781	0,66278685
hsa-miR-9-3p	16,1377961	27,1379506	1,68163921	0,74986821
hsa-miR-320a	128,994564	220,894564	1,71243312	0,77604764
hsa-miR-130b-3p	36,5925236	64,0705441	1,75091898	0,80811233
hsa-let-7d-3p	45,2820924	79,3932652	1,75330381	0,81007601
hsa-miR-15a-5p	395,659367	714,374758	1,80552975	0,85242219
hsa-miR-378a-3p	1640,88831	2979,12517	1,81555634	0,8604117
hsa-miR-5196-3p	0,60520952	1,13237295	1,87104285	0,9038426
U8	8,52969929	16,0056899	1,87646591	0,90801808
hsa-miR-17-5p	760,301861	1459,10735	1,91911585	0,94044181
hsa-miR-93-5p	435,005647	848,558101	1,95068295	0,96397932
hsa-miR-148b-3p	10,8586183	21,4930433	1,97935343	0,98502924
hsa-miR-92a-3p	514,239652	1087,12036	2,11403449	1,07999891
hsa-miR-652-3p	4,94477161	10,6976917	2,16343495	1,11332374
hsa-miR-193b-5p	0,96833524	2,12319929	2,19262834	1,13266129
hsa-miR-25-3p	33,2805438	82,361757	2,47477197	1,3072956
hsa-miR-361-5p	10,0950106	26,3165503	2,60688683	1,38232796
hsa-miR-7-5p	206,282514	539,019549	2,61301619	1,38571607
hsa-miR-146b-5p	26,1228744	68,4775066	2,62136186	1,39031652
hsa-miR-3529-3p	202,05502	539,019549	2,66768699	1,4155894
hsa-miR-221-3p	46,6304235	127,305526	2,73009586	1,44895161
hsa-miR-24-3p	22,9492099	67,6898807	2,94955169	1,56049569
hsa-miR-330-3p	1,33146095	4,10485195	3,08296833	1,62432007
hsa-miR-30e-5p	106,724948	329,175609	3,08433609	1,62495998
hsa-miR-378d	50,8464041	157,812183	3,10370391	1,63399093
hsa-miR-301b-3p	0,84729333	2,68938576	3,17409055	1,66634328
hsa-miR-877-5p	2,65394866	10,04981	3,78673864	1,92095585
hsa-miR-23b-3p	20,0003558	84,0692838	4,20338941	2,07155312
mgU2-19	1,93667048	8,64129411	4,4619331	2,15766888
hsa-miR-589-5p	0,72625143	4,03904317	5,56149428	2,47547256
hsa-miR-9-5p	58,0482584	324,294462	5,58663552	2,4819797
hsa-miR-421	1,3038096	10,2720589	7,87849619	2,97792028
hsa-miR-106a-5p	18,8488472	152,953862	8,1147595	3,02054834
hsa-miR-146a-5p	100,394086	1048,87712	10,4475987	3,38509948
hsa-miR-378e	1,08937714	12,1022359	11,1093169	3,47369821
hsa-miR-568	2,03006103	24,3238976	11,9818553	3,58277942
hsa-miR-3184-3p	43,6528499	571,625968	13,0948144	3,71092371
hsa-miR-423-5p	43,6528499	571,625968	13,0948144	3,71092371
hsa-miR-125b-5p	21,8098873	360,423602	16,5256976	4,04663927
hsa-miR-142-3p	3,13811628	56,3911571	17,9697475	4,16749823
hsa-miR-27b-3p	12,9447136	247,306477	19,1048241	4,25586507
hsa-miR-145-5p	3,60360579	156,258643	43,3617471	5,43835098

9. Appendix

hsa-miR-222-3p	3,11943817	244,373913	78,3390788	6,29166026
hsa-miR-223-3p	4,71166105	386,16441	81,9592933	6,35683564
hsa-miR-1246	1,3038096	191,328267	146,745558	7,19717302
ACA3	0	0,77850641	Inf	Inf
ACA63	0	0,63695979	Inf	Inf
HBII-202	0	0,35386655	Inf	Inf
HBII-85-10	0	12,3563516	Inf	Inf
hsa-let-7e-5p	0	2,61861245	Inf	Inf
hsa-miR-100-5p	0	1,4862395	Inf	Inf
hsa-miR-10a-5p	0	0,63695979	Inf	Inf
hsa-miR-10b-5p	0	27,0342749	Inf	Inf
hsa-miR-122-5p	0	178,352722	Inf	Inf
hsa-miR-125a-5p	0	9,2104593	Inf	Inf
hsa-miR-126-3p	0	171,157881	Inf	Inf
hsa-miR-126-5p	0	167,169644	Inf	Inf
hsa-miR-1268a	0	1,27391957	Inf	Inf
hsa-miR-1268b	0	0,7077331	Inf	Inf
hsa-miR-1297	0	0,56618648	Inf	Inf
hsa-miR-130a-3p	0	8,00632013	Inf	Inf
hsa-miR-136-5p	0	3,61440332	Inf	Inf
hsa-miR-138-1-3p	0	0,35386655	Inf	Inf
hsa-miR-139-5p	0	53,5691025	Inf	Inf
hsa-miR-141-3p	0	0,49541317	Inf	Inf
hsa-miR-143-3p	0	33,7497336	Inf	Inf
hsa-miR-144-3p	0	62,3239233	Inf	Inf
hsa-miR-144-5p	0	16,7802247	Inf	Inf
hsa-miR-150-5p	0	59,7663425	Inf	Inf
hsa-miR-151a-3p	0	2,33551922	Inf	Inf
hsa-miR-152-3p	0	2,61861245	Inf	Inf
hsa-miR-194-5p	0	1,98165267	Inf	Inf
hsa-miR-195-5p	0	1,69855943	Inf	Inf
hsa-miR-197-5p	0	0,42463986	Inf	Inf
hsa-miR-199a-3p	0	12,1918745	Inf	Inf
hsa-miR-199a-5p	0	2,97744353	Inf	Inf
hsa-miR-199b-3p	0	12,1918745	Inf	Inf
hsa-miR-200c-3p	0	0,92005302	Inf	Inf
hsa-miR-203a-3p	0	1,98165267	Inf	Inf
hsa-miR-203b-5p	0	0,49541317	Inf	Inf
hsa-miR-214-3p	0	27,5436356	Inf	Inf
hsa-miR-218-5p	0	9972,54205	Inf	Inf
hsa-miR-22-5p	0	3,33230299	Inf	Inf
hsa-miR-23a-3p	0	142,324334	Inf	Inf
hsa-miR-27a-3p	0	17,4520143	Inf	Inf
hsa-miR-3074-5p	0	7,0842813	Inf	Inf
hsa-miR-30a-5p	0	7,22483501	Inf	Inf
hsa-miR-3194-5p	0	1,27391957	Inf	Inf
hsa-miR-320b	0	3,89253203	Inf	Inf
hsa-miR-320c	0	2,1939726	Inf	Inf
hsa-miR-320d	0	1,4862395	Inf	Inf
hsa-miR-326	0	1,13237295	Inf	Inf

9. Appendix

hsa-miR-328-3p	0	0,63695979	Inf	Inf
hsa-miR-331-3p	0	0,42463986	Inf	Inf
hsa-miR-331-5p	0	5,6678222	Inf	Inf
hsa-miR-335-5p	0	8,57548533	Inf	Inf
hsa-miR-339-3p	0	6,58191779	Inf	Inf
hsa-miR-340-3p	0	29,6099935	Inf	Inf
hsa-miR-34a-5p	0	107,293735	Inf	Inf
hsa-miR-34c-5p	0	0,49541317	Inf	Inf
hsa-miR-3591-3p	0	172,894241	Inf	Inf
hsa-miR-3667-5p	0	1,27391957	Inf	Inf
hsa-miR-367-3p	0	445,317105	Inf	Inf
hsa-miR-369-3p	0	2,97843644	Inf	Inf
hsa-miR-374a-5p	0	3,26053677	Inf	Inf
hsa-miR-376b-3p	0	3,54462291	Inf	Inf
hsa-miR-376c-3p	0	23,8774138	Inf	Inf
hsa-miR-378f	0	2,61861245	Inf	Inf
hsa-miR-378g	0	2,12319929	Inf	Inf
hsa-miR-409-3p	0	0,49541317	Inf	Inf
hsa-miR-409-5p	0	0,56618648	Inf	Inf
hsa-miR-411-5p	0	0,49541317	Inf	Inf
hsa-miR-412-5p	0	0,49541317	Inf	Inf
hsa-miR-424-5p	0	4,25334892	Inf	Inf
hsa-miR-433-3p	0	10,2969597	Inf	Inf
hsa-miR-4424	0	0,84927971	Inf	Inf
hsa-miR-4466	0	0,35386655	Inf	Inf
hsa-miR-449a	0	0,35386655	Inf	Inf
hsa-miR-451a	0	868,38312	Inf	Inf
hsa-miR-455-3p	0	0,35386655	Inf	Inf
hsa-miR-486-3p	0	2,97843644	Inf	Inf
hsa-miR-486-5p	0	221,987836	Inf	Inf
hsa-miR-492	0	12,3563516	Inf	Inf
hsa-miR-494-3p	0	62,7686555	Inf	Inf
hsa-miR-494-5p	0	35,0096629	Inf	Inf
hsa-miR-520g-5p	0	3,47484251	Inf	Inf
hsa-miR-526b-5p	0	3,47484251	Inf	Inf
hsa-miR-542-3p	0	0,35386655	Inf	Inf
hsa-miR-574-3p	0	0,63695979	Inf	Inf
hsa-miR-615-3p	0	0,35386655	Inf	Inf
hsa-miR-619-5p	0	3,75098541	Inf	Inf
hsa-miR-627-5p	0	0,63695979	Inf	Inf
hsa-miR-664a-5p	0	0,35386655	Inf	Inf
hsa-miR-6731-3p	0	0,35386655	Inf	Inf
hsa-miR-6810-3p	0	0,49541317	Inf	Inf
hsa-miR-7641	0	2,48203036	Inf	Inf
hsa-miR-885-5p	0	18,5345274	Inf	Inf
hsa-miR-940	0	0,63695979	Inf	Inf
hsa-miR-941	0	0,49541317	Inf	Inf
hsa-miR-942-5p	0	0,49541317	Inf	Inf
hsa-miR-99b-5p	0	1,06159964	Inf	Inf
SNORD127	0	3,68616953	Inf	Inf

9. Appendix

U32A	0	0,35386655	Inf	Inf
U64	0	0,49541317	Inf	Inf
U68	0	0,35386655	Inf	Inf
U96b	0	2,48203036	Inf	Inf
ACA4	0,72625143	0	0	-Inf
ACA61	11,3729768	0	0	-Inf
ACA62	0,60520952	0	0	-Inf
ACA7	1,69458667	0	0	-Inf
ACA7B	1,69458667	0	0	-Inf
hsa-miR-1273g-3p	0,60520952	0	0	-Inf
hsa-miR-1275	22,9962709	0	0	-Inf
hsa-miR-1285-5p	0,60520952	0	0	-Inf
hsa-miR-16-2-3p	7,0211621	0	0	-Inf
hsa-miR-181b-3p	4,9260935	0	0	-Inf
hsa-miR-190a-3p	2,05771238	0	0	-Inf
hsa-miR-190a-5p	8,5893496	0	0	-Inf
hsa-miR-191-3p	0,96833524	0	0	-Inf
hsa-miR-219b-5p	0,60520952	0	0	-Inf
hsa-miR-26b-3p	2,17875429	0	0	-Inf
hsa-miR-29a-5p	0,84729333	0	0	-Inf
hsa-miR-29b-1-5p	16,5767024	0	0	-Inf
hsa-miR-29c-5p	6,5743507	0	0	-Inf
hsa-miR-301a-5p	0,60520952	0	0	-Inf
hsa-miR-3615	0,60520952	0	0	-Inf
hsa-miR-3653-5p	0,96833524	0	0	-Inf
hsa-miR-4284	549,455387	0	0	-Inf
hsa-miR-4323	2,03006103	0	0	-Inf
hsa-miR-4521	11,8262137	0	0	-Inf
hsa-miR-4791	2,15110293	0	0	-Inf
hsa-miR-548aa	7,96184599	0	0	-Inf
hsa-miR-548t-3p	7,96184599	0	0	-Inf
hsa-miR-576-5p	0,72625143	0	0	-Inf
hsa-miR-579-3p	2,53290676	0	0	-Inf
hsa-miR-582-5p	73,7723183	0	0	-Inf
hsa-miR-616-5p	0,72625143	0	0	-Inf
hsa-miR-664a-3p	37,0106154	0	0	-Inf
hsa-miR-769-3p	0,60520952	0	0	-Inf
hsa-miR-7974	0,60520952	0	0	-Inf
hsa-miR-7975	0,72625143	0	0	-Inf
hsa-miR-942-3p	0,60520952	0	0	-Inf
mgU6-47	1,45250286	0	0	-Inf
mgU6-77	1,81562857	0	0	-Inf
SNORD119	10,131627	0	0	-Inf
SNORD121A	9,87983835	0	0	-Inf
SNORD121B	0,60520952	0	0	-Inf
SNORD125	0,96833524	0	0	-Inf
SNORD126	2,89603247	0	0	-Inf
snR38A	4,8416762	0	0	-Inf
U102	29,6934715	0	0	-Inf
U103	0,96833524	0	0	-Inf

9. Appendix

U103B	0,96833524	0	0	-Inf
U105	0,72625143	0	0	-Inf
U106	1,57354476	0	0	-Inf
U14A	0,60520952	0	0	-Inf
U14B	1,21041905	0	0	-Inf
U15A	1,45250286	0	0	-Inf
U16	19,9752522	0	0	-Inf
U18B	1,08937714	0	0	-Inf
U18C	4,64665347	0	0	-Inf
U22	17,9613215	0	0	-Inf
U24	23,3209723	0	0	-Inf
U29	18,7170323	0	0	-Inf
U35B	13,5104224	0	0	-Inf
U36A	2,41186485	0	0	-Inf
U36B	21,2043412	0	0	-Inf
U38A	3,6222839	0	0	-Inf
U43	3,51021524	0	0	-Inf
U46	3,38917334	0	0	-Inf
U48	0,72625143	0	0	-Inf
U50	1,93667048	0	0	-Inf
U53	18,2533508	0	0	-Inf
U54	23,8956543	0	0	-Inf
U57	65,615778	0	0	-Inf
U58B	23,3428631	0	0	-Inf
U60	1,57354476	0	0	-Inf
U71b	0,96833524	0	0	-Inf
U73a	32,858171	0	0	-Inf
U77	20,4073299	0	0	-Inf
U81	10,503726	0	0	-Inf
U82	20,8336552	0	0	-Inf
U84	0,96833524	0	0	-Inf
U87	2,15110293	0	0	-Inf
U89	0,84729333	0	0	-Inf
U90	5,8197163	0	0	-Inf
U94	0,60520952	0	0	-Inf
U95	8,86590526	0	0	-Inf
U97	0,72625143	0	0	-Inf
Z17B	1,57354476	0	0	-Inf

9.6 Jurkat small RNA sequencing results (log2foldchange >±2)

id	baseMeanA cell	baseMeanB exo	foldChange	log2FoldChange
hsa-miR-378f	2238,37161	2,6925824	0,00120292	-9,699243354
hsa-let-7e-5p	3696,4514	8,07774721	0,00218527	-8,837972232
hsa-miR-378g	2240,22856	8,07774721	0,00360577	-8,115477217

9. Appendix

U24	459,781657	2,6925824	0,00585622	-7,415814604
U48	314,939294	2,6925824	0,00854953	-6,869939459
hsa-miR-101-3p	246,603409	2,6925824	0,01091868	-6,517058436
snR39B	395,53107	8,07774721	0,02042254	-5,613694219
U42B	373,61902	8,07774721	0,02162028	-5,531471094
U38B	122,930314	2,6925824	0,02190332	-5,512706412
U52	226,176922	5,38516481	0,02380952	-5,392317423
hsa-let-7f-5p	6971,003	169,632691	0,02433404	-5,360880111
U34	314,567903	8,07774721	0,02567887	-5,283274663
HBII-210	1207,39109	37,6961537	0,03122116	-5,001331924
U27	1245,27294	40,3887361	0,03243364	-4,946365177
hsa-miR-3607-5p	835,629022	29,6184064	0,03544444	-4,818296672
U18A	69,0786658	2,6925824	0,0389785	-4,681177816
hsa-miR-3607-3p	734,239367	29,6184064	0,0403389	-4,631684542
hsa-miR-15b-5p	1220,01837	51,1590657	0,04193303	-4,575769147
hsa-miR-590-3p	62,3936336	2,6925824	0,04315476	-4,534336428
hsa-miR-181d-5p	373,990411	16,1554944	0,04319762	-4,532904472
hsa-miR-1260b	231,376391	10,7703296	0,04654896	-4,425107358
U78	635,820838	29,6184064	0,04658294	-4,424054373
U58B	53,8516481	2,6925824	0,05	-4,321928095
SNORD121A	52,737476	2,6925824	0,05105634	-4,291766124
U45B	50,1377413	2,6925824	0,0537037	-4,218834602
U96a	50,1377413	2,6925824	0,0537037	-4,218834602
hsa-miR-9-5p	47,9093973	2,6925824	0,05620155	-4,15324626
HBII-429	93,5904504	5,38516481	0,05753968	-4,119298928
U76	45,3096625	2,6925824	0,05942623	-4,072756342
U44	630,249978	37,6961537	0,05981143	-4,063434932
mgh28S-2409	223,205797	13,462912	0,06031614	-4,051312091
U31	1530,12959	94,2403841	0,06158981	-4,02116461
U57	87,2768089	5,38516481	0,06170213	-4,018535951
hsa-miR-29a-3p	730,896851	51,1590657	0,06999492	-3,836605997
hsa-miR-7-5p	595,710645	43,0813185	0,0723192	-3,789477431
SNORD119	34,9107236	2,6925824	0,07712766	-3,696607857
hsa-let-7a-5p	7082,04881	565,442305	0,07984163	-3,646715056
hsa-miR-3529-3p	535,545355	43,0813185	0,08044383	-3,635874454
U49B	64,250587	5,38516481	0,08381503	-3,576647233
hsa-miR-100-5p	62,7650243	5,38516481	0,08579882	-3,542898441
hsa-miR-340-3p	187,180901	16,1554944	0,08630952	-3,534336428
U30	62,022243	5,38516481	0,08682635	-3,525723297
hsa-miR-29c-5p	30,4540355	2,6925824	0,08841463	-3,499571009
hsa-miR-130b-5p	180,124478	16,1554944	0,08969072	-3,478897441
hsa-miR-19a-3p	14292,2274	1375,90961	0,09626978	-3,376773174
U79	54,9658201	5,38516481	0,09797297	-3,351472371
U95	108,074687	10,7703296	0,09965636	-3,326894348
U61	26,368738	2,6925824	0,10211268	-3,291766124
hsa-miR-7-1-3p	25,254566	2,6925824	0,10661765	-3,229481846
U104	225,06275	24,2332416	0,10767327	-3,215267987

9. Appendix

hsa-miR-98-5p	337,222734	37,6961537	0,11178414	-3,16121257
hsa-miR-4286	237,690033	26,925824	0,11328125	-3,142019005
hsa-miR-374b-5p	443,811858	51,1590657	0,11527197	-3,116886394
hsa-miR-374c-3p	443,811858	51,1590657	0,11527197	-3,116886394
hsa-miR-218-5p	21,5406592	2,6925824	0,125	-3
hsa-let-7d-5p	2277,36763	293,491482	0,12887313	-2,955976662
U63	62,3936336	8,07774721	0,12946429	-2,949373927
U60	20,0550965	2,6925824	0,13425926	-2,896906507
hsa-miR-577	19,6837059	2,6925824	0,13679245	-2,869939459
U45A	134,814816	18,8480768	0,13980716	-2,838489821
hsa-miR-20a-5p	1499,67555	215,406592	0,14363546	-2,799516105
hsa-miR-30c-5p	816,688097	118,473626	0,14506594	-2,785219275
hsa-miR-505-3p	219,49189	32,3109888	0,14720812	-2,764070824
U80	108,074687	16,1554944	0,14948454	-2,741931847
hsa-miR-454-3p	124,787267	18,8480768	0,15104167	-2,726981506
hsa-miR-19b-3p	14749,4093	2250,99889	0,15261621	-2,712019929
HBII-142	17,4553618	2,6925824	0,15425532	-2,696607857
hsa-miR-15a-3p	17,0839711	2,6925824	0,1576087	-2,665580961
U35A	17,0839711	2,6925824	0,1576087	-2,665580961
hsa-miR-29c-3p	785,862671	126,551373	0,16103497	-2,634554065
hsa-miR-30a-5p	199,436793	32,3109888	0,16201117	-2,625834782
hsa-let-7c-5p	497,663506	80,7774721	0,16231343	-2,623145695
U16	15,9697991	2,6925824	0,16860465	-2,56828376
hsa-miR-548aa	46,7952252	8,07774721	0,17261905	-2,534336428
hsa-miR-548t-3p	46,7952252	8,07774721	0,17261905	-2,534336428
hsa-miR-98-3p	30,4540355	5,38516481	0,17682927	-2,499571009
HBII-95B	14,8556271	2,6925824	0,18125	-2,4639471
hsa-miR-142-5p	58,6797269	10,7703296	0,1835443	-2,445799753
hsa-miR-4454	277,800226	51,1590657	0,18415775	-2,440985951
U25	86,9054183	16,1554944	0,18589744	-2,427421224
U42A	57,9369455	10,7703296	0,18589744	-2,427421224
U81	27,8543007	5,38516481	0,19333333	-2,370837695
hsa-miR-18b-5p	277,800226	53,8516481	0,19385027	-2,36698537
U50	27,4829101	5,38516481	0,19594595	-2,351472371
U33	26,7401287	5,38516481	0,20138889	-2,311944006
U74	283,371086	59,2368129	0,20904325	-2,258126633
hsa-miR-455-3p	391,445773	83,4700545	0,21323529	-2,229481846
hsa-miR-424-5p	73,5353539	16,1554944	0,21969697	-2,186413124
hsa-miR-340-5p	12,2558923	2,6925824	0,21969697	-2,186413124
U49A	96,1901852	21,5406592	0,22393822	-2,158827293
hsa-miR-181a-2-3p	22,6548313	5,38516481	0,23770492	-2,072756342
hsa-miR-25-3p	53,8516481	215,406592	4	2
hsa-miR-331-5p	3,34251609	13,462912	4,02777778	2,009984089
hsa-miR-877-5p	62,022243	258,487911	4,16766467	2,059239203
hsa-miR-671-3p	1,85695338	8,07774721	4,35	2,121015401
hsa-miR-345-5p	115,873891	522,360986	4,50801282	2,172491618
hsa-miR-629-5p	17,8267525	80,7774721	4,53125	2,17990909

9. Appendix

hsa-miR-24-3p	214,29242	985,48516	4,59878683	2,201253325
hsa-miR-339-3p	8,54198556	40,3887361	4,72826087	2,241309635
hsa-miR-3184-3p	26,368738	126,551373	4,79929578	2,262822727
hsa-miR-423-5p	26,368738	126,551373	4,79929578	2,262822727
hsa-miR-200c-3p	4,45668812	21,5406592	4,83333333	2,273018494
hsa-miR-1908-5p	1,11417203	5,38516481	4,83333333	2,273018494
hsa-miR-222-5p	1,11417203	5,38516481	4,83333333	2,273018494
hsa-miR-34a-5p	1,11417203	5,38516481	4,83333333	2,273018494
hsa-miR-3928-3p	1,11417203	5,38516481	4,83333333	2,273018494
hsa-miR-6804-5p	1,11417203	5,38516481	4,83333333	2,273018494
U85	1,11417203	5,38516481	4,83333333	2,273018494
hsa-miR-320c	5,94225082	29,6184064	4,984375	2,317412614
U3-3	263,31599	1335,52087	5,0719323	2,342535488
U3	265,915724	1354,36895	5,09322626	2,348579808
hsa-miR-1303	2,97112541	16,1554944	5,4375	2,442943496
hsa-miR-2110	1,48556271	8,07774721	5,4375	2,442943496
hsa-miR-22-3p	6,3136415	35,0035713	5,54411765	2,470957872
hsa-miR-3184-5p	16,7125804	94,2403841	5,63888889	2,495410916
hsa-miR-4661-5p	1,85695338	10,7703296	5,8	2,5360529
hsa-miR-28-3p	36,3962863	215,406592	5,91836735	2,565199246
hsa-miR-320b	8,54198556	51,1590657	5,98913044	2,582346553
U8	34,5393329	207,328845	6,00268817	2,585608725
U3-2	193,123152	1176,65851	6,09278846	2,607102652
U3-2B	193,123152	1176,65851	6,09278846	2,607102652
U3-4	192,00898	1171,27335	6,10009671	2,608832116
hsa-miR-7974	2,97112541	18,8480768	6,34375	2,665335917
HBII-166	5,57086015	37,6961537	6,76666667	2,758445322
hsa-miR-320d	2,97112541	21,5406592	7,25	2,857980995
hsa-miR-1226-5p	2,59973473	18,8480768	7,25	2,857980995
hsa-miR-3909	2,22834406	16,1554944	7,25	2,857980995
hsa-miR-203a-3p	1,11417203	8,07774721	7,25	2,857980995
U100	1,11417203	8,07774721	7,25	2,857980995
HBII-85-10	0,74278135	5,38516481	7,25	2,857980995
hsa-miR-1286	0,74278135	5,38516481	7,25	2,857980995
hsa-miR-647	0,74278135	5,38516481	7,25	2,857980995
14qII-20	0,37139068	2,6925824	7,25	2,857980995
14qII-22	0,37139068	2,6925824	7,25	2,857980995
14qII-23	0,37139068	2,6925824	7,25	2,857980995
14qII-25	0,37139068	2,6925824	7,25	2,857980995
14qII-28	0,37139068	2,6925824	7,25	2,857980995
14qII-29	0,37139068	2,6925824	7,25	2,857980995
14qII-9	0,37139068	2,6925824	7,25	2,857980995
ACA11	0,37139068	2,6925824	7,25	2,857980995
hsa-miR-192-3p	0,37139068	2,6925824	7,25	2,857980995
hsa-miR-193b-5p	0,37139068	2,6925824	7,25	2,857980995
hsa-miR-3667-5p	0,37139068	2,6925824	7,25	2,857980995
hsa-miR-373-3p	0,37139068	2,6925824	7,25	2,857980995

9. Appendix

hsa-miR-4687-3p	0,37139068	2,6925824	7,25	2,857980995
hsa-miR-6821-3p	0,37139068	2,6925824	7,25	2,857980995
hsa-miR-130b-3p	90,619325	673,145601	7,42827869	2,893027942
hsa-miR-1246	27,8543007	212,71401	7,63666667	2,932943053
hsa-miR-139-5p	18,1981431	140,014285	7,69387755	2,943710869
hsa-miR-151a-3p	12,9986737	107,703296	8,28571429	3,050626073
hsa-miR-10b-5p	1,48556271	13,462912	9,0625	3,17990909
hsa-miR-199a-3p	2,97112541	29,6184064	9,96875	3,317412614
hsa-miR-199b-3p	2,97112541	29,6184064	9,96875	3,317412614
hsa-miR-1273h-3p	1,85695338	18,8480768	10,15	3,343407822
ACA63	2,59973473	26,925824	10,3571429	3,372554168
hsa-miR-320a	168,611367	1766,33406	10,4757709	3,388984512
hsa-miR-3194-3p	0,74278135	8,07774721	10,875	3,442943496
hsa-miR-497-5p	0,74278135	8,07774721	10,875	3,442943496
U93	0,74278135	8,07774721	10,875	3,442943496
HBII-289	5,19946947	67,3145601	12,9464286	3,694482263
hsa-miR-203b-5p	0,74278135	10,7703296	14,5	3,857980995
hsa-miR-3940-3p	0,74278135	10,7703296	14,5	3,857980995
hsa-miR-125a-3p	0,37139068	5,38516481	14,5	3,857980995
hsa-miR-1468-5p	0,37139068	5,38516481	14,5	3,857980995
hsa-miR-4660	0,37139068	5,38516481	14,5	3,857980995
hsa-miR-4684-3p	0,37139068	5,38516481	14,5	3,857980995
hsa-miR-4726-5p	0,37139068	5,38516481	14,5	3,857980995
hsa-miR-568	0,37139068	5,38516481	14,5	3,857980995
hsa-miR-643	0,37139068	5,38516481	14,5	3,857980995
hsa-miR-7704	0,37139068	5,38516481	14,5	3,857980995
hsa-miR-891a-5p	0,37139068	5,38516481	14,5	3,857980995
hTR	0,37139068	5,38516481	14,5	3,857980995
hsa-miR-7641	1,11417203	18,8480768	16,9166667	4,080373416
ACA47	1,48556271	32,3109888	21,75	4,442943496
hsa-miR-320e	0,37139068	8,07774721	21,75	4,442943496
hsa-miR-449b-3p	0,37139068	8,07774721	21,75	4,442943496
hsa-miR-6516-3p	1,11417203	26,925824	24,1666667	4,594946589
hsa-miR-589-5p	3,71390676	113,088461	30,45	4,928370323
hsa-miR-619-3p	0,37139068	32,3109888	87	6,442943496
hsa-miR-130a-3p	0,37139068	35,0035713	94,25	6,558420713
hsa-miR-145-5p	2,59973473	341,957965	131,535714	7,03931076
hsa-miR-122-5p	0,37139068	59,2368129	159,5	7,317412614
hsa-miR-486-5p	1,11417203	255,795328	229,583333	7,842874103
hsa-miR-143-3p	0,74278135	201,94368	271,875	8,086799686
hsa-miR-451a	0	651,604942	Inf	Inf
hsa-miR-494-3p	0	166,940109	Inf	Inf
hsa-miR-376c-3p	0	72,6997249	Inf	Inf
hsa-miR-214-3p	0	61,9293953	Inf	Inf
hsa-miR-526b-5p	0	53,8516481	Inf	Inf
hsa-miR-379-5p	0	48,4664833	Inf	Inf
hsa-miR-3609	0	40,3887361	Inf	Inf

9. Appendix

hsa-miR-6087	0	32,3109888	Inf	Inf
hsa-miR-199a-5p	0	26,925824	Inf	Inf
hsa-miR-3591-3p	0	24,2332416	Inf	Inf
hsa-miR-574-3p	0	24,2332416	Inf	Inf
hsa-miR-409-3p	0	21,5406592	Inf	Inf
hsa-miR-382-5p	0	18,8480768	Inf	Inf
hsa-miR-487b-3p	0	18,8480768	Inf	Inf
hsa-miR-637	0	13,462912	Inf	Inf
hsa-miR-217	0	10,7703296	Inf	Inf
hsa-miR-486-3p	0	10,7703296	Inf	Inf
hsa-miR-495-3p	0	10,7703296	Inf	Inf
hsa-miR-124-5p	0	8,07774721	Inf	Inf
hsa-miR-31-5p	0	8,07774721	Inf	Inf
hsa-miR-412-5p	0	8,07774721	Inf	Inf
hsa-miR-487a-3p	0	8,07774721	Inf	Inf
hsa-miR-493-3p	0	8,07774721	Inf	Inf
hsa-miR-144-5p	0	5,38516481	Inf	Inf
hsa-miR-210-5p	0	5,38516481	Inf	Inf
hsa-miR-3126-3p	0	5,38516481	Inf	Inf
hsa-miR-411-5p	0	5,38516481	Inf	Inf
hsa-miR-4689	0	5,38516481	Inf	Inf
hsa-miR-5010-3p	0	5,38516481	Inf	Inf
hsa-miR-520g-5p	0	5,38516481	Inf	Inf
hsa-miR-611	0	5,38516481	Inf	Inf
hsa-miR-6500-3p	0	5,38516481	Inf	Inf
hsa-miR-6789-5p	0	5,38516481	Inf	Inf
hsa-miR-6791-3p	0	5,38516481	Inf	Inf
hsa-miR-6878-3p	0	5,38516481	Inf	Inf
mgU12-22	0	5,38516481	Inf	Inf
U108	0	5,38516481	Inf	Inf
U91	0	5,38516481	Inf	Inf
ACA19	0	2,6925824	Inf	Inf
HBII-52-26	0	2,6925824	Inf	Inf
HBII-52-31	0	2,6925824	Inf	Inf
HBII-52-41	0	2,6925824	Inf	Inf
hsa-miR-127-3p	0	2,6925824	Inf	Inf
hsa-miR-144-3p	0	2,6925824	Inf	Inf
hsa-miR-205-5p	0	2,6925824	Inf	Inf
hsa-miR-224-5p	0	2,6925824	Inf	Inf
hsa-miR-299-5p	0	2,6925824	Inf	Inf
hsa-miR-3120-5p	0	2,6925824	Inf	Inf
hsa-miR-3157-3p	0	2,6925824	Inf	Inf
hsa-miR-329-3p	0	2,6925824	Inf	Inf
hsa-miR-3605-5p	0	2,6925824	Inf	Inf
hsa-miR-369-5p	0	2,6925824	Inf	Inf
hsa-miR-377-3p	0	2,6925824	Inf	Inf
hsa-miR-3939	0	2,6925824	Inf	Inf

9. Appendix

hsa-miR-4463	0	2,6925824	Inf	Inf
hsa-miR-4497	0	2,6925824	Inf	Inf
hsa-miR-4508	0	2,6925824	Inf	Inf
hsa-miR-4659b-5p	0	2,6925824	Inf	Inf
hsa-miR-4723-5p	0	2,6925824	Inf	Inf
hsa-miR-4754	0	2,6925824	Inf	Inf
hsa-miR-518c-5p	0	2,6925824	Inf	Inf
hsa-miR-518d-5p	0	2,6925824	Inf	Inf
hsa-miR-520c-5p	0	2,6925824	Inf	Inf
hsa-miR-526a	0	2,6925824	Inf	Inf
hsa-miR-6729-5p	0	2,6925824	Inf	Inf
hsa-miR-6771-5p	0	2,6925824	Inf	Inf
hsa-miR-6794-5p	0	2,6925824	Inf	Inf
hsa-miR-6831-3p	0	2,6925824	Inf	Inf
hsa-miR-6831-5p	0	2,6925824	Inf	Inf
hsa-miR-937-5p	0	2,6925824	Inf	Inf
hsa-miR-378b	2324,16285	0	0	-Inf
hsa-miR-378i	2015,16581	0	0	-Inf
hsa-miR-181c-5p	572,684423	0	0	-Inf
hsa-miR-196b-5p	237,318642	0	0	-Inf
hsa-miR-4318	121,073361	0	0	-Inf
hsa-miR-4289	111,417203	0	0	-Inf
hsa-miR-1304-3p	106,217733	0	0	-Inf
U73a	106,217733	0	0	-Inf
U82	106,217733	0	0	-Inf
U58C	83,5629022	0	0	-Inf
HBII-419	82,0773395	0	0	-Inf
U102	80,9631675	0	0	-Inf
hsa-miR-7975	79,8489954	0	0	-Inf
U45C	76,87787	0	0	-Inf
U54	75,3923073	0	0	-Inf
hsa-miR-23c	51,9946947	0	0	-Inf
U46	46,0524439	0	0	-Inf
hsa-miR-1301-3p	42,3385371	0	0	-Inf
hsa-miR-7977	42,3385371	0	0	-Inf
HBII-316	41,5957558	0	0	-Inf
U75	41,5957558	0	0	-Inf
U88	35,2821143	0	0	-Inf
hsa-miR-505-5p	34,9107236	0	0	-Inf
U29	33,4251609	0	0	-Inf
hsa-miR-33a-5p	31,9395982	0	0	-Inf
U37	28,2256914	0	0	-Inf
mgH18S-121	27,1115194	0	0	-Inf
hsa-miR-4521	26,7401287	0	0	-Inf
U105B	25,6259567	0	0	-Inf
hsa-miR-4448	25,254566	0	0	-Inf
ACA36B	24,140394	0	0	-Inf

9. Appendix

HBII-180C	23,7690033	0	0	-Inf
HBII-276	23,7690033	0	0	-Inf
hsa-miR-664a-3p	23,7690033	0	0	-Inf
hsa-miR-181b-2-3p	23,3976126	0	0	-Inf
U32A	23,3976126	0	0	-Inf
hsa-miR-301a-5p	23,0262219	0	0	-Inf
HBII-55	21,9120499	0	0	-Inf
hsa-miR-181b-3p	21,5406592	0	0	-Inf
hsa-miR-500b-5p	21,5406592	0	0	-Inf
hsa-miR-1290	21,1692686	0	0	-Inf
SNORD121B	20,7978779	0	0	-Inf
hsa-miR-140-5p	19,6837059	0	0	-Inf
hsa-miR-542-3p	19,6837059	0	0	-Inf
hsa-miR-652-5p	19,6837059	0	0	-Inf
HBII-108B	18,5695338	0	0	-Inf
HBII-13	17,4553618	0	0	-Inf
HBII-82B	15,9697991	0	0	-Inf
U36B	15,9697991	0	0	-Inf
HBII-240	15,5984084	0	0	-Inf
hsa-miR-500a-5p	15,5984084	0	0	-Inf
hsa-miR-153-3p	15,2270177	0	0	-Inf
U106	15,2270177	0	0	-Inf
HBII-239	14,1128457	0	0	-Inf
hsa-let-7f-2-3p	14,1128457	0	0	-Inf
hsa-miR-16-2-3p	14,1128457	0	0	-Inf
U53	12,9986737	0	0	-Inf
hsa-miR-96-5p	12,627283	0	0	-Inf
HBII-95	11,8845016	0	0	-Inf
hsa-miR-1254	11,8845016	0	0	-Inf
hsa-miR-660-3p	11,8845016	0	0	-Inf
U101	11,513111	0	0	-Inf
hsa-miR-30e-3p	11,1417203	0	0	-Inf
hsa-miR-3619-5p	11,1417203	0	0	-Inf
HBII-234	10,3989389	0	0	-Inf
hsa-miR-550a-5p	10,3989389	0	0	-Inf
hsa-miR-766-5p	10,0275483	0	0	-Inf
U56	10,0275483	0	0	-Inf
snR38A	9,65615759	0	0	-Inf
U83	9,65615759	0	0	-Inf
HBII-180A	9,28476691	0	0	-Inf
hsa-miR-362-5p	9,28476691	0	0	-Inf
hsa-miR-501-5p	9,28476691	0	0	-Inf
HBII-296A	8,91337623	0	0	-Inf
hsa-miR-500b-3p	8,91337623	0	0	-Inf
hsa-miR-545-5p	8,91337623	0	0	-Inf
hsa-miR-378h	8,54198556	0	0	-Inf
U77	8,54198556	0	0	-Inf

9. Appendix

HBII-296B	8,17059488	0	0	-Inf
U103	8,17059488	0	0	-Inf
U103B	8,17059488	0	0	-Inf
U18C	8,17059488	0	0	-Inf
hsa-let-7g-3p	7,7992042	0	0	-Inf
U36C	7,7992042	0	0	-Inf
hsa-miR-550a-3-5p	7,42781353	0	0	-Inf
hsa-miR-942-5p	7,42781353	0	0	-Inf
hsa-miR-548ap-3p	7,05642285	0	0	-Inf
ACA10	6,68503217	0	0	-Inf
E3	6,68503217	0	0	-Inf
hsa-miR-3200-3p	6,68503217	0	0	-Inf
hsa-miR-744-3p	6,3136415	0	0	-Inf
HBII-99	5,94225082	0	0	-Inf
hsa-miR-26b-3p	5,94225082	0	0	-Inf
hsa-miR-1224-3p	5,57086015	0	0	-Inf
hsa-miR-18a-3p	5,57086015	0	0	-Inf
hsa-miR-502-5p	5,57086015	0	0	-Inf
hsa-miR-574-5p	5,57086015	0	0	-Inf
hsa-miR-92b-5p	5,57086015	0	0	-Inf
U86	5,57086015	0	0	-Inf
hsa-miR-183-3p	5,19946947	0	0	-Inf
hsa-miR-212-3p	5,19946947	0	0	-Inf
hsa-miR-3182	5,19946947	0	0	-Inf
hsa-miR-504-5p	5,19946947	0	0	-Inf
snR38B	5,19946947	0	0	-Inf
U51	5,19946947	0	0	-Inf
ACA51	4,82807879	0	0	-Inf
ACA9	4,82807879	0	0	-Inf
hsa-miR-8485	4,82807879	0	0	-Inf
hsa-miR-99b-3p	4,82807879	0	0	-Inf
U36A	4,82807879	0	0	-Inf
HBII-251	4,45668812	0	0	-Inf
HBII-295	4,45668812	0	0	-Inf
HBII-85-12	4,45668812	0	0	-Inf
hsa-miR-219b-5p	4,45668812	0	0	-Inf
hsa-miR-221-5p	4,45668812	0	0	-Inf
ACA61	4,08529744	0	0	-Inf
ACA7	4,08529744	0	0	-Inf
HBII-85-23	4,08529744	0	0	-Inf
hsa-miR-25-5p	4,08529744	0	0	-Inf
hsa-miR-301b-5p	4,08529744	0	0	-Inf
hsa-miR-374a-5p	4,08529744	0	0	-Inf
hsa-miR-548av-5p	4,08529744	0	0	-Inf
HBI-43	3,71390676	0	0	-Inf
HBII-85-11	3,71390676	0	0	-Inf
hsa-miR-1273f	3,71390676	0	0	-Inf

9. Appendix

hsa-miR-29a-5p	3,71390676	0	0	-Inf
hsa-miR-4472	3,71390676	0	0	-Inf
hsa-miR-624-5p	3,71390676	0	0	-Inf
hsa-miR-769-3p	3,71390676	0	0	-Inf
ACA7B	3,34251609	0	0	-Inf
hsa-miR-3130-5p	3,34251609	0	0	-Inf
hsa-miR-4791	3,34251609	0	0	-Inf
hsa-miR-616-3p	3,34251609	0	0	-Inf
hsa-miR-619-5p	3,34251609	0	0	-Inf
hsa-miR-6797-3p	3,34251609	0	0	-Inf
SNORD127	3,34251609	0	0	-Inf
U71b	3,34251609	0	0	-Inf
ACA43	2,97112541	0	0	-Inf
hsa-miR-132-5p	2,97112541	0	0	-Inf
hsa-miR-16-1-3p	2,97112541	0	0	-Inf
hsa-miR-2467-3p	2,97112541	0	0	-Inf
hsa-miR-450b-5p	2,97112541	0	0	-Inf
hsa-miR-545-3p	2,97112541	0	0	-Inf
hsa-miR-6511a-3p	2,97112541	0	0	-Inf
hsa-miR-6511b-3p	2,97112541	0	0	-Inf
hsa-miR-6799-3p	2,97112541	0	0	-Inf
mgU2-25	2,97112541	0	0	-Inf
ACA22	2,59973473	0	0	-Inf
HBII-382	2,59973473	0	0	-Inf
hsa-miR-103a-2-5p	2,59973473	0	0	-Inf
hsa-miR-1179	2,59973473	0	0	-Inf
hsa-miR-1256	2,59973473	0	0	-Inf
hsa-miR-1273d	2,59973473	0	0	-Inf
hsa-miR-128-1-5p	2,59973473	0	0	-Inf
hsa-miR-199b-5p	2,59973473	0	0	-Inf
hsa-miR-3150a-5p	2,59973473	0	0	-Inf
hsa-miR-3653-5p	2,59973473	0	0	-Inf
hsa-miR-548k	2,59973473	0	0	-Inf

9.7 DG75 small RNA sequencing results (log2foldchange >±2)

id	baseMeanA	baseMeanB	foldChange	log2FoldChange
U29	197,796297	1,63299316	0,00825593	-6,920352855
HBII-429	333,742978	3,26598632	0,00978593	-6,67507492
hsa-miR-4521	10374,2014	104,511562	0,01007418	-6,633193917
hsa-miR-3607-5p	2527,26104	58,7877538	0,02326145	-5,425915222
hsa-miR-20a-5p	10153,135	404,982304	0,03988742	-4,647922577
hsa-miR-505-5p	39,8042083	1,63299316	0,04102564	-4,607330314
U101	38,5794635	1,63299316	0,04232804	-4,562242424

9. Appendix

U74	1611,76425	70,218706	0,04356636	-4,52064152
hsa-miR-95-3p	28,169132	1,63299316	0,05797101	-4,108524457
ACA3	27,5567596	1,63299316	0,05925926	-4,076815597
hsa-miR-33a-3p	80,8331615	4,89897949	0,06060606	-4,044394119
hsa-miR-16-2-3p	25,7196423	1,63299316	0,06349206	-3,977279923
U104	1085,73633	71,8516991	0,06617785	-3,917507703
hsa-miR-19b-1-5p	172,076654	11,4309521	0,06642942	-3,912033899
U25	364,361599	24,4948974	0,06722689	-3,894817763
U45C	235,763388	16,3299316	0,06926407	-3,851749041
U102	304,349101	21,2289111	0,06975184	-3,841624824
U31	1921,6247	143,703398	0,07478224	-3,741160519
HBI-61	21,4330353	1,63299316	0,07619048	-3,714245518
hsa-miR-106b-5p	2115,74677	163,299316	0,07718283	-3,695576306
HBII-336	20,8206628	1,63299316	0,07843137	-3,672425342
SNORD126	20,8206628	1,63299316	0,07843137	-3,672425342
U38A	20,8206628	1,63299316	0,07843137	-3,672425342
hsa-miR-378a-5p	143,907522	11,4309521	0,07943262	-3,654124525
hsa-miR-4284	605,023967	48,9897949	0,08097166	-3,626439137
U44	1014,70113	84,9156444	0,08368538	-3,57888067
hsa-miR-28-5p	205,144766	17,9629248	0,08756219	-3,513548167
U18C	35,5176013	3,26598632	0,09195402	-3,442943496
U50	34,9052288	3,26598632	0,09356725	-3,417852515
SNORD119	51,4392846	4,89897949	0,0952381	-3,392317423
hsa-miR-548aa	34,2928564	3,26598632	0,0952381	-3,392317423
hsa-miR-548t-3p	34,2928564	3,26598632	0,0952381	-3,392317423
hsa-miR-182-5p	152,480737	14,6969385	0,09638554	-3,375039431
hsa-miR-942-5p	16,5340558	1,63299316	0,09876543	-3,339850003
U19	16,5340558	1,63299316	0,09876543	-3,339850003
hsa-miR-7-5p	676,671541	66,9527196	0,09894419	-3,33724115
U58B	246,786092	24,4948974	0,09925558	-3,332707934
hsa-miR-3529-3p	621,558022	62,0537402	0,0998358	-3,324298999
hsa-miR-365a-3p	556,034172	55,5217675	0,09985316	-3,324048147
hsa-miR-365b-3p	556,034172	55,5217675	0,09985316	-3,324048147
hsa-miR-99a-5p	904,474088	93,0806102	0,10291131	-3,280526597
hsa-let-7a-5p	7002,4788	751,176855	0,10727299	-3,220641195
U73a	332,518233	35,9258496	0,10804174	-3,21033927
hsa-miR-29c-3p	584,815676	63,6867333	0,10890052	-3,198917205
HBII-419	313,534687	34,2928564	0,109375	-3,192645078
hsa-miR-18a-5p	12721,425	1433,768	0,11270498	-3,149376782
snR39B	2202,70365	249,847954	0,11342786	-3,140153102
hsa-miR-29b-3p	4710,98115	545,419716	0,11577625	-3,110588801
hsa-miR-1307-5p	463,565934	55,5217675	0,11977103	-3,061649149
U58A	272,505734	34,2928564	0,1258427	-2,990306604
ACA21	12,8598212	1,63299316	0,12698413	-2,977279923
hsa-miR-1303	12,8598212	1,63299316	0,12698413	-2,977279923
hsa-miR-148b-5p	12,8598212	1,63299316	0,12698413	-2,977279923
hsa-miR-500a-5p	12,8598212	1,63299316	0,12698413	-2,977279923

9. Appendix

Z17B	76,5465545	9,79795897	0,128	-2,965784285
hsa-miR-18a-3p	24,4948974	3,26598632	0,13333333	-2,906890596
U81	107,165176	14,6969385	0,13714286	-2,866248611
hsa-miR-130b-5p	105,328059	14,6969385	0,13953488	-2,841302254
HBII-85-27	11,6350763	1,63299316	0,14035088	-2,832890014
U58C	781,387228	112,676528	0,14420063	-2,793850658
hsa-let-7d-5p	1735,46348	251,480947	0,14490708	-2,786800003
hsa-let-7f-5p	4673,01406	690,756108	0,14781811	-2,758105059
E3	22,0454077	3,26598632	0,14814815	-2,754887502
HBII-85-25	11,0227038	1,63299316	0,14814815	-2,754887502
HBII-99	11,0227038	1,63299316	0,14814815	-2,754887502
hsa-miR-616-5p	11,0227038	1,63299316	0,14814815	-2,754887502
U87	11,0227038	1,63299316	0,14814815	-2,754887502
U82	219,229332	32,6598632	0,14897579	-2,746850183
mgh18S-121	216,779842	32,6598632	0,15065913	-2,730639956
hsa-miR-629-3p	21,4330353	3,26598632	0,15238095	-2,714245518
HBII-142	31,8433667	4,89897949	0,15384615	-2,700439718
hsa-miR-4286	559,708406	86,5486376	0,15463166	-2,693092401
U63	198,408669	31,0268701	0,1563786	-2,67688499
U77	61,849616	9,79795897	0,15841584	-2,658211483
HBII-420	374,159558	62,0537402	0,16584834	-2,592063557
ACA51	9,79795897	1,63299316	0,16666667	-2,584962501
hsa-miR-501-5p	9,79795897	1,63299316	0,16666667	-2,584962501
U88	9,79795897	1,63299316	0,16666667	-2,584962501
hsa-miR-101-3p	631,355981	106,144556	0,16812157	-2,572423305
hsa-miR-18b-5p	58,1753814	9,79795897	0,16842105	-2,569855608
SNORD121A	112,676528	19,5959179	0,17391304	-2,523561956
hsa-miR-9-5p	56,3382641	9,79795897	0,17391304	-2,523561956
hsa-miR-3653-5p	28,169132	4,89897949	0,17391304	-2,523561956
hsa-miR-219b-5p	9,18558654	1,63299316	0,17777778	-2,491853096
hsa-miR-3667-5p	9,18558654	1,63299316	0,17777778	-2,491853096
U67	9,18558654	1,63299316	0,17777778	-2,491853096
hsa-miR-17-3p	673,609679	122,474487	0,18181818	-2,459431619
U28	17,7588006	3,26598632	0,18390805	-2,442943496
hsa-miR-183-5p	70,4228301	13,0639453	0,18550725	-2,430452552
hsa-miR-339-5p	175,750889	32,6598632	0,18583043	-2,427941333
U18A	157,379716	29,3938769	0,18677043	-2,420662048
hsa-miR-589-3p	34,9052288	6,53197265	0,1871345	-2,417852515
U50B	43,4784429	8,16496581	0,18779343	-2,412781525
U35B	52,051657	9,79795897	0,18823529	-2,409390936
U90	8,5732141	1,63299316	0,19047619	-2,392317423
hsa-miR-4454	212,493235	40,8248291	0,19212296	-2,379898164
hsa-miR-142-3p	1508,27331	295,571762	0,19596698	-2,351317526
hsa-miR-34a-5p	261,48303	52,2557812	0,19984387	-2,32305476
SNORD125	24,4948974	4,89897949	0,2	-2,321928095
hsa-miR-324-3p	55,7258917	11,4309521	0,20512821	-2,285402219
hsa-miR-140-5p	39,8042083	8,16496581	0,20512821	-2,285402219

9. Appendix

U54	31,8433667	6,53197265	0,20512821	-2,285402219
ACA14b	7,96084166	1,63299316	0,20512821	-2,285402219
HBII-316	176,975634	37,5588427	0,21222607	-2,236326227
U57	122,474487	26,1278906	0,21333333	-2,22881869
HBII-234	15,3093109	3,26598632	0,21333333	-2,22881869
hsa-miR-25-5p	15,3093109	3,26598632	0,21333333	-2,22881869
hsa-miR-582-5p	105,328059	22,8619043	0,21705426	-2,203872333
hsa-miR-660-5p	320,270784	70,218706	0,21924793	-2,189364882
hsa-let-7a-3p	52,051657	11,4309521	0,21960784	-2,186998515
hsa-miR-1285-3p	28,7815045	6,53197265	0,22695036	-2,139551352
hsa-miR-532-3p	28,7815045	6,53197265	0,22695036	-2,139551352
hsa-miR-1260b	399,266828	91,4476171	0,22903886	-2,126335733
hsa-let-7f-1-3p	35,5176013	8,16496581	0,22988506	-2,121015401
hsa-miR-29a-3p	1752,60991	403,349311	0,23014209	-2,119403226
hsa-miR-29c-5p	14,084566	3,26598632	0,23188406	-2,108524457
hsa-miR-1180-3p	20,8206628	4,89897949	0,23529412	-2,087462841
ACA9	6,73609679	1,63299316	0,24242424	-2,044394119
hsa-miR-4791	6,73609679	1,63299316	0,24242424	-2,044394119
hsa-miR-641	6,73609679	1,63299316	0,24242424	-2,044394119
U96a	60,0124987	14,6969385	0,24489796	-2,029747343
hsa-miR-15b-5p	1331,29768	326,598632	0,24532352	-2,027242536
U43	98,5919622	24,4948974	0,24844721	-2,008988783
U79	327,006881	81,6496581	0,24968789	-2,001802243
hsa-miR-589-5p	13,4721936	53,8887743	4	2
ACA41	4,89897949	19,5959179	4	2
hsa-miR-526b-5p	4,89897949	19,5959179	4	2
hsa-miR-7641	3,67423461	14,6969385	4	2
hsa-miR-378f	2,44948974	9,79795897	4	2
HBII-52-23	1,22474487	4,89897949	4	2
hsa-miR-25-3p	88,1816307	364,157475	4,12962963	2,046012398
hsa-miR-194-5p	17,7588006	75,1176855	4,22988506	2,08061846
U3-3	556,646544	2356,40913	4,23322332	2,0817566
U3	569,506365	2444,59076	4,29247312	2,101809099
hsa-miR-619-5p	2,44948974	11,4309521	4,66666667	2,222392421
ACA47	5,51135192	26,1278906	4,74074074	2,245112498
U3-2	453,767975	2282,92444	5,03103914	2,330856412
U3-2B	453,767975	2282,92444	5,03103914	2,330856412
U3-4	439,683409	2279,65845	5,18477252	2,374280692
hsa-miR-320b	8,5732141	45,7238085	5,33333333	2,415037499
hsa-miR-320d	4,89897949	26,1278906	5,33333333	2,415037499
HBII-202	1,22474487	6,53197265	5,33333333	2,415037499
hsa-miR-129-2-3p	0,61237244	3,26598632	5,33333333	2,415037499
hsa-miR-129-5p	0,61237244	3,26598632	5,33333333	2,415037499
hsa-miR-182-3p	0,61237244	3,26598632	5,33333333	2,415037499
hsa-miR-193a-3p	0,61237244	3,26598632	5,33333333	2,415037499
hsa-miR-200b-3p	0,61237244	3,26598632	5,33333333	2,415037499
hsa-miR-4511	0,61237244	3,26598632	5,33333333	2,415037499

9. Appendix

hsa-miR-4779	0,61237244	3,26598632	5,33333333	2,415037499
hsa-miR-7850-5p	0,61237244	3,26598632	5,33333333	2,415037499
hsa-miR-99b-5p	0,61237244	3,26598632	5,33333333	2,415037499
HBII-85-8	4,28660705	24,4948974	5,71428571	2,514573173
HBII-276	4,28660705	26,1278906	6,0952381	2,607682577
hsa-miR-152-3p	1,83711731	11,4309521	6,22222222	2,637429921
U99	1,83711731	11,4309521	6,22222222	2,637429921
HBII-85-6	4,28660705	27,7608838	6,47619048	2,695145418
hsa-miR-320c	5,51135192	35,9258496	6,51851852	2,704544116
HBII-85-10	1,22474487	8,16496581	6,66666667	2,736965594
hsa-miR-643	1,22474487	8,16496581	6,66666667	2,736965594
ACA63	3,06186218	22,8619043	7,46666667	2,900464326
HBII-85-3	5,51135192	42,4578222	7,7037037	2,945552216
HBII-85-9	5,51135192	42,4578222	7,7037037	2,945552216
hsa-miR-150-5p	50,8269122	393,551352	7,74297189	2,952887404
ACA8	0,61237244	4,89897949	8	3
hsa-miR-133a-3p	0,61237244	4,89897949	8	3
hsa-miR-138-1-3p	0,61237244	4,89897949	8	3
hsa-miR-196b-5p	0,61237244	4,89897949	8	3
hsa-miR-4492	0,61237244	4,89897949	8	3
hsa-miR-885-5p	0,61237244	4,89897949	8	3
SNORA84	0,61237244	4,89897949	8	3
HBII-85-5	4,28660705	37,5588427	8,76190476	3,131244533
HBII-85-7	4,28660705	37,5588427	8,76190476	3,131244533
hsa-miR-486-3p	1,83711731	16,3299316	8,88888889	3,152003093
hsa-miR-146a-5p	58,1753814	519,291826	8,92631579	3,158064846
HBII-85-1	4,28660705	39,1918359	9,14285714	3,192645078
HBII-436	1,22474487	11,4309521	9,33333333	3,222392421
U61	1,22474487	11,4309521	9,33333333	3,222392421
hsa-miR-3074-5p	6,73609679	63,6867333	9,45454546	3,2410081
HBII-85-2	4,28660705	42,4578222	9,90476191	3,308122295
SNORA38B	0,61237244	6,53197265	10,66666667	3,415037499
U49B	0,61237244	6,53197265	10,66666667	3,415037499
hsa-let-7e-5p	1,83711731	21,2289111	11,55555556	3,530514717
hsa-miR-3651	0,61237244	8,16496581	13,33333333	3,736965594
hsa-miR-6087	0,61237244	8,16496581	13,33333333	3,736965594
hsa-miR-760	0,61237244	9,79795897	16	4
U89	0,61237244	9,79795897	16	4
HBII-85-4	2,44948974	40,8248291	16,66666667	4,058893689
hsa-miR-199a-3p	5,51135192	101,245576	18,3703704	4,199308808
hsa-miR-199b-3p	5,51135192	101,245576	18,3703704	4,199308808
U47	1,22474487	22,8619043	18,66666667	4,222392421
hsa-miR-655-3p	0,61237244	11,4309521	18,66666667	4,222392421
hsa-miR-1246	34,2928564	658,096244	19,1904762	4,262318606
hsa-miR-619-3p	0,61237244	13,0639453	21,33333333	4,415037499
hsa-miR-647	0,61237244	13,0639453	21,33333333	4,415037499
HBII-289	6,12372436	140,437412	22,93333333	4,519374159

9. Appendix

U32A	3,06186218	91,4476171	29,8666667	4,900464326
hsa-miR-199a-5p	0,61237244	24,4948974	40	5,321928095
hsa-miR-3607-3p	1,22474487	52,2557812	42,6666667	5,415037499
hsa-miR-126-5p	7,34846923	331,497612	45,1111111	5,495410916
hsa-miR-486-5p	12,2474487	664,628217	54,2666667	5,761994389
hsa-miR-30a-5p	0,61237244	39,1918359	64	6
hsa-miR-223-3p	26,9443872	1817,52139	67,4545455	6,075843758
hsa-miR-130a-3p	0,61237244	65,3197265	106,666667	6,736965594
hsa-miR-126-3p	3,06186218	581,345566	189,866667	7,568842835
hsa-miR-125a-5p	0,61237244	138,804419	226,666667	7,824428435
hsa-miR-451a	0,61237244	1085,94045	1773,33333	10,79224803
hsa-miR-145-5p	0	357,625502	Inf	Inf
hsa-miR-494-3p	0	311,901694	Inf	Inf
hsa-miR-203b-5p	0	153,501357	Inf	Inf
hsa-miR-203a-3p	0	145,336391	Inf	Inf
hsa-miR-143-3p	0	133,905439	Inf	Inf
hsa-miR-221-3p	0	112,676528	Inf	Inf
hsa-miR-376c-3p	0	112,676528	Inf	Inf
hsa-miR-214-3p	0	66,9527196	Inf	Inf
hsa-miR-379-5p	0	55,5217675	Inf	Inf
hsa-miR-455-3p	0	52,2557812	Inf	Inf
hsa-miR-144-3p	0	39,1918359	Inf	Inf
hsa-miR-222-3p	0	39,1918359	Inf	Inf
hsa-miR-409-3p	0	29,3938769	Inf	Inf
hTR	0	29,3938769	Inf	Inf
hsa-miR-122-5p	0	26,1278906	Inf	Inf
hsa-miR-144-5p	0	22,8619043	Inf	Inf
hsa-miR-411-5p	0	17,9629248	Inf	Inf
hsa-miR-487b-3p	0	16,3299316	Inf	Inf
hsa-miR-382-5p	0	14,6969385	Inf	Inf
hsa-miR-10b-5p	0	13,0639453	Inf	Inf
hsa-miR-224-5p	0	13,0639453	Inf	Inf
hsa-miR-376a-5p	0	11,4309521	Inf	Inf
hsa-miR-483-3p	0	11,4309521	Inf	Inf
hsa-miR-10a-5p	0	9,79795897	Inf	Inf
hsa-miR-326	0	9,79795897	Inf	Inf
hsa-miR-329-3p	0	9,79795897	Inf	Inf
hsa-miR-409-5p	0	9,79795897	Inf	Inf
hsa-miR-493-3p	0	9,79795897	Inf	Inf
hsa-miR-204-3p	0	8,16496581	Inf	Inf
hsa-miR-376a-3p	0	8,16496581	Inf	Inf
hsa-miR-376c-5p	0	8,16496581	Inf	Inf
hsa-miR-412-5p	0	8,16496581	Inf	Inf
hsa-miR-493-5p	0	8,16496581	Inf	Inf
hsa-miR-1249-3p	0	6,53197265	Inf	Inf
hsa-miR-26a-2-3p	0	6,53197265	Inf	Inf
hsa-miR-299-5p	0	6,53197265	Inf	Inf

9. Appendix

hsa-miR-3609	0	6,53197265	Inf	Inf
hsa-miR-381-3p	0	6,53197265	Inf	Inf
hsa-miR-487a-3p	0	6,53197265	Inf	Inf
hsa-miR-206	0	4,89897949	Inf	Inf
hsa-miR-335-5p	0	4,89897949	Inf	Inf
hsa-miR-3653-3p	0	4,89897949	Inf	Inf
hsa-miR-433-3p	0	4,89897949	Inf	Inf
hsa-miR-496	0	4,89897949	Inf	Inf
ACA54	0	3,26598632	Inf	Inf
hsa-miR-143-5p	0	3,26598632	Inf	Inf
hsa-miR-145-3p	0	3,26598632	Inf	Inf
hsa-miR-200a-5p	0	3,26598632	Inf	Inf
hsa-miR-340-3p	0	3,26598632	Inf	Inf
hsa-miR-34c-5p	0	3,26598632	Inf	Inf
hsa-miR-3591-3p	0	3,26598632	Inf	Inf
hsa-miR-3648	0	3,26598632	Inf	Inf
hsa-miR-33a-5p	179,425124	0	0	-Inf
hsa-miR-590-3p	137,171426	0	0	-Inf
U36B	100,42908	0	0	-Inf
hsa-miR-1275	59,4001263	0	0	-Inf
snR38A	53,8887743	0	0	-Inf
ACA36B	50,8269122	0	0	-Inf
hsa-miR-664a-3p	48,3774224	0	0	-Inf
HBII-13	41,0289532	0	0	-Inf
U105	28,7815045	0	0	-Inf
U84	28,169132	0	0	-Inf
HBII-239	27,5567596	0	0	-Inf
hsa-miR-7974	23,882525	0	0	-Inf
U15A	23,882525	0	0	-Inf
HBII-108B	22,0454077	0	0	-Inf
hsa-miR-579-3p	19,5959179	0	0	-Inf
hsa-miR-181b-3p	17,7588006	0	0	-Inf
U105B	17,1464282	0	0	-Inf
U71b	16,5340558	0	0	-Inf
hsa-miR-3618	14,6969385	0	0	-Inf
hsa-miR-500b-5p	14,6969385	0	0	-Inf
hsa-miR-545-3p	14,084566	0	0	-Inf
hsa-miR-34a-3p	12,8598212	0	0	-Inf
hsa-miR-4485-3p	12,8598212	0	0	-Inf
hsa-miR-362-5p	11,6350763	0	0	-Inf
ACA2b	11,0227038	0	0	-Inf
hsa-miR-877-3p	11,0227038	0	0	-Inf
HBII-251	10,4103314	0	0	-Inf
hsa-miR-132-5p	10,4103314	0	0	-Inf
ACA23	9,79795897	0	0	-Inf
hsa-miR-192-3p	9,79795897	0	0	-Inf
HBII-180A	9,18558654	0	0	-Inf

9. Appendix

hsa-miR-3074-3p	8,5732141	0	0	-Inf
hsa-miR-33b-5p	8,5732141	0	0	-Inf
hsa-miR-597-5p	8,5732141	0	0	-Inf
hsa-miR-96-5p	8,5732141	0	0	-Inf
ACA62	7,96084166	0	0	-Inf
hsa-miR-26b-3p	7,96084166	0	0	-Inf
hsa-miR-4323	7,96084166	0	0	-Inf
hsa-miR-183-3p	7,34846923	0	0	-Inf
hsa-miR-3613-5p	7,34846923	0	0	-Inf
hsa-miR-642a-3p	7,34846923	0	0	-Inf
hsa-miR-642b-5p	7,34846923	0	0	-Inf
ACA33	6,73609679	0	0	-Inf
hsa-miR-3179	6,73609679	0	0	-Inf
hsa-miR-642a-5p	6,73609679	0	0	-Inf
hsa-miR-652-5p	6,73609679	0	0	-Inf
ACA36	6,12372436	0	0	-Inf
hsa-let-7g-3p	6,12372436	0	0	-Inf
hsa-miR-4461	6,12372436	0	0	-Inf
hsa-miR-576-5p	6,12372436	0	0	-Inf
hsa-miR-874-5p	6,12372436	0	0	-Inf
mgU6-77	6,12372436	0	0	-Inf
ACA35	5,51135192	0	0	-Inf
hsa-miR-1254	5,51135192	0	0	-Inf
hsa-miR-1296-3p	5,51135192	0	0	-Inf
hsa-miR-2110	5,51135192	0	0	-Inf
hsa-miR-550a-3p	5,51135192	0	0	-Inf
hsa-miR-550b-2-5p	5,51135192	0	0	-Inf
mgU2-25	5,51135192	0	0	-Inf
U65	5,51135192	0	0	-Inf
U71d	5,51135192	0	0	-Inf
ACA52	4,89897949	0	0	-Inf
ACA53	4,89897949	0	0	-Inf
hsa-let-7c-3p	4,89897949	0	0	-Inf
hsa-miR-1-3p	4,89897949	0	0	-Inf

9.8 HeLa small RNA sequencing results (log2foldchange >±1)

id	baseMeanA cell	baseMeanB exo	log2FoldChange
hsa-miR-204-5p	423,0920113	2,261919333	-7,547280156
hsa-miR-4284	917,8046138	6,785758	-7,079533269
hsa-miR-95-3p	34,04188596	2,261919333	-3,911691582
U74	131,7465197	9,047677333	-3,864073562
hsa-miR-454-3p	27,41034974	2,261919333	-3,599101352

9. Appendix

hsa-miR-125b-5p	1283,423311	117,6198053	-3,44779418
U80	72,94689849	6,785758	-3,426264755
U29	21,22091593	2,261919333	-3,229867542
HBII-429	20,33671111	2,261919333	-3,168466997
HBII-142	19,45250627	2,261919333	-3,10433666
mgH28S-2411	17,24199419	2,261919333	-2,93030726
hsa-miR-582-5p	98,58883857	13,571516	-2,86084244
U24	49,07336808	6,785758	-2,854358407
U48	15,91568694	2,261919333	-2,814830043
hsa-miR-1260b	99,4730434	15,83343533	-2,65133131
hsa-miR-99a-5p	1104,813935	192,2631433	-2,522649291
U44	84,44156129	15,83343533	-2,414978947
hsa-miR-455-3p	46,42075359	9,047677333	-2,359150559
hsa-miR-10b-5p	68,96797676	13,571516	-2,345344759
U97	11,49466279	2,261919333	-2,345344759
hsa-miR-551b-3p	68,52587434	13,571516	-2,336066946
U38A	11,05256038	2,261919333	-2,288761231
hsa-miR-26a-5p	389,0501253	88,21485399	-2,140862536
hsa-miR-361-3p	19,45250627	4,523838666	-2,10433666
HBII-240	9,726253133	2,261919333	-2,10433666
hsa-let-7f-5p	402,3131978	95,00061199	-2,082310353
hsa-miR-3117-3p	18,56830144	4,523838666	-2,037222464
hsa-miR-10a-5p	81,7889468	20,357274	-2,0063615
hsa-miR-4454	398,334276	101,78637	-1,968435241
hsa-miR-182-5p	77,36792265	20,357274	-1,926191152
hsa-miR-30c-5p	246,2510452	65,59566066	-1,908457563
hsa-miR-590-3p	8,399945887	2,261919333	-1,892832555
hsa-miR-125a-5p	607,4487184	169,64395	-1,840252639
U50	7,957843472	2,261919333	-1,814830043
hsa-miR-4286	237,8510993	70,11949933	-1,762171093
U16	7,515741057	2,261919333	-1,732367882
hsa-miR-365a-3p	58,79962121	18,09535467	-1,700187477
hsa-miR-365b-3p	58,79962121	18,09535467	-1,700187477
hsa-miR-374b-5p	36,69450045	11,30959667	-1,698016378
hsa-miR-374c-3p	36,69450045	11,30959667	-1,698016378
hsa-miR-339-5p	29,1787594	9,047677333	-1,689299161
hsa-miR-1275	7,073638642	2,261919333	-1,644905041
hsa-miR-148b-5p	7,073638642	2,261919333	-1,644905041
U82	7,073638642	2,261919333	-1,644905041
U87	7,073638642	2,261919333	-1,644905041
hsa-let-7e-5p	188,7777313	61,071822	-1,628109799
U21	20,77881351	6,785758	-1,614531392
hsa-miR-30b-5p	79,57843472	27,143032	-1,551795637
U88	6,631536227	2,261919333	-1,551795637
hsa-miR-210-3p	45,09444634	15,83343533	-1,509975461
U62A	87,97838061	31,66687066	-1,47417474
U62B	87,97838061	31,66687066	-1,47417474

9. Appendix

HBII-239	6,189433812	2,261919333	-1,452259963
hsa-miR-151a-5p	256,8615032	97,26253133	-1,40103464
HBII-180C	17,6840966	6,785758	-1,381870635
hsa-miR-98-5p	17,6840966	6,785758	-1,381870635
hsa-miR-151b	264,3772442	101,78637	-1,377053619
hsa-let-7a-5p	1067,677333	445,5981086	-1,260660695
HBII-99	5,305228981	2,261919333	-1,229867542
hsa-miR-32-5p	5,305228981	2,261919333	-1,229867542
hsa-miR-876-5p	5,305228981	2,261919333	-1,229867542
hsa-miR-505-3p	15,47358453	6,785758	-1,189225557
hsa-miR-139-5p	66,75746468	29,40495133	-1,182870062
hsa-miR-99a-3p	9,726253133	4,523838666	-1,10433666
hsa-miR-500a-3p	4,863126566	2,261919333	-1,10433666
U71b	4,863126566	2,261919333	-1,10433666
U73a	4,863126566	2,261919333	-1,10433666
hsa-miR-99b-5p	152,5253332	72,38141866	-1,075357593
hsa-miR-30d-5p	179,4935805	364,1690126	1,02067592
hsa-let-7d-3p	6,631536227	13,571516	1,033166864
hsa-miR-296-5p	6,631536227	13,571516	1,033166864
U75	4,421024151	9,047677333	1,033166864
HBII-166	2,210512076	4,523838666	1,033166864
hsa-miR-1254	2,210512076	4,523838666	1,033166864
hsa-miR-1292-5p	2,210512076	4,523838666	1,033166864
U27	42,88393427	90,47677333	1,077110212
hsa-miR-574-3p	102,5677603	217,144256	1,082076464
U33	10,61045796	22,61919333	1,092060553
hsa-miR-224-3p	5,305228981	11,30959667	1,092060553
U17b	25,19983766	54,286064	1,107167445
hsa-miR-152-3p	16,79989177	36,19070933	1,107167445
hsa-miR-23a-3p	1801,567342	3928,953882	1,124892654
hsa-miR-181a-5p	43,32603668	95,00061199	1,132702537
hsa-miR-877-3p	3,094716906	6,785758	1,132702537
U18A	3,094716906	6,785758	1,132702537
hsa-miR-19b-3p	1716,241575	3833,95327	1,159580114
hsa-miR-186-5p	10,16835555	24,88111266	1,290964621
hsa-miR-24-3p	935,4887104	2384,062977	1,349630198
hsa-miR-224-5p	62,77854295	160,5962727	1,355094959
U20	6,189433812	15,83343533	1,355094959
hsa-miR-1306-5p	4,421024151	11,30959667	1,355094959
hsa-miR-3607-5p	4,421024151	11,30959667	1,355094959
U34	3,536819321	9,047677333	1,355094959
U58A	2,652614491	6,785758	1,355094959
hsa-miR-92b-5p	1,76840966	4,523838666	1,355094959
U37	1,76840966	4,523838666	1,355094959
ACA33	0,88420483	2,261919333	1,355094959
ACA43	0,88420483	2,261919333	1,355094959
HBI-43	0,88420483	2,261919333	1,355094959

9. Appendix

HBII-202	0,88420483	2,261919333	1,355094959
hsa-miR-1237-3p	0,88420483	2,261919333	1,355094959
hsa-miR-1268a	0,88420483	2,261919333	1,355094959
hsa-miR-1287-5p	0,88420483	2,261919333	1,355094959
hsa-miR-181a-3p	0,88420483	2,261919333	1,355094959
hsa-miR-183-3p	0,88420483	2,261919333	1,355094959
hsa-miR-196b-3p	0,88420483	2,261919333	1,355094959
hsa-miR-221-5p	0,88420483	2,261919333	1,355094959
hsa-miR-25-5p	0,88420483	2,261919333	1,355094959
hsa-miR-301b-3p	0,88420483	2,261919333	1,355094959
hsa-miR-326	0,88420483	2,261919333	1,355094959
hsa-miR-4488	0,88420483	2,261919333	1,355094959
hsa-miR-6787-3p	0,88420483	2,261919333	1,355094959
U85	0,88420483	2,261919333	1,355094959
hsa-miR-452-5p	75,15741057	199,0489013	1,405135641
hsa-let-7b-3p	8,842048302	24,88111266	1,492598483
U26	31,83137389	90,47677333	1,507098052
U52	3,978921736	11,30959667	1,507098052
hsa-miR-1180-3p	11,05256038	31,66687066	1,518593691
hsa-miR-185-5p	43,7681391	131,1913213	1,583719334
ACA45	11,93676521	36,19070933	1,600207457
hsa-miR-25-3p	15,47358453	47,500306	1,618129365
hsa-miR-93-3p	12,37886762	38,45262866	1,635202878
hsa-miR-501-3p	3,536819321	11,30959667	1,677023054
hsa-miR-107	87,97838061	289,5256746	1,718470338
hsa-miR-361-5p	21,22091593	72,38141866	1,770132458
hsa-miR-421	17,24199419	58,80990266	1,770132458
hsa-miR-22-5p	3,978921736	13,571516	1,770132458
HBII-276	1,326307245	4,523838666	1,770132458
hsa-miR-138-1-3p	1,326307245	4,523838666	1,770132458
U58B	1,326307245	4,523838666	1,770132458
U42B	11,05256038	38,45262866	1,79870161
hsa-miR-149-5p	24,75773525	90,47677333	1,869668132
hsa-miR-126-3p	18,56830144	67,85758	1,869668132
hsa-miR-15b-3p	18,56830144	67,85758	1,869668132
hsa-miR-423-3p	132,6307245	490,8364953	1,887827501
hsa-miR-145-5p	97,70463374	361,9070933	1,889120494
HBII-85-1	3,536819321	13,571516	1,94005746
HBII-85-2	3,536819321	13,571516	1,94005746
hsa-miR-454-5p	3,536819321	13,571516	1,94005746
HBII-295	1,76840966	6,785758	1,94005746
hsa-miR-579-3p	1,76840966	6,785758	1,94005746
hsa-miR-629-3p	1,76840966	6,785758	1,94005746
U17a	22,98932559	92,73869266	2,012207245
hsa-miR-590-5p	88,86258544	361,9070933	2,025971363
ACA61	2,210512076	9,047677333	2,033166864
hsa-miR-92a-1-5p	2,210512076	9,047677333	2,033166864

9. Appendix

mgU2-19	20,3367111	85,95293466	2,079460516
hsa-miR-15a-5p	58,3575188	248,8111266	2,092060553
hsa-let-7i-5p	171,5357371	744,1714606	2,11712589
U8	10,16835555	45,23838666	2,153461098
hsa-miR-21-3p	3,536819321	15,83343533	2,162449881
hsa-miR-93-5p	244,924738	1124,173909	2,198454834
hsa-miR-132-3p	10,61045796	49,76222533	2,229564077
hsa-miR-615-3p	12,37886762	58,80990266	2,248179755
hsa-miR-20a-5p	481,8916325	2372,75338	2,299781502
HBII-85-3	4,863126566	24,88111266	2,355094959
HBII-85-9	4,863126566	24,88111266	2,355094959
HBII-85-4	2,652614491	13,571516	2,355094959
ACA3	0,88420483	4,523838666	2,355094959
hsa-miR-589-3p	0,88420483	4,523838666	2,355094959
hsa-miR-873-3p	0,88420483	4,523838666	2,355094959
U14B	0,88420483	4,523838666	2,355094959
U41	0,88420483	4,523838666	2,355094959
ACA21	0,442102415	2,261919333	2,355094959
ACA41	0,442102415	2,261919333	2,355094959
ACA55	0,442102415	2,261919333	2,355094959
HBII-234	0,442102415	2,261919333	2,355094959
HBII-438A	0,442102415	2,261919333	2,355094959
HBII-438B	0,442102415	2,261919333	2,355094959
hsa-let-7f-1-3p	0,442102415	2,261919333	2,355094959
hsa-miR-105-5p	0,442102415	2,261919333	2,355094959
hsa-miR-125b-2-3p	0,442102415	2,261919333	2,355094959
hsa-miR-1268b	0,442102415	2,261919333	2,355094959
hsa-miR-190a-5p	0,442102415	2,261919333	2,355094959
hsa-miR-191-3p	0,442102415	2,261919333	2,355094959
hsa-miR-616-3p	0,442102415	2,261919333	2,355094959
hsa-miR-619-5p	0,442102415	2,261919333	2,355094959
mgU6-47	0,442102415	2,261919333	2,355094959
U105B	0,442102415	2,261919333	2,355094959
U54	0,442102415	2,261919333	2,355094959
U92	0,442102415	2,261919333	2,355094959
mgh28S-2409	7,515741057	40,714548	2,437557119
hsa-miR-143-3p	13,70517487	74,64333799	2,445292768
hsa-miR-221-3p	32,71557872	183,215466	2,485491596
hsa-miR-193b-3p	159,5989719	920,6011686	2,528124916
hsa-let-7b-5p	273,2192925	1587,867372	2,538959151
HBII-85-6	2,652614491	15,83343533	2,57748738
HBII-85-8	2,652614491	15,83343533	2,57748738
HBII-210	13,70517487	90,47677333	2,722826743
HBII-316	2,652614491	18,09535467	2,770132458
hsa-miR-130b-3p	8,842048302	61,071822	2,788054366
hsa-miR-378d	22,98932559	167,3820307	2,864108606
U83A	3,978921736	29,40495133	2,885609676

9. Appendix

hsa-miR-130a-3p	127,767598	968,1014746	2,921636263
hsa-miR-497-5p	1,76840966	13,571516	2,94005746
ACA47	0,88420483	6,785758	2,94005746
hsa-miR-378f	0,88420483	6,785758	2,94005746
hsa-miR-589-5p	0,88420483	6,785758	2,94005746
U14A	0,88420483	6,785758	2,94005746
hsa-miR-3074-5p	49,51547049	393,573964	2,990683533
hsa-miR-940	3,978921736	31,66687066	2,992524879
HBII-85-5	3,094716906	24,88111266	3,007171655
HBII-85-7	3,094716906	24,88111266	3,007171655
hsa-miR-92a-3p	248,4615573	2056,084674	3,048805123
E3	1,326307245	11,30959667	3,092060553
hsa-miR-3613-3p	2,652614491	24,88111266	3,229564077
hsa-miR-335-5p	12,37886762	122,143644	3,302627539
hsa-miR-484	533,1755126	5297,415078	3,312606127
hsa-miR-181b-5p	36,69450045	373,21669	3,346377742
hsa-miR-1285-3p	1,76840966	18,09535467	3,355094959
hsa-miR-16-2-3p	0,442102415	4,523838666	3,355094959
hsa-miR-2278	0,442102415	4,523838666	3,355094959
hsa-miR-340-5p	0,442102415	4,523838666	3,355094959
hsa-miR-3940-3p	0,442102415	4,523838666	3,355094959
hsa-miR-4508	0,442102415	4,523838666	3,355094959
hsa-miR-6516-3p	0,442102415	4,523838666	3,355094959
hsa-miR-6516-5p	0,442102415	4,523838666	3,355094959
mgU12-22	0,442102415	4,523838666	3,355094959
U28	0,442102415	4,523838666	3,355094959
U71d	0,442102415	4,523838666	3,355094959
U91	0,442102415	4,523838666	3,355094959
U42A	1,76840966	20,357274	3,52501996
U83B	3,094716906	36,19070933	3,547740037
hsa-miR-320a	543,7859706	6629,685566	3,607829611
hsa-miR-3184-5p	6,631536227	95,00061199	3,840521786
hsa-miR-3529-3p	2,210512076	31,66687066	3,840521786
hsa-miR-7-5p	2,210512076	31,66687066	3,840521786
hsa-miR-92b-3p	45,53654876	671,790042	3,882913552
hsa-miR-203b-5p	0,88420483	13,571516	3,94005746
hsa-miR-2110	0,88420483	13,571516	3,94005746
ACA63	0,442102415	6,785758	3,94005746
hsa-miR-18a-3p	0,442102415	6,785758	3,94005746
hsa-miR-6747-3p	0,442102415	6,785758	3,94005746
hsa-miR-22-3p	16,35778936	264,644562	4,016006313
hsa-miR-3184-3p	31,83137389	542,86064	4,092060553
hsa-miR-423-5p	31,83137389	542,86064	4,092060553
hsa-miR-126-5p	6,631536227	135,71516	4,355094959
hsa-miR-629-5p	9,726253133	212,6204173	4,450252192
hsa-miR-125a-3p	1,76840966	40,714548	4,52501996
hsa-miR-320e	1,76840966	40,714548	4,52501996

9. Appendix

U104	1,76840966	40,714548	4,52501996
U96a	0,88420483	20,357274	4,52501996
U22	11,49466279	278,216078	4,597169746
hsa-miR-574-5p	9,284150718	226,1919333	4,606633726
U61	0,442102415	11,30959667	4,677023054
hsa-miR-378a-3p	166,2305081	4446,933409	4,741553713
hsa-miR-296-3p	4,421024151	119,8817247	4,761087318
U3	174,1883516	5163,961838	4,889758284
U3-3	167,5568153	5143,604564	4,94005746
hsa-miR-193a-5p	13,26307245	443,3361893	5,062914207
hsa-miR-378c	7,515741057	253,3349653	5,07498704
U3-2	124,2307786	5075,746984	5,352525599
U3-2B	124,2307786	5075,746984	5,352525599
U3-4	123,3465738	5071,223145	5,36154421
HBII-289	3,536819321	156,072434	5,463619416
hsa-miR-378e	1,326307245	63,33374133	5,57748738
hsa-miR-877-5p	3,978921736	203,57274	5,677023054
hsa-miR-138-5p	15,03148211	902,5058139	5,907877054
hsa-miR-148a-3p	0,442102415	40,714548	6,52501996
hsa-miR-193b-5p	0,442102415	45,23838666	6,677023054
hsa-miR-320b	14,5893797	1687,391823	6,85373266
hsa-miR-320c	10,61045796	1531,319389	7,173144482
hsa-miR-150-5p	0,88420483	128,929402	7,187984973
hsa-miR-320d	7,957843472	1275,722504	7,32472131
hsa-miR-340-3p	2,652614491	450,1219473	7,406757079
hsa-miR-1246	8,842048302	2194,061753	7,955007801
hsa-miR-376c-3p	0,88420483	377,7405286	8,738799251
hsa-miR-223-3p	0	531,5510433	Inf
hsa-miR-451a	0	484,0507373	Inf
hsa-miR-486-5p	0	217,144256	Inf
hsa-miR-134-5p	0	104,0482893	Inf
hsa-miR-494-3p	0	81,42909599	Inf
hsa-miR-323a-3p	0	76,90525733	Inf
hsa-miR-409-3p	0	61,071822	Inf
hsa-miR-200a-3p	0	56,54798333	Inf
hsa-miR-376a-3p	0	47,500306	Inf
hsa-miR-382-5p	0	38,45262866	Inf
hsa-miR-122-5p	0	29,40495133	Inf
hsa-miR-3591-3p	0	29,40495133	Inf
hsa-miR-144-3p	0	27,143032	Inf
hsa-miR-142-3p	0	24,88111266	Inf
hsa-miR-206	0	20,357274	Inf
hsa-miR-154-5p	0	15,83343533	Inf
hsa-miR-200b-3p	0	15,83343533	Inf
hsa-miR-200c-3p	0	15,83343533	Inf
hsa-miR-425-3p	0	15,83343533	Inf
hsa-miR-214-3p	0	11,30959667	Inf

9. Appendix

hsa-miR-329-3p	0	11,30959667	Inf
hsa-miR-543	0	11,30959667	Inf
hsa-miR-7854-3p	0	11,30959667	Inf
U95	0	11,30959667	Inf
hsa-miR-29b-1-5p	0	9,047677333	Inf
hsa-miR-3607-3p	0	9,047677333	Inf
hsa-miR-373-3p	0	9,047677333	Inf
hsa-miR-379-5p	0	9,047677333	Inf
hsa-miR-487b-3p	0	9,047677333	Inf
hsa-miR-495-3p	0	9,047677333	Inf
hsa-miR-6777-3p	0	9,047677333	Inf
hsa-miR-885-5p	0	9,047677333	Inf
hsa-miR-1-3p	0	6,785758	Inf
hsa-miR-136-3p	0	6,785758	Inf
hsa-miR-144-5p	0	6,785758	Inf
hsa-miR-199a-3p	0	6,785758	Inf
hsa-miR-199b-3p	0	6,785758	Inf
hsa-miR-3679-5p	0	6,785758	Inf
hsa-miR-380-3p	0	6,785758	Inf
hsa-miR-382-3p	0	6,785758	Inf
hsa-miR-432-5p	0	6,785758	Inf
hsa-miR-486-3p	0	6,785758	Inf
hsa-miR-5100	0	6,785758	Inf
14qI-8	0	4,523838666	Inf
14qII-14	0	4,523838666	Inf
14qII-26	0	4,523838666	Inf
HBI-6	0	4,523838666	Inf
hsa-miR-127-3p	0	4,523838666	Inf
hsa-miR-1273g-3p	0	4,523838666	Inf
hsa-miR-1285-5p	0	4,523838666	Inf
hsa-miR-142-5p	0	4,523838666	Inf
hsa-miR-197-5p	0	4,523838666	Inf
hsa-miR-215-5p	0	4,523838666	Inf
hsa-miR-2355-3p	0	4,523838666	Inf
hsa-miR-23a-5p	0	4,523838666	Inf
hsa-miR-299-3p	0	4,523838666	Inf
hsa-miR-300	0	4,523838666	Inf
hsa-miR-3194-5p	0	4,523838666	Inf
hsa-miR-337-5p	0	4,523838666	Inf
hsa-miR-34c-5p	0	4,523838666	Inf
hsa-miR-365a-5p	0	4,523838666	Inf
hsa-miR-376b-3p	0	4,523838666	Inf
hsa-miR-381-3p	0	4,523838666	Inf
hsa-miR-411-5p	0	4,523838666	Inf
hsa-miR-4429	0	4,523838666	Inf
hsa-miR-4492	0	4,523838666	Inf
hsa-miR-4725-3p	0	4,523838666	Inf

9. Appendix

hsa-miR-485-3p	0	4,523838666	Inf
hsa-miR-493-5p	0	4,523838666	Inf
hsa-miR-665	0	4,523838666	Inf
hsa-miR-760	0	4,523838666	Inf
hsa-miR-938	0	4,523838666	Inf
U63	26,52614491	0	-Inf
U81	18,56830144	0	-Inf
U84	16,35778936	0	-Inf
U76	15,47358453	0	-Inf
hsa-miR-324-5p	13,26307245	0	-Inf
hsa-miR-28-5p	11,93676521	0	-Inf
hsa-miR-4521	11,93676521	0	-Inf
U36C	11,49466279	0	-Inf
hsa-miR-378a-5p	10,16835555	0	-Inf
U45A	8,842048302	0	-Inf
hsa-miR-664a-3p	7,957843472	0	-Inf
U106	7,957843472	0	-Inf
ACA36B	7,515741057	0	-Inf
HBII-180A	7,515741057	0	-Inf
hsa-miR-196b-5p	7,073638642	0	-Inf
mgh18S-121	7,073638642	0	-Inf
U101	7,073638642	0	-Inf
U103	7,073638642	0	-Inf
U103B	7,073638642	0	-Inf
HBII-55	6,631536227	0	-Inf
U51	6,631536227	0	-Inf
U60	6,631536227	0	-Inf
U43	6,189433812	0	-Inf
snR38B	5,747331397	0	-Inf
U45B	5,747331397	0	-Inf
U86	5,747331397	0	-Inf
hsa-miR-27a-5p	5,305228981	0	-Inf
hsa-miR-532-3p	5,305228981	0	-Inf
hsa-miR-675-3p	5,305228981	0	-Inf
U55	5,305228981	0	-Inf
hsa-miR-502-3p	4,863126566	0	-Inf
U13	4,863126566	0	-Inf
U49A	4,863126566	0	-Inf
hsa-miR-192-5p	4,421024151	0	-Inf
hsa-miR-548aa	4,421024151	0	-Inf
hsa-miR-548t-3p	4,421024151	0	-Inf
U15A	4,421024151	0	-Inf
U50B	4,421024151	0	-Inf
HBII-85-21	3,978921736	0	-Inf
hsa-miR-545-3p	3,978921736	0	-Inf
U58C	3,978921736	0	-Inf
U65	3,978921736	0	-Inf

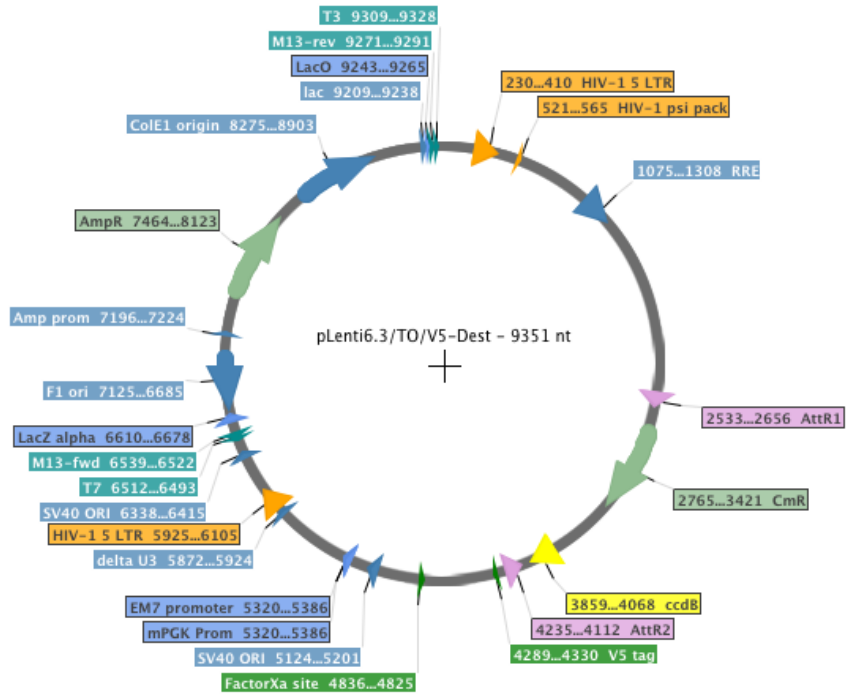
9. Appendix

HBII-85-14	3,536819321	0	-Inf
HBII-85-16	3,536819321	0	-Inf
HBII-85-17	3,536819321	0	-Inf
HBII-85-18	3,536819321	0	-Inf
HBII-85-19	3,536819321	0	-Inf
HBII-85-20	3,536819321	0	-Inf
HBII-85-22	3,536819321	0	-Inf
HBII-95B	3,536819321	0	-Inf
hsa-miR-132-5p	3,536819321	0	-Inf
HBII-85-15	3,094716906	0	-Inf
HBII-85-25	3,094716906	0	-Inf
HBII-85-27	3,094716906	0	-Inf
HBII-85-29	3,094716906	0	-Inf
hsa-miR-362-5p	3,094716906	0	-Inf
U15B	3,094716906	0	-Inf
U59B	3,094716906	0	-Inf
U77	3,094716906	0	-Inf

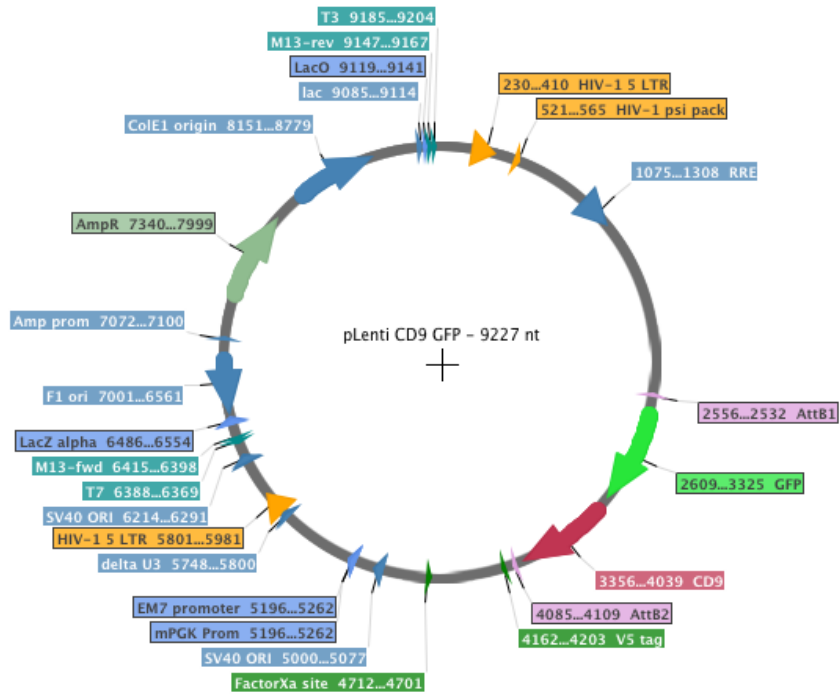
9. Appendix

9.9 Plasmid maps

9.9.1 Destiny vector for lentiviral construct generation

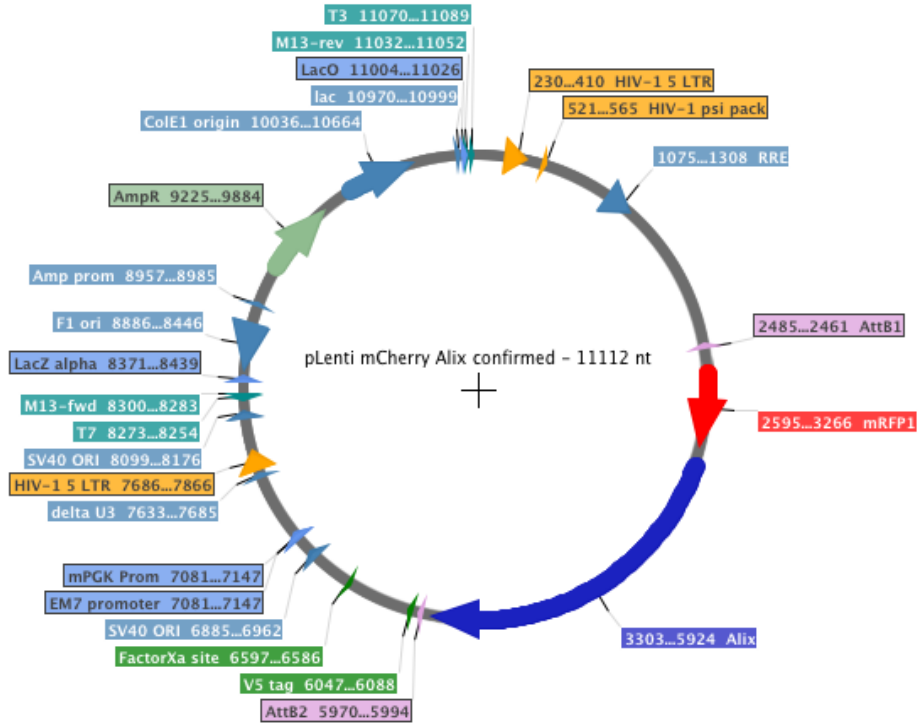


9.9.2. Lentivirus vector for stable CD9_{GFP} expression

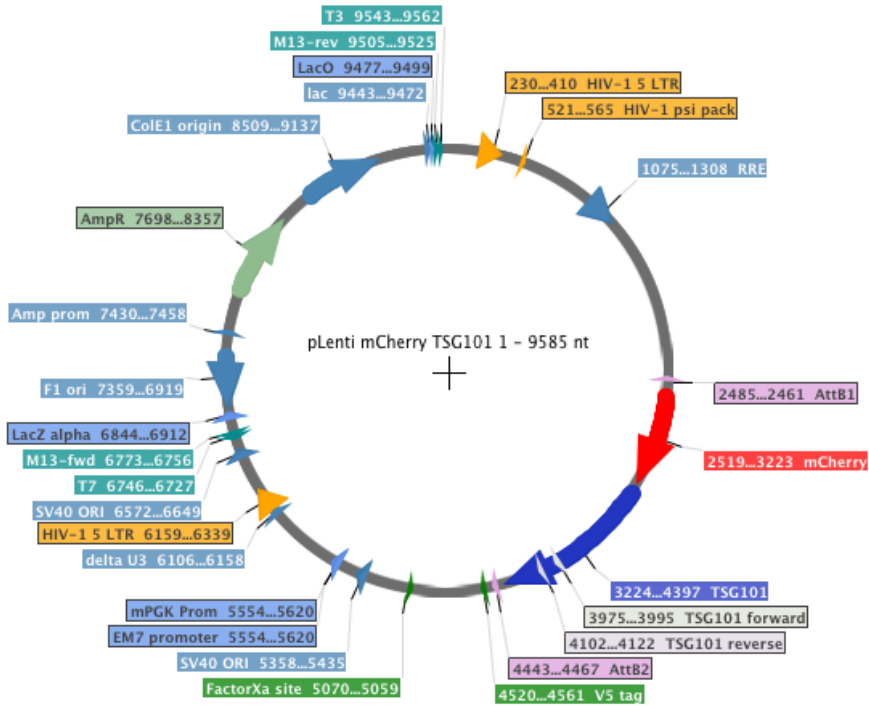


9. Appendix

9.9.3. Lentivirus vector for stable *Alix*_{mCherry} expression



9.9.4. Lentivirus vector for stable *TSG101*_{mCherry} expression



9.10 Curriculum vitae

Personal data

Date of birth 18.09.1985
Born in Herford
Nationality German



Education

05.2013 – 11.2016 **Promotion at the German Primate Center (Uni Göttingen)**
Acceptance at the Göttingen Graduate School for
Neurosciences, Biophysics, and Molecular Biosciences
(GGNB)

Emphases: Molecular Biology (RNA isolation, NGS),
Cell Biology (Cell Culture, Transfection), Bioinformatic (NGS
Data Analysis by R-software)

10.2010 – 01.2013

Biochemistry (Master), University Bielefeld

Emphases: Proteincrystallography, Cell Biology, Genetics

Master thesis: „Untersuchungen zur

Transkriptionsregulation der humanen Xylosyltransferasen

(Grade: 1.0)

Graduation: Bachelor of Science (Note: 1.4)

10.2006 – 09.2010

Biochemistry (Bachelor), University Bielefeld

Emphases: Gentechnology, Cell Biology, Immunology

Bachelor thesis: „Funktionale Charakterisierung einer ZF5-
Transkriptionsfaktorbindestelle im XT-II Promotor“

(Grade: 1.3)

Graduation: Bachelor of Science (Note: 2.4)

9. Appendix

10.2005 – 09.2006

Bioinformatics and Genome Research, Universität Bielefeld

Study abroad

01.2012 – 04.2012

Research Internship, Biomedical Center,
Uppsala University, Sweden

- Cell culture of chinese hamster ovary cells
- Cell stimulation with FGF
- SDS-PAGE protein separation and western blotting
- Separation of GAGs by sizing column chromatography
- Enzymatic and chemical cleavage of GAGs

10.2003

Great Whirley High school Exchange, UK

Further Qualification

Languages

German (native language)

English (advanced)

Latin (basic)

EDV knowledge

Operation systems: MS Windows, MacOS, Linux

Programming: R-software

Data processing: Origin 8.6, Graphpad, Fiji, Chemdraw

Awards

Admission to Göttingen Graduate School for Neurosciences, Biophysics, and Molecular Biosciences (GGNB) in 2013.

Posterprize at the 12th international PhD symposium „Horizons in Molecular Biology“, Göttingen in 2014.

Publications

Hoffmann DB, **Böker KO**, Schneider S, Eckermann-Felkl E, Schuder A, Komrakova M, Sehmisch S, Gruber J. In Vivo siRNA Delivery Using JC Virus-like Particles Decreases the Expression of RANKL in Rats. *Mol Ther Nucleic Acids*. 2016 Mar 22;5:e298. doi: 10.1038/mtna.2016.15.

Liedigk R, Kolleck J, **Böker KO**, Meijaard E, Md-Zain BM, Abdul-Latiff MA, Ampeng A, Lakim M, Abdul-Patah P, Tosi AJ, Brameier M, Zinner D, Roos C. Mitogenomic phylogeny of the common long-tailed macaque (*Macaca fascicularis fascicularis*). *BMC Genomics*. 2015 Mar 21;16:222. doi: 10.1186/s12864-015-1437-0.

Faust I, **Böker KO**, Eirich C, Akkermann D, Kuhn J, Knabbe C, Hendig D. Identification and characterization of human xylosyltransferase II promoter single nucleotide variants. *Biochem Biophys Res Commun*. 2015 Mar 20;458(4):901-7. doi: 10.1016/j.bbrc.2015.02.056.

Faust I, **Böker KO**, Lichtenberg C, Kuhn J, Knabbe C, Hendig D. First description of the complete human xylosyltransferase-I promoter region. *BMC Genet*. 2014 Dec 5;15:129. doi: 10.1186/s12863-014-0129-0.